THE JOURNAL
OF
CHEMICAL PHYSICS

VOLUME 18, NUMBER 8 AUGUST, 1950

The Recombination of Iodine Atoms in Solution

RICHARD M. NOYES
Department of Chemistry, Columbia University, New York, New York
(Received February 13, 1950)

A simple theory involving jumps between lattice sites has been used to treat the recombination of atoms produced in solution by photo-chemical dissociation. The results have been applied to experimental data obtained previously on the photo-dissociation of iodine in hexane at 25°C.

The treatment indicates that if a pair of atoms is separated by one molecular diameter in the dissociation process, then the probability is 0.40 to 0.50 that these atoms will recombine by diffusion in a period of 10^{-6} second or less. The experimental data for light of 436 mμ indicate that if some of the atoms undergo "primary recombination" without escaping from the cage of solvent molecules in which they are formed, then a larger number of atoms must become separated by two or more molecular diameters as a result of the photo-dissociation.

For light of 578 mμ the data and calculations indicate that about 35 percent of the atoms become completely separated and ultimately combine with atoms from other molecules, about 30 percent become separated by a molecular diameter but recombine rapidly by diffusion, and about 35 percent either fail to undergo predissociation or recombine without escaping from the cage of solvent molecules in which they are formed.

WE have shown[1] that when iodine atoms are produced photo-chemically from molecules in hexane at 25°C, the apparent quantum efficiencies are 0.59 at 436 mμ and 0.37 at 578 mμ. The experimental procedure was such that we measured only the quantum efficiency for the production of atoms which recombined at a rate proportional to the square root of the intensity of illumination. This restriction means that we have measured the quantum efficiency only for the production of atoms which ultimately combine with iodine atoms from other molecules. The iodine atoms which recombine with their original partners do so at a rate proportional to the first power of the intensity of illumination. If a molecule in solution has just undergone photo-dissociation, the separation of the atoms is certainly much less than the probable distance to the nearest atom formed from another molecule; hence the fraction of original partners which subsequently recombine by diffusion will surely be appreciable. Moreover, this fraction will depend at least slightly upon the photo-stationary concentration of iodine atoms, for an increase in the concentration of atoms will increase the probability that an atom which would otherwise recombine with its original partner will react first with an atom from another molecule.

[1] J. Zimmerman and R. M. Noyes, J. Chem. Phys. **18**, 658 (1950).

In this paper we shall attempt to treat the recombination by diffusion of atoms originally from the same molecule, and shall demonstrate that the fraction of original partners which recombine with each other is virtually independent of the atom concentration over any range attainable experimentally.

THEORETICAL

Relative Diffusion of Atoms

In order to treat the change in separation of two atoms, let us assume that the atoms move through the solution by making jumps of constant distance a but in random directions. Since only the relative displacement of the two atoms is important, we may treat one atom as a stationary origin and consider the motion of the other atom relative to it.

Let us consider the space around the origin to be composed of a series of concentric spherical shells of thickness a. An atom is considered to be in shell n if its center is more than $(n-1/2)a$ and less than $(n+1/2)a$ from the origin.

Let M_n be the probability that an atom, initially situated at random in shell n, will leave this shell by entering shell $(n-1)$. This probability will certainly be very nearly the ratio of the inner surface area of the

shell to the total surface area.[2] Then

$$M_n=\frac{(n-1/2)^2}{(n-1/2)^2+(n+1/2)^2}=\frac{n^2-n+1/4}{2n^2+1/2}$$

$$=1/2-\frac{n^2}{2n(n^2+1/4)}. \quad (1)$$

For $n>5$ we may assume to an excellent approximation that $M_n=(n-1)/2n$.

Then, let R_n be the probability that an atom in shell n will undergo a specified reaction near the origin before it shall have gotten into shell $(n+1)$.

$$R_n=M_nR_{n-1}+M_n(1-R_{n-1})M_nR_{n-1}$$
$$+[M_n(1-R_{n-1})]^2M_nR_{n-1}$$
$$+[M_n(1-R_{n-1})]^3M_nR_{n-1}+\cdots$$
$$=\frac{M_nR_{n-1}}{1-M_n(1-R_{n-1})}. \quad (2)$$

The probability that an atom in shell n will jump into shell $(n+1)$ at some time before it has undergone reaction near the origin of the system is

$$1-R_n=1-M_n+M_n(1-R_{n-1})(1-M_n)$$
$$+[M_n(1-R_{n-1})]^2(1-M_n)+\cdots$$
$$=\frac{1-M_n}{1-M_n(1-R_{n-1})}. \quad (3)$$

Finally, let F_n be the probability that an atom initially located at a site inside of shell n will undergo reaction near the origin of the system before it has jumped outside of shell n.

$$F_n=F_{n-1}+(1-F_{n-1})R_n. \quad (4)$$

If the values of R and F are known for some shell s at a small distance from the origin, they can be calculated for any shell farther away. For distances more than a few molecular diameters from the origin we may treat M_n, R_n, and F_n as continuous functions of n and use the approximation that $M_n=(n-1)/2n$. Then let $dR_n/dn=(R_{n+1}-R_{n-1})/2$. This assumption is exact if d^3R_n/dn^3 and all higher derivatives are zero; this condition is very nearly fulfilled. Then

$$\frac{dR_n}{dn}=-\frac{2n+1+n^2R_n}{(n+2+nR_n)(n-1)(1-R_n)}R_n. \quad (5)$$

[2] This treatment of the probability was suggested by Dr. J. M. Miller. We have also investigated three other more complicated approximation methods of calculating M_n. All methods agree that $M_n=1/2-(1/2n)f(n)$ where $f(n)$ is a function of n which rapidly approaches unity as n increases. The value of $f(1)$ by the different treatments varied from 0.750 to 0.857 and is 0.800 by this treatment. Certainly the deviation of the results of our calculations from reality will be caused more by our over-simplified picture of the diffusion process than by any errors arising from this treatment of probability.

The terms in R_n in the denominator are small and will tend to cancel each other. Actually R_n decreases rapidly enough so that they have no serious effect for $n>10$. Also R_n is approximately inversely proportional to n^2; so the term in the numerator can be corrected for by the introduction of a constant. Let $n^2R_n=b$. In no case of interest to us was b greater than 0.8. Then

$$\frac{dR_n}{R_n}=-\frac{2n+1+b}{(n+2)(n-1)}dn, \quad (6)$$

and

$$R_n/R_s=\frac{(s+2)(s-1)}{(n+2)(n-1)}\left[\frac{(s-1)(n+2)}{(s+2)(n-1)}\right]^{b/3}. \quad (7)$$

By a similar treatment we find that for values of n greater than 10 we can write

$$\frac{dF_n}{1-F_n}=R_ndn. \quad (8)$$

An approximate value of F_n can then be calculated with the expression

$$\ln\frac{1-F_s}{1-F_n}=R_s(s+2)(s-1)\int_s^n\frac{dn}{(n+2)(n-1)}$$
$$=\frac{R_s(s+2)(s-1)}{3}\ln\frac{(n-1)(s+2)}{(n+2)(s-1)}. \quad (9)$$

In every case of interest to us this value of F_n is mathematically correct to 0.003 or better.

Conditions Resulting in Recombination

The recursion formulas developed in the preceding section are concerned with the probability that two atoms will diffuse together if they are separated by a few molecular diameters. In order to apply this treatment to the problem of the recombination of atoms produced photo-chemically, we must make additional assumptions as to the initial separation of the atoms and the probability that they will react before they have diffused farther apart. We have examined three separate sets of assumptions. Two sets were selected to correspond to the extreme limits which could be expected, and the third set was based on the assumptions which seemed to us the most plausible.

Assumption I. Let us postulate that in the photochemical process the second atom is removed a distance of $1.00a$ from the first atom and that in the neighborhood of the origin it can only occupy sites in a cubic closest-packed lattice. Let us also assume that two atoms in adjacent lattice sites cannot react unless one moves toward the other with sufficient energy to carry it to any adjacent site. This situation would exist if iodine atoms were situated in the interstices between

the larger hexane molecules and did not significantly distort the lattice. If atoms which are in contact in the solution automatically react, Assumption I will lead to the smallest possible fraction of recombination by diffusion of those atoms which are not separated by more than one jump before they have lost the excess energy absorbed from the quantum which caused dissociation.

By examining the probability that an atom initially located at a distance of $1.00a$ in a cubic closest-packed lattice will reach the origin before it has reached a distance of more than $2.00a$, we find $F_{1.5}=0.1660$. A similar treatment for an initially random probability distribution in shell 1.5 gives $R_{1.5}=0.0623$. With these results it is possible to evaluate F for larger values of n.

Assumption II. Let us postulate that in the photochemical process the second atom may be removed with equal probability to any one of the 30 sites in a cubic closest-packed lattice of which 6 are located at a distance of $1.414a$ and 24 are located at a distance of $1.732a$. Let us assume also that any atom in a site adjacent to another atom will automatically react. This situation would exist if the atoms were equal to the solvent molecules in size and behavior and combined without activation energy. This assumption will lead to the greatest possible amount of recombination by diffusion.

An analysis of the probabilities of various displacements in shell 1.5 of a cubic closest-packed lattice indicates that the mathematical description of this assumption is $F_{1.5}=0.2912$ and $R_{1.5}=0.3750$.

Assumption III. This assumption is based on an attempt to obtain the most plausible answer with the use of quantities calculated from the properties of hexane and from the observed rate of combination of atoms from different molecules. Hexane at 25° has a density of 0.655 g/ml and therefore contains 4.58×10^{21} molecules/ml. If these molecules can be considered as occupying sites in a closest-packed lattice, the distance between adjacent sites is 6.75A. We do not know the diffusion coefficient for iodine atoms in hexane, but the diffusion coefficient for iodine molecules in heptane at 20°C is 2.76×10^{-5} cm²/sec.[3] Let us assume that for atoms in hexane at 25° $D=3.0\times10^{-5}$ cm²/sec. However, we can also write $D=\nu l^2/6$[4] where ν is the frequency of jumps and l is the root-mean-square jump length $=6.75$A in our example. Then $\nu=4.0\times10^{10}$ sec.$^{-1}$, and the frequency of jumps which affect the relative position of two atoms is 8.0×10^{10} sec.$^{-1}$. We have observed[1] that in this system the rate constant for the reaction $I+I\rightarrow I_2$ is 1.8×10^{-11} (atom/ml)$^{-1}$ sec.$^{-1}$. Then the frequency of recombination of two atoms in a volume of 1 ml is 7.2×10^{-11} sec.$^{-1}$. The number of different relative configurations which the atoms occupy on the average before they combine[5] is $8.0\times10^{10}/7.2\times10^{-11}=1.1\times10^{21}$. Then for one atom in a given position the number of lattice sites available to the other which lead to recombination is $4.58\times10^{21}/1.11\times10^{21}=4.12$. If this number were 1.0, we would have the situation in Assumption I. If the number were 13, we would have the situation in Assumption II. Since the number is intermediate, we shall assume that the atoms react at an average distance of $(3.12/12)^{\frac{1}{3}}a=0.64a$. It is interesting to note that this distance of 4.32A is identical to the 4.30A van der Waals diameter of an iodine atom!

The recombination diameter of two atoms was taken to be zero in Assumption I and to be $1.00a$ in Assumption II. The reasoning of the preceding paragraph suggests that the most plausible value of this quantity is $0.64a$. In the absence of any better procedure, we have chosen to calculate $F_{1.5}$ and $R_{1.5}$ for Assumption III by a linear interpolation between the values for the first two assumptions. Then $F_{1.5}=0.2461$ and $R_{1.5}=0.2624$.

TABLE I. Recombination of iodine atoms produced photo-chemically.

	Assumption I	Assumption II	Assumption III
$F_{1.5}$	0.166	0.291	0.246
$F_{2.5}$	0.188	0.393	0.325
$F_{4.5}$	0.208	0.463	0.384
$F_{9.5}$	0.224	0.511	0.427
$F_{99.5}$	0.240	0.554	0.466
$F_{999.5}$	0.241	0.558	0.470
F_{∞}	0.242	0.559	0.470

RESULTS AND DISCUSSION

We have treated the above three sets of assumptions by making summations with recursion Eqs. (2) and (4) up to and including shell 9.5 and have evaluated F for larger values of n by integration with Eq. (9). The results are presented in Table I.

We have investigated the possibility of introducing additional refinements into the development of Assumption III. Modifications of the diffusion coefficient within reasonable limits and corrections for screening of the center lattice site by the surrounding sites only varied the recombination diameter between $0.59a$ and $0.66a$. A correction of the type discussed in reference 5 might increase the value to about $0.75a$. No assumptions which seem reasonable to us give values of F_{∞} outside of the range 0.40 to 0.50. The theory cannot justify a choice between these limits.

Our experimental data indicated apparent quantum

[3] C. C. Miller, Proc. Royal Soc. (London) **106A**, 724 (1924).
[4] A. Einstein, Ann. d. Physik **17**, 549 (1905).

[5] This treatment was suggested by the work of E. Rabinowitch, Trans. Faraday Soc. **33**, 1225 (1937). It is based on the assumption that the probability of reaction after any displacement is n/N where n is the number of sites at which reaction occurs and N is the total number of sites in the solution. Such a treatment is strictly valid only if the n reactive sites are distributed at random. We have not developed a quantitative treatment for the existing situation in which the reactive sites are all located in a small region. Therefore, the true number of effective lattice sites may be larger than the value calculated here.

yields of 0.59 at 436 mμ and 0.37 at 578 mμ. The deviation of these numbers from unity is a measure of the fraction of pairs in which the original atoms either undergo "primary recombination" before they escape from the cage in which they are formed or else undergo "secondary recombination" by diffusion according to the process considered in this paper. Although the structure of the liquid is not regular enough to justify a clean-cut distinction between primary and secondary recombination, such a distinction can probably be made in a large fraction of the recombinations which occur.

Within the accuracy of our data the value of the quantum efficiency at 436 mμ agrees exactly with the result to be expected from Assumption III if there is no primary recombination and if the absorption of a quantum separates the atoms by only one jump. However, if two normal atoms are produced by light of 436 mμ, they have a combined excess energy of about 30 kcal./mole, and many of the pairs may become separated by more than one jump before they have lost this excess energy. The probability that these atoms will recombine by diffusion is considerably less. On the other hand, if the molecule fails to undergo predissociation after absorbing a quantum, the excess energy of the two atoms is only about 8 kcal./mole, and there may be some primary recombination. If more than a very few percent of the atoms do recombine without escaping from the cage in which they are formed, the data and theory require that a larger fraction of the pairs are separated by more than one molecular diameter before they have lost their excess energy.

The low quantum yield at 578 mμ cannot be entirely explained by secondary recombination even with the use of Assumption II. If we accept the conclusion of Assumption III that about 45 percent of the atoms which are separated by one jump will recombine by diffusion, then our data indicate that about 35 percent of the molecules which absorb a quantum undergo primary recombination, about 30 percent undergo secondary recombination, and about 35 percent eventually combine with other atoms in the solution. If two normal atoms are produced, they have a combined excess energy of about 13 kcal./mole; however, it may be that not all of the molecules which absorb a quantum undergo predissociation. Of course we are experimentally unable to detect the difference between primary recombination and failure to predissociate.

The presence of a considerable fraction of the atoms which recombine with their original partners by diffusion apparently contradicts the fact that the atom concentration is very closely proportional to the square root of the absorbed intensity. However, an examination of Table I shows that over 99 percent of the original partners which recombine by diffusion do so before they have diffused apart to a distance of 100 molecular diameters. Since the frequency of jumps is 8×10^{10} sec.$^{-1}$, these atoms recombine in a period of the order of 10^{-6} seconds or less. In our experiments the mean lifetime for combination of atoms from different pairs was of the order of 0.3 second. Although we were working with dilute solutions and low light intensities, it would hardly be possible to increase the concentration of atoms (and hence to decrease their mean lifetime) by a factor of more than 10^3. Therefore, we see that the concentration of atoms will not have a detectable effect on the fraction of original partners which recombine. Moreover, we determined the concentration of free atoms by an exchange reaction which had a frequency of the order of 10^3 sec.$^{-1}$. Hence we were virtually unable to detect the presence of atoms from pairs which recombined, and our quantum yields refer to the formation of atoms which ultimately combine with iodine atoms from other molecules.

We have developed the above theory to treat the case of photo-chemical dissociation in which the atoms separate with energies of the order of one electron volt or less and in which the atoms react only with each other and not with the solvent. It may be that a modification of this approach will also be helpful in treating the behavior of "hot" recoil fragments from nuclear processes.

ACKNOWLEDGMENT

The author is indebted to Drs. George E. Kimball and Joseph Zimmerman for helpful discussions during the development of these ideas. He is especially grateful to Dr. J. M. Miller for very careful and critical reviews of several drafts of the paper.

The Concentration and Mobility of Vacancies in Sodium Chloride

HOWARD W. ETZEL* AND ROBERT J. MAURER**
Carnegie Institute of Technology, Pittsburgh, Pennsylvania
(Received February 17, 1950)

The electrical conductivity of sodium chloride, containing cadmium chloride as an impurity, has been determined as a function of temperature. From these data it is calculated that the mobility of the positive ion vacancies is given by the equation $\mu=(19600/T)\exp(-9860/T)$ cm.^{2}/volt-sec. between 250°C and 400°C. The concentration of positive ion vacancies in a "pure" sodium chloride crystal was 1.0×10^{17} cm^{-3} and independent of temperature below 550°C.

INTRODUCTION

IT is generally accepted that ionic mobility in the crystalline alkali halides is the result of the presence of vacancies, i.e., lattice sites at which ions are missing.[1,2] A fundamental problem is the determination of the concentration and mobility of the vacancies and the temperature dependence of these quantities. Since the electrical conductivity, σ, is of the form

$$\sigma=ne\mu, \tag{1}$$

where e is the electronic charge, the measurement of the conductivity yields only the product, $n\mu$, of the concentration, n, of positive ion vacancies and their mobility, μ.[3]

Koch and Wagner[4] have suggested and applied to the silver halides a method for the determination of the quantities n and μ which consists in measuring the conductivity as a function of the concentration of a positive divalent ion which is dissolved in the crystal. As applied to an alkali halide such as sodium chloride, the method of Koch and Wagner assumes that the divalent ion enters the lattice substitutionally. Since the crystal must be electrically neutral, it is also assumed that each divalent impurity ion replaces two sodium ions with the result that an excess concentration of positive ion vacancies equal to the concentration of impurity ion is introduced into the crystal. According to Eq. (1) and to a first approximation, the conductivity of the impure salt is a linear function of the concentration of impurity ion.

A pure crystal contains equal concentrations of positive and negative ion vacancies. The effect of the vacancies which are introduced into the crystal by the divalent impurity is to shift the equilibrium existing between positive and negative ion vacancies, promoting their combination. As a result, the equilibrium concentration of positive ion vacancies in the impure crystal is less than the sum of the original concentration in the pure crystal and the concentration of the divalent impurity ion.

As pointed out by Stasiw and Teltow,[5] who have given a lucid presentation of the theory of Koch and Wagner, a second reaction, between divalent impurity ions and positive ion vacancies, must be taken into account. Because of its double charge, a positive divalent ion attracts a positive ion vacancy, which has an effective negative charge. The fraction of positive ion vacancies which are nearest neighbors of a positive divalent ion exceeds that expected on the basis of chance and a vacancy tends to remain a nearest neighbor of a divalent ion for a time greater than the normal jump time of a vacancy. Such an association between a vacancy and a divalent ion will be called a complex. Figure 1 is a schematic representation of a crystal containing vacancies, divalent impurity ions, and complexes.

A difference in size between the divalent impurity ion and the sodium ion promotes the formation of complexes because the vacancy may relieve the local stress surrounding the impurity ion. The effect of complex formation is to reduce the concentration of free positive ion vacancies which contribute to the conductivity of the crystal.

THEORY

It is assumed that the vacancies, positive divalent impurity ions, and complexes behave as the components of an ideal solution. The reaction between positive and negative ion vacancies by which they combine and

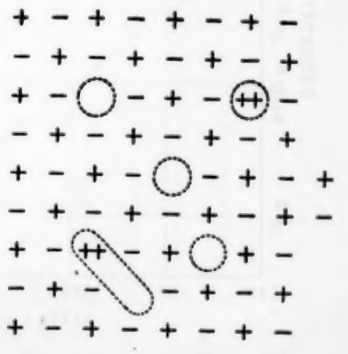

FIG. 1. Schematic representation of vacancies, divalent impurity ions, and complexes in a sodium chloride crystal.

* Now at the University of Paris, Paris, France.
** Now at the University of Illinois, Urbana, Illinois.
[1] F. Seitz, *Modern Theory of Solids* (McGraw-Hill Company, Inc., New York, 1940).
[2] N. Mott and R. Gurney, *Electric Phenomena in Ionic Crystals* (Oxford University Press, London, 1940), Chapter II.
[3] The data of Tubandt (Part III, Hdb. der Exp. Physik, Vol. XII, 1932) indicates that the contribution of the chloride ion, in sodium chloride, to the conductivity is negligible below 400°C.
[4] E. Koch and C. Wagner, Zeits. f. physik. Chemie **B38**, 295 (1937).
[5] O. Stasiw and J. Teltow, Ann. d. Physik (6) **1**, 261 (1947).

TABLE I.

Element*	% Impurity	Element*	% Impurity
Cd	<0.01	Cu	<0.001
Fe	<0.001	Ag	<0.01
B	<0.001	Zn	<0.01
Be	<0.001	Ni	<0.01
Si	<0.001	Co	<0.01
Mn	<0.01	Li	<0.001
Mg	<0.01	K	<0.01
As	<0.01	Ba	<0.01
Sn	<0.01	Ca	<0.01
Sb	<0.01	Cr	<0.001
P	<0.01	Al	<0.01
Hg	<0.01	Zr	<0.01
Pb	<0.01	Ti	<0.01

* Molybdenum, tungsten, and vanadium not detected.

migrate to the surface of the crystal is represented by the chemical equation,

$$V_p + V_n \rightleftharpoons \text{perfect crystal.} \tag{2}$$

Similarly, the reaction between positive ion vacancies (V_p) and divalent impurity ions (I) to form complexes (C) is represented by

$$V_p + I \rightleftharpoons C. \tag{3}$$

Application of the mass action law to these reactions yields the following equations,

$$x_p \cdot x_n = 1/K_1, \tag{4}$$

$$(y - x_c)x_p/x_c = 1/K_2. \tag{5}$$

The mole fractions of positive and negative ion vacancies are represented by x_p and x_n respectively; x_c is the mole fraction of the complexes present; and y is the mole fraction of impurity ion added to the crystal.

By combining the equation

$$y - x_c = x_p - x_n, \tag{6}$$

which expresses the condition that the crystal is electrically neutral, with Eqs. (4) and (5), one obtains

$$y = x_0\left[H(Z^2-1) + \left(Z - \frac{1}{Z}\right)\right], \tag{7}$$

where H is defined by the two equilibrium constants,

$$H = K_2/K_1^{\frac{1}{2}}. \tag{8}$$

The dimensionless quantity, z, is given by

$$z = x_p/x_0 = \sigma/\sigma_0, \tag{9}$$

since the mobility, μ, of the positive ion vacancies is assumed independent of the concentration of impurity ion. The conductivity of the pure crystal and the mole fraction of positive ion vacancies present in it are represented by σ_0 and x_0, respectively. According to Eq. (4)

$$x_0 = 1/K_1^{\frac{1}{2}}. \tag{10}$$

When z is much greater than unity, as in the present work, Eq. (7) is adequately approximated by the quadratic

$$y = L\sigma^2 + F\sigma, \tag{11}$$

where

$$L = x_0 H/\sigma_0^2, \tag{12}$$

$$F = x_0/\sigma_0 = M/\rho N_0 e\mu. \tag{13}$$

By fitting experimental data of conductivity *versus* mole fraction of impurity, at constant temperature, to Eq. (11), the constants L and F are evaluated. The mobility, μ, of the positive ion vacancies is obtained directly by substituting in Eq. (13) the known values of the electronic charge, e, Avogadro's number, N_0, the molecular weight, M, and the density, ρ, of sodium chloride. The concentration, n, of free positive ion vacancies is given by Eq. (1) when the mobility is known. The degree of association of impurity ions in the form of complexes, α, defined as

$$\alpha = x_c/y \tag{14}$$

is given by

$$\alpha = 1/1 + F/L\sigma \tag{15}$$

and the equilibrium constant, K_2, is

$$K_2 = L/F^2. \tag{16}$$

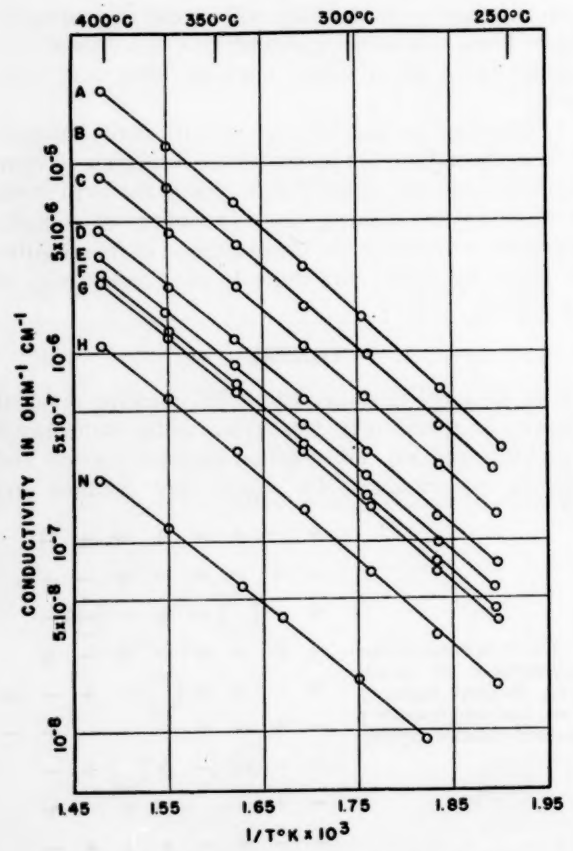

FIG. 2. The temperature dependence of the electrical conductivity of NaCl-$CdCl_2$ crystals.

The heat of formation of the complexes, Q, can be obtained, if the temperature dependence of K_2 is known, by means of the van't Hoff equation,

$$Q=\frac{d(\ln K_2)}{d(1/RT)}. \quad (17)$$

EXPERIMENTAL

Single crystals were grown from the melt by the Kyropoulos method using a platinum crucible.[6] Eimer and Amend Tested Purity sodium chloride and Baker and Adamson cadmium chloride were used as source materials.

Cadmium was chosen as the divalent impurity because its ionic radius is within five percent of that of sodium.[7] In addition, polarographic analysis for cadmium is convenient, sensitive, and precise.[8]

The single crystals were cleaved into cubes approximately one centimeter on edge and annealed in an atmosphere of helium. Annealing of the crystals consisted in heating them to 770°C at the rate of 6°C/min. and holding them at this temperature for one hour. They were then cooled to room temperature at the rate of 1°C/min.

Tests conducted upon "pure" crystals and upon one containing 0.02 mole percent cadmium showed that the conductivity was not altered when the rate of cooling was changed to either 3°C or 0.3°C/min. The conductivity of a quenched "pure" crystal which was rapidly cooled in air by removing it from the oven at 770°C was the same as that of a crystal cooled at 1°C/min. A quenched crystal containing cadmium had a low temperature conductivity approximately 70 percent greater than that of the same crystal cooled at 1°C/min.

For measurement of the electrical conductivity, the crystal cubes were cleaved into plates approximately one millimeter thick. One such plate was used for the determination of the conductivity of a sample and the adjacent plates were analyzed for the cadmium content.

As electrodes, both platinum, evaporated on the crystal surfaces in a vacuum, and colloidal graphite, painted on in alcohol solution, were used. Over the entire temperature range from 250°C to 700°C, these electrode materials yielded identical results. Platinum electrodes disappeared rather rapidly above 600°C. Because of traces of oxygen present in the helium atmosphere of the oven, the graphite electrodes slowly oxidized at the higher temperatures.

During the conductivity measurements the crystals were mounted between platinum clad nickel electrodes in a quartz tube. The quartz tube was surrounded by an electrically heated oven, the temperature of which was held constant by a conventional temperature regulator. A ballistic galvanometer measured the charge passed through the crystal upon application of a square pulse of voltage of known magnitude and duration. The resistance of the crystal was determined by replacing the crystal in the circuit by a precision variable resistor which was adjusted to duplicate the deflection of the galvanometer obtained with the crystal. The charge passed through the crystal for a single measurement varied from 2×10^{-8} coulomb at low temperatures to 2×10^{-7} coulomb at the higher temperatures. The direction of the current was reversed after each measurement. The independence of the measured crystal resistance of the duration of the voltage pulse, which was varied between 0.050 and 0.20 second was established, as was the validity of Ohm's law. The accuracy of the conductivity determinations is estimated as ±5 percent.

TABLE II.

Sample	Mole ratio Cd/Na $\times10^{-5}$
A	68.6
	64.0
B	39.0
	38.5
C	19.0
D	8.8
E	5.0
F	5.1
G	3.6
H	1
N	0

RESULTS

The conductivity as a function of temperature is shown in Fig. 2 for eight sodium chloride crystals containing cadmium as an impurity (curves *A* through *H*). Curve *N* of Fig. 2 is data obtained from a "pure"

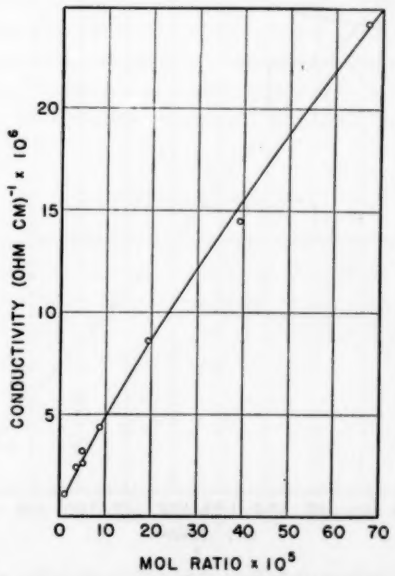

FIG. 3. Electrical conductivity *versus* mole ratio Cd/Na at 403°C.

[6] S. Kyropoulos, Zeits. f. anorg. allgem. Chemie **154**, 308 (1926).
[7] F. Seitz, reference 1, p. 93.
[8] I. Kolthoff and J. Lingane, *Polarography* (Interscience Publishers, Inc., New York, 1941).

TABLE III.

Temperature (°C)	(cm²/volt-sec.)	L	F
403	$(1.35\pm0.26)\times10^{-5}$	$(0.301\pm0.058)\times10^{8}$	$(0.206\pm0.040)\times10^{3}$
344	$(3.70\pm0.75)\times10^{-6}$	$(0.525\pm0.105)\times10^{7}$	$(0.755\pm0.152)\times10^{2}$
295	$(1.03\pm0.21)\times10^{-6}$	$(0.133\pm0.028)\times10^{9}$	$(0.270\pm0.056)\times10^{3}$
256	$(3.03\pm0.65)\times10^{-7}$	$(0.263\pm0.057)\times10^{10}$	$(0.922\pm0.200)\times10^{3}$

sodium chloride crystal. Spectroscopic analysis of this "pure" crystal revealed the accidental impurities shown in Table I. The cadmium content of crystals A through H is given in Table II. The analysis for cadmium is believed accurate to ±5 percent. In two cases, sufficient material was available for duplicate analyses with the results indicated in Table II.

A typical curve of conductivity *versus* mole fraction of cadmium is shown in Fig. 3 for a temperature of 403°C. The solid curve of Fig. 3 represents a least squares fit of Eq. (11) to the experimental points. Table III gives the mobility, μ, calculated from the data of Fig. 2 for four temperatures. The mobility as a function of temperature is given by the equation,

$$\mu=\left(\frac{19{,}600}{T}\right)\exp\left(-\frac{9860}{T}\right)\text{ cm}^2/\text{volt sec.} \quad (18)$$

Between 250°C and 400°C, the concentration of free positive ion vacancies in the "pure" crystal (curve N of Fig. 2) is $1.0\pm0.2\times10^{17}$ cm^{-3} and independent of temperature. This value is similar to that found by Breckenridge[9] as the result of dielectric loss measurements on sodium chloride. The equilibrium constant, K_2, as a function of temperature is shown in Fig. 4. The heat of formation, Q, of complexes is of the order of 0.3 electron volt per complex. In crystal A having the largest cadmium content, the degree of association, α, is about 25 percent at 403°C and increases to 50 percent at 256°C.

In Fig. 5 (curve N), the conductivity of a "pure" crystal of sodium chloride is shown over the temperature range of 300°C to 700°C. In the high temperature region, this data satisfies the relation

$$\sigma=\left(\frac{3.72\times10^{8}}{T}\right)\exp\left(-\frac{21{,}600}{T}\right)\Omega^{-1}\text{ cm}^{-1}. \quad (19)$$

The form of curve N, Fig. 5, is typical of the "pure" alkali halides. Above the knee of the curve, it has been suggested that both the concentration and the mobility of the vacancies depend upon the temperature. Simple theory (2) predicts a temperature dependence of these

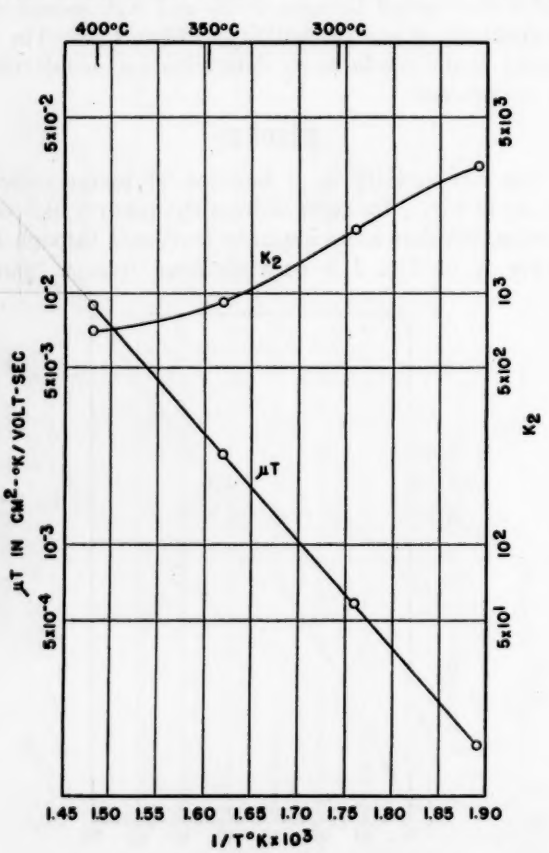

FIG. 4. The temperature dependence of the mobility, μ, of positive ion vacancies; and of the equilibrium constant K_2.

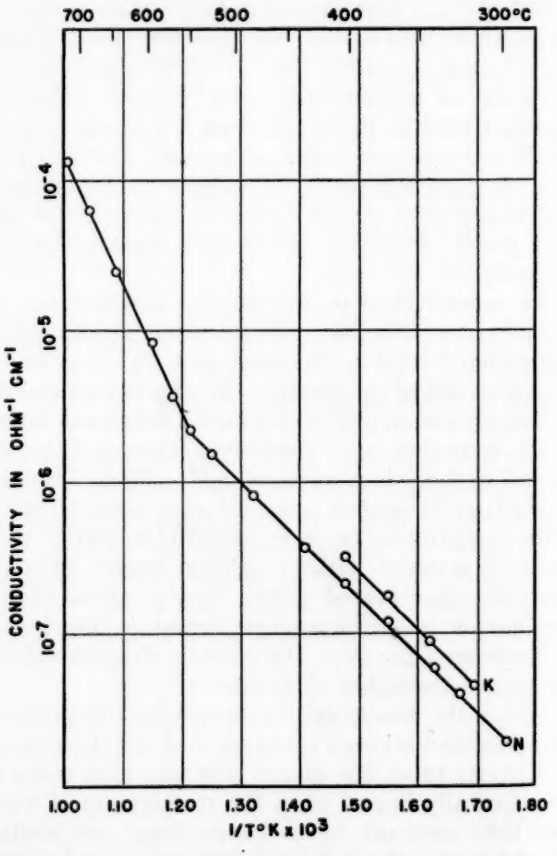

FIG. 5. The temperature dependence of the conductivity of "pure" NaCl and NaCl-KCl.

[9] R. G. Breckenridge, J. Chem. Phys. **16**, 959 (1948).

quantities given by the expressions

$$n = n_0 \exp(-W/2kT), \tag{20}$$

$$\mu = (\mu_0/T) \exp(-u/kT), \tag{21}$$

where U is the activation energy for the jump of a vacancy and W is the energy necessary to form a pair of isolated positive and negative ion vacancies within the crystal. Extrapolation of Eq. (18) into the high temperature region and combination of it with Eq. (19) leads to the equation

$$n = 1.2 \times 10^{23} \exp(-11{,}700/T) \text{ cm}^{-3}. \tag{22}$$

for the concentration of positive ion vacancies in the region of high temperature. The experimental values of U and W are 0.85 ev and 2.02 ev respectively. The experimental values of μ_0 and n_0 are in reasonable agreement with the predictions of the simple theory (2).

A prime assumption of the present work is that the increase in conductivity observed when cadmium chloride is dissolved in sodium chloride is due entirely to the divalent character of the cadmium ion. To test this assumption, a crystal was grown from a melt containing one mole percent of potassium chloride. On the basis of the results of McFee[10] and the results obtained with cadmium chloride, it is expected that the concentration of potassium chloride in the crystal was about a tenth of its concentration in the melt. As shown by curve K of Fig. 5, this crystal possessed a conductivity about 65 percent greater than that of "pure" sodium chloride. The effect of the monovalent ion, potassium, upon the conductivity, is therefore, negligible by comparison with that of the divalent ion, cadmium, although the ionic radius of potassium is considerably larger than that of cadmium.

When the conductivity of sodium chloride crystals, containing cadmium as an impurity was measured in the neighborhood of 500°C, the conductivity was observed to decrease with the time. An explanation of this effect which is illustrated in Fig. 6 has not been found. If a crystal was held at constant temperature, the percentage decrease of the conductivity increased with the concentration of cadmium present. The effect of cycling a crystal between 270°C and 520°C is shown in Fig. 7. The effect is absent if the temperature of the crystal remains below 400°C and is not observed at any temperature with "pure" crystals. Reannealing of the crystals does not restore the conductivity to its original

[10] R. McFee, J. Chem. Phys. **15**, 856 (1947).

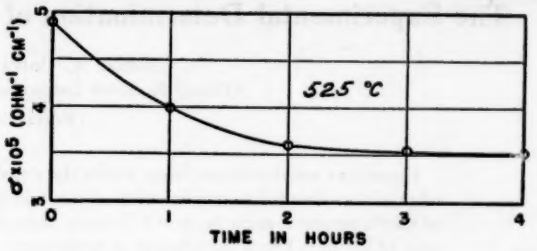

FIG. 6. Decrease of conductivity with time for crystal E (see Fig. 2) at 525°C.

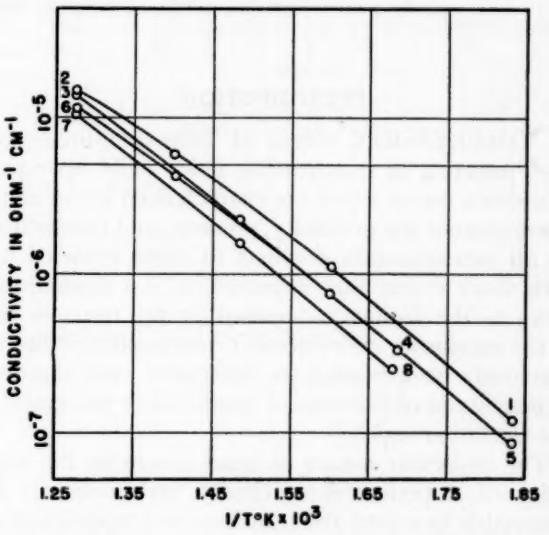

FIG. 7. Decrease of conductivity of crystal C on cycling with maximum temperature of 525°C. The numbers indicate the order in which the points were determined.

value. Experiments in which crystals, both with and without electrodes, were annealed in the neighborhood of 500°C indicated that at least a part of the decrease in conductivity may be ascribed to the presence of the electrodes. The observed conductivity decrease correlates, however, with the observation that quenched crystals containing cadmium possessed a somewhat larger low temperature conductivity than those which were cooled slowly.

ACKNOWLEDGMENT

The determination of the cadmium content of the crystals was performed at the U. S. Naval Research Laboratory through the courtesy of Dr. James Schulman. This research was partially supported by the ONR of the U. S. Navy Department.

The Experimental Determination of the Thickness of a Shock Front in a Gas* †

GEORGE R. COWAN** AND DONALD F. HORNIG
Metcalf Research Laboratory, Brown University, Providence, R. I.
(Received February 20, 1950)

Equations are developed from which the density profile of a shock front may be calculated from a knowledge of its reflectivity as a function of wave-length and angle of incidence. The reflectivities of shock fronts of shock pressure ratio $p_2/p_1=1.71$ have been measured in nitrogen at initial pressure, p_1, equal to 85, 68, and 42 lb./in.^{2}. From the change of reflectivity with wave-length, the thickness of the fronts was found to be 1.8×10^{-5} cm, 2.0×10^{-5} cm, and 3.2×10^{-5} cm with an accuracy of twenty-five percent. An independent but less accurate check was provided by the change of reflectivity with initial pressure, yielding a thickness of 1.5×10^{-5} cm for $p_1=85$ lb./in.^{2}. The weighted mean value, 1.7×10^{-5} cm, for $p_1=85$ lb./in.^{2} is significantly greater than that calculated from the theory of Thomas, 1.0×10^{-5} cm.

INTRODUCTION

COMPRESSION waves of finite amplitude propagating in compressible fluids build up rapidly into shock waves which are characterized by an almost discontinuous rise in density, pressure, and temperature. In all measurements previous to those reported here such shock fronts have appeared to be a discontinuity down to the limitation imposed by the response time of the measuring instruments. Consequently, it has not previously been possible to determine even the order of magnitude of the time of transition or the extent of the transition region.

The molecular nature of gases precludes the possibility of a perfect discontinuity and makes it unreasonable to expect the transition in properties at the shock front to occur in a distance less than the mean free path of the gas molecules. If the disturbance is described by the hydrodynamic equations for a continuum, the inclusion of thermal conductivity and viscosity terms also leads to the conclusion that the transition in properties must take place over a finite region of space and in the case of gases that this region must be of the order of magnitude of a few mean free paths. Theoretical investigations of the detailed nature of a shock front have been carried out both from the kinetic theory and hydrodynamic points of view by a number of authors, including Rankine,[1] Rayleigh,[2] Taylor,[3] Becker,[4] and Thomas.[5]

Although these theories are definitely approximate, a reasonably valid conclusion is that for all but the weakest shocks the transition takes place in a very few mean free paths; a molecule on the average undergoes only a very few collisions in traversing the transition region. The investigation of the phenomenon in detail should afford data regarding kinetic processes in individual collisions such as the efficiency of collisional transfer of translational to rotational energy.

Recently a measurement technique which is peculiarly suited to the investigation of the shock front has been suggested.[6] It is based on the fact that the wave-length of visible light is of the same order of magnitude as the theoretically predicted thickness of a shock front in a gas under ordinary conditions of temperature and pressure. Hence, the optical properties of a shock front should be sensitive to its thickness and, in particular, the reflectivity should be a suitable property for experimental measurement. The reflectivities of moving shock waves in nitrogen have now been measured at various wave-lengths and for various angles of incidence and the thickness of the shock fronts determined to within an error estimated at twenty-five percent.

REFLECTIVITY OF A SHOCK FRONT

Since the index of refraction of a pure substance is a single valued function of its density, a plane shock front can be characterized by an index of refraction which is a continuous function, $n(x)$, of the distance, x, perpendicular to the front. The total change in n in passing through the front is very small compared to n; for example, for nitrogen at standard temperature and pressure, $n=1.0003$, while if the density is increased ten times $n=1.0030$. Under these circumstances the transition region may be regarded as a superposition of infinitesimal plane interfaces and since the total amplitude of the reflected light wave is negligible compared to the incident amplitude, all cross terms between the effects of different interfaces may be neglected. The reflecting layer is thus regarded as a first-order perturbation of the incident electromagnetic radiation. This approximation is valid when the reflectivity is very much less than unity.

If we denote by A_1, A_2, B_1 and B_2 the amplitudes of the electric field intensity parallel (1) with and perpendicular (2) to the plane of incidence of the light for the incident (A) and the reflected (B) beams; and

* Based on a thesis presented by George R. Cowan in partial fulfillment of the requirements for the degree of Doctor of Philosophy, Brown University, 1949.

† The work reported here was supported by ONR under contract N7onr-358, Task 3.

** Present address: Department of Physical Chemistry, University of Minnesota, Minneapolis, Minnesota.

[1] W. V. M. Rankine, Phil. Trans. **160**, 277 (1870).
[2] Lord Rayleigh, Proc. Roy. Soc. **A84**, 247 (1910).
[3] G. I. Taylor, Proc. Roy. Soc. **A84**, 371 (1910).
[4] R. Becker, Zeits. f. Physik **8**, 321 (1922).
[5] L. H. Thomas, J. Chem. Phys. **12**, 449 (1944).
[6] D. F. Hornig, Phys. Rev. **72**, 179 (1947).

if we denote the angles of incidence and of transmission by θ and $\theta+\delta\theta$, then if $\delta\theta$ is vanishingly small Fresnel's Laws take the form

$$B_1/A_1=-\delta\theta/\tan 2\theta, \tag{1}$$

$$B_2/A_2=\delta\theta/\sin 2\theta. \tag{2}$$

Under the same circumstances, Snell's Law of Refraction becomes:

$$n\delta\theta=-\delta n\tan\theta. \tag{3}$$

The substitution of (3) in (1) and (2) yields the reflectivity coefficients for reflection from an infinitesimal interface. These are

$$B_1/A_1=\delta n(1-\tan^2\theta)/2n, \tag{4}$$

$$B_2/A_2=-\delta n(1+\tan^2\theta)/2n. \tag{5}$$

Since in any given region of the shock front the index of refraction change is given by

$$\delta n=(dn/dx)\delta x, \tag{6}$$

the coefficient for reflection from the entire layer characterized by $n=n(x)$ is, in this approximation,

$$\frac{B_1}{A_1}=\frac{1-\tan^2\theta}{2}\int_{-\infty}^{\infty}\frac{1}{n}\left(\frac{dn}{dx}\right)\exp\left[-\frac{2\pi i\xi(x)}{\lambda}\right]dx, \tag{7}$$

where the exponential gives the relative phases of the reflected beams from various layers. In this equation λ is the wave-length of the light and $\xi(x)$ is the difference in path between the light reflected from the layer x and that from the layer at $x=0$.

Since the total change in index of refraction is negligible, n may be taken, in this approximation, equal to a constant value n_0 and in the case of gases it is safe to set $n_0=1$. Furthermore, refraction may be neglected so that the path difference is given by the simple expression

$$\xi(x)=2x\cos\theta. \tag{8}$$

Therefore,

$$\frac{B_1}{A_1}=\frac{1-\tan^2\theta}{2}\int_{-\infty}^{\infty}\left(\frac{dn}{dx}\right)\exp(-2\pi ixy)dx \tag{9}$$

$$=(1-\tan^2\theta)F(y)/2$$

where we have set

$$y=2\cos\theta/\lambda. \tag{10}$$

Similarly,

$$B_2/A_2=-(1+\tan^2\theta)F(y)/2. \tag{11}$$

Equations (9) and (11) are Fourier integrals so that their inverses can also be found, using the Fourier integral theorem. This yields

$$\frac{dn}{dx}=\int_{-\infty}^{\infty}F(y)\exp(2\pi ixy)dy. \tag{12}$$

The reflectivity, R, is the ratio of reflected to incident power, and is given by

$$R=\frac{|B|^2}{|A|^2}=\frac{|B_1|^2+|B_2|^2}{|A_1|^2+|A_2|^2}. \tag{13}$$

If the incident light is nonpolarized

$$|A_1|^2=|A_2|^2=|A|^2/2 \tag{14}$$

so that

$$2R=\left|\frac{B_1}{A_1}\right|^2+\left|\frac{B_2}{A_2}\right|^2. \tag{15}$$

Using Eqs. (9) and (11), one obtains in this case

$$R=(1+\tan^4\theta)|F(y)|^2/4. \tag{16}$$

From this equation one can then predict the reflectivity as a function of the angle of incidence and the wave-length for any assumed density (and hence index of refraction) profile of the front.

In the limit $y\to 0$, which is realized physically at long wave-lengths or at grazing incidence, the reflectivity becomes independent of the shock front model and is given by

$$R(0)=(\Delta n)^2(1+\tan^4\theta)/4, \tag{17}$$

where (Δn) is the total change in the index of refraction. This limiting reflectivity may be used to measure Δn and hence also $\Delta\rho$ and Δp in the shock front.

All of the preceding equations, having been derived for a first-order perturbation, are valid only when $R\ll 1$. In the cases to which we apply them R is in the range 10^{-5} to 10^{-7} so that they may be used with confidence.

In order to interpret the experimental data it is necessary to compare the measured reflectivities with those calculated from appropriate models. For this purpose R was derived for two simple functions $n(x)$. In the first, Model I, the shock front is approximated by a linearly rising index of refraction whose slope is the average slope of the front.

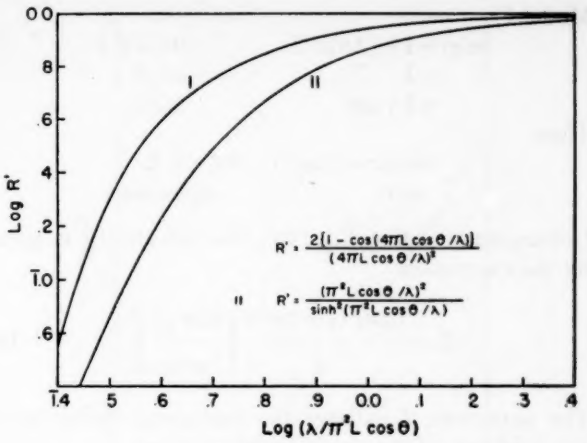

FIG. 1. Theoretical reflectivities of Model I and Model II shock fronts.

Model I

$$\begin{aligned} n(x) &= 1+(\Delta n)x/L && 0\leqslant x\leqslant L \\ &= 1 && x\leqslant 0 \\ &= 1+\Delta n && x\geqslant L. \end{aligned}$$

Then

$$\begin{aligned} dn/dx &= (\Delta n)/L && 0\leqslant x\leqslant L \\ &= 0 && \text{elsewhere.} \end{aligned}$$

Consequently, using Eq. (16), the reflectivity is given by the expression

$$R_{\mathrm{I}}=\frac{(\Delta n)^2(1+\tan^4\theta)}{4}\left[\frac{\sin\pi yL}{\pi yL}\right]^2. \tag{18}$$

The parameter L satisfies the customary definition of the thickness of the shock front

$$L=(\Delta n)/(dn/dx)_{\max}=(\Delta\rho)/(d\rho/dx)_{\max}. \tag{19}$$

This model is special in that the maximum slope is identical with the average slope.

The second function, Model II, is a very close approximation to the profile of the front obtained theoretically by Thomas.[5]

Model II

$$n(x)=1+\frac{\Delta n}{1+\exp(-4x/L)}$$

$$R_{\mathrm{II}}=\frac{(\Delta n)^2(1+\tan^4\theta)}{4}\left[\frac{\pi^2yL/2}{\sinh(\pi^2yL/2)}\right]^2. \tag{20}$$

The parameter L again gives the thickness of the front in terms of the maximum slope (which is greater than the average slope). For these and other models the solutions to equation (16) are best found using the Fourier transforms tabulated by Campbell and Foster.[7]

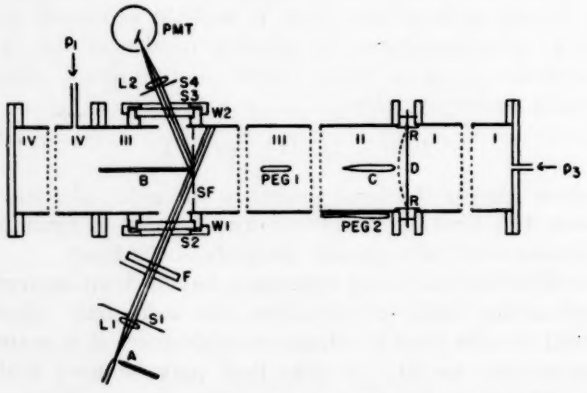

FIG. 2. Schematic drawing of shock tube and optical system.

A	carbon arc	*SF*	shock front
L	lens	*PEG*	piezoelectric gauge
S	slit	*D*	diaphragm
W	window	*R*	diaphragm cutting rings
B	baffle	*C*	diaphragm catcher
PMT	photo-multiplier tube		

[7] G. A. Campbell and R. M. Foster, "Fourier Integrals for Practical Applications," Mathematical Physics Monograph B-584 (Bell Telephone System Technical Publications, 1942).

Epstein[8] has given an exact solution of the wave equation for reflection of the perpendicular component of the light for a special function, $n(x)$, which reduces to Model II if Δn is small. His exact solution becomes coincident, as it should, with that part of Eq. (20) which is due to the perpendicular component under these same conditions.

Since all models will yield the $(\Delta n)^2$ and $1+\tan^4\theta$ terms, it is convenient, in comparing models, to define a quantity R' which includes only that part of Eqs. (19) and (20) which is included in square brackets. That is

$$R'=4R/(\Delta n)^2(1+\tan^4\theta). \tag{21}$$

The functions R_{I}' and R_{II}' are plotted in Fig. 1. It is seen that the two models do not differ drastically but that the differences should be sufficient to distinguish between them.

EXPERIMENTAL PROCEDURE

In order to measure the reflectivity of a shock front, a plane shock front was generated in a cylindrical tube and propagated down the tube until it intersected a beam of light. As the shock front passed through the light beam a pulse of reflected light was generated. This reflected beam was focussed on a photo-multiplier tube and recorded on an oscilloscope. The reflected pulse had an intensity approximately 10^{-5} to 10^{-7} times that of the incident beam and a duration of approximately 20 microseconds. A schematic drawing of the apparatus used is shown in Fig. 2.

The chief reason for the choice of this scheme rather than any method using stationary shock waves was the necessity of distinguishing the weak reflected beam from the constant background of scattered light. This is easily done when the front moves through the beam but quite impossible in a static method. Moreover, generating a plane moving shock wave is easy and inexpensive while stationary fronts require elaborate experimental arrangements.

The shock tube was a cylindrical brass tube whose inner diameter was $2\frac{7}{8}$ in. and whose thickness was $\frac{1}{16}$ in., made up of four flanged sections, each 2 feet in length, which were bolted together. The shock wave was set up in this tube by the bursting diaphragm method which has been used by many workers.[9,10] Section I (see Fig. 2) of the shock tube was the compression chamber to which gas was admitted through an inlet (p_3) in the end plate. Section I was separated from the remainder of the tube, the expansion chamber, by a copper diaphragm (D) which was clamped between steel rings (R). The inside edge of the face of the ring on the low pressure side of the diaphragm acted as the cutting edge when the diaphragm sheared

[8] P. S. Epstein, Proc. N. A. S. **16**, 627 (1930).

[9] W. Payman and W. F. C. Shepherd, Proc. Roy. Soc. **A186**, 293 (1946).

[10] Bleakney, Weimer, and Fletcher, Rev. Sci. Inst. **20**, 807 (1949).

off; it was raised very slightly above the face of the ring and was kept quite sharp. When the tube was being filled with gas the pressure was made somewhat higher first on one side of the diaphragm, then on the other, so that the diaphragm was snapped from deformation in one direction to the other. This procedure, usually repeated twice, tended to weaken the diaphragm at the edge, thus increasing the possibility of shearing off a perfect circular disk. It also gave some measure of control over the final bursting pressure p_3. No device for initiating the bursting was provided; after adjustment of the pressure p_1 in the expansion chamber the pressure in the compression chamber was increased slowly until the diaphragm burst.

Just behind the diaphragm a flat strip of brass (C) was soldered to the inside of the tube. Its purpose was to prevent the sheared-off diaphragm from traveling down the tube. The leading edge of the post was about $\frac{1}{2}$ in. behind the undeformed diaphragm so that just before bursting the center of the diaphragm was almost touching the post. On bursting, the circular disk became wrapped around the catching post, offering little resistance to the flow of the gas. Subsequently, on reversal of the gas flow (by reflection of the rarefaction wave from the high pressure end or reflection of the shock wave from the low pressure end) the disk was knocked free from the catcher and in virtually every case came to rest at the high pressure end of the shock tube. This method of shearing off a circular disk and preventing it from traveling down the tube was found quite suitable for thin sheet copper, thicknesses of .010 in., .008 in. and .005 in. being used to obtain bursting pressure differences (p_3-p_1) of 205, 164 and 103 lb./in.^{2} on the average. The mean deviation from the mean of p_3 on bursting was 3.5 percent, but on the last thirty-five determinations it was 1.6 percent at 275 lb./in.^{2}, 2.3 percent at 230 lb./in.^{2} and 3.2 percent at 130 lb./in.^{2}.

The bursting of the diaphragm produced a compressional disturbance which built up into a shock wave as it travelled down the tube. It was judged from the data of Payman and Shepherd[9] that the distance of $3\frac{1}{2}$ feet from the diaphragm to the reflection point was sufficient to allow the compression wave to produce a shock front and, although no experiments were performed as a direct check, this appears to have been the case. The pressure distribution in the tube after the shock front had formed is shown schematically in Fig. 3. Assuming an idealized bursting process, Payman

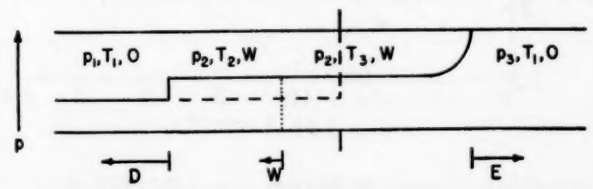

FIG. 3. Pressure distribution in shock tube after formation of a shock front. D represents the shock front and E the rarefaction wave. W and T are the flow velocity and temperature of the gas.

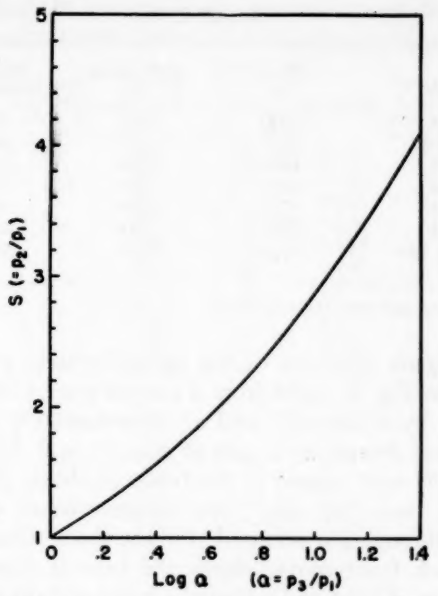

FIG. 4. Shock pressure ratio calculated from bursting pressure ratio in nitrogen at 25°C.

and Shepherd[9] obtained equations which yield the shock pressure ratio, $S=p_2/p_1$, in terms of the bursting pressure ratio, $\alpha=p_3/p_1$. This relation is

$$(S-1)/[(S\zeta+1)(\zeta+1)]^{\frac{1}{2}}=1-(S/\alpha)^{1/(\zeta+1)}, \quad (22)$$

where $\zeta=(\gamma+1)/(\gamma-1)$ and γ is the ratio of heat capacities. This relationship is plotted in Fig. 4 as S *vs.* $\log\alpha$ for $\zeta=5.95$ (N_2 at 25°C).

Section III contained the windows for the incident and reflected light beams as well as a baffle to prevent any light from the incident beam from passing directly to the exit window. It was also provided with a port through which was inserted a tourmaline piezoelectric gauge (PEG 1) which was used to trip the apparatus for recording the reflected light as well as to record the passage of the shock front in measurements of its velocity.

Section IV was added merely to provide extra volume so that the final pressure would not rise to values which would give leakage problems and to prevent the high pressures resulting from reflection of the shock wave from the end plate from being impressed on the windows. It was also provided with a gas inlet tube for adjustment of the pressure p_1 in the expansion chamber.

The important requirements of an optical system for the detection and measurement of reflection of light from a moving shock front are that it must be sensitive enough to measure extremely small reflectivities; it must be capable of detecting the reflection in the very short time available, about 20 microseconds; it must be able to distinguish the reflection signal from a considerable background of scattered light; and none of the components of the optical system must interfere with the shock front during the time of measurement.

TABLE I.

Filter	Mid-λ (A)	Half-width (A)	Relative transmission
18	3900	100	7.20
35+47	4300	200	24.0
75	4890	180	23.3
74	5300	150	13.4
73	5720	120	8.75
25	6100	200	23.2
44+15[a]	5330	150	20.2

[a] Used for only three measurements.

The main elements of the optical system used are shown in Fig. 2. Light from a carbon arc (A) was collimated by a lens (L_1) and an approximately parallel beam was defined by a pair of slits (S_1 and S_2). Color filters (F) were placed in the beam to obtain different spectral bands of light. The incident beam of light passed through a window (W_1) in the shock tube. When the shock front moved down the tube it intersected this beam of light and reflected a beam of light through the second window (W_2). A pair of slits (S_3 and S_4) selected the part of the reflected pulse of light which was reflected from the central region of the shock front, at the same time minimizing the amount of light scattered from the shock tube wall which could reach the detector. The reflected beam was focussed by a lens (L_2) on the detector, an RCA 1P21 photo-multiplier tube. The dashed line SF in Fig. 2 shows the position of the shock front at the instant of maximum reflection.

The photo-multiplier tube was clearly the most suitable detector on the basis of its characteristics, which have been reported by several investigators.[11,12] Not only is it very sensitive but it remains so when the duration of the measurement becomes very short. Since the pulse of light to be detected lasts only 20 microseconds, the photo-multiplier tube has a distinct advantage over photographic film which derives its sensitivity from integration of the signal over time. The limiting sensitivity of the photo-multiplier tube in this application was not the dark current noise but rather the much larger noise signal due to the considerable background of light scattered by the shock tube walls. The photo-multiplier tube offers a distinct advantage in discriminating between the reflected beam and the scattered light since the steady current arising from the scattered light is readily eliminated by a filter in the recording system. This discrimination could not be achieved so easily and so well in a photographic detector. On the other hand, if sensitive enough, a photographic method could be used together with a prism to measure the complete reflectivity spectrum on a single shock front. The photo-multiplier tube was operated from a well-regulated power supply which supplied 67 volts per stage.

The light source used was a Bausch and Lomb 4.5 amp. d.c. carbon arc. The greatest improvement in the sensitivity of the method used here undoubtedly could be obtained by the substitution of higher intensity light sources. Since the parallel beam optics use only a very small area of the source, the intensity available in the beam depends entirely on the *brightness* rather than total light output of the source. In this respect the carbon arc is the most satisfactory simple source but it seems likely that much greater luminosities could be obtained, for example, from condenser discharges.

The lenses in the optical system were both two element achromats with a diameter of 18 mm and a focal length of 34.4 mm. The slit system consisted of an 8 mm slit (S_1) at the collimating lens, a 7 mm slit (S_4) at the detector lens and two slits (S_2 and S_3), 7 mm wide ×13 mm high at the entrance and exit windows of the shock tube. The distance from S_1 to S_2 was 10 cm, from S_2 to S_3, 13 cm and from S_3 to S_4, 5 cm. With this slit system the illuminated area of the shock front was a square, approximately $\frac{1}{2}$ in. × $\frac{1}{2}$ in. The color filters (F) used to obtain different spectral bands were placed in the incident beam between slits S_1 and S_2. The shock tube windows were 2 in. diameter circles of $\frac{1}{4}$ in. plate glass.

It has been mentioned previously that the measurements were limited by the noise generated in the photo-multiplier tube by the background of scattered light.

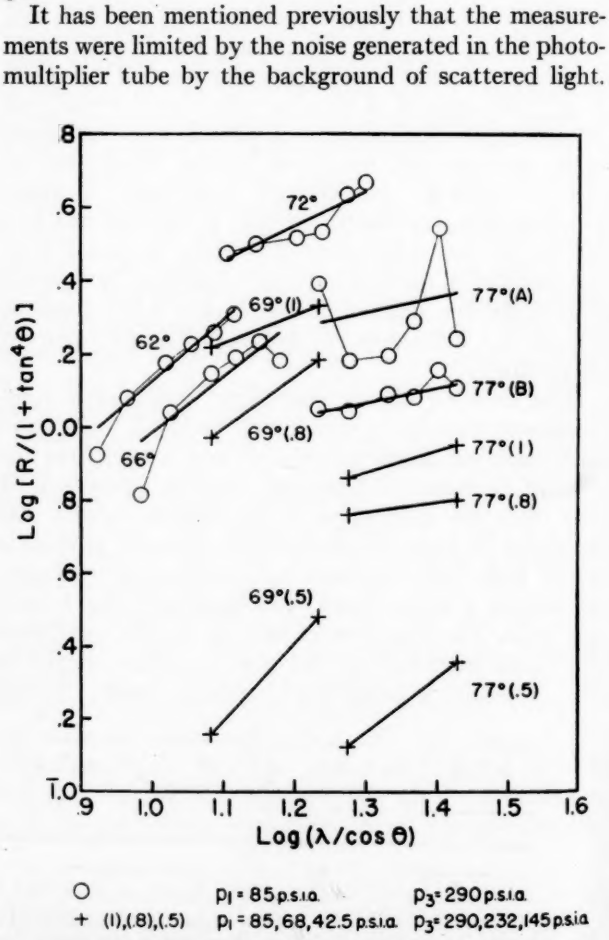

FIG. 5. Measured reflectivity of shock fronts.

[11] R. D. Sard, J. App. Phys. **17**, 768 (1946).
[12] R. W. Engstrom, J. Opt. Soc. Am. **37**, 420 (1947).

In order to cut down the intensity of the scattered light the shock tube walls were smoothed and coated with Kodak dull black lacquer except just in front of the windows where they were covered with a glossy black paint. The glossy paint tended to reflect non-absorbed light up the shock tube whereas a dull paint tended to scatter it into the vicinity of the beam. The combination of baffle (B) and paint cut the scattered light to a point where shock front reflectivities as low as 10^{-7} could be measured.

The recording system consisted of a preamplifier with a gain of about 100 and a Dumont type 208 cathode-ray oscilloscope which had been modified by doubling the accelerating voltage and increasing the frequency response, the latter by lowering the load resistances of the vertical amplifier stages. In order to minimize noise from all sources it was desirable to make the band width of the recording system as narrow as was consistent with reasonable reproduction of the signal to be recorded. The rise time constant, which primarily determined the band width, was 5 microseconds. The decay time constant was varied from 50 microseconds to 2 milliseconds without noticeable effect. The measurements were all made using as a time base a single sweep of 100 microseconds per inch velocity. It was tripped after a 400 microsecond delay by the signal from the piezoelectric gauge (PEG 1).

The velocity of some of the shock waves was also recorded. This was done by measuring the time interval between the pulse from the piezoelectric gauge and the pulse from the photo-multiplier tube. To do so the piezoelectric gauge signal was differentiated to produce a "pip," passed through a biased diode to remove "hash" and applied to the vertical plates of a second oscilloscope, the timing oscilloscope. The signal from the photo-multiplier tube was obtained by tapping the vertical deflection plates of the recording oscilloscope, passed through a biased diode and applied to the vertical amplifier of the timing oscilloscope. A timing wave, usually 10 kc per second, was obtained from a General Radio Type 1302A oscillator. The linear time base for the velocity measurements was initiated from a time delay unit triggered by a pulse from another piezoelectric gauge (PEG 2) which was taped to the outside of the shock tube so that it delivered a signal when the diaphragm burst. The measured velocities (D) were used to calculate the shock pressure ratio S from the relation

$$D^2=p_1v_1(S\zeta+1)/(\zeta-1). \tag{23}$$

With the equipment used it was also possible to obtain a shock pressure measurement from the amplitude of the signal generated by the piezoelectric gauge (PEG 1) but this method was found to be less accurate than the velocity method.

In order to compare the experimental data obtained at different wave-lengths of the light it was necessary to calibrate the optical system. In calculating the wave-lengths it was assumed that the carbon arc source had the spectral distribution of a black body at 4000°K. The transmission of the Wratten filters was taken from the data supplied by the manufacturer and the spectral sensitivity of the RCA 1P21 photo-multiplier tube was taken from the data of Engstrom.[11] The relative magnitude of the transmission of each spectral band was determined by measuring with a sensitive galvanometer the current from the photomultiplier tube exposed to light from the carbon arc after passing through the filter and a suitable attenuator consisting of defocussed lenses and pinholes. Table I gives the Wratten filter combinations used, the mean wave-length value, the estimated half-width (containing half the area), and the relative transmission. The accuracy of this calibra-

TABLE II. Average values of shock front reflectivity.

Angle of incidence	Initial pressure (lbs./in.²)	Bursting pressure (lbs./in.²)	Mean wave-length (cm ×10⁵)	Relative reflectivity	Number of measurements	Average deviation (%)
62°	85	292	3.90	0.117	5	12.8
		291	4.30	0.168	5	30.2
		285	4.89	0.209	5	12.1
		298	5.30	0.236	5	5.8
		296	5.72	0.252	6	30.8
		295	6.10	0.283	5	12.2
66°	85	291	3.90	0.179	5	27.3
		283	4.30	0.302	6	14.4
		287	4.89	0.385	5	26.7
		293	5.30	0.426	5	22.5
		298	5.72	0.472	5	20.3
		298	6.10	0.417	5	9.6
72°	85	304	3.90	2.86	4	6.8
		291	4.30	3.03	6	10.9
		293	4.89	3.16	9	25.4
		293	5.30	3.24	6	14.2
		304	5.72	4.10	6	9.1
		296	6.10	4.37	4	11.2
77°(A)	85	294	3.90	8.36	3	5.1
		292	3.90	10.4	3	10.6
		296	4.30	5.16	4	5.8
		298	4.89	5.31	6	21.6
		291	5.32	6.63	4	9.1
		308	5.72	11.77	3	5.3
		283	6.10	5.94	3	4.4
77°(B)	85	291	3.90	3.81	6	20.4
		292	4.30	3.74	5	16.6
		283	4.89	4.17	5	9.7
		282	5.30	4.10	5	7.7
		287	5.72	4.84	5	18.8
		286	6.10	4.32	6	9.9
77°	42.5	147	4.30	0.450	6	9.0
	42.5	146	6.10	0.769	7	12.0
	68	247	4.30	1.95	5	17.4
	68	235	6.10	2.13	4	1.9
	85	288	4.30	2.47	5	12.5
	85	286	6.10	3.03	5	7.1
69°	42.5	145	4.30	0.0698	4	22.6
	42.5	147	6.10	0.149	5	8.4
	68	238	4.30	0.455	4	13.1
	68	252	6.10	0.748	4	5.0
	85	287	4.30	0.803	5	10.5
	85	292	6.10	1.038	4	4.3

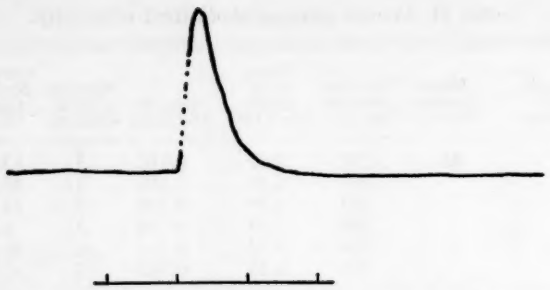

FIG. 6. Typical record of reflected intensity *vs.* time. Scale divisions indicate 50 microsecond intervals.

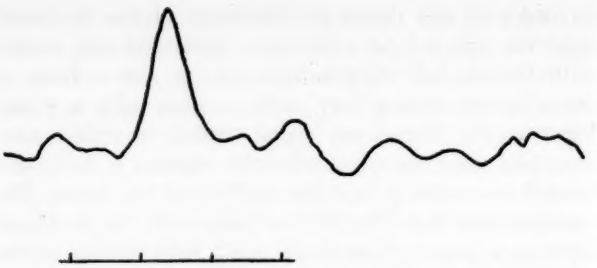

FIG. 7. Reflected intensity *vs.* time at $\theta=69°$ and $p_1=42$ lb./in.^{2}, showing noise level. Scale divisions indicate 50 microsecond intervals.

tion was limited by the motion of the positive crater of the arc but the transmissions are believed to be accurate to within two percent.

A preliminary experiment was conducted to determine approximately the minimum reflectivity that could be measured by the apparatus. Using the carbon arc source and a photo-multiplier tube detector, short pulses of light were obtained by the use of a small plane mirror placed tangentially on a shaft driven by an 1800 r.p.m. motor. A system of slits and lenses provided a known attenuation. The optics were adjusted to give a 20 microsecond reflected pulse and the band pass filter was adjusted for maximum signal to noise ratio. It was concluded that a reflectivity of about 10^{-7} could be detected if the background light could be kept at a low level. Under the conditions used in the measurements reported here the calculated values of the shock front reflectivity lay in the range 10^{-5} to 10^{-7}; no attempt was made to determine the absolute values of the reflectivity experimentally.

EMPIRICAL RESULTS

The reflectivity of shock fronts was studied experimentally as a function of the wave-length of the reflected light (from 3900A to 6100A), the angle of incidence and the pressure p_1 of the stationary gas into which the shock front moved. In all of the measurements the ratio of the pressure behind the front to that ahead of it, the shock pressure ratio, p_2/p_1, was kept constant by making the bursting pressure ratio, p_3/p_1, as close to 3.41 as possible. This particular value was chosen in the following way; p_3 was made as great as seemed feasible in the shock tube used and the reflectivity as a function of the bursting pressure ratio, p_3/p_1, was estimated from Eq. (22), the shock front thickness derived by Thomas and the non-oscillating part of the reflectivity Eq. (18). The value chosen was one estimated to give the highest reflectivity. When the initial pressure p_1 was 85 lb./in.^{2}, 151 reflectivity measurements were made at wave-lengths of 3900A, 4300A, 4890A, 5300A, 5700A, and 6100A and at four angles 77°, 72°, 66°, and 62°. The decay time constant of the amplifier filter was much shorter for the measurements at 77°(A) and at 72° than for the others, and the window slits slightly larger, so that the values may not be directly comparable with the others. Another set of 35 measurements was made in two spectral bands centered on 4300A and 6100A at two angles of incidence, 69° and 77°, with three different values of the pressure p_1, 85, 68, and 42 lbs./in.^{2} while p_3/p_1 was equal to 3.41 in each case. The average reflectivities under each of these conditions are listed in Table II and presented graphically in Fig. 5.

A typical reflection pulse at all but 62° and 42 lbs./in.^{2} is shown in Fig. 6. At the smallest angle of incidence (62°) or the lowest initial pressure (42 lb./in.^{2}), the magnitude of the reflected pulse was not much greater than the noise background. A typical reflected pulse under these conditions is shown in Fig. 7.

It was established in a variety of ways that the observed pulses were actually due to reflection from the shock front. The time elapsed between the piezoelectric gauge pulse and the reflected light pulse was determined in some of the experiments. Velocities calculated from these times on the assumption that the pulse was occurring at the shock front were found to be slightly more than one percent lower than the shock front velocities calculated from the bursting pressure, p_3. This result is consistent with the results of other workers[9,10] and is not unreasonable because of the reduction of the flow velocity of the gas behind the shock front by the caught diaphragm, the piezoelectric gauge and the shock tube walls as well as the idealization of the bursting process which is used in the derivation of the expression connecting the bursting pressure and the velocity.

The duration of the pulse in an ideal optical arrangement would be just the time required for the shock front to traverse the light beam. The width at half height of twenty randomly selected pulses was found to be 23 microseconds with an average deviation of 6 percent. The calculated value is about 18 microseconds. The discrepancy can be attributed to distortion by the coupling filters in the amplifiers.

Finally, the dependence of the pulse height on wavelength, angle of incidence and initial pressure is convincing evidence that the pulse is a true reflection from the shock front. The pulse height, within a rather large experimental error, agrees with the calculated $1+\tan^4\theta$ angle dependence, as may be seen from Fig. 5 where

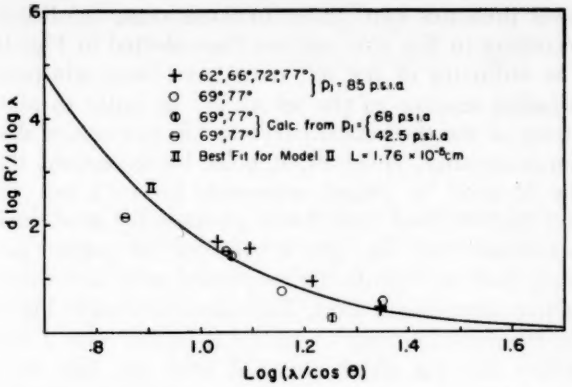

FIG. 8. Slope of reflectivity with respect to wave-length.

$R/(1+\tan^4\theta)$ is plotted. If the $1+\tan^4\theta$ law is correct, the results obtained at the same initial pressure p_1, should lie at about the same value of $R/(1+\tan^4\theta)$. In fact they scatter by about a factor of two but since the reflectivity changes by a factor of twenty-three between 62° and 77° this is reasonable agreement. The dependence on pressure (at constant p_3/p_1) is greater than p_1^2 as it should be. The slope with respect to wave-length is always positive and increases with decreasing angle of incidence and pressure.

Although there can be no doubt that measurements of reflection from the shock front were obtained, the large scatter in the data of Table II and Fig. 5, particularly in comparing data taken for differing angles of incidence or independent sets of data at the same angle of incidence, makes it difficult to compare the measured reflectivities with the theoretical expressions in a straightforward way. However, a careful analysis of the errors involved shows that neither the systematic errors nor the scatter is as great if the change in reflectivity with wave-length or with initial pressure is used as a basis for calculation.

Because of the crudeness of the optical arrangement which necessitated a realignment of the system at each new angle setting, the major reason for the differences between sets of data in Fig. 5 is that the over-all transmission of the system changed when the angle of incidence was changed. No such systematic error occurred, however, within a set of measurements when only the wave-length or the initial pressure was varied. This difficulty is circumvented if the quantity $dR/R = d\ln R$ is taken as the basic datum since the transmission occurs equally in the numerator and denominator and therefore is eliminated. In particular, the quantities $d\ln R/d\lambda$ or $d\ln R/d\ln\lambda$ may be compared with the theory. Alternatively, the comparison of $\log R$ at several initial pressures may also be used if the angle is kept constant.

Aside from the systematic error due to transmission changes, the mean deviation of individual measurements from the mean values listed in Table II is 13 percent. Consequently, the precision of these means is approximately 10 percent. A consideration of the possible errors in the response curves for the various spectral bands and the precision in setting the angle of incidence (about one degree) leads to the conclusion that the parameter $\lambda/\cos\theta$ is accurate to better than 10 percent within the entire range of angles used. Finally, it is estimated that the absolute value of the shock pressure ratio used has a systematic error of less than five percent and a somewhat smaller random error. This ratio was calculated from the bursting pressure ratio p_3/p_1 but, in accord with previous observations and the few velocity measurements made, the experimental value of this ratio was reduced by 10 percent in calculating p_2/p_1.

THE THICKNESS OF THE SHOCK FRONT

A. From the Change of Reflectivity with Wave-Length

It has been previously pointed out that the systematic errors arising from the change in the transmission of the system do not occur in $d\ln R'/d\ln\lambda$. This quantity is plotted in Fig. 8 for each of the sets of measurements at a given angle and pressure. Since the experimental points in Fig. 5 at any given angle of incidence show no significant curvature they were fitted by least squares to the straight lines drawn through them. The slopes of these lines on the logarithmic plot constitute the points in Fig. 8. The smooth curve in Fig. 8 is $d\log R_{II}'/d\log\lambda$ with the abscissa chosen to give the best fit to the experimental points. The value of L for best fit with Model II is 1.8×10^{-5} cm. The average deviation of the abscissae of the experimental points from this curve is .06, equivalent to 15 percent, or a range of L from 1.5 to 2.0×10^{-5} cm. Taking ±3 average deviations, we conclude that, with a probability of 90 percent, the value of L, the shock front thickness, is between 1.1 and 2.7×10^{-5} cm for a shock with $p_2/p_1=1.71$ propagating into nitrogen at 25°C and static pressure $p_1=85$ lb./in.^{2}.

The data taken at lower pressures have been included in Fig. 8 by assuming that $L=\text{constant}/p_1$ when p_2/p_1 is kept constant. That is, the abscissae of the points for $p_1=42$ and 68 lbs./in.^{2} have been changed by $-\log 0.5$ and $-\log 0.8$ and included in the graph for $p_1=85$ lb./in.^{2}. This assumption has strong theoretical foundation since a change in p_1 with p_2/p_1 constant is merely a change in the distance and time scale of the shock front. It is rigorous to the extent that the Boltzmann equation is valid; i.e., to the extent that only binary collisions are important. The fact that these points agree with the others indicates that, within the experimental error, the assumption is justified.

The data at the three pressures $p_1=85$, 68 and 42 lb./in.^{2} have also been fitted separately in exactly the same fashion, yielding the values $L=1.8$, 2.0 and 3.2×10^{-5} cm, respectively. A quantitative test of the scaling assumption is obtained if these values are all scaled to $p_1=85$ lb./in.^{2}, yielding values of 1.8, 1.6,

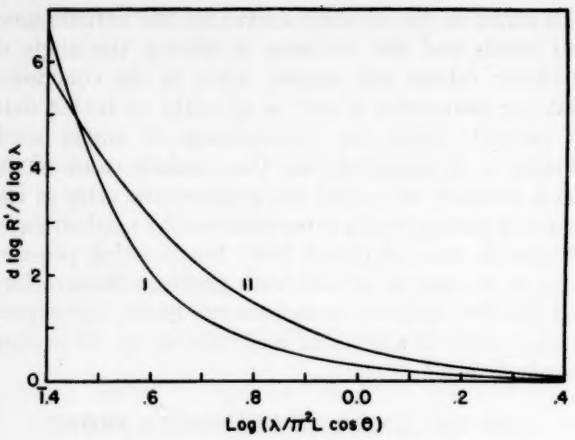

FIG. 9. Theoretical slope of reflectivity with respect to wave-length for Models I and II.

and 1.6×10^{-5} cm which are, to the present accuracy, in good agreement.

The theoretical curve from Model I has not been shown in Fig. 8 because it does not give nearly as good a fit as Model II, having too great a curvature. The two models are compared in this respect in Fig. 9. It appears that although not accurate enough to determine a detailed profile, even the present data are sufficient to distinguish between the two models. However, in view of the large experimental error, Model I cannot be ruled out with certainty.

B. From the Change in Reflectivity with Pressure

The scaling law which was described and tested to some extent in the previous section provides a method for obtaining an independent, although less reliable, measurement of the shock front thickness. On the basis of this assumption, there are two effects when p_1 is changed; since isothermally the change in index of refraction, Δn, is proportional to p_1, the reflectivity is proportional to p_1^2; secondly, the function R' depends on $\lambda/L\cos\theta$ so that a change in p_1 produces a change in the corresponding value of $\lambda/\cos\theta$. Consequently, to the extent that this scaling assumption is valid, the reflectivity spectrum R_a for $p_1=p_a$ is determined from the spectrum R_b for $p_1=p_b$ by the equation

$$R_a\left(\frac{\lambda}{\cos\theta}\right)=\frac{p_a^2}{p_b^2}R_b\left(\frac{p_b\lambda}{p_a\cos\theta}\right). \tag{24}$$

As a consequence of the second effect variation of the initial pressure p_1 offers a means of extending the effective wave-length range of the measurements.

The last two sets of data in Table II (at 69° and 77° incidence) each contained measurements at pressure p_1 with relative values 0.5, 0.8 and 1.0. Each set also contained measurements at two wave-lengths, 4300A and 6100 A. The reflectivities obtained at the two lower pressures were scaled to those at $p_1=85$ lb./in.^{2} according to Eq. (24) and are thus plotted in Fig. 10. The ordinates of the 69° data have been arbitrarily adjusted relative to the set at 77° in order to allow fitting of the theoretical curve to the two sets of data simultaneously. However, it must be recognized that the fit must be judged separately for each set. The fact that each set does define a reasonably good curve is evidence that Eq. (24) is valid for the present purpose, both as regards the amplitude term and the effective wave-length term. The smooth curves in Fig. 10 are theoretical curves. Curve (a) is $\log R_{II}'$ with $L=1.8\times10^{-5}$ cm, the value obtained from the best fit to $d\log R_{II}'/d\log\lambda$. Curve (b) is the best fit to $\log R_{II}'$, yielding $L=1.5\times10^{-5}$ cm. Curve (c) is the best fit to $\log R_I'$, yielding $L=2.0\times10^{-5}$ cm.

As mentioned previously, the meaning of L in Model I and Model II is not quite the same. If for example, the distance between the point in the shock front where $\rho-\rho_1=0.2\Delta\rho$ and the point where $\rho-\rho_1=0.8\Delta\rho$ is compared, it is found that it is $0.6L$ for Model I and $0.694L$ for Model II. In the Thomas shock front profile for $p_2/p_1=1.5$ it is $0.704L$, for comparison. On this basis, $L_I=2.0\times10^{-5}$ cm would be equivalent to $L_{II}=1.7\times10^{-5}$ cm. It may then be concluded that, within the experimental error, the scaling law does hold and that the shock front thickness obtained in this way is in satisfactory agreement with that obtained from the dependence of reflectivity on wave-length, the thickness of a shock front of pressure ratio $p_2/p_1=1.71$ propagating in nitrogen at 25°C and 85 lb./in.^{2} being 1.7×10^{-5} cm within an error estimated at ±25 percent.

COMPARISON WITH THEORY

The expression obtained by Thomas[5] for the thickness of a shock front, using the hydrodynamic theory of Becker[4] but including the fact that the viscosity and thermal conductivity have a temperature dependence given by the kinetic theory of gases for hard sphere

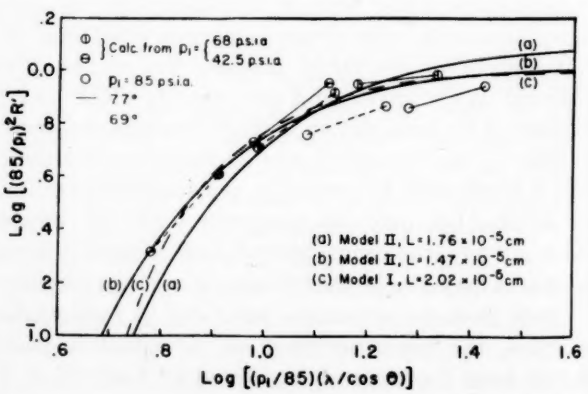
Calc. from p₁ = 68 p.s.i.a
42.5 p.s.i.a
p₁ = 85 p.s.i.a.
77°
69°
(a) Model II, L = 1.76 × 10⁻⁵ cm
(b) Model II, L = 1.47 × 10⁻⁵ cm
(c) Model I, L = 2.02 × 10⁻⁵ cm
Log [(85/p₁)²R']
Log [(p₁/85)(λ/cos θ)]

FIG. 10. Reflectivity spectrum obtained by scaling results obtained at varying initial pressures.

molecules, is as follows:

$$L_T=(\omega_1-\omega_2)(ds/d\omega)_{\min.}$$
$$=\frac{4}{3}\left(\frac{2}{\pi}\right)^{\frac{1}{2}}\nu\left\{\frac{(\omega_1-\omega_2)[\{\omega_1+\omega_2\}\{\omega_1\omega_2-(\omega_1+\omega_2-1)\omega^2\}]^{\frac{1}{2}}}{(\omega_1-\omega)(\omega-\omega_2)}\right\}_{\min.}. \quad (25)$$

In this equation $\omega=(a/b)u$ where u is the mass velocity of the gas relative to a coordinate system moving with the shock front, a is the rate of flow of mass past any point, b is the rate of flow of momentum, $\nu=0.998$, s represents distance measured in mean free paths and the subscripts one and two denote the initial and final states of the gas.

In order to put Eq. (25) in a form suitable for comparison with experiment it is necessary to define an experimental thickness by

$$L=(\rho_2-\rho_1)(dx/d\rho)_{\min.}$$
$$=(1/\omega_2-1/\omega_1)[\omega^2(dx/d\omega)]_{\min.}. \quad (26)$$

Furthermore

$$\frac{dx}{d\omega}=\frac{dx}{ds}\cdot\frac{ds}{d\omega}=l\frac{ds}{d\omega}=l_1\frac{\omega}{\omega_1}\frac{ds}{d\omega}. \quad (27)$$

The quantity l is the mean free path. The kinetic theory expression for the mean free path of hard spheres of diameter σ is

$$l=1/\sqrt{2}\pi n\sigma^2 \quad (28)$$

where n is the number density of molecules. However, the kinetic theory equation for the viscosity, μ, allows us to eliminate σ since, for hard spheres,

$$\frac{1}{\pi\sigma^2}=\frac{\pi^{\frac{1}{2}}}{\nu}\frac{\mu}{(kmT)^{\frac{1}{2}}} \quad (29)$$

where k is Boltzmann's constant, T is the absolute temperature and m is the mass of a molecule. Consequently, it is found that

$$l=\left(\frac{\pi}{2}\right)^{\frac{1}{2}}\frac{\mu}{\nu n(kmT)^{\frac{1}{2}}}=\left(\frac{\pi}{2}\right)^{\frac{1}{2}}\frac{\mu}{\nu(\rho p)^{\frac{1}{2}}}. \quad (30)$$

Taking $ds/d\omega$ from Thomas' expression, Eq. (25), one then obtains for the experimental thickness

$$L=\frac{4}{3}\frac{\mu_1}{(\rho_1 p_1)^{\frac{1}{2}}\omega_1}\left(\frac{1}{\omega_2}-\frac{1}{\omega_1}\right)$$
$$\times\left\{\frac{\omega^3[\{\omega_1+\omega_2\}\{\omega_1\omega_2-(\omega_1+\omega_2-1)\omega^2\}]^{\frac{1}{2}}}{(\omega_1-\omega)(\omega-\omega_2)}\right\}_{\min.}$$
$$=\frac{4}{3}\frac{\mu_1}{(\rho_1 p_1)^{\frac{1}{2}}}\Phi_{\min.}. \quad (31)$$

For nitrogen at 25°C and one atmos., $\mu_1=1.77\times10^{-4}$ poises,[13] $p_1=1.013\times10^6$ dyne/cm² and $\rho_1=1.146\times10^{-3}$ gm/cm³. Consequently, if p_1 is expressed in atmospheres Eq. (31) becomes

$$Lp_1=6.92\times10^{-6}\Phi_{\min.}\text{ cm. atmos.} \quad (32)$$

Values of the thickness calculated from Eq. (32) are plotted in Fig. 11. For $p_2/p_1=1.71$ the calculated L is 1.0×10^{-5} cm if p_1 is 85 lb./in.² This value appears to be considerably lower than the experimental value. The probability that the theoretical value is too low is estimated to be about 95 percent.

There appear to be at least two reasons why the actual thickness may be greater than the theoretical value. In the first place, nitrogen is a diatomic molecule and the use of the theory in its present form implies complete equilibrium between rotational and translational degrees of freedom. Since the entire shock front phenomenon takes place in very few mean free paths such equilibrium may not be reached immediately. If the rotational heat capacity lagged, the gas would heat more rapidly than expected, the density would rise more slowly and a thicker shock front would result. Secondly, the theory in its present form may not be adequate even for a monatomic gas. Thomas has

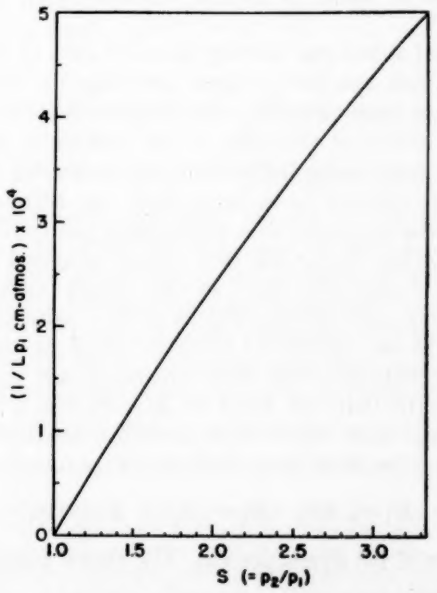

FIG. 11. Becker-Thomas shock front thickness in nitrogen at 25°C.

[13] M. Trautz and P. B. Baumann, Ann. d. Physik **394**, 733 (1929).

already argued that the third approximation in the Chapman-Enskog expansion would increase the calculated thickness. An experimental decision on this score might be reached by studying the thickness of shock fronts in a monatomic gas and such measurements have been undertaken in argon.

ACKNOWLEDGMENT

We should like gratefully to acknowledge the aid given to us by Dr. Paul M. Fye and the Explosives Division of the Naval Ordnance Laboratory by loaning us the shock tube and much of the recording equipment used in this work.

THE JOURNAL OF CHEMICAL PHYSICS VOLUME 18, NUMBER 8 AUGUST, 1950

The Vibrational Spectra and Structure of Inorganic Molecules. II. Sulfur S_8, Sulfur Chloride S_2Cl_2, Phosphorous P_4

H. J. BERNSTEIN AND J. POWLING*
National Research Council, Ottawa, Canada

(Received February 27, 1950)

The infra-red spectra from 2–25μ have been obtained for S_8 as solid and in CS_2 solution; for S_2Cl_2 as liquid and in CS_2 solution; and for P_4 in CS_2 solution. A satisfactory assignment of the Raman and infra-red spectrum of S_8 has been made on the basis of D_{4d} symmetry. The spectrum and valence force calculations are consistent with the C_2 structure for S_2Cl_2, and together with the electron diffraction data exclude the C_{2v} form. The vibrational spectrum of P_4 is interpreted unequivocally on the basis of the tetrahedral structure (T_d).

I. SULFUR S_8

THE x-ray analysis[1] of rhombic sulfur shows that the molecule is S_8 with symmetry of the D_{4d} point group. The distance between the S atoms is found to be 2.12A, and the bond angle 105°. Cryoscopic measurements on rhombic sulfur in solution show that the molecule is again S_8. This is indeed borne out by the similarity between the Raman spectrum of the solid and of sulfur in solution (columns 2, 3, and 4 of Table I).

Table I shows the existing infra-red data of the solid and Raman spectra of solid and solution. Although these data seem extensive, the assignment of the fundamental modes of vibration to the symmetry types of the D_{4d} point group leaves much to be desired. Valence force calculations have been made by Bhagavantam and Venkatarayudu[2] with a complete quadratic potential function. Using the two strong polarized lines at 470 cm^{-1} and 216 cm^{-1} as the totally symmetrical vibrations approximate values of the principal force constants are calculated for zero value of the interaction constant.[2] These force constants are then used to indicate that the band at 243 cm^{-1} is a type E_2 vibration. With these three identified frequencies the values of the three force constants were found to be

$$K_1=2.309, \quad K_2=0.903, \quad K_3=0.067$$

in units of 10^5 dynes per cm. The above authors then calculated all the frequencies from these force constants and matched them with the available experimental data as shown in Table II, columns 3, 4, and 5. The discrepancy between ν_{10}(calc) and ν_{10}(obs) was later cleared up by further investigation of the Raman spectrum[3] when a line was observed at 520 cm^{-1}. However there are two strong objections to the above assignment. Firstly, on the basis of this assignment the strong infra-red band at 150 cm^{-1} and the strong wide band at 200–250 cm^{-1} in the spectrum of the solid (Table I, column 5) cannot be satisfactorily explained and choice of 200 cm^{-1} for one of the fundamentals would seem rather arbitrary. Secondly, since the valence force calculations are accurate to within 10 percent for all frequencies except ν_9 it suggests that since ν_9 is calculated too low the calculated value of ν_8 is too high. The assignment indicated by the calculation then is that ν_8 is 185 cm^{-1} rather than 243 cm^{-1}, and that ν_{11} is 243 cm^{-1}. Because of these criticisms it seemed worth while attempting to improve this assignment both by a new valence force calculation and by investigation of the infra-red spectrum in solid and solution at long paths so that as many overtones and combination tones as possible could be observed.

Experimental

The infra-red spectrum of a 60 percent solution of sulfur in CS_2 and of the crystal was obtained with a Perkin-Elmer spectrometer (Model 12C). The results are shown in Fig. 1 and also included in Table I (columns 6 and 7).

* National Research Laboratories Postdoctorate Fellow 1949–50.

[1] B. E. Warren and J. T. Burwell, J. Chem. Phys. 3, 6 (1935).

[2] S. Bhagavantam and T. Venkatarayudu, Proc. Ind. Acad. Sci. 8A, 101, 115 (1938).

[3] Reported in K. W. F. Kohlrausch, *Ramanspektren* (Edwards Bros., Ann Arbor, Michigan, 1945), p. 394.

TABLE I. Raman and infra-red spectra of S_8.*

	Raman			Infra-Red			
	CS_2 sol.[a]	$C_{10}H_8$ sol.[a]	solid[b]	solid[c]	solid[d]	CS_2 sol.[d]	Assignment
1	[e]	86(m)	85(5)D				$267-185=82(E_2)$
2				87(w)			$243-152=91(E_1+E_3)$
3				103(w)			
4			114(0)				$267-152=115(E_2)$
5				150(s)			†
6	151(9)	153(m)	152(10)P				$\nu_9(E_2)$
7		184(v.v.w.)	185(0b)D				$\nu_8(E_2)$
8				200–250(s)			†
9	218(11)	217(m)	216(10)P				$\nu_2(A_1)$
10	248(3)	248(v.v.w.)	243(1b)D				$\nu_{11}(E_3)$
11				267(w)			$\nu_4(B_2)$
12	299(1)						$2\times152=304(A_1+B_1+A_2+B_2)$
13	334(2)?						$185+152=337(A_1+B_1+B_2)$
14				400(w)			$216+190=406(E_1)$
15					435(w)		$190+243=433(B_1+B_2+E_2)$
16	437(1)	437(v.w.)	434(2b)D				$\nu_7(E_2)$
17				465(s)	465(s)	471(s)	$\nu_5(E_1)$
18	474(10)	476(m)	470(10)P				$\nu_1(A_1)$
19					509(w)		$267+243=510(E_1)$
20			520(0)[f]				$\nu_{10}(E_3)$
21					549(w)	544(w)	$2\times152+243=547(E_3+2E_1)$
22		591(v.v.w.)			584(w)	592(w)	$152+434=586(A_1+B_1+A_2+B_2)$
23					618(w)	622(w)	$434+185=619(A_1+B_1+A_2+B_2)$
24					659(w)		$470+190=660(E_1)$
25				686(w)[g]	678(w)	686(w)	$216+465=681(E_1)$
26					710(w)	714(w)	$190+520=710(B_1+B_2+E_2)$
27				841(m)[g]	840(m)	854(m)	$2\times190+465=845(E_3+2E_1)$
28					869(w)		$2\times434=868(A_1+B_1+B_2)$
29					901(w)	912(w)	$465+434=899(E_1+E_3)$
30				932(w)[g]	937(w)	942(w)	$465+470=935(E_1)$
31					986(w)		$465+520=985(B_1+B_2+E_2)$
32					1052(w)		$532+520=1052(E_1)$
33				1290(w)[g]	1300(w)	1315(w)	$840+465=1305(B_1+B_2+E_2+E_3+2E_1)$
34					1510(w)		$840+678=1518(B_1+B_2+E_2+E_3+2E_1)$

* D = depolarized, P = polarized, b = diffuse, w = weak, m = medium, s = strong, v = very.
† The fundamental $\nu_6=190(E_1)$ interacts with the difference tone $434-243=191(E_1+E_3)$ to give Fermi splitting observed at 150 cm^{-1} and 230 cm^{-1}. The intensity and width of the band at 230 is further enhanced by superposition of $465-243=222(B_1+B_2+E_2)$ and Fermi resonance between 230 and $434-190=244(E_1+E_3)$.
[a] H. Gerding and R. Westrik, Rec. Trav. Chim. Pays-Bas, **62**, 68 (1943).
[b] C. S. Venkateswaran, Proc. Ind. Acad. Sci. **4A**, 345 (1936).
[c] R. B. Barnes, Phys. Rev. **39**, 570 (1932).
[d] This work.
[e] Overlapped by CS_2 wing, see reference b.
[f] Reported in K. W. F. Kohlrausch, *Ramanspektren* (Edwards Bros., Ann Arbor, Michigan, 1945), p. 394.
[g] Taylor and Rideal, Proc. Roy. Soc. (London), **115A**, 589 (1927).

Discussion

It would appear from Table I that all the Raman lines are due to internal vibrations (i.e., not lattice vibrations), since they are present in solution. For this reason it seems not unreasonable to consider the observed infra-red spectrum as entirely due to the S_8 molecule. An assignment of the fundamentals must account therefore for all of the 34 observed infra-red and Raman lines listed in Table I.

From the Raman spectrum of the solid one can readily assign the two strong polarized lines at 470 cm^{-1} and 216 cm^{-1} to ν_1 and ν_2. Of the three allowed infra-red active fundamentals (ν_4, ν_5, ν_6) ν_5 is assigned as 465 cm^{-1} since it corresponds to a stretching mode whereas ν_4 and ν_6 would be much lower since they are bending modes.[2] Without the aid of a calculation of the frequencies from a quadratic potential function it would be extremely difficult and laborious to assign the remaining 8 frequencies.

With the unambiguous assignment of $\nu_1=470$, $\nu_2=216$ and $\nu_5=465$ cm^{-1} the force constants were calculated from the equations of Bhagavantam and Venkatarayudu[2] to be

$$K_1=2.042,\quad K_2=0.920,\quad K_3=0.182\times10^5 \text{ dynes per cm.}$$

With these force constants all the frequencies were calculated and are given in the last column of Table II. These values differ only very slightly from the values calculated by Bhagavantam and Venkatarayudu (Table II, column 3) because both calculations give a value of ~250 cm^{-1} for ν_8. As can be seen from Table II the following assignments can be made unambiguously:

$$\nu_4=267,\quad \nu_7=434,\quad \nu_9=152 \quad \text{and} \quad \nu_{10}=520.^3$$

Again since ν_7 and ν_9 are calculated too low,[4] the calcu-

[4] It is not surprising that the equations for the frequencies do not yield better agreement between the observed and calculated frequencies for this symmetry type. All of the equations involve R^2, R^4, and R^8 as coefficients where R is the S–S bond distance and is given by 2.12 ± 0.03A. The error in these coefficients may be large but for the first and second degree equations there should be reasonable internal consistency. For a third degree equation, however, the errors have increased and the agreement between observed and calculated frequencies could not be expected to be as good as for equations of lesser degree.

TABLE II. Fundamental vibration frequencies for S_8.

Type		Calc.[a]	Obs.[b] I.R.	Obs.[b] R.	Calc.[c]
A_1	ν_1	481		470(p)	470
	ν_2	197		216(P)	216
B_1	ν_3	557			524
B_2	ν_4	255	267(w)		277
E_1	ν_5	481	465(s)		465
	ν_6	181	200(s)		202
E_2	ν_7	452		434(D)	410
	ν_8	243		243	258
	ν_9	122		152(D)	131
E_3	ν_{10}	542		114?	515
	ν_{11}	211		185	232

[a] Calculated by Bhagavantam and Venkatarayudu from $\nu_1=470$, $\nu_2=216$, $\nu_3=243$.
[b] Experimental data used by Bhagavantam and Venkatarayudu.
[c] Calculated in this work from $\nu_1=470$, $\nu_2=216$, $\nu_8=465$.

lated value of ν_8 is much too high indicating that ν_8 should be 185 cm^{-1} rather than 243 cm^{-1}. With $\nu_8=185$ cm^{-1} and $\nu_{11}=243$ cm^{-1} the difference tone $\nu_7-\nu_{11}=434-243=191$ cm^{-1} (E_1+E_3) could interact with a fundamental [say $\nu_6=190$ cm^{-1} (E_1)] to give Fermi splitting observed at 150 cm^{-1} and 230 cm^{-1}. This would account for the strong band at 150 cm^{-1} and account for a strong band in the region 200–250 cm^{-1}. The width of this band (200–250 cm^{-1}) could be explained by overlapping with $465-243=222$ cm^{-1} $(B_1+B_2+E_2)$ and further Fermi resonance between 230 cm^{-1} and $434-190=244$ cm^{-1} (E_1+E_2). It is worth emphasizing, that it was found impossible to explain the strong infra-red bands at 150 cm^{-1} and 200–250 cm^{-1} with any other reasonable choice for ν_6 but $\nu_6=190$ cm^{-1}. The choice of 150 cm^{-1} and the middle of 200–250 cm^{-1} as the fundamentals can be excluded as an assignment since the resulting interpretation of the spectrum is highly unsatisfactory.

The only unassigned fundamental is ν_3 which is both Raman and infra-red inactive. However, the band at 1052 cm^{-1} observed in the infra-red spectrum of the solid can be interpreted as a binary combination tone only by combination of $\nu_3+\nu_{10}(E_1)$ from which, by difference $\nu_3=1052-520=532$ cm^{-1}. This value for ν_3 is further supported by the valence force calculation of $\nu_3\sim524$ cm^{-1}. The values of the frequencies of the fundamental modes of solid rhombic sulfur and their assignment to symmetry types as indicated by this work are:

Type			
A_1	$\nu_1=470$	$\nu_2=216$	
B_1	$\nu_3=532$		
B_2	$\nu_4=267$		
E_1	$\nu_5=465$	$\nu_6=190$	
E_2	$\nu_7=434$	$\nu_8=185$	$\nu_9=152$
E_3	$\nu_{10}=520$	$\nu_{11}=243$	

The interpretation of the 34 observed bands and lines is given in the last column of Table I and appears quite satisfactory.

II. SULFUR CHLORIDE S_2Cl_2

The work of Gerding and Westrik[5] on the Raman spectrum of liquid S_2Cl_2 limits the choice for the structure of S_2Cl_2 molecule to either the planar C_{2v} form or the non-planar C_2 form.

The symmetry types, number of vibrations and selection rules for these point groups are given in Table III.

Both C_{2v} and C_2 models should have 6 lines in their Raman spectrum. For the C_{2v} model, 3 are polarized and 3 depolarized while for the C_2 model 4 are polarized and 2 depolarized.

The Raman spectrum obtained by Gerding and Westrik[5] gave: 106(depol), 245(depol), 537(depol) 206(pol) and 443(pol). Only 5 lines were observed and 3 are depolarized. Since there is no doubt as to the depolarization of 245 cm^{-1} and 537 cm^{-1} and since the above authors quote 106 cm^{-1} as depolarized the C_2 model was rejected and the C_{2v} structure was adopted for S_2Cl_2.

To account for the 6th line which was not observed they assume that 443 cm^{-1} is the resultant of two coincident polarized lines due to the S-S and S-Cl symmetrical stretching vibrations. Venkateswaran[6] working under higher dispersion notes that this line is diffuse on the short wave-length side but obtained no resolution into two lines.

In contradiction to the above interpretation the electron diffraction by the vapor indicates that the structure is C_2 with the S-Cl bonds at 90° with respect to each other.[7] Since the interpretation of the spectroscopic data does not agree with the results obtained from electron diffraction, we have re-examined the spectroscopic data and have obtained also the infra-red spectrum of S_2Cl_2.

Results and Discussion

The S_2Cl_2 used in this work was the redistilled product of the General Chemical Company, New York, b.p. 135–136°C. The infra-red spectra from 2–25μ of S_2Cl_2 as liquid and a solution in CS_2 were obtained with a Perkin-Elmer spectrometer (Model 12C). The results are shown in Fig. 2 and in Table IV.

In dilute solution with CS_2 there are indeed two intense bands at 438 cm^{-1} and 448 cm^{-1} which are presumably fundamentals.

The line at 443 cm^{-1} in the Raman spectrum of the liquid is due to two fundamentals of the same frequency, as surmised by Gerding and Westrik. In dilute solution with CS_2 it is resolved in the infra-red into two bands.

It is interesting that no splitting of the two fundamentals at 443 cm^{-1} was observed in the Raman spec-

[5] H. Gerding and R. Westrik, Rec. Trav. Chim. Pays-Bas **60**, 702 (1941).
[6] S. Venkateswaran, Ind. J. Phys. **6**, 275 (1931).
[7] K. J. Palmer, J. Am. Chem. Soc. **60**, 2360 (1938).

trum due to Fermi resonance.[8] This is probably due to the fact that there is little interaction between the two vibrations.

In the present authors' opinion it seems highly improbable that Gerding and Westrik could distinguish between a weakly polarized line and a depolarized line at 106 cm^{-1} which shows considerable overlapping with the exciting line on their microphotometer trace.*

If it is assumed then that the line at 106 cm^{-1} is weakly polarized, the spectroscopic data are consistent with the C_2 structure and the assignment is:

Type *A*	106	206	438	448
Type *B*	245	537		

Morino and Mizushima[9] have obtained the secular equations for the vibrations of the S_2Cl_2 molecule of symmetry C_2 in which the S-Cl bonds are at 90° to each other. They employ a quadratic potential function with 5 force constants which is independent of azimuthal angle. In this way an expression for the symmetrical frequencies is obtained which does not include the torsional vibration. Using $K_{S-Cl}=2.42\times10^5$ dynes per cm, $K_{S-S}=1.87\times10^5$ dynes per cm, $K'=0.35\times10^5$ dynes per cm, $\delta=0.30\times10^5$ dynes per cm, and $\delta'=0.00\times10^5$ dynes per cm in their expression for the fre-

TABLE III.

		C_{2v}				C_2	
Type	No. of vibrations	Raman	*I.R.*	Type	No. of vibrations	Raman	*I.R.*
A_1	3	+(pol)	+	*A*	4	+(pol)	+
A_2	1	+(depol)	−	*B*	2	+(depol)	+
B_1	2	+(depol)	+		6	6	6
B_2	0	+(depol)	+				
	6	6	5				

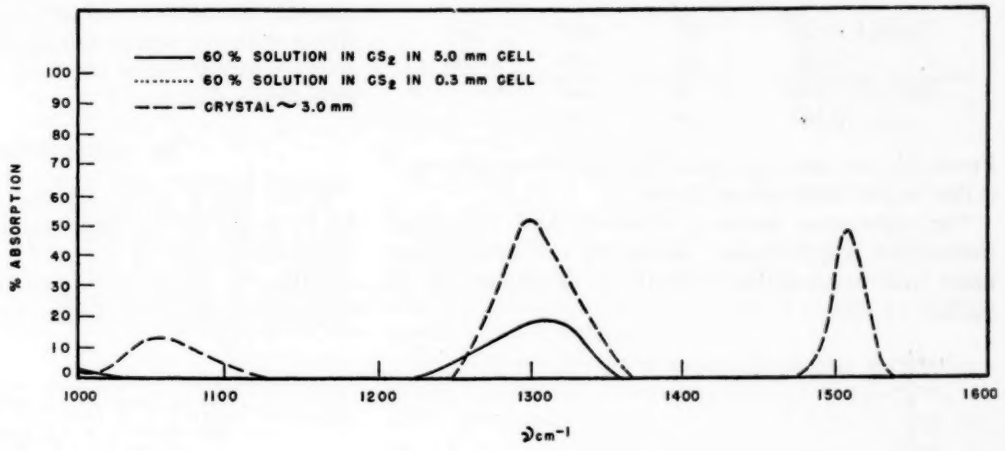

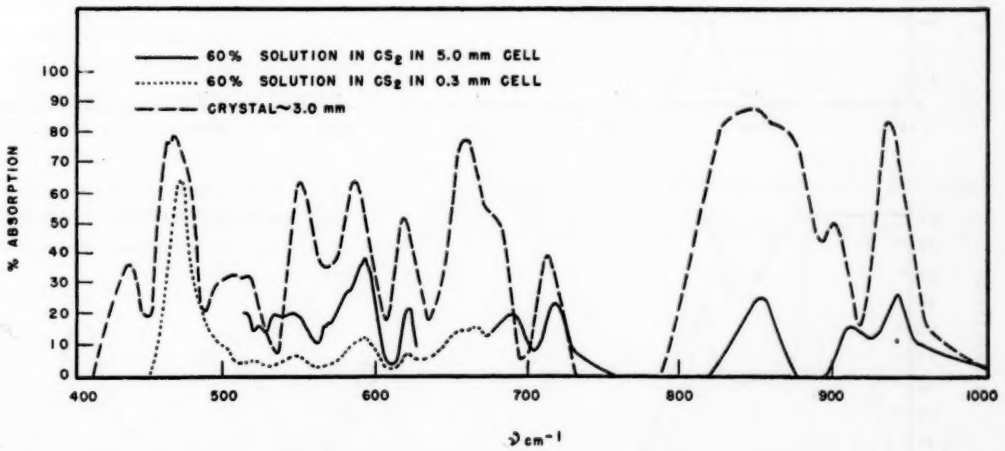

FIG. 1. Infra-red spectrum of solid sulfur and in CS_2 solution.

[8] G. Herzberg, *Infrared and Raman Spectra* (D. Van Nostrand Company, New York, 1945), p. 215.

* The earlier measurement by R. Ananthakrishnan, Proc. Ind. Acad. Sci. **5A**, 285 (1937) of the polarization of the line at 123 cm^{-1} in the Raman spectrum of dichloroethane showed the line to be depolarized. More recent measurements by Neu, Ottenberg, and Gwinn [J. Chem. Phys. **16**, 1004 (1948)] show the line to be weakly polarized ($\rho=0.63$). The difficulties encountered in obtaining the polarization of lines near the exciting line are well known and doubt as to the depolarization of the line at 106 cm^{-1} in S_2Cl_2 is perhaps justified.

[9] Y. Morino and S. Mizushima, Sci. Pap. Phys. Chem. Res. Tokyo **32**, 220 (1937).

TABLE IV. The vibrational spectrum of liquid S_2Cl_2.

ν cm^{-1} Raman[a]	I.R.[b]	Assignment C_2
106 (depol)		A
206 (pol)		A
245 (depol)		B
443 (pol)	438 s	A
	448 s	A
537 (depol)	538 s	B
	779 w	537+245 (B)
	881 m	448+438 (A)
	984 w	537+448 (B)
	1073 w	537+537 (A)
	1333 w	878+448 (A)

[a] Gerding and Westrik, reference 5.
[b] This work.

quencies the following frequencies for the symmetrical and antisymmetrical modes of the S_2Cl_2 molecule are calculated, *viz.*:

Type A (calc)	493	445	184
(obs)	446	438	208
Type B (calc)	536	242	
(obs)	536	242	

From this one may conclude that the line at 106 cm^{-1} is due to the torsional oscillation.

The agreement between observed and calculated frequencies is quite good considering the assumptions made and is consistent with the C_2 configuration of S_2Cl_2.

TABLE V.

	D_{4h}			T_d			
Type	No. of vibrations	Raman	I.R.	Type	No. of vibrations	Raman	I.R.
A_{1g}	1	+(pol)	−	A_1	1	+(pol)	−
B_{1g}	1	+(depol)	−	E	1	+(depol)	−
B_{1u}	1	−	−	F_2	1	+(depol)	+
B_{2g}	1	+(depol)	−		3	3	1
E_u	1	−	+				
	5	3	1				

In Table IV the observed Raman and infra-red spectra are given with an assignment based on the C_2 structure. Although the vibrational spectrum alone is not sufficient to decide the structure of S_2Cl_2 it is not inconsistent with a C_2 structure if the line at 106 cm^{-1} in the Raman spectrum is taken as weakly polarized rather than depolarized. Also, the calculated frequencies for the C_2 model agree well with those observed. Along with the results obtained from the electron diffraction by the vapor the total evidence favors the C_2 structure rather than C_{2v}.

III. PHOSPHOROUS P_4

If the four P atoms are equivalent, suitable models for P_4 would be the plane square model (D_{4h}) and the tetrahedral model (T_d).

Table V shows the symmetry types, number of vibrations and selection rules for the two models.

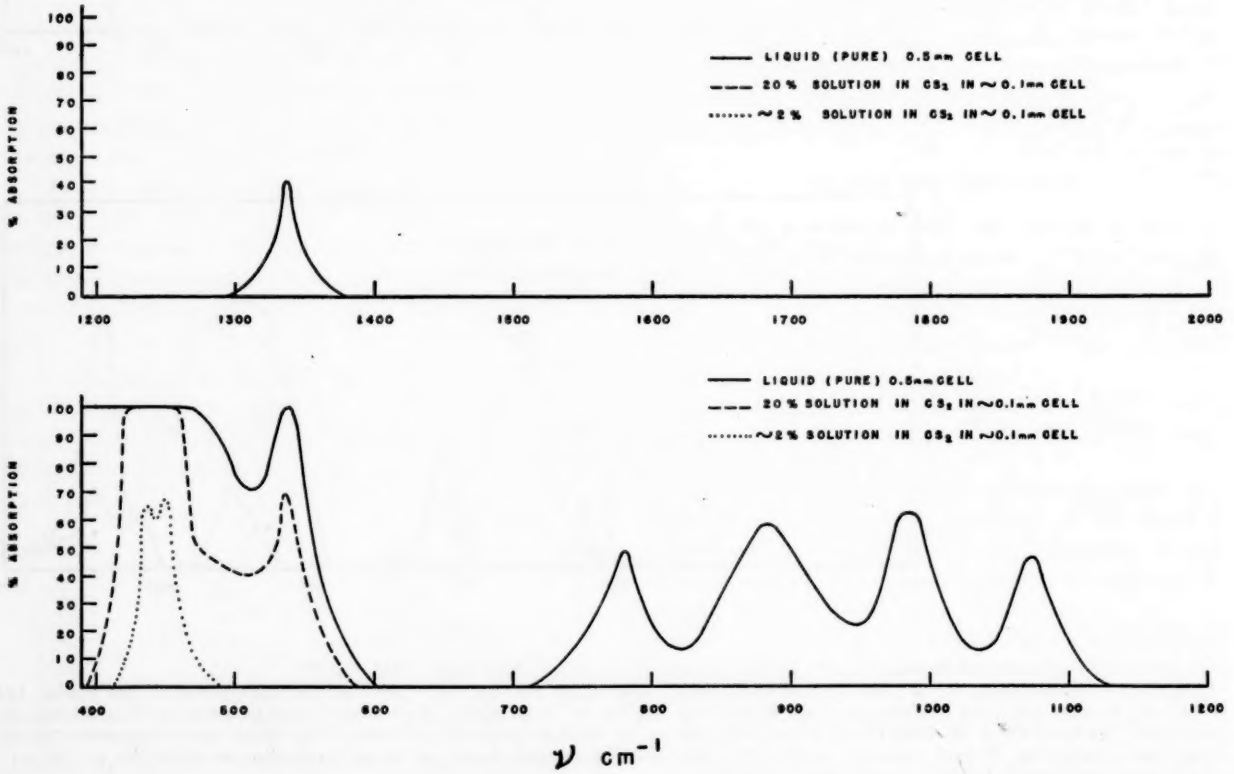

FIG. 2. Infra-red spectrum of S_2Cl_2.

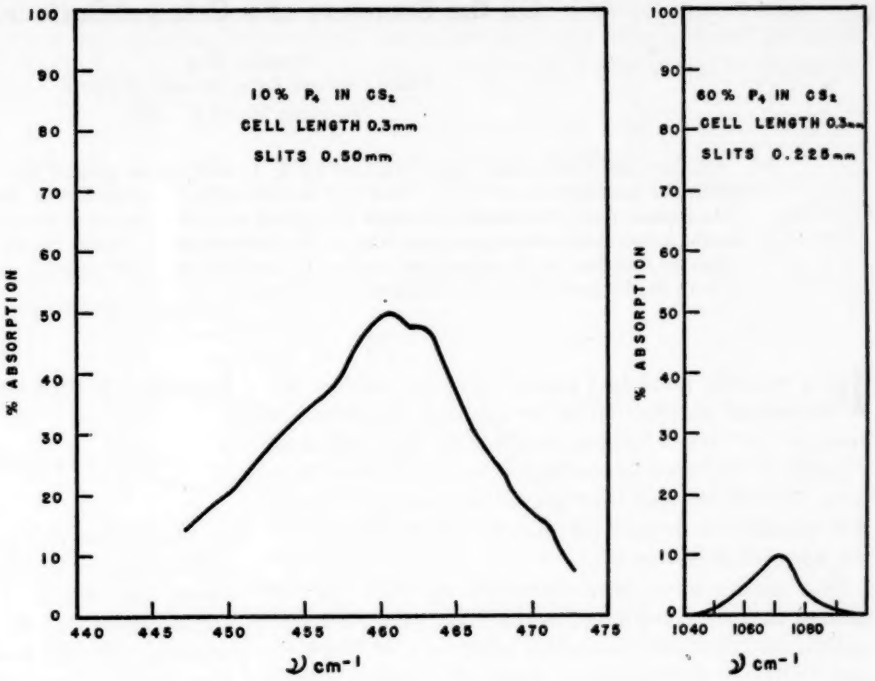

FIG. 3. Infra-red spectrum of phosphorus. [The abscissae in the smaller figure should be moved one division to the right.]

In both cases there should be one polarized line and two depolarized lines in the Raman spectrum.

In the infra-red spectrum there should be no correspondence with a Raman band for the D_{4h} model, whereas, the infra-red active fundamental should correspond to one of the two depolarized Raman lines for the T_d model.

The infra-red spectrum of a solution of yellow phosphorous P_4 in CS_2 was obtained in a 0.3 mm cell with a Perkin-Elmer model 12C spectrometer.

One strong band was observed at 461 cm^{-1} and a weak one at 1062 cm^{-1} (see Fig. 3). Since the Raman spectrum of liquid phosphorous[10] contains a polarized line at 606 cm^{-1} and two depolarized lines at 363 cm^{-1} and 465 cm^{-1} it seems quite definite that the infra-red band at 461 cm^{-1} (in CS_2 solution) corresponds to the Raman line at 465 cm^{-1} (liquid) and that this frequency corresponds to the type F_2 vibration of the T_d model.

Since 606 cm^{-1} is polarized it is necessarily of type A_1 so that 363 cm^{-1} is of type E.

Furthermore since A_1+F_2 is infra-red active the weak band observed at 1062 cm^{-1} is 606+461=1067. The Raman and infra-red spectra of yellow P_4 clearly indicate then the T_d structure.

Calculations of the frequencies of the tetrahedral model from a two constant quadratic potential function[11] show also that 465 cm^{-1} is of type F_2 and 363 cm^{-1} is of type E when 606 cm^{-1} is taken as type A_1.

Further, the tetrahedral structure has been deduced from the electron diffraction data.[12]

ACKNOWLEDGMENT

Thanks are due W. Le B. Ross of the University of British Columbia for obtaining the infra-red spectrum of S_8 in CS_2 solution and to Miss E. Miller for reducing the spectra.

[10] C. S. Venkateswaran, Proc. Ind. Acad. Sci. **2A**, 260 (1935); **4A**, 345 (1936).

[11] S. Bhagavantam and T. Venkatarayudu, Proc. Ind. Acad. Sci. **8A**, 119 (1938).

[12] Maxwell, Hendricks, and Mosely, J. Chem. Phys. **3**, 699 (1935).

On the Structure of a Catalyst Surface. II

ROBERT SIPS
Union Chimque Belge, Brussels, Belgium
(Received March 2, 1950)

Our previous results have been criticized by T. L. Hill on the ground that we considered energies of adsorption ranging from $-\infty$ to ∞. We have accordingly revised our former theory.

It appears that, if we assume localized adsorption without interaction, the possible mathematical forms for the adsorption isotherm are very limited. We have studied in detail, for the simplest of these, the distribution function for the adsorption energy. It turns out that this simplest isotherm is a generalization of both the Freundlich and the Langmuir isotherms.

IN a recently published paper,[1] we have studied the statistical distribution of the energies of adsorption amongst the active centers existing on the surface of a catalyst. We have shown that, if we admit that there is no interaction and that the adsorption is localized, it is possible to deduce the distribution function from the adsorption isotherm.

Our results have been criticized by Hill[2] on the ground that we considered, as did Halsey and Taylor,[3] energies of adsorption extending from $q=-\infty$ to $q=\infty$, and therefore containing a range of negative values which cannot have any real existence.

It must be admitted that this objection is well founded and we have thus been led to a re-examination of the problem. In what follows, we shall show that the assumption of localized adsorption without interaction implies rather severe restrictions on the possible mathematical form of the adsorption isotherm. If these are verified, however, it is always possible to obtain, from the isotherm, a unique distribution function for the adsorption energy.

We shall only consider the case of adsorption without dissociation.

If $N(q)dq$ is the fraction of sites whose energy of adsorption per mole lies between q and $q+dq$, the adsorption isotherm is given by

$$\vartheta(p)=\int_0^\infty \frac{N(q)dq}{1+(a/p)\exp(-q/RT)}, \qquad (1)$$

where a is a function of the temperature only and where we have taken as zero the energy of a molecule in its lowest free state in the gas, and ϑ is the ratio of the total number of adsorbed molecules to the number of available sites.

In our first paper, we took as limits of integration $-\infty$ and ∞, thus introducing negative values of q of no possible significance.

The problem we have now to solve is to find the function $N(q)$ when $\vartheta(p)$ is known. Let us put

$$\frac{a}{p}+1=y \quad \exp(q/RT)-1=x. \qquad (2)$$

Equation (1) then takes the form

$$\vartheta[a/(y-1)]=RT\int_0^\infty \frac{N[RT\log(x+1)]}{x+y}dx, \qquad (3)$$

so that $\vartheta(a/y-1)$ is the Stieltjes transform of $N(RT\log(x+1))$. The general theory of this transform shows that $\vartheta(a/y-1)$ is an analytical function of y, single-valued in the complex plane cut along the negative real axis from 0 to $-\infty$.* It results from this that (p) is also a single-valued analytical function of p in the complex plane cut this time on the real negative axis from $p=0$, corresponding to $y=-\infty$, to $p=-a$, corresponding to $y=0$.

Furthermore, the function $\vartheta(p)$ must, on physical grounds, be such that

$$\vartheta(0)=0, \quad \vartheta(\infty)=1.$$

The first of these conditions is automatically satisfied, while the second only means that

$$\int_0^\infty N(q)dq=1.$$

The restrictions thus imposed on the mathematically possible forms for the adsorption isotherm are severe. It can be seen, for instance, that the Freundlich equation is not acceptable, because the function

$$\vartheta(p)=Ap^c$$

can be made uniform only if the complex plane is cut on the negative real axis from 0 to $-\infty$.

The simplest possible form for $\vartheta(p)$ seems to be

$$\vartheta(p)=(p/p+a)^c, \qquad (4)$$

where c is a constant. It is easily seen that it satisfies all the conditions imposed on $\vartheta(p)$ if $0<c<1$.

This form of $\vartheta(p)$ reduces to the Freundlich isotherm when p is small, while, at the same time, it avoids the difficulty of increasing indefinitely with p. We believe therefore that the function (4), at least for small values of p, and assuming localized adsorption

[1] Robert Sips, J. Chem. Phys. **16**, 490 (1948).
[2] Terrill L. Hill, J. Chem. Phys. **17**, 762 (1949).
[3] G. Halsey and H. S. Taylor, J. Chem. Phys. **15**, 624 (1947).

* More precisely, the y complex plane must be cut along every interval of the negative real axis $(y, y+dy)$ such that $N(RT\log(x+1))$ is $\neq 0$ for $-y>x>-(y+dy)$.

without interaction, is the correct mathematical form of the experimental isotherms which are usually represented by a Freundlich formula, and we shall accordingly call it the generalized Freundlich isotherm. If we are right, measurements made with a sufficient accuracy would give the value of the function $a(T)$ and therefore information about the physical state of the adsorbed molecules.

We shall now obtain the distribution function which corresponds to the generalized Freundlich isotherm. We only have to apply formula (6) of our first paper. If we write

$$f(y)=\frac{1}{RT}\vartheta(a/y-1)=\frac{y^{-c}}{RT}\quad N(RT\log(x+1))=\varphi(x) \tag{5}$$

so that (3) becomes

$$f(y)=\int_0^\infty \frac{\varphi(x)}{x+y}dx, \tag{6}$$

we find that

$$\varphi(x)=\frac{1}{RT}\frac{(xe^{-\pi i})^{-c}-(xe^{\pi i})^{-c}}{2\pi i}=\frac{1}{RT}\frac{\sin\pi c}{\pi}x^{-c}$$

and

$$N(q)=\frac{1}{RT}\frac{\sin\pi c}{\pi}(\exp q/RT-1)^{-c}. \tag{7}$$

We thus have

$$\left(\frac{p}{p+a}\right)^c=\frac{\sin\pi c}{\pi}\times\int_0^\infty\frac{dq}{(\exp q/RT-1)^c\left(1+\frac{a}{p}\exp(-q/RT)\right)}. \tag{8}$$

If, in this, we let $p\to\infty$, we find

$$1=\frac{\sin\pi c}{\pi}\int_0^\infty\frac{dq}{(\exp q/RT-1)^c},$$

a result easy to verify.

Let us now examine more thoroughly the distribution to which we have thus been led. The function

$$(\exp q/RT-1)^{-c}$$

is infinite for $q=0$ and decreases steadily to zero when q increases. Physically, the fact that $N(q)$ becomes infinite for $q=0$ seems at first sight rather unrealistic, but if, as we have assumed earlier, $0<c<1$, the number of active centers whose energy of adsorption lies between 0 and q, when q is very small, is approximately proportional to

$$\int_0^q\frac{dq}{q^c}=\frac{q^{1-c}}{1-c}$$

and therefore tends to zero at the same time as q. This shows that the fact that $N(q)$ becomes infinite for $q=0$ does not constitute a real objection. At the same time, we now see more clearly why it was necessary to assume that $c<1$.

When $c=1$, our generalized Freundlich isotherm reduces to the well-known Langmuir isotherm, so that our formula (4) actually is also a generalization of the Langmuir formula. As we now have $\sin\pi c=0$, it appears that $N(q)$ is zero for all values of q, $q=0$ excepted, where it is infinite, in such a way, nevertheless, that

$$\lim_{c\to1}\frac{1}{RT}\frac{\sin\pi c}{\pi}\int_0^\infty(\exp q/RT-1)^{-c}dq=1,$$

which means that all the active centers have now the same energy of adsorption.

To illustrate these results, we have represented on Fig. 1 the curve $RTN(q)$ as a function of q/RT for different values of c. It will be seen that, when $c\to1$, the curve has, for $q\neq0$, ordinates that become smaller and smaller, while, at the same time, it increases constantly in the neighborhood of $q=0$.

On the other hand, when c decreases towards zero, the curves tend to become horizontals with steadily decreasing ordinates.

It has been suggested by Hill[4] that another interesting form for the isotherm is

$$\vartheta(p)=(p/p+A)^c,$$

where $A<a$. It is easy to see that this case does not differ from the one we have just considered. We only have to put, in (8)

$$q=q'-b,\quad a=A,\quad a\exp b/RT=a'$$

so that it becomes

$$\left(\frac{p}{p+A}\right)^c=\frac{\sin\pi c}{\pi}\times\int_b^\infty\frac{dq'}{(\exp[(q'-b)/RT]-1)^c[1+(a'/p)\exp(-q'/RT]}$$

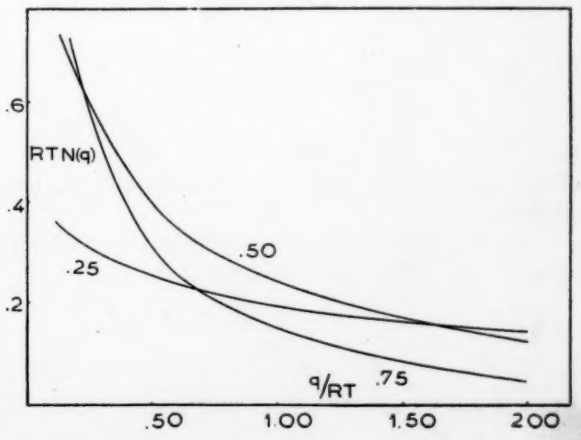

FIG. 1. Distribution curve for various values of c.

[4] Terrill L. Hill, private communication.

and this can also be written

$$\left(\frac{p}{p+A}\right)^c=\int_0^\infty \frac{N(q)dq}{1+(a/p)\exp(-q/RT)}$$

with

$$N(q)=0, \quad 0\leqslant q<b$$

$$N(q)=\frac{\sin\pi c}{\pi}(\exp[(q-b)/RT]-1)^{-c}, \quad b<q.$$

The distribution has thus only been shifted without actual change.

There are, of course, infinitely many possible forms for the $\vartheta(p)$ function, although it is not easy to find simple ones. A satisfactory formula would be, for instance, obtained by taking a finite sum of expressions of the form (4), with various values of c, all of which must satisfy the condition $0<c\leqslant 1$. It is obviously very easy to find the corresponding distribution function.

But there is another possibility. We have stated before that the cut along the negative real axis, which makes the analytic function $\vartheta(p)$ single-valued in the complex plane, need not extend from $p=-a$ to $p=0$, if the function $N(q)$ is not $\neq 0$ in the whole range $0\leqslant q\leqslant\infty$. This shows, for instance, that a function of the form

$$\vartheta(p)=\frac{1}{\log k}\log\frac{kp+a}{p+a}, \tag{9}$$

where k is a constant >1, would also be a possible form of isotherm. We have in fact

$$\vartheta(0)=0 \quad \vartheta(\infty)=1,$$

and the function is single-valued if the real negative axis is cut from $p=-a$ to $p=-a/k$. If k is very large, this cut will not be very different from the cut from $p=-a$ to $p=0$ used before.

On the other hand, if a and k are large, we shall have approximately, for small values of p

$$\vartheta(p)=\frac{1}{\log k}\log\frac{kp}{a}=A\log cp \tag{10}$$

where

$$A=1/\log k, \quad c=k/a,$$

and we therefore are led to the Temkin and Pyzhev[5] isotherm.

It is easy to find the distribution function which corresponds to (9). We have first

$$f(y)=\frac{1}{RT\log k}\log\frac{y+(k-1)}{y}.$$

Then

$$\varphi(x)=\lim_{\eta=0}\frac{1}{RT\log k}\left[\log\frac{-x+(k-1)-i\eta}{-x-i\eta}-\log\frac{-x+(k-1)+i\eta}{-x+i\eta}\right],$$

so that

$$\varphi(x)=\frac{1}{RT\log k}=N(q),$$

if $0<x<k-1$, or $0<q<RT\log k$, and

$$\varphi(x)=0,$$

if $k-1<x$ or $RT\log k<q$.

The possible isotherm (9) thus corresponds to a distribution characterized by $N(q)=$ constant in one interval and zero everywhere else.

We have, so far, considered a as independent of q. This assumption, which seems to have been made for the first time by Fowler,[6] without however any apparent justification, has also been criticized by Hill.[7] To conclude the present paper, we shall show that, at least in principle, our method can be used in the general case where a is a known function of q.

We now have to solve the following integral equation

$$\vartheta(p)=\int_0^\infty \frac{N(q)dq}{1+[a(q)/p]\exp(-q/RT)}. \tag{11}$$

We shall assume that $a(0)\neq 0$ and that, when $q\to\infty$, $a(q)\exp(-q/RT)\to 0$. Let us put

$$x=\frac{a(0)}{a(q)}\exp(q/RT)-1 \quad y=1+a(0)/p.$$

The first of these gives x as a monotonously increasing function of q. It can therefore be inverted in the form

$$q=F(x)$$

(11) now becomes

$$\vartheta\left(\frac{a(0)}{y-1}\right)=\int_0^\infty \frac{N[F(x)]F'(x)(1+x)dx}{x+y} \tag{13}$$

and this, being once again a Stieltjes transform, can be solved in the usual way.

If $a(q)=a(0)$ is a constant

$$q=F(x)=RT\log(1+x)$$

and (13) is of course identical with (3).

[5] Temkin and Pyzhev, Acta Physicochemica (USSR) **12**, 327 (1940).

[6] R. H. Fowler, *Statistical Mechanics* (Cambridge University Press, London, 1936), 2nd. Ed., p. 833.

[7] Terrill L. Hill, J. Chem. Phys. **17**, 763 (1949).

Thermal Diffusion in the Critical Region. II

E. B. GILLER, R. B. DUFFIELD,* AND H. G. DRICKAMER
Department of Chemistry, University of Illinois, Urbana, Illinois

(Received March 9, 1950)

The previous measurements on thermal diffusion in the critical region for the system ethane-xenon are extended and completed, with the use of a modified radioactive tracer technique. A rough calculation of cluster size in the critical region is made. A mechanism of molecular motion in the dense gas above the critical point, consistent with the data is present. It is shown that the transformation between dense gas and liquid occurs without discontinuity as far as thermal diffusion is concerned.

The thermal diffusion columns operated in the region of turbulent heat transfer gave a separation as predicted by the modified theory of the column.

THIS paper extends the previous work[1] on thermal diffusion in the critical region using the same gases (ethane-xenon). The columns used were those described previously by one of the authors,[2] but with several important refinements in the temperature control and measurement, pressure measurement, and particularly in the method of analysis.

The column was set in a bath where the temperature could be held to $\pm 0.01°C$. The inner tube was heated by a hot wire embedded in sand. Since the heavy metal heads presented a short circuit for the heat, the heads were heated with glas-col heaters. In order to insure that no vertical gradients occurred, a dummy column was constructed with seven couples peened to the outer wall of the inner column. The necessary heater currents to maintain zero vertical gradient for various densities, temperatures, and ΔT's were thus established, as well as the temperature drop through the walls. This permitted accurate calculation of the temperature and ΔT across the gap.

The pressures in the range 0–1000 psia were measured by means of a dead weight gauge accurate to ± 0.1 psia, permitting considerably greater accuracy in the calculation of ρ and β.

Third and most important, the method of analysis was modified. The xenon concentration at the top and bottom of the column was measured by two radiation detectors installed directly in the column rather than by external counters to which samples were removed for analysis. The detectors were anthracene crystals, the radiation-induced scintillations of which were counted by 1P28 photo-multiplier tubes. The light was conducted from the crystals through the wall of the column to the photo-tubes by Lucite rods. The column details are shown in Fig. 1. The electrical circuit and the details of the analytical system are discussed in

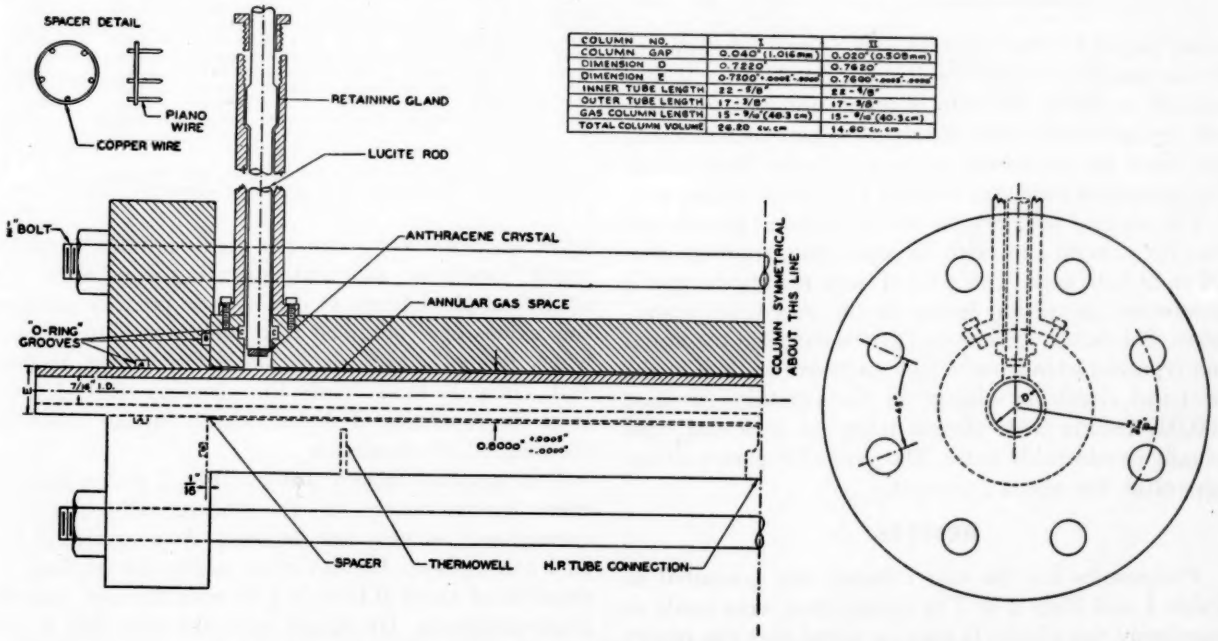

FIG. 1. Thermal diffusion column. Material: cold-rolled steel. Scale: 1 in. = 1 in.

* R. B. Duffield is also in the Department of Physics.

[1] Pierce, Duffield, and Drickamer, J. Chem. Phys. 18, 950 (1950).

[2] Drickamer, Mellow, and Tung, J. Chem. Phys. 18, 945 (1950).

TABLE I.

Run	Temp. °C	Press. atmos.	Column II ρ g/cc	ΔT °C	$q/B/T$	α'[a]	α[b]
1	33.08	49.26	0.181	1.25	0.745	−19.30	−0.434
2	33.08	49.42	0.200	1.25	0.740	−31.80	−0.497
3	33.08	49.53	0.216	1.25	0.781	−21.20	−0.392
4	32.93	48.53	0.150	1.15	0.654	−11.00	−0.583
5	33.08	49.73	0.231	1.35	0.784	−18.40	−0.350
6	33.25	51.36	0.275	2.10	0.821	− 7.41	−0.163
7	33.25	56.18	0.310	2.10	0.929	− 1.18	−0.0350
8	33.27	59.22	0.321	1.87	0.947	− 0.648	−0.0234
9	33.40	61.71	0.324	2.00	1.017	+ 0.138	+0.00627
10	33.37	63.21	0.328	1.97	1.032	+ 0.238	+0.0114
11	38.08	70.70	0.316	3.35	1.021	+ 0.150	+0.00561
12	38.07	65.14	0.302	3.43	0.962	− 0.388	−0.0124
13	38.10	57.69	0.265	3.40	0.769	− 6.05	−0.131
14	38.18	55.45	0.227	3.36	0.672	−13.50	−0.267
15	38.08	54.50	0.209	3.21	0.622	−16.80	−0.404
16	37.99	54.12	0.201	3.13	0.621	−17.10	−0.436
17	37.95	53.48	0.182	2.94	0.596	−15.10	−0.484
18	38.03	52.21	0.152	3.15	0.532	− 8.80	−0.440
19	46.18	58.75	0.154	3.85	0.539	− 4.48	−0.298
20	46.44	53.75	0.117	4.17	0.430	− 2.76	−0.309
21	46.10	61.44	0.193	3.80	0.618	− 6.21	−0.263
22	46.23	63.44	0.215	3.95	0.677	− 6.00	−0.198
23	46.25	64.13	0.221	4.10	0.705	− 5.53	−0.170
24	46.15	67.49	0.252	3.95	0.769	− 3.10	−0.0992
25	46.21	75.33	0.281	3.82	0.923	− 0.582	−0.0221
26	46.11	82.68	0.304	3.82	1.033	+ 0.236	+0.0093
27	46.10	85.54	0.311	3.80	1.068	+ 0.397	+0.01591
28	54.14	99.63	0.309	3.57	1.107	+ 0.520	+0.0234
29	54.22	87.17	0.276	3.65	0.962	− 0.268	−0.0116
30	54.27	80.50	0.250	3.75	0.822	− 1.58	−0.0664
31	54.35	74.65	0.221	3.80	0.705	− 3.50	−0.145
32	54.40	71.04	0.203	3.95	0.632	− 4.25	−0.205
33	54.49	66.81	0.182	4.12	0.561	− 3.95	−0.249
34	54.64	62.48	0.138	4.28	0.484	− 2.73	−0.340
35	54.55	57.53	0.116	4.30	0.430	− 1.95	−0.286
36	33.00	47.49	0.126	1.40	0.452	− 8.60	−0.876
37	32.84	48.37	0.146	0.88	0.592	−13.50	−0.910
38	30.20	43.41	0.102	1.80	0.368	− 3.65	−0.567
39	30.16	44.56	0.111	1.86	0.394	− 5.50	−0.637
40L	30.18	47.78	0.300	1.75	0.742	− 5.96	−0.196
41L	30.16	50.10	0.313	1.84	0.801	− 2.91	−0.103
42L	30.00	78.87	0.358	1.60	0.981	− 0.067	−0.00523
43L	31.85	82.00	0.354	1.50	1.022	+ 0.0074	+0.00616
44L	31.90	57.90	0.327	1.64	0.943	− 0.544	−0.0261
45	33.32	60.18	0.322	2.13	1.006	+ 0.0546	+0.00226
46	33.28	63.24	0.328	2.00	1.031	+ 0.228	+0.0108
47	32.55	56.84	0.319	0.90	0.993	− 0.0876	−0.0052
48	33.39	47.79	0.128	2.03	0.669	− 4.32	−0.328
49	33.26	49.49	0.190	1.74	0.797	−20.50	−0.370
50	33.32	52.38	0.282	1.85	0.820	− 5.93	−0.150

TABLE I.—(*Continued*)

Run	Temp. °C	Press. atmos.	Column II ρ g/cc	ΔT °C	$q/B/T$	α'[a]	α[b]
51	33.44	53.90	0.296	2.13	0.861	− 3.47	−0.0881
52	33.44	54.97	0.301	2.13	0.881	− 2.44	−0.0656
53	33.30	59.00	0.320	1.85	0.925	− 1.11	−0.0394
54L	23.00	42.00	0.342	2.16	1.034	+ 0.248	+0.0109
55L	22.97	47.90	0.350	2.14	1.062	+ 0.353	+0.0173
56L	9.84	40.48	0.392	2.08	1.195	+ 0.833	+0.0388
57L	9.88	37.35	0.391	2.04	1.205	+ 0.970	+0.0427
58L	29.97	48.75	0.308	1.89	0.775	− 3.77	−0.123
59L	30.12	55.20	0.331	2.12	0.870	− 1.32	−0.0528
60	33.03	49.69	0.238	2.05	0.830	−15.70	−0.248
61	35.28	52.70	0.245	2.08	0.816	− 9.60	−0.221
62	37.96	56.40	0.249	2.08	0.816	− 6.44	−0.238
63	42.07	62.20	0.246	2.14	0.820	− 3.23	−0.132
64	46.10	67.90	0.260	2.16	0.830	− 2.08	−0.0989
65	50.09	73.30	0.246	2.11	0.944	− 1.54	−0.0855
66	32.30	50.54	0.290	1.50	0.869	− 4.43	−0.184
67	32.54	49.22	0.260	1.43	0.849	−10.40	−0.192
68	32.39	47.79	0.140	1.18	0.879	−10.65	−0.717
69	30.16	43.16	0.101	1.92	0.523	− 2.23	−0.359
70	30.27	38.70	0.076	2.13	0.466	− 0.758	−0.305
71	14.95	31.10	0.064	3.34	0.218	− 1.44	−0.460
72	14.94	25.60	0.046	3.45	0.192	− 0.514	−3.360
73L	14.81	38.27	0.374	3.52	1.074	+ 0.310	+0.0120
74L	26.00	45.88	0.331	2.04	1.003	+ 0.027	+0.00246
75L	28.18	49.76	0.326	1.99	1.039	+ 0.471	+0.0145
76L	30.11	52.99	0.324	1.95	1.039	+ 0.421	+0.0169
			Column I				
77	24.95	37.87	0.083	3.70	0.950	− 1.25	−0.114
78	25.63	34.00	0.063	3.85	0.993	− 0.0645	−0.0108
79	15.03	31.69	0.066	3.85	0.955	− 0.794	−0.0838
80	15.73	27.08	0.048	4.75	1.007	+ 0.0280	+0.00673
81	− 1.15	20.71	0.038	3.90	1.009	+ 2.0230	+0.0086
82	− 1.15	17.83	0.031	4.30	1.103	+ 0.131	+0.0652
83	−15.10	14.25	0.025	3.80	0.998	− 0.00176	−0.00102
84	−14.89	4.43	0.0065	5.27	0.959	− 0.0308	−0.0417
85	0.14	4.90	0.0070	11.08	0.922	− 0.0167	−0.0197
86	15.44	4.83	0.0063	15.12	0.919	− 0.0141	−0.0169
87	25.65	33.79	0.062	3.90	0.989	− 0.102	−0.0181
88	29.73	8.32	0.0107	14.65	0.954	− 0.0059	−0.00530
89	29.78	4.49	0.0055	14.75	1.024	+ 0.00477	+0.00705
90	44.49	4.76	0.0057	14.42	1.060	+ 0.0225	+0.0299
91	44.42	8.48	0.0103	14.33	1.205	+ 0.025	+0.0253
92	53.90	8.73	0.0102	14.70	1.142	+ 0.0166	+0.0161
93	53.85	4.23	0.0050	14.80	1.104	+ 0.0401	+0.0567
94	44.18	8.25	0.0100	14.14	1.211	+ 0.0273	+0.0276
95	46.30	44.61	0.079	3.80	0.944	− 0.729	−0.100
96	46.39	53.80	0.118	4.13	0.882	− 6.580	−0.329
97T	46.31	61.35	0.189	4.02	0.906	−18.70	−0.320
98T	47.67	61.74	0.179	6.57	0.909	−15.90	−0.247
99T	47.72	66.83	0.233	6.77	0.899	−23.30	−0.238
100	46.40	53.70	0.118	4.10	0.894	− 5.80	−0.287
101T	45.75	61.20	0.195	2.90	0.902	−22.70	−0.470
102	45.02	60.88	0.199	1.50	0.861	−35.40	−0.910
103	33.06	46.78	0.118	1.72	0.894	−12.50	−0.595
104	33.23	40.53	0.078	1.85	0.955	− 0.78	−0.129
105	25.73	34.01	0.062	3.75	0.991	− 0.0830	−0.0147

[a] α' = calculated by method of Furry, Jones, and Onsager.
[b] α = calculated by method of Drickamer, Mellow, and Tung.

other papers.[3,4] This method had several advantages; it was possible to operate at constant density, it was possible to follow the rate of separation and to establish beyond doubt when steady state had been reached, and since the chambers at the ends were blanked off, the relaxation time was reduced by a large factor.

The method of operation was as follows: gas was let into the column and, with no separation, readings were taken at both ends. The ratio of these readings supplied a constant correction factor to the measured separations. The factor was checked at the end, and the initial run repeated from time to time to insure no drift in the electrical circuit or change in the crystals. At least 100,000 counts were always taken at each end, and usually considerably more. The over-all accuracy of the apparatus was about 1 percent.

RESULTS

The results for the two columns are presented in Table I and Figs. 2–4. The calculations were made as previously described.[1] It may be noted that the results agree quantitatively with the previous ones, obtained under somewhat different operating conditions and analytical procedures. It can also be pointed out that the values of χ obtained from the two columns agree when the method of calculation of Drickamer, Mellow, and Tung[2] is used, while the classical method gives large discrepancies. This provides a further check on the method of calculation.

It is apparent from a study of Fig. 2 that α behaves even approximately in the theoretically predicted manner only at very low densities. At pressures as low as 4 atmospheres the deviation is already marked. At densities of about 0.15–0.16 g/cc goes through a rather sharp minimum. (It should be noted that this is well below the critical density of 0.212 g/cc.) At higher densities α approaches zero and eventually becomes positive. It is important to note that there is no discontinuity in this procedure at the phase boundary,

[3] Timmerhaus, Giller, Tung, Duffield, and Drickamer, Rev. Sci. Inst. **21**, 261 (1950).
[4] Timmerhaus, Giller, Duffield, and Drickamer, Nucleonics (June, 1950).

and α is still negative at least 4°C below the critical point in the liquid phase. These results can be explained in the following manner. Let us assume that the ethane molecules form clusters while the xenon molecules do not. By a cluster we mean a group of molecules with a distinct correlation between the velocities of neighboring molecules, which correlation must last for macroscopic periods of time. As these clusters are more dense than the surrounding medium, xenon generally will move around the cluster rather than through it, so that separation occurs between ethane clusters and xenon. As the density of the system increases, the space available for movement of a cluster decreases, so the cluster mobility decreases. Further, the average density of the system approaches that of the cluster, so that the relative probability of a xenon molecule moving through rather than around a cluster increases.

Based on this picture, and some simplifying assumptions, a crude calculation of cluster size can be made.

TABLE II. Molecules per cluster.

	33°C		54°C	
Density g/cc	C_2H_6	Xe	C_2H_6	Xe
0.01	2–3	1	2	1
0.155	26	1	10	1

The theoretical equation for α for a dense gas with one component almost pure can be written[5]

$$\alpha=\frac{-5(C-1)}{Q_2'}S_2'\frac{1+\frac{2}{5}\pi n_2\sigma_2^3\chi_2}{\chi_{12}}, \qquad (1)$$

where

$$S_2'=\frac{\chi_2}{\chi_{12}}\left(\frac{r_{02}}{r_{012}}\right)^2\frac{M_2}{(M_1)^{\frac{1}{2}}}\sqrt{2}A\frac{W_2^{(2)}(2)}{W_{12}^{(2)}(2)}$$
$$-M_1[3(M_1-M_2)+4M_2A]$$

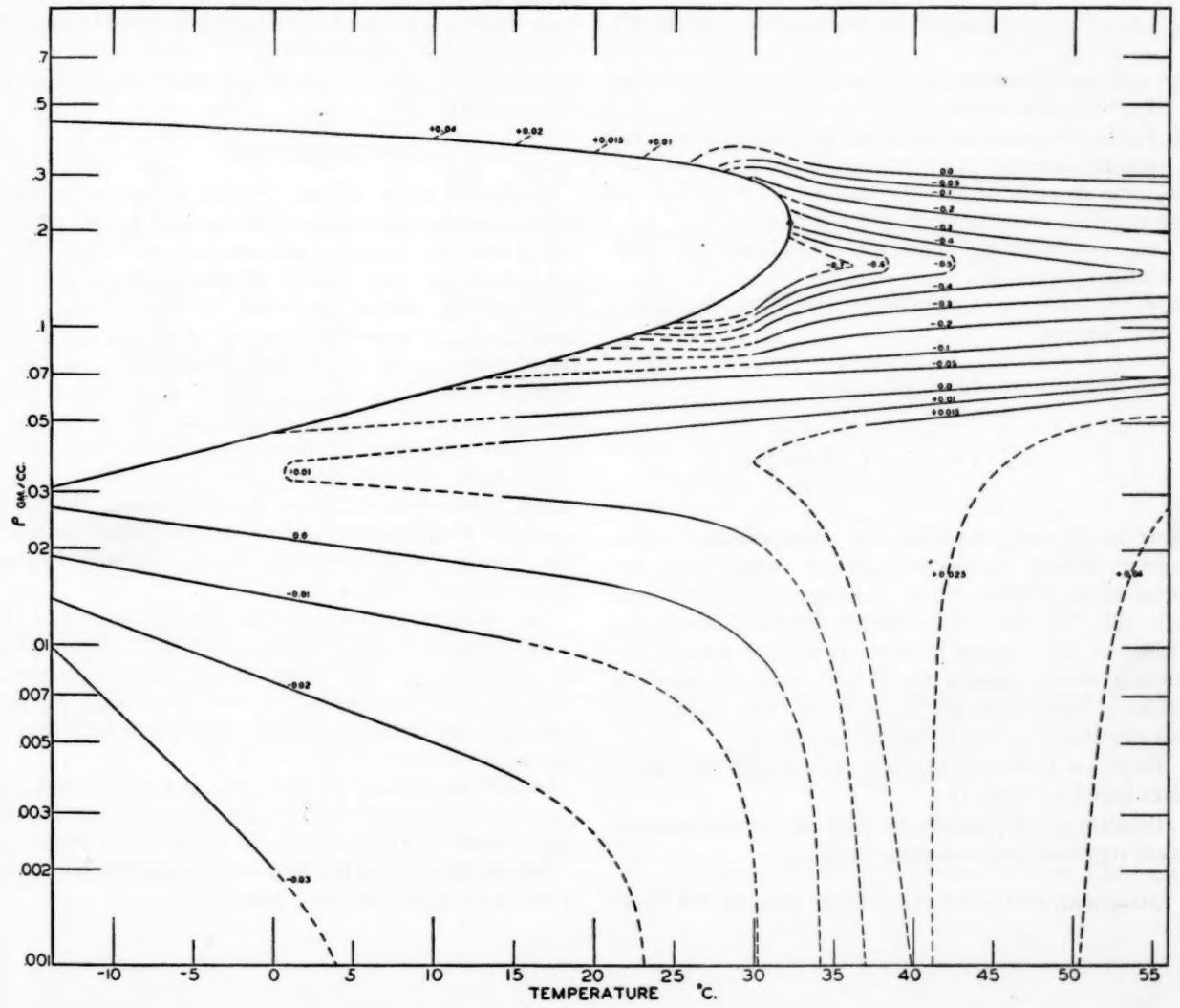

FIG. 2. ρ-T-α plot.

[5] S. Chapman and T. G. Cowling, *Mathematical Theory of Non-Uniform Gases* (Cambridge University Press, London, 1939).

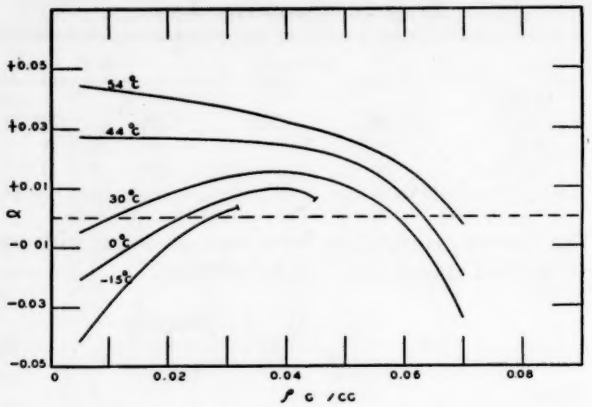

FIG. 3. α at low densities.

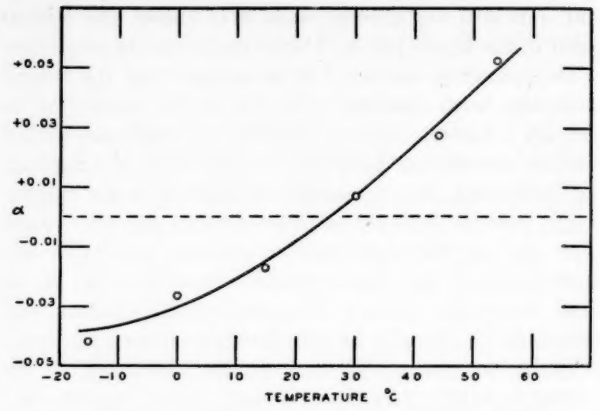

FIG. 4. Effect of temperature on α at a density of 0.005 g/cc.

$$Q_2' = \frac{\chi_2}{\chi_{12}} \frac{\sqrt{2}}{(M_1)^{\frac{1}{2}}} \frac{W_2^{(2)}(2)}{W_{12}^{(2)}(2)} A \left(\frac{r_{02}}{r_{012}}\right)^2 \times [6M_1^2 + M_2^2(5-4B) + 8M_1M_2A],$$

r_0 = collision diameter for Lennard-Jones molecules, $W_{12}^{(2)}(2)$, $W_2^{(2)}(2)$,

A, B, C = cross section integrals depending on the interaction energy,

$M_1 = m_1/(m_1m_2)$,

m_1, m_2 = molecular mass of species 1 and 2,

$\sigma_1, \sigma_2, \sigma_{12}$ = molecular diameters calculated for solid elastic spheres,

n_1, n_2 = number of molecules of species 1 and 2 per unit volume,

$$\chi_2 = 1 + (5/12)\pi n_2 \sigma_2^3$$

$$\chi_{12} = 1 + \frac{\pi}{12} n_2 \sigma_2^3 \left(8 - \frac{3\sigma_2}{\sigma_{12}}\right).$$

Now let us make the following assumptions: (1) The cluster density is constant at any temperature and equal to the density, where α changes sign in the dense gas. (2) The interaction energy between xenon and cluster is the same as between xenon and ethane permitting us to evaluate the $W_{(2)}^{(2)}$ integrals from the tables of Hirshfelder *et al.*[6] (3) Within the accuracy of our calculation r_0 can be substituted for σ.

Based on these assumptions one obtains the cluster sizes found in Table II.

Because of the limited validity of the assumptions these represent order of magnitude only.

[6] Hirshfelder, Bird, and Spotz, J. Chem. Phys. 16, 968 (1948).

Since α is as sensitive as it is to the intermolecular forces, the fact that there is absolutely no discontinuity in going from the dense gas to the liquid indicates that the forces in the liquid state must not differ appreciably from those in a gas for a considerable interval below the critical, and it must be only at comparatively low temperatures that it assumes its essentially solid-like characteristics.

TURBULENCE

It appears to be of some interest to append a note concerning the operation of the column in the region where the heat transfer was definitely turbulent. This point could be very clearly established. As described previously in normal operation, it was necessary to heat the heads to prevent the ends of the column from being colder than the center. When turbulent heat transfer was obtained by increasing density or T this heating was entirely unnecessary. The break between turbulent and non-turbulent heat transfer was very sharp. Even when turbulence was very evident, separation proceeded as before in the laminar film and could be predicted by the theory developed earlier.[2] The runs in Table I marked T were definitely in the turbulent heat transfer region.

The authors wish to acknowledge the assistance of L. H. Tung, K. D. Timmerhaus, and W. L. Robb with the construction and operation of the equipment. Assistance in obtaining the electronic and other equipment was received from the du Pont Fund for Fundamental Research.

One of the authors (E.B.G.) engaged in the work as partial fulfillment of the requirements for the Ph.D. degree while on active duty with the U. S. Air Force.

The cooperation of the Argonne National Laboratory of the AEC made the work possible.

Thermal Diffusion in the System Methane-Xenon

L. H. TUNG AND H. G. DRICKAMER
Department of Chemistry, University of Illinois, Urbana, Illinois

(Received March 9, 1950)

Thermal diffusion measurements have been carried out for the system methane-xenon at a temperature 100°C above the critical using two thermal diffusion columns. The results confirm the column theory presented in an earlier paper, and are consistent with the results obtained on the system ethane-xenon.

THERMAL diffusion measurements have been made in the system methane-xenon using the equipment and techniques previously described.[1-3]

The methane was 99.9 percent pure material obtained from Phillips Petroleum. The xenon was spectroscopically pure and was obtained from the Matheson Company and irradiated by the AEC at the Argonne National Laboratory. The gas mixture contained about 0.15 mole percent xenon. The results are presented in Table I and Fig. 1.

TABLE I. Thermal diffusion in the system CH_4-Xe.

Run No.	T (°K)	P (atmos.)	ρ (g/ml)	q	ΔT (°C)	α'[a]	α[b]
Column II							
1	298.7	10.34	0.0068	1.176	15.6	0.083	0.128
2	297.8	10.41	0.0068	1.135	11.4	0.116	0.178
3	298.1	77.89	0.0581	12.32	14.8	0.454	0.176
4	299.1	77.89	0.0581	11.23	11.6	0.440	0.187
5	299.3	97.96	0.0752	8.85	11.9	0.676	0.229
6	299.0	97.96	0.0752	9.65	15.4	0.700	0.221
7	298.4	99.32	0.0764	10.78	15.6	0.762	0.234
8	299.0	60.34	0.0439	18.25	16.6	0.292	0.141
9	299.3	40.27	0.0283	16.00	17.4	0.149	0.109
10	298.3	20.82	0.0214	2.619	16.1	0.107	0.123
11	298.5	10.20	0.0067	1.565	16.8	0.201	0.307
12	298.5	99.93	0.0770	9.641	15.5	0.734	0.226
13	297.8	10.34	0.0068	1.149	10.8	0.145	0.224
Column I							
14	298.4	60.68	0.0440	1.582	12.8	0.703	0.148
15	297.8	60.54	0.0439	1.726	20.1	0.839	0.133
16	296.7	78.91	0.0589	1.719	18.5	1.59	0.164
17	298.0	98.57	0.0758	1.677	16.3	2.59	0.204
18	298.4	98.91	0.0758	1.658	12.7	2.56	0.234
19	298.9	44.69	0.0318	1.736	12.5	0.404	0.144
20	298.5	44.69	0.0318	1.724	16.1	0.398	0.121
21	298.9	30.41	0.0210	1.998	16.8	0.204	0.101
22	298.1	20.41	0.0138	2.299	15.7	0.120	0.0826
23	297.8	20.41	0.0138	2.187	11.8	0.129	0.0985
24	298.2	20.48	0.0139	1.996	7.5	0.166	0.151
25	297.9	10.34	0.0068	1.580	11.6	0.116	0.147
26	298.9	10.37	0.0068	1.921	16.8	0.0886	0.103
27	298.1	4.456	0.0029	1.208	15.8	0.135	0.207
28	297.6	60.34	0.0439	1.729	20.2	0.821	0.130
29	275.5	59.73	0.0490	1.689	11.6	1.43	0.224
30	275.7	44.97	0.0356	1.620	12.5	0.595	0.148

[a] α' calculated by the equations of Furry, Jones, and Onsager.
[b] α calculated by the equations of Drickamer, Tung, and Mellow.

The values of α were calculated as for the previous system. The p-v-t properties were those of Matthews and Hurd.[4] The viscosity at atmospheric pressure was obtained from Johnston and McCloskey,[5] and corrected for pressure by use of Enskog's dense gas correction. The diffusion coefficients were calculated from theory assuming a Lennard-Jones interaction potential as in the previous work. It may be noted that the modified column theory of Drickamer, Mellow, and Tung[1] gives consistent results between the two columns, while the classical theory does not.

It can be seen that α is everywhere positive, starting out not far from the theoretical value, at first decreasing with increasing density and then increasing. If one notes that these data were obtained about 100°C above the critical point these results become consistent with the previously reported data for ethane-xenon. The minimum in the α-density curve is at about two-thirds of the critical density just as the minimum occurred for the ethane -xenon system. It is apparent that even 100°C above the critical point the assumption of molecular chaos is not entirely justified at densities somewhat above atmospheric.

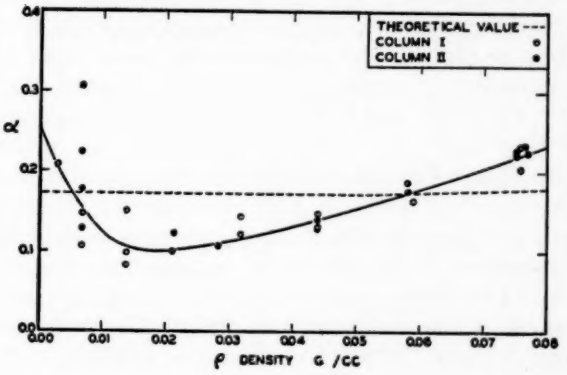

FIG. 1. Thermal diffusion ratio of the system CH_4-Xe.

[1] Drickamer, Mellow, and Tung, J. Chem. Phys. **18**, 945 (1950).
[2] Pierce, Duffield, and Drickamer, J. Chem. Phys. **18**, 950 (1950).
[3] Giller, Duffield, and Drickamer, J. Chem. Phys. **18**, 1027 (1950).
[4] C. S. Matthews and C. O. Hurd, Trans. A.I.Ch.E. **42**, 55 (1946).
[5] H. L. Johnston and K. E. McCloskey, J. Chem. Phys. **44**, 1038 (1940).

THE JOURNAL OF CHEMICAL PHYSICS VOLUME 18, NUMBER 8 AUGUST, 1950

The Electrostatic Contribution to the Lattice Energy of Some Ordered Spinels

F. DE BOER, J. H. VAN SANTEN AND E. J. W. VERWEY
Philips Research Laboratories, N. V. Philips' Gloeilampenfabrieken, Eindhoven, Netherlands
(Received March 9, 1950)

The electrostatic contribution to the lattice energy of some ordered spinels is calculated. It is made plausible that also in the case of certain spinels that do not show any long-range ordering, a considerable amount of short-range order is to be expected. As a consequence the lattice energy of "inversed" spinels containing different ions at octahedral positions, is increased with respect to the corresponding "normal" spinels containing one type of ions at octahedral interstices.

1. INTRODUCTION

In previous papers[1,2] we have calculated the electrostatic contribution to the lattice energy for spinels with different types of arrangement of the cations, i.e., with a different partition of the cations between the two different lattice positions occurring in the spinel structure (the tetrahedral and octahedral sites respectively). This cation arrangement appeared to be of importance for the understanding of various physical properties of these substances. The electronic conductivity of Fe_3O_4[3,4] and of solid solutions of Fe_3O_4 and other spinels could be explained in detail[5] in terms of this arrangement. The low temperature transition point of Fe_3O_4[6] could be interpreted on this basis, too.[5]

Also the magnetic properties of the Fe^{3+}-spinels (gross formula $Me^{2+}Fe_2^{3+}O_4$) are directly related to this cation arrangement. Within the accuracy given by direct or indirect x-ray evidence we found[1] that the ferromagnetic Fe-spinels (i.e., the ferrites of Mg, Mn^{2+}, Fe^{2+}, Co^{2+}, Ni^{2+} and Cu^{2+}) are all of the inversed type: $Fe^{3+}(Fe^{3+}Me^{2+})O_4$. The non-ferromagnetic spinels, $ZnFe_2O_4$ and $CdFe_2O_4$, however, proved to be of the normal type: $Me^{2+}(Fe^{3+}{}_2)O_4$. A physical theory for the magnetism of these ferrites, from the point of view of this arrangement of the cations, has recently been given by Néel.[7] This theory appears to be able to explain various aspects of the magnetic behavior of these materials. Among these the solid solutions of $ZnFe_2O_4$ and a ferromagnetic ferrite are of special importance.[8] The relatively high values of the magnetic saturation of these solid solutions can be satisfactorily explained as the result of the unequal distribution of Fe^{3+} between tetrahedral and octahedral positions in the solid solution of the normal and the inversed spinel.[9] In the case of the ferrites of Mg and Cu[7], one must also assume that the arrangement is not completely inversed but admixed with a small contribution of normal spinel, e.g., $Fe^{3+}{}_{0.9}Mg_{0.1}(Mg_{0.9}Fe^{3+}{}_{1.1})O_4$. Obviously in this case the energy difference between the normal and inversed arrangement is small. Actually by proper changes in the heat treatment, with the result that the cation arrangement is frozen in at different temperatures, minor changes in the degree of inversion can be effected, as is indicated by corresponding changes of the magnetic properties.[7,9,10]

These results show the importance of the problem of the relative stability of the normal and inversed arrangement, and therefore of the energies corresponding to both types of spinel lattices.

In the calculations referred to above it has been assumed, in accordance with the concept of Barth and Posnjak,[11] that in the inversed spinels the distribution of the ions of different valency over the octahedral lattice position is a completely random one. Hence the energy effect of a possible short-range order has been neglected. Such a short-range order can occur due to the fact that an ion of one type has a tendency to be surrounded by ions of the other type in essentially the same way as in electrolytic solutions the ions are surrounded by ionic clouds carrying an excess charge of the opposite sign. The amount of order will correspond to the temperature below which the cations lose their diffusion mobility (roughly of the order of 700°–800°K) with the exception of those spinels where the ions of different charge are derived from the same metal and the exchange can occur by an electron transfer. The latter case is realized in Fe_3O_4, and the possibility of such a type of order in inversed spinels is actually suggested by the physical behavior of this substance at low temperatures. At about 120°K Fe_3O_4 shows a transition point, and the strongly decreased and anisotropic electronic conductivity below the transition temperature has led to the assumption of a long-range order in the octahedral spinel sites.[5]

Meanwhile a second type of long-range order in the

[1] E. J. W. Verwey and E. L. Heilmann, J. Chem. Phys. **15**, 174 (1947).
[2] Verwey, de Boer, and van Santen, J. Chem. Phys. **16**, 1091 (1948).
[3] E. J. W. Verwey and J. H. de Boer, Rec. Trav. Chim. Pays-Bas, **55**, 531 (1936).
[4] J. H. de Boer and E. J. W. Verwey, Proc. Phys. Soc. **59A**, 59 (1937).
[5] Verwey, Haayman, and Romeyn, J. Chem. Phys. **15**, 181 (1947).
[6] E. J. W. Verwey and P. W. Haayman, Physica, 's-Grav. **8**, 979 (1941).
[7] L. Néel, Ann. de Physique **3**, 137 (1948).
[8] J. L. Snoek, *New developments in ferromagnetic materials* (Amsterdam-New York, 1947).
[9] E. W. Gorter, Nature, **165**, 798 (1950).
[10] F. G. Brockman (to be published).
[11] T. F. W. Barth and E. Posnjak, Zeits. f. Krist. **82**, 325 (1932).

octahedral position has been established,[12] namely in the case of the Li-Fe spinel $Fe(Fe_{1.5}Li_{0.5})O_4$. The transition temperature is here about 1200°K.

For a better understanding of these long-distance order-disorder phenomena we must possess a better knowledge of the energies involved. Accordingly, in the present paper we give calculations of the electrostatic contribution to the lattice energy for both types of order in the distribution of ions of different charges over the octahedral lattice points. From the above it will be clear that the results of these calculations will also be important for the question of relative stabilities of normal and inversed spinels.

2. ORDERING IN MAGNETITE

As indicated above the distribution of the Fe ions in Fe_3O_4 (magnetite) is of the inversed type, i.e., Fe^{3+} at tetrahedral and $Fe^{2+}+Fe^{3+}$ at octahedral interstices.

As shown by Verwey and Haayman,[6] the electrical conductivity decreases sharply at about 120°K. The following explanation has been proposed: at high temperatures the electrical conduction takes place by an electron transfer between Fe ions at octahedral interstices according to the scheme (Verwey and de Boer):[3,4]

$$Fe^{2+}Fe^{3+}Fe^{3+}\rightarrow Fe^{3+}Fe^{2+}Fe^{3+}$$

and occurring particularly along rows of Fe ions with [110] directions. At temperatures under 120°K an ordering of the extra electrons at the Fe^{2+} ions exists so that rows of Fe ions pointing in the [110] directions are entirely built up of either Fe^{2+} ions or Fe^{3+} ions, the electron-exchange mechanism being confined to regions where the ordering happens to be less severe.

In this arrangement the Fe ions are distributed in such a way that planes perpendicular to one of the cubic axes, say the c-axis, entirely consist of either Fe^{2+} or Fe^{3+} ions:

Fe^{2+} ions at	0 0 0	$\frac{1}{2}\frac{1}{2}$ 0	$\frac{1}{4}\frac{1}{4}$ 0	$\frac{3}{4}\frac{3}{4}$ 0
	$\frac{1}{2}$ 0 $\frac{1}{2}$	0 $\frac{1}{2}\frac{1}{2}$	$\frac{3}{4}\frac{1}{4}\frac{1}{2}$	$\frac{1}{4}\frac{3}{4}\frac{1}{2}$
Fe^{3+} ions at	0 $\frac{1}{4}\frac{1}{4}$	$\frac{1}{2}\frac{3}{4}\frac{1}{4}$	$\frac{1}{4}$ 0 $\frac{1}{4}$	$\frac{3}{4}\frac{1}{2}\frac{1}{4}$
	$\frac{3}{4}$ 0 $\frac{3}{4}$	$\frac{1}{2}\frac{1}{4}\frac{3}{4}$	0 $\frac{3}{4}\frac{3}{4}$	$\frac{1}{4}\frac{1}{2}\frac{3}{4}$

We calculated by means of Ewald's[13] method the effect of this "magnetite" ordering on the electrostatic contribution to the lattice energy for a general spinel

$$A^{p+}(B_{(1)}{}^{q_1+}B_{(2)}{}^{q_2+})O_4{}^{2-},$$

for the simple situation where both in the disordered and in the ordered states the parameter u[1] has the same value. In the former case all ions at octahedral interstices are supposed to carry the same charge $\frac{1}{2}(q_1+q_2)$ whereas in the latter case the ions $B_{(1)}$ and $B_{(2)}$ have their real charges q_1 and q_2.

We shall omit all details of the calculation but give only the result that the magnetite ordering gives rise to a gain in electrostatic energy per "molecule" $A^{p+}(B_{(1)}{}^{q_1+}B_{(2)}{}^{q_2+})O_4{}^{2-}$

$$\Delta V=1.001(q_1-q_2)^2(e^2/a), \tag{1}$$

where e denotes the electronic charge and a stands for the edge of the unit cell.

For Fe_3O_4 ($q_1=2$, $q_2=3$, $a=8.39$A) formula (1) yields

$$\Delta V=1.71eV=39.6 \text{ kcal./mole.} \tag{1a}$$

3. LITHIUM-FERRITE ORDERING*

The arrangement of the cations in $LiFe_5O_8$ or $Li_{1/2}Fe_{5/2}O_4$ has been investigated by Braun[12] with the aid of x-rays. The ions are distributed in the following way: Fe^{3+} at tetrahedral and $\frac{1}{2}Li^{+}+\frac{3}{2}Fe^{3+}$ at octahedral positions.

At temperatures above 1200°K the Li^+ and Fe^{3+} ions are distributed at random over the octahedral interstices (space group Fd3m). At lower temperatures, however, an ordering of the ions at the octahedral position takes place in such a way that every Li^+ ion is surrounded only by Fe^{3+} ions (space group P 4_33), one of the energetically equivalent arrangements being

Fe^{3+} ions at	0 0 0	0 $\frac{1}{4}\frac{1}{4}$	$\frac{1}{4}$ 0 $\frac{1}{4}$	
	$\frac{1}{2}\frac{1}{2}$ 0	$\frac{3}{4}\frac{1}{2}\frac{1}{4}$	$\frac{3}{4}\frac{3}{4}$ 0	
	$\frac{1}{2}$ 0 $\frac{1}{2}$	$\frac{1}{2}\frac{1}{4}\frac{3}{4}$	$\frac{3}{4}\frac{1}{4}\frac{1}{2}$	
	0 $\frac{3}{4}\frac{3}{4}$	$\frac{1}{4}\frac{1}{2}\frac{3}{4}$	$\frac{1}{4}\frac{3}{4}\frac{1}{2}$	
Li^+ ions at	$\frac{1}{4}\frac{1}{4}$ 0	$\frac{1}{2}\frac{3}{4}\frac{1}{4}$	$\frac{3}{4}$ 0 $\frac{3}{4}$	0 $\frac{1}{2}\frac{1}{2}$.

Again with the aid of Ewald's[8] method we calculated the effect of this "lithium-ferrite ordering" on the electrostatic part of the lattice energy for a general lithium ferrite spinel

$$A^{p+}((B_{(1)}{}^{q_1+})_{3/2}(B_{(2)}{}^{q_2+})_{1/2})O_4{}^{2-},$$

for the simple case that both in the disordered and in the ordered states the parameter u assumes the same value. In the disordered state all ions at octahedral

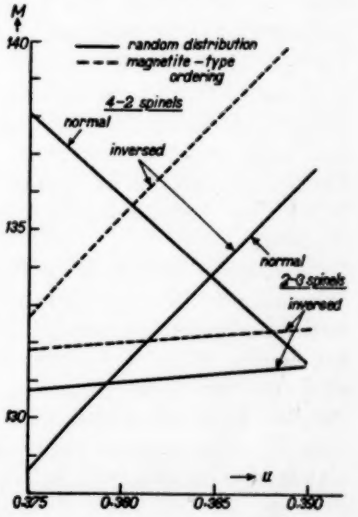

FIG. 1. Plot of electrostatic contribution to the lattice energy in units e^2/a against u.

[12] P. B. Braun, Acta Cryst. (to be published).
[13] P. P. Ewald, Ann. d. Physik, 64, 253 (1921).

* By "lithium ferrite" is meant the spinel $LiFe_5O_8$, not to be confused with $LiFeO_2$ showing sodium chloride structure.

interstices are supposed to have charges $\frac{1}{4}(3q_1+q_2)$ whereas in the ordered state $B_{(1)}$ and $B_{(2)}$ have their real charges q_1 and q_2.

It was calculated that the lithium-ferrite ordering causes a gain of electrostatic energy per "molecule" $Li_{1/2}Fe_{5/2}O_4$

$$\Delta V=0.712(q_1-q_2)^2(e^2/a). \quad (2)$$

For lithium ferrite itself ($q_1=3$, $q_2=1$, $a=8.4$A) we obtain from (2)

$$\Delta V=4.88eV=113 \text{ kcal./mole}. \quad (2a)$$

4. DISCUSSION

In order to obtain the real energies of ordering the electrostatic energies calculated above must be corrected for the effects of polarization and ionic displacement. An analysis shows that such corrections have a tendency to increase the energy of ordering. The polarization is mainly caused by the oxygen ions, and restricting ourselves to the effect of the nearest neighbors of oxygen we can show that the effect of ordering is such as to increase the energy gain accompanying the ordering by about 25 percent both for magnetite and lithium ferrite. Also ionic displacements caused by the ordering will probably favor the ordered situation because in the latter the lattice is in a better position to take advantage of less symmetrical structures. To a first approximation, however, the real energies of ordering will be given by the electrostatic values of ΔV calculated above.

The energy effects (cf. Eqs. (1a) and (2a)) are large compared with the energy of thermal motion at the transition temperatures. Therefore, also above these temperatures a very pronounced order must be present. Such a situation might seem paradoxical but it is also realized in the melting phenomena of heteropolar compounds. In the solid state long-range and short-range order occur whereas in the liquid state only short-range order can be present. The energy effect of the melting process (taken at constant volume) is only a small fraction of the lattice energy. It is probable that a pronounced short-range order and a corresponding large energy of ordering also above the temperature at which long-range order is destroyed, is a typical feature of Coulomb interaction in contrast to the nearest-neighbor interaction commonly considered in order-disorder theories.

As discussed already in the introduction, our previous calculations[1,2] of the electrostatic contribution to the lattice energy of inversed spinels must be corrected for the energy effect of a strong short-range order. It is obvious that these corrections have a tendency to stabilize inversed spinels with respect to the normal ones. In order to get an impression of the order of magnitude of these effects we have plotted the electrostatic contribution to the lattice energy M (in units e^2/a) for 1) no short-range order and 2) fully developed magnetite-type order (Fig. 1).

The correction (cf. Eq. (1)) is smallest for 2–3 spinels. Even is we assume that the energy effect of the short-range order approaches the value corresponding to a fully developed magnetite-type order, the conclusions concerning the relative stability of normal and inversed spinels given in our previous papers[1,2] are not materially affected. The limit of the stability region of normal spinels is shifted from $u=0.379$ to $u=0.381$. This limit cannot be taken too strictly, as the normal and inversed arrangements of the same spinel will not have exactly the same values of lattice dimension a and parameter u, and also other energy effects should be taken into account. The values of the parameter as found experimentally for normal 2–3 spinels, such as the aluminates or chromites, are generally well above 0.381 and therefore in the region where the electrostatic contribution to the lattice energy is actually larger for the normal arrangement.

Somewhat smaller values of u have been reported for the ferrites ($CuFe_2O_4$ 0.380 ± 0.005; $ZnFe_2O_4$ 0.380 ± 0.005; $Cu_{0.5}Zn_{0.5}Fe_2O_4$ 0.380 ± 0.005[1]; Fe_3O_4 0.379; LiFe-spinel 0.382 ± 0.005 (above 1200°K)).[12] Though the accuracy of these determinations is generally rather low a smaller value of u for the Fe spinels seems plausible in view of the larger size of the Fe^{3+} ion. Accepting these u values the theoretical lattice energy values seem to be in good agreement with experimental evidence, showing that for the ferrites the inversed arrangement is the more stable one (though the energy difference may be small), except in the case of the ferrites of Zn and Cd where probably specific valency forces play a part.

For 4–2 spinels the correction is rather important. We find now that from an electrostatic point of view the ordered inversed spinel arrangement is more stable than the normal one for $u>0.381$. As all investigated 4–2 spinels were found to be of the inversed type, the corrected values appear to be in a better agreement with experimental facts than the uncorrected values because the parameter values determined up till now, though rather scanty, are mostly about 0.385. More definite conclusions are not yet possible because these parameter values are not very accurate.

The conclusion that such a pronounced short-range order exists in these inversed spinels is also important for those phenomena in which the interaction between neighboring ions and therefore the number of cations of different species surrounding each cation, plays a part. Hence it should be taken into account, for instance, in quantitative theories both of the magnetic and the electric properties of the materials indicated in Section 1.

THE JOURNAL OF CHEMICAL PHYSICS VOLUME 18, NUMBER 8 AUGUST, 1950

X-Ray Diffraction by Solid Soaps

A. J. STOSICK
Department of Chemistry, University of Southern California, Los Angeles, California
(Received March 24, 1950)

Arguments are presented to show that x-ray diagrams obtained by using the powder technique for common soap samples can be interpreted in terms of two kinds of disordering. The first kind of disorder, a stacking disorder of micellar layers, makes the layers optically independent for certain diffraction maxima so that continuous diffraction bands arise rather than discrete maxima. A second kind of disorder within a layer in which long chain ions are randomly oriented with respect to rotation about their long axes causes all but one set of bands to be weak. A consideration of these two disorders permits extensive unification of the results of x-ray diffraction experiments for poorly crystallized soaps. The use of such diffraction patterns for phase studies is subject to severe uncertainties.

THE x-ray diffraction patterns of solid soaps, in particular the metal salts of fatty acids, have been examined by a number of investigators over a period covering many years. In a few instances the investigators succeeded in obtaining single crystals sufficiently well-ordered to produce an essentially normal single crystal diffraction pattern.[1] The unit cells found in these cases have two relatively short axes whose lengths are apparently simply related to the packing diameter of a fatty acid chain. The remaining axis of the unit cell is much longer and is approximately equal to some even multiple of the length of a fatty acid ion. The approximate nature of the equality arises from the fact that there must be a positive ion layer, a van der Waals end packing distance, and from the possibility that the chains may be tilted.

A unit cell of this kind produces a series of diffraction maxima $(00l)$, labeling the long axis $\mathbf{a}_3$, which begins at very small angles and which extends out to very large angles. Depending on the space group and the detailed internal arrangement, the $(00l)$ spectra may be present only when l runs through the successive permitted values. In the small angle region these are the only diffraction maxima possible, and this permits an unequivocal determination of $\mathbf{b}_3$ the length of the axis reciprocal to $\mathbf{a}_3$.

The other diffraction maxima for which both h and k are not zero occur at larger angles, and actually consist of a band of closely spaced lines whose resolution increases with increasing scattering angle. This arises from the fact that, for this kind of cell, as l varies, for a given h and k not both zero, the reciprocal lattice vectors $\mathbf{H}=h\mathbf{b}_1+k\mathbf{b}_2+l\mathbf{b}_3$ are very nearly equal for several low values of l, but become progressively better resolved as l becomes large. This point has been discussed both by Buerger[1] and Vand.[2] On single crystal Weissenberg photographs this resolution can always be achieved, but on rotation photographs or on powder patterns there may be several unresolved diffraction maxima for low values of l. However, even on powder photographs of well-crystallized materials, these lines have been resolved for moderate values of l, say l equal to ± 2 or more.

For soap single crystals, the diffraction maxima extend to moderately large diffraction angles, with an intensity decline not significantly different from that for other organic crystals. This conclusively indicates that the absence of wide angle scattering maxima for other soap patterns cannot be attributed solely to temperature lattice vibrations, but is strong presumptive evidence for lattice disorder.

A second kind of diffraction diagram corresponds to a powder, with each crystallite giving a diagram with well-defined and resolved maxima extending to large scattering angles. A powder diagram of this sort is no different from that of any other organic substance except for features which are related to the exceptional length of one of the crystal axes. Diagrams of this kind have been obtained by Vand[3] for several soaps.

A third kind of diagram, not yet published, was obtained by Dr. J. D. Grandine, II, in these laboratories. It is the diagram of a naturally oriented bundle of fibers of sodium stearate, possibly hydrated. These fiber bundles produced rotation diagrams with well-defined layer lines with a considerable number of resolved reflections on each layer line. The layer line spacing, which directly gives the length of a crystal axis rather than a plane spacing, corresponded to some short crystallographic axis.

The fourth and far more common kind of diagram, which we shall call a powder diagram for simplicity, is notorious for its variability. It is this type of diagram[4] which has been most used in attempts to determine phase behavior of soaps. These diagrams are obtained when the x-ray powder technique is applied to soap samples for which no special attempts have been made to obtain good crystal growth. A given sample may produce a diffraction pattern which changes with time.

[1] M. J. Buerger, Am. Mineral. **30**, 551 (1945). J. E. Miner and E. C. Lingafelter, J. Am. Chem. Soc. **71**, 1145 (1949).
[2] V. Vand, Acta Cryst. **1**, 109 (1948).
[3] Vand, Aitken, and Campbell, Acta Cryst. **2**, 398 (1949).
[4] P. A. Thiessen and J. Stauff, Zeits. f. physik. Chem. **A176**, 397 (1936). Ferguson, Rosevear, and Stillman, Ind. Eng. Chem. **35**, 1005 (1943). Buerger, Smith, Ryer, and Spike, Proc. Nat. Acad. Sci. **31**, 226 (1945). Vold, Grandine, and Vold, J. Colloid Sci. **3**, 339 (1948).

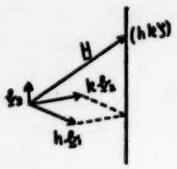

FIG. 1. Space reciprocal to $\mathbf{a}_1$, $\mathbf{a}_2$, $\mathbf{a}_3$.

If a sample is heated and then restored to room temperature, the diagrams obtained before and after the treatment may be greatly different. Two investigators may obtain significantly different diagrams for their respective preparations even though the materials prepared should have been the same.

This kind of powder diagram is characterized by a series of (00l) diffraction maxima beginning in the small angle region. In addition there is a broad diffraction band in the vicinity of $2\theta \approx 20°$ (for copper K radiation). This broad band almost never shows sharply resolved substructure, but it may resolve into two or more broad sub-maxima. At larger scattering angles there is frequently a series of small and relatively narrow maxima running out to $2\theta \approx 40°$ or more. Almost without exception, no other broad bands are observed which are like the band at $2\theta \approx 20°$, but at larger values of θ. It is the purpose of this paper to show that diagrams of this kind can be interpreted as resulting from a random parallel stacking of micellar layers.

The problem of disordered stacking of layer lattices has been discussed by several investigators. For the purpose at hand, the discussion of Warren[5] for complete randomness of stacking will be used. The idea of disordered layer stacking was used earlier by Maegdefrau and Hofmann[6] in an interpretation of the x-ray diffraction by montmorillonite containing varying amounts of water.

Warren showed that if a solid consists of randomly stacked, identical, two-dimensional lattices, then characteristic effects appear in the diffraction pattern. The randomness of stacking may consist of random displacement parallel to the layer, with the direction and magnitude of the lateral displacement arbitrary. The stacking thickness of the parallel layers is assumed to be constant. The random lateral displacements alone are sufficient to make the layers optically independent for certain sets of Miller indices. The added possibility of random rotation about the normal to the layers does not introduce any new effects not caused by the displacement randomness alone.

Suppose we characterize the two-dimensional lattice of the layers by vectors $\mathbf{a}_1$ and $\mathbf{a}_2$ which define a regular two-dimensional net. Let $\mathbf{a}_3$ be a third vector whose projection on the normal to the layer is the layer repeat thickness. Warren, in discussing carbon black, chose $\mathbf{a}_3$ as normal to the $\mathbf{a}_1$, $\mathbf{a}_2$ net. For the soaps, whose layers are many atoms thick, it will be convenient to choose $\mathbf{a}_3$ parallel to the axis of the long chain ion. It is readily shown that this does not in any way alter the applicability of Warren's discussion to the problem at hand. For an ideal well-ordered crystal the vectors $\mathbf{L}=l_1\mathbf{a}_1+l_2\mathbf{a}_2+l_3\mathbf{a}_3$, with the l_i integers, represent translations between identical points in the distribution of scattering matter. For stacking disorder, this is true for the vectors $\mathbf{L}'=l_1\mathbf{a}_1+l_2\mathbf{a}_2$ in a single net, but not for the vectors $\mathbf{L}$ above. This means that the translations $l_3\mathbf{a}_3$ are not lattice translations for the disordered stacking.

For the case of random stacking, only two kinds of diffraction maxima are possible. These are the (00l) spectra which are in no way affected by the stacking disorder. The other kind of diffraction maxima are (hk) maxima, with at least one of the pair h, k not zero. These maxima are diffraction maxima of the two-dimensional gratings which comprise the lattice of the individual layers. For these maxima the integral index l has become meaningless and can be replaced by a quantity ζ, a continuously variable coordinate in reciprocal space. The indices h and k are always "good indices" if the layers have sufficiently large lateral dimensions.

This means that for the soaps, with stacking disorder, we expect to find a sequence of sharp spectra, the (00l) series, beginning at small angles and continuing out to large angles. They will provide no indication of stacking disorder, their broadness may provide information concerning the number of consecutive layers in a disordered crystallite. We also expect to find a series of broad bands beginning at larger angles, each band arising from a set of indices (hk). For a given (hk) pair we expect a continuous variation of intensity with scattering angle, but no resolved sharp lines.

In Fig. 1 a portion of the space reciprocal to $\mathbf{a}_1$, $\mathbf{a}_2$, $\mathbf{a}_3$ is shown. For a given index pair (hk), diffraction is possible if $2\sin\theta/\lambda$ corresponds to the length of a reciprocal vector, $\mathbf{H}$, from the origin to any point on the line through (hk) and parallel to $\mathbf{b}_3$. The coordinate along this line is ζ. If the layers are one atom thick, $\mathbf{a}_3$ can be most simply chosen to be normal to $\mathbf{a}_1$, $\mathbf{a}_2$. Then $\mathbf{b}_3$ will be normal to $\mathbf{b}_1$, $\mathbf{b}_2$, and the resulting ($hk\zeta$) band will rise rapidly at the low angle edge and decline slowly in intensity with increasing scattering angle. The decline is in part caused by the decrease in scattering power of the atoms with increasing angle, and in part caused by the Lorentz factor as discussed by Warren. For carbon black, Warren's results show that the (10) band extends almost to the (11) band of the graphite-like layers. If the layers are many atoms thick, the intensity in a band will decline more rapidly with increasing scattering angle; and if the layers show regular internal structure along $\mathbf{a}_3$, then the intensity decline within a band need not be monotomic, but may rise and fall more than once.

From the known dimensions of long chain fatty acid groups, we know that in the first approximation they can be regarded as cylinders. Such cylinders will have

[5] B. E. Warren, Phys. Rev. **59**, 693 (1941).
[6] E. Maegdefrau and V. Hofmann, Zeits. f. Krist. **98**, 299 (1937).

optimum packing if they pack in a two-dimensional hexagonal close-packed array. The metal ions will move to locations of maximum coulomb energy consistent with the packing of the negative ions. For such a layer the $\mathbf{a}_1$, $\mathbf{a}_2$ net will be hexagonal with the axes making an angle of 120°. The axes $\mathbf{b}_1$, $\mathbf{b}_2$ reciprocal to $\mathbf{a}_1$, $\mathbf{a}_2$ will also form a hexagonal net with the angle between $\mathbf{b}_1$, $\mathbf{b}_2$ having the value 60°. For this reciprocal net we find that the three index pairs (and their negatives), (10), (01), and $(1\bar{1})$ have the same value of $\sin\theta$ and hence lead to superimposing bands. Putting in the dimensions of the acid ions, assumed to be cylinders, the value of 2θ is about 20° for CuKα x-rays. The next band should occur with a $\sin\theta$ which is $\sqrt{3}$ larger, corresponding to the superposition of the bands (11), $(2\bar{1})$, $(1\bar{2})$, and their negatives. Following this, with a $\sin\theta$ which is twice that of the first band, is the superposition of the bands (20), (02), $(2\bar{2})$, and their negatives.

Hence we see that we expect a sequence of bands the first with $2\theta\approx 20°$, the second with $2\theta\approx 35°$, and the third with $2\theta\approx 40°$. No other side-spacing bands can occur in this region.

Suppose next that the nets are not exactly hexagonal, but nearly so since the long ions are nearly cylindrical. In this case the reciprocal net will also be almost, but not quite, hexagonal. If we change only the angle $\mathbf{a}_1$, $\mathbf{a}_2$ a little from 120°, then the (10) and (01) bands still superimpose, but the $(1\bar{1})$ band now occurs at a slightly different angle. If we change both the angle and the relative lengths of $\mathbf{a}_1$, $\mathbf{a}_2$ we find that the (10), (01), and $(1\bar{1})$ bands all occur at nearly equal but different values of θ. In no case can we get more than three (hk) bands near $2\theta\approx 20°$ for the kind of net we have described. This means that for randomly stacked soap layers the diffraction region at $2\theta\approx 20°$ must be describable as the superposition of at most three (hk) bands and of one or more of the $(00l)$ series of long spacings. In a similar way the bands near $2\theta\approx 35°$ and $2\theta\approx 40°$ must be describable in terms of similar sets of three (hk) bands and long spacings.

If sharp diffraction maxima are observed between $2\theta\approx 20°$ and $2\theta\approx 35°$, then either they must be high orders of $(00l)$, or they must be resolved lines (hkl) of an ordered layer stacking for one of the sets $(10l)$, $(01l)$, or $(1\bar{1}l)$. An examination of the data obtained by Professor R. D. Vold in these laboratories shows that these lines can be identified as high orders of $(00l)$. Additional resolution tests on the 20° band for calcium stearate have been made by Professor Vold. Two sharp maxima are almost completely resolved by his instrument in this angle region if they differ in 2θ by 18′. This is sufficient to resolve some of the soap (hkl) lines in this region if the index l has meaning. No such resolution has been observed for the commonly used soap "powder" samples.

STRUCTURE OF THE BANDS

Two additional items concerning the broad bands need to be discussed. The first is the nearly universal failure to find strong bands at $2\theta\approx 35°$ and $2\theta\approx 40°$ for the common powder samples. The second concerns the distribution of intensity in the $2\theta\approx 20°$ band. The problem involved is the calculation of the Fourier transform from the crystal space of two-dimensional gratings with a thickness of many atom layers to the reciprocal space (ξ, η, ζ). Since the layers show two-dimensional periodicity of periods $\mathbf{a}_1$ and $\mathbf{a}_2$, the only values of ξ and η which enter are the integral values (hk). Because of the periodicity with respect to $\mathbf{a}_1$ and $\mathbf{a}_2$, a micellar layer can be regarded as a parallel array of unit cells having relative translations $l_1\mathbf{a}_1+l_2\mathbf{a}_2$. The Fourier transform of the layer's scattering density then factors into two terms, one related to the lattice function, and the other to the distribution of scattering matter in the unit cell. If we let x, y, z be coordinates along $\mathbf{a}_1$, $\mathbf{a}_2$, $\mathbf{a}_3$, with $0\leqslant x, y, z\leqslant 1$, or $-\frac{1}{2}\leqslant x, y, z\leqslant+\frac{1}{2}$

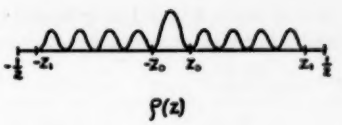

FIG. 2. Fourier transform.

$$F(\xi,\eta,\zeta)=\int_{-\frac{1}{2}}^{+\frac{1}{2}}\rho(x,y,z)\times\exp[-2\pi i(\xi x+\eta y+\zeta z)]dxdydz$$

is the structure factor of a unit cell. The function $\rho(x, y, z)$ is the scattering density distribution function. The function $F(\xi, \eta, \zeta)$ is a continuous function in reciprocal space. The lattice function is responsible for the sharpness of diffraction maxima, and for the problem at hand requires that (ξ, η) be integers (h, k), so that the scattered waves have amplitudes $F(hk\zeta)$. Our problem, therefore, is one of devising a physically reasonable function $\rho(x, y, z)$ which accounts for the observed relative intensities of the $(hk\zeta)$ bands and the $(00l)$ sharp lines.

As a model we can adopt the following array. Let us suppose that each of the fatty acid ions is nearly cylindrical in shape so that it can be rotated by arbitrary amounts around its long axis, and let us suppose that this disorder is permanent within a layer except for a slow ageing process which leads to removal of this disorder. The scattering amplitude for a layer of this kind can be calculated to a high degree of correctness by replacing each long ion by an ion "smeared-out" by rotating it about its long axis. The result of this process is the possibility of factoring $\rho(x, y, z)$ into $\rho(x, y)$ and $\rho(z)$ for which we can separately calculate the Fourier transforms. In a strict sense the proposed factoring can be accomplished only if the chains are normal to the median plane of the layer. However, since this condition is nearly satisfied for the soaps, the introduction of this factorization will not lead to a serious error. For the kind of distribution proposed $\rho(x, y)$ can be represented by the function $\rho(x, y)=1+\cos 2\pi x+\cos 2\pi y+\cos 2\pi(x-y)$ to a high degree of correctness. For a hexagonal (or near hexagonal) net the

TABLE I. α-sodium stearate (powder).

d/n obsd. 51.63±0.15A (d_{001})	d/n calcd.	Indices
5.76	5.74	0 0 9
5.18	5.16	0 0 10
4.68	4.69	0 0 11
4.68	—	(10ζ), (01ζ)
4.32	4.31	0 0 12
4.32	—	(1$\bar{1}\zeta$)
4.01	3.98	0 0 13
3.71	3.69	0 0 14
3.46	3.45	0 0 15
3.24	3.23	0 0 16
3.06	3.04	0 0 17
2.88	2.87	0 0 18
2.73	2.72	0 0 19
2.46	2.46	0 0 21
2.35	2.35	0 0 22
2.32	2.34	(20ζ), (02ζ)
2.25	2.25	0 0 23
2.16	2.16	(22$\bar{\zeta}$)
2.13	2.15	0 0 24
2.09	2.07	0 0 25

scattering matter corresponding to $\rho(x, y)$ is concentrated near integral values for x and y and declines to low values when x and y are near half-integers. Higher order Fourier terms are needed for a correct representation of $\rho(x, y)$, but their amplitudes must be much smaller than the terms listed above. The density distribution above has the property that only $F_{00\zeta}$, $F_{01\zeta}$, $F_{10\zeta}$, and $F_{1\bar{1}\zeta}$ have non-zero values. This means that only the bands at $2\theta\approx 20°$ and the (00l) series, including (000), will appear. The bands at $2\theta\approx 35°$ and $2\theta\approx 40°$ appear only if higher order terms are needed to represent $\rho(x, y)$ correctly. Thus the band with scattering amplitude $F_{11\zeta}$ arises only from including the term $\cos 2\pi(x+y)$ in $\rho(x, y)$, and similarly the band with amplitude $F_{20\zeta}$ arises only from including the term $\cos 2\pi(2x)$ in $\rho(x, y)$. The non-appearance of the bands at $2\theta\approx 35°$ and $2\theta\approx 40°$ means that the corresponding terms in $\rho(x, y)$ must be small or zero. The non-appearance of the bands cannot be ascribed solely to lattice vibrations since the corresponding single crystal patterns show higher order (hkl) maxima.

In order to determine whether or not individual ($hk\zeta$) bands can show structure, we must evaluate the Fourier transform for a reasonable function $\rho(z)$. Such a function is shown in Fig. 2. For convenience the origin is located at the center, the location of the metal ion layer, and $-\frac{1}{2}\leqslant z\leqslant\frac{1}{2}$. The function shown is made up of cosine terms joined together at z_0, and having an integral number of cycles from z_0 to z_1. The cosine term from z_0 to z_1 represents the carbon chain. The gap from z_1 to $z=\frac{1}{2}$ represents the van der Waals end packing term.

This function $\rho(z)$ is

$$\begin{aligned}
(z)&=\tfrac{1}{2}\rho_1[1-\cos 2\pi n(z+z_0)] && -z_1\leqslant z\leqslant -z_0\\
(z)&=\tfrac{1}{2}\rho_0[1-\cos 2\pi(1/2z_0)z] && -z_0\leqslant z\leqslant +z_0\\
(z)&=\tfrac{1}{2}\rho_1[1-\cos 2\pi n(z-z_0)] && z_0\leqslant z\leqslant z_1
\end{aligned}$$

with $n=[(z_1-z_0)a_3]/r_0$, and in which r_0 is the projection of a C−C bond on the long axis of the fatty acid ion. No special term is included for the carboxyl oxygen atoms, one of these can be regarded as just another carbon atom in the chain, and the other is simply neglected. It will be seen that n is one greater than the number of C atoms in the chain if we count one oxygen as an added carbon atom.

The Fourier transform for this function $\rho(z)$ was calculated, and the following properties of the transform ($F_{hk\zeta}$) were noted. The terms corresponding to the average scattering power, i.e. $\rho_1\times\frac{1}{2}$, and $\rho_0\times\frac{1}{2}$, introduce terms of the form $(\sin 2\pi\zeta z_1-\sin 2\pi\zeta z_0)/\pi\zeta$ and $(\sin 2\pi\zeta z_0)/\pi\zeta$, whereas the oscillating parts of the scattering density, i.e. $[-\cos 2\pi n(z-z_0)-\cos 2\pi n(z+z_0)]$ introduce a term in the form

$$\frac{\sin 2\pi\zeta z_0}{\pi(\zeta+n)}+\frac{\sin 2\pi\zeta z_0}{\pi(\zeta-n)}-\frac{\sin 2\pi[(\zeta+n)(z_1-z_0)+\zeta z_0]}{\pi(\zeta+n)}-\frac{\sin 2\pi[(\zeta-n)(z_1-z_0)+\zeta z_0]}{\pi(\zeta-n)}.$$

This reduces to $2(z_1-z_0)\cos 2\pi n z_0$ when $\zeta=\pm n$, and is small for all other values of ζ. The term $[-\cos 2\pi\times(1/2z_0)z]$ introduces a term of the form

$$\frac{\sin 2\pi(\zeta+1/2z_0)z_0}{\pi(\zeta+1/2z_0)}+\frac{\sin 2\pi(\zeta-1\zeta 2z_0)z_0}{\pi(\zeta-1/2z_0)}$$

which can be rearranged to

$$(2\zeta\sin 2\pi\zeta z_0)/[\pi(\zeta^2-1/4z_0^2)].$$

This is small except when $\zeta=\pm 1/2z_0$. Thus we expect $F_{hk\zeta}$ to be large near $\zeta=0$, $\zeta=\pm 1/2z_0$, and again near $\zeta=\pm n$. The contribution to $F_{hk\zeta}$ from the right and left oscillating terms have a relative phase factor which depends on the value of z_0. If $2z_0\approx r_0/a_3$, they reinforce; if $2z_0\approx pr_0/2a_3$, then they cancel. If the former is true, the (00l) series should have large values of F_{00l} for $l\approx n$; if the latter is true F_{00l} will not be unusually large near $l\approx n$. The essential correctness of these arguments is supported by the x-ray data for cetyl palmitate published by Kohlhaus.[7] This ester has a chain of 33 atoms of uniform periodicity except for a slight difference between C−C and C−O bonds at the center. For this crystal the (00l) series has values for F_{00l} which are moderate for small l, nearly vanishing for $l\approx 20$, very large for $l\approx 34$, and again small for $l\approx 38$.

Since we have assumed that we can factor $\rho(x, y, z)$ into $\rho(x, y)$ and $\rho(z)$, the ζ dependence of $F_{hk\zeta}$ does not depend on (hk). This means that the values of $F_{hk\zeta}$ along the reciprocal space lines (00ζ), (10ζ), (01ζ), and (1$\bar{1}\zeta$) must be the same. For the (00ζ) line only integral values of ζ are permitted. Qualitatively this means that in each ($hk\zeta$) band we expect the same envelope of values of $F_{hk\zeta}$ as for the series F_{00l}, but for

[7] Kohlhaus, Zeits. f. Krist. 98, 418 (1938).

TABLE II. ζ-sodium palmitate (powder).

d/n obsd. 41.69 ±0.20A (d_{110})	d/n calcd.	Indices
5.22	5.22	0 0 8
4.37	—	(10ζ)
4.19	4.17	0 0 10
3.98	—	(1$\bar{1}\zeta$)
3.85	—	(01ζ)
3.49	3.48	0 0 12
3.22	3.21	0 0 13
2.99	2.98	0 0 14
2.78	2.78	0 0 15
2.62	2.61	0 0 16
2.46	2.46	0 0 17
2.39	2.38	(11ζ)
2.33	2.32	0 0 18

TABLE III. β-sodium palmitate (powder). 0.23 percent H_2O.

d/n obsd. 42.30A (d_{001})	d/n calcd.	Indices
21.30	21.15	0 0 2
13.90	14.10	0 0 3
10.60	10.58	0 0 4
8.48	8.46	0 0 5
6.05	6.04	0 0 7
4.15	—	(10ζ)
3.75	—	(01ζ)
3.23	3.25	0 0 13
3.07	—	(1$\bar{1}\zeta$)
2.85	2.82	0 0 15
2.63	2.64	0 0 16
2.48	2.48	0 0 17
2.35	2.35	0 0 18
1.88	1.88	(02ζ)
1.79	1.77	0 0 24

the ($hk\zeta$) bands the angle range is compressed. Because of the differences in the Lorentz factors for the (00l) series and the ($hk\zeta$) bands, this similarity may not appear obvious from an examination of the corresponding intensities. No attempt will be made here to evaluate the Lorentz factor for the ($hk\zeta$) bands, but qualitatively we can forsee the possibility that an ($hk\zeta$) band may consist of more than one region of large intensity, and that the point of maximum intensity need not necessarily correspond to $\zeta=0$.

INTERPRETATION OF SOME PATTERNS

To illustrate the application of these ideas in interpreting powder diagrams of poorly crystallized soaps, possible sets of indices will be assigned to several such patterns. The examples listed are only a few of a much larger number of patterns which have been similarly identified as combinations of (00l) lines and ($hk\zeta$) bands. The data for α sodium stearate (not necessarily Buerger's crystalline α hemihydrate) and for ζ sodium palmitate are taken from the Doctoral Dissertation of Joseph D. Grandine, II,[8] and were furnished to the writer by Dr. R. D. Vold. This assistance of Dr. Vold is gratefully acknowledged, as is his information concerning the reliability of the measured data. The third example is that of β-sodium palmitate with 0.23 percent water, the data being that of Ferguson, Rosevear, and Nordsieck.[9] These data are presented in Tables I, II, and III, respectively.

In the first column of each table the values of d_{001} (layer thickness), or the measured values of the long spacing, are listed together with all other reported maxima. Column two lists the calculated positions of (00l) maxima or ($hk\zeta$) bands, the location of higher order bands being calculated from the maxima identified as (10ζ), (01ζ), and (1$\bar{1}\zeta$) bands. For the latter calculation the measured maxima are assumed to correspond to the region ($hk0$) of the band. This assumption is justified. The third column of each table lists the corresponding line or band indices.

[8] J. D. Grandine, II, Doctoral Dissertation, University of Southern California, 1949.

[9] Ferguson, Rosevear, and Nordsieck, J. Am. Chem. Soc. **69**, 141 (1947).

For none of these patterns are the orders of (00l) for which $l \approx n$ (the number of atoms in the chain) exceptionally strong. Hence we conclude that the bands should show a maximum only near $\zeta=0$. This justifies our procedure for identifying band maxima with the region $\zeta=0$ of the ($hk\zeta$) bands. In any case no serious error will result so long as the ζ values in the different bands are nearly the same for all band maxima.

A point which might be raised concerning the correctness of this interpretation for some soap patterns is the close similarity of some patterns for different soaps in the region 2θ greater than 20°, i.e. past the 20° band system. As one goes through an homologous series, changing the length of the fatty acid chains, for a given "Greek letter phase," there is often a set of lines which appears almost at the same position for the different substances. This deceptively suggests that these diffraction maxima must necessarily be side spacings, and cannot be identified as orders of (00l). This argument is false.

The positions of these lines are characterized by d/n values, for a given λ. Clearly if d/n is the same, or nearly the same, the diffraction maxima occur at the same angle. Suppose that for some soap, d_{001} is 45.0A, and for a higher member of the series d_{001} is 4.5A larger, i.e. $d'_{001}=49.5$A. Then the order $n=20$ of the first exactly coincides with $n'=22$ of the second soap. Simple arithmetic calculation will show that this equality remains nearly true for several orders higher and lower than the values corresponding to exact coincidence. It is therefore expected that several members of an homologous series may exhibit this deceptively similar appearance for disordered samples, and the observation of nearly identical positions for a set of maxima is no guarantee that they represent "side spacings."

CONCLUSIONS

From the preceding discussions several important conclusions can be reached. The great bulk of x-ray diffraction results for powder samples of soaps, those for which no special efforts have been made to obtain good crystal growth, can be interpreted as the random

superposition of micellar layers. For such samples we find a series of relatively sharp $(00l)$ reflections extending out to relatively large angles, and series of $(hk\zeta)$ bands near 20°, 35°, and 40°. Most of the lines which have been called short spacings or side spacings are merely high orders of the $(00l)$ series. From arguments presented earlier we may also expect randomness of orientation of the large ions in the micellar layers. If this randomness is also present, we expect that the only strong band will be the band system near 20°. In part, the weakness or absence of the other bands may be due to anisotropic thermal vibrations.

It is also clear that any attempt to use such powder diagrams in phase studies of the soaps is, at best, beset by the gravest of uncertainties. Thus a sample of unchanging composition might give a great range of distinguishably different diffraction patterns corresponding to varying degrees of order. Since these will in general not be equilibrium arrangements, although they may have a long temporal stability, there is at least a serious doubt as to whether they should properly be called phases in the thermodynamic sense. In the strictest sense, thermodynamics and the notion of a phase involve equilibrium concepts.

THE JOURNAL OF CHEMICAL PHYSICS VOLUME 18, NUMBER 8 AUGUST, 1950

Radial Distribution Functions and the Equation of State of a Fluid Composed of Rigid Spherical Molecules*

JOHN G. KIRKWOOD, EUGENE K. MAUN, AND BERNI J. ALDER
Gates and Crellin Laboratories of Chemistry, Pasadena, California
(Received March 20, 1950)

The integral equation for the radial distribution function of a fluid of rigid spherical molecules has been integrated numerically in the Kirkwood approximation and in the Born-Green approximation over a wide range of densities. The distribution functions so obtained have been used to calculate the equation of state and excess entropy of the fluid. The results are compared with those obtained by means of the free volume theory of the liquid state.

I.

IN the statistical-mechanical theory of liquids composed of molecules possessing a potential of intermolecular force of the form,

$$V_N=\sum_{i<k=1}^{N} V(R_{ik}), \tag{1}$$

the average density $\rho^{(2)}(\mathbf{R}_1, \mathbf{R}_2)$ in the configuration space of molecular pairs plays a central role. In the fluid states of aggregation, gas or liquid, it is possible to define a function $g(R_{12})$, called the radial distribution function, by the relation,

$$\begin{aligned}\rho^{(2)}&=[\rho^{(1)}]^2 g(R_{12}),\\ \rho^{(1)}&=N/v,\end{aligned} \tag{2}$$

where the average number density $\rho^{(1)}$ in singlet space is uniform and equal to the reciprocal of the volume per molecule, and R_{12} is the scalar distance in the relative configuration space of a representative molecular pair. As is well known, the radial distribution function may be determined experimentally by the x-ray scattering technique.[1]

The thermodynamic functions of a liquid are related to the potential of intermolecular force $V(R)$ and the radial distribution function by the theories of Kirkwood,[2] Born and Green,[3] Mayer,[4] and Yvon,[5] which are basically equivalent although differing in certain details. The equation of state is given by

$$\frac{pv}{NkT}=1-\frac{2\pi N}{3vkT}\int_0^\infty R^3\frac{dV}{dR}g(R)dR, \tag{3}$$

the internal energy by

$$\frac{E}{NkT}=\frac{3}{2}+\frac{2\pi N}{vkT}\int_0^\infty R^2V(R)g(R)dR, \tag{4}$$

and the chemical potential by

$$\frac{\mu}{NkT}=\log p+\frac{\mu^E}{NkT}+\frac{\mu^*(T)}{NkT};\quad \mu^*(T)=\lim_{p\to 0}[\mu-NkT\log p]$$

$$\mu^E=\frac{4\pi N^2}{v}\int_0^1\int_0^\infty R^2V(R)g(R,\xi)dRd\xi -NkT\log\frac{pv}{NkT}, \tag{5}$$

* This work was carried out under Task Order XIII of Contract N6onr-244 between the ONR and the California Institute of Technology.

[1] F. Zernike and J. A. Prins, Zeits. f. Physik **41**, 184 (1927); P. Debye and H. Menke, Physik. Zeits. **31**, 797 (1930); B. E. Warren, J. App. Phys. **8**, 645 (1937); A. Eisenstein and N. S. Gingrich, Phys. Rev. **62**, 261 (1942).

[2] J. G. Kirkwood, J. Chem. Phys. **3**, 300 (1935).

[3] M. Born and H. S. Green, Proc. Roy. Soc. **A188**, 10 (1946).

[4] J. E. Mayer, J. Chem. Phys. **15**, 187 (1947).

[5] J. Yvon, *Actualités Scientifiques et Industrielles* (Hermann et Cie, Paris, 1935), p. 203. Because of its relative inaccessibility, the pioneering work of Yvon has been largely overlooked by other investigators.

where $g(R, \xi)$ is the radial distribution function for a pair of molecules, one of which, i, is partially coupled to those of the rest of the fluid, corresponding to a potential of intermolecular force,

$$V_N(\xi)=V_{N-1}+\xi\sum_{k=1}^{N}V(R_{ik}). \tag{6}$$

$\mu^*(T)$ is the ideal gas reference value of the chemical potential, depending on temperature alone.

Systems of integro-differential equations for the average densities in the configuration space of subsets of n molecules of a liquid have been developed in equivalent forms by Kirkwood,[2] Born and Green,[3] Mayer,[4] and Yvon.[5] In general, one has

$$\rho^{(n)}=\frac{N!}{(N-n)!}\frac{1}{v^n}e^{-\beta W^{(n)}}$$

$$\beta=1/(kT), \tag{7}$$

where $W^{(n)}$ is the potential of average force acting on the molecular subset n, the resultant of their direct interaction and their average interactions with the other $N-n$ molecules of the liquid. When $W^{(3)}(123)$ is approximated by

$$W^{(3)}(123)=W^{(2)}(12)+W^{(2)}(13)+W^{(2)}(23), \tag{8}$$

where 1, 2, 3 denote the coordinates of a molecular triplet, the several sets of integro-differential equations may be closed to give an integral equation for the pair function and thus for the radial distribution function. This approximation, superposition of mean forces between pairs in a set of triplets may be regarded as analogous to the Hartree approximation in quantum mechanics, applied to the density $\rho^{(3)}$ in the space of triplets as the product of the densities $\rho^{(2)}$ for the sets in the space of molecular pairs. As has been shown by one of us,[6] the corresponding Hartree-like approximation in singlet space leads to the free-volume theory of liquids.

The resulting integral equation for the radial distribution function for a pair of molecules, one of which is partially coupled to other molecules of the fluid according to the potential of Eq. (6), takes the form

$$\log g(R, \xi)=-\beta\xi V(R)$$

$$+\frac{\pi N}{vR}\int_0^\infty[K(R-r, \xi)-K(R+r, \xi)]r[g(r)-1]dr,$$

$$K(t, \xi)=-2\beta\int_0^\xi\int_{|t|}^\infty sV(s)g(s, \xi)dsd\xi; \quad \text{K}$$

$$K(t, \xi)=\beta\xi\int_{|t|}^\infty(s^2-t^2)\frac{dV}{ds}g(s, \xi)ds; \quad \text{BGY} \tag{9}$$

[6] J. G. Kirkwood, J. Chem. Phys. **18**, 380 (1950).

where now as henceforth $g(r)$ denotes $g(r, 1)$, with $\xi=1$. The kernel designated by K refers to the Kirkwood theory and that designated by BGY refers to the Born-Green-Yvon theory. Although the original sets of integro-differential equations in the two theories are exact, the superposition approximation, Eq. (8), leads to the two different kernels of Eq. (9). The numerical discrepancies, reflecting the influence of the superposition approximation are not great and will be discussed later. Since the essentials of the derivation of Eqs. (9) have been given elsewhere[2,3,7] they will not be reproduced here.

The potential of intermolecular force $V(R)$ is conveniently expressed in the form,

$$V(R)=\epsilon\gamma(x),$$
$$x=R/a, \tag{10}$$

where ϵ is an energy and a is a length characteristic of the molecules. Thus for a Lennard-Jones potential, we have

$$\gamma(x)=(1/x^n)-(1/x^6) \tag{11}$$

where n is an exponent in the neighborhood of 12 and a and ∞ are the two values of R for which $V(R)$ vanishes. For rigid spheres,

$$\lim_{\epsilon\to\infty}e^{-\beta\epsilon\gamma(x)}=0; \quad 0\leqslant x\leqslant 1,$$
$$=1; \quad x>1, \tag{12}$$

where a is the diameter of the spheres. If we define a function $\psi(x)$ by the relation

$$g(x, \xi)=e^{-\beta\xi\epsilon\gamma(x)+[\psi(x, \xi)/x]},$$
$$g(-x)=g(x),$$
$$\gamma(-x)=\gamma(x),$$
$$\psi(-x)=-\psi(x), \tag{13}$$

and extend the definitions of $g(x)$ and $\gamma(x)$ to the negative real axis by means of the last three of Eqs. (13), the integral equation, Eq. (9), becomes

$$\psi(x, \xi)=\frac{\lambda_0}{4}\int_{-\infty}^{\infty}K(x-s, \xi)s[g(s)-1]ds$$

$$\lambda_0=(4\pi Na^3)/v$$

$$K(t, \xi)=-2\beta\epsilon\int_{|t|}^\infty\int_0^\xi s\gamma(s)g(s, \xi)d\xi ds; \quad \text{K}$$

$$K(t, \xi)=\xi\beta\epsilon\int_{|t|}^\infty(s^2-t^2)\frac{d\gamma(s)}{ds}g(s, \xi)ds; \quad \text{BGY}. \tag{14}$$

The solution of Eq. (14) with the Lennard-Jones potential, Eq. (11), by numerical methods with the use of International Business Machine equipment is at present under investigation. Since direct iterative operation on a sequence of trial functions $g(s)$ with the integral

[7] J. G. Kirkwood and E. M. Boggs, J. Chem. Phys. **10**, 394 (1942).

operator $\int_{-\infty}^{\infty} ds K(x-s)$ in general fails to give convergent results for values of λ_0 appropriate to liquid densities, other methods are being developed, which depend on starting with a relatively good zero approximation to $g(s)$. In order to obtain a set of trial functions for the zero approximation base, as well as for their intrinsic interest, we have undertaken the integration of Eq. (14) for fluids composed of rigid spheres.

For rigid spheres, Eq. (14) becomes,

$$\begin{aligned}\psi(x)&=\frac{\lambda}{4}\int_{-\infty}^{\infty} K_0(x-s)s[g(s)-1]ds\\ g(s)&=e^{\psi(s)/s} \quad |s|\geqslant 1\\ &=0 \quad |s|<1\\ K_0(t)&=t^2-1 \quad |t|\leqslant 1\\ &=0 \quad |t|>1 \end{aligned} \tag{15}$$

where $\psi(x)$ denotes $\psi(x, 1)$. The parameter λ is related to the density in different ways according to the Kirkwood theory and the Born-Green theory (see Appendix)

$$\begin{aligned}&[g_1(\lambda)]^{-\frac{1}{2}}\int_0^{\lambda}[g_1(\lambda')]^{-\frac{1}{2}}d\lambda'=4\pi\sqrt{2}v_0/v; \quad \text{K}\\ &[g_1(\lambda)]^{-1}\lambda=4\pi\sqrt{2}(v_0/v); \quad \text{BG}\\ &v_0=Na^3/\sqrt{2},\end{aligned} \tag{16}$$

where v_0 is the close-packed volume of the system of spheres and $g_1(\lambda)$ denotes $g(1+\epsilon, \lambda)$ as $\epsilon\to+0$. The two systems of integro-differential equations underlying the Kirkwood and the Born and Green theories are equivalent and exact. However, the superposition approximation in the space of triplets leads to different equations in the space of pairs. The discrepancy reflected in Eq. (16) is thus a measure of the error produced by this approximation.

Equation (15), linearized with respect to the function $\psi(x)$, assumes the form,

$$\begin{aligned}\psi(x)=\frac{\lambda}{4}\int_{-\infty}^{\infty} K_0(x-s)[&A\{|s|-1\}\psi(s)\\ &-[1-A\{|s|-1\}]s]ds,\\ A\{t\}&=1 \quad t\geqslant 0,\\ &=0 \quad t<0,\end{aligned} \tag{17}$$

where $A(t)$ is the unit step-function. Equation (17) has been given approximate analytical solutions by Kirkwood and Boggs[7] for several values of λ. The present numerical solutions of the non-linear equation, Eq. (15), cover a wider range of the parameter λ than those of Kirkwood and Boggs. For the same values of λ in the linear approximation, they are found to agree with the analytical solutions for large values of x and to correct the latter in the neighborhood of the first peak of the radial distribution function.

II.

We shall now describe the methods employed in the numerical solution of Eq. (15), which we write in the form

$$\begin{aligned}\psi(x)&=\frac{\lambda}{4}\int_{-\infty}^{\infty} K_0(x-s)\varphi(s)ds\\ \varphi(x)&=x[g(x)-1]\\ g(x)&=A(|x|-1)e^{\psi(x)/x}.\end{aligned} \tag{18}$$

The resolvent kernel $k(t)$ of $K_0(t)$ may be expressed in the form[8]

$$\begin{aligned}k(t)&=-\frac{\lambda}{\pi}\int_0^{\infty}\frac{G(u)}{1-\lambda G(u)}\cos utdu\\ G(u)&=\frac{1}{4}\int_{-\infty}^{\infty}K_0(t)e^{iut}dt=\frac{u\cos u-\sin u}{u^3}.\end{aligned} \tag{19}$$

By the method of Fourier transforms, we obtain from Eq. (18)

$$\begin{aligned}\psi(x)&=-\int_{-\infty}^{\infty}k(x-s)f(s)ds\\ f(x)&=\varphi(x)-\psi(x)\end{aligned} \tag{20}$$

from which $\psi(x)$ may be determined for $x>1$ when $f(x)$ is known. An alternative form of Eq. (20) is

$$f(x)=\varphi(x)+\int_{-\infty}^{\infty}k(x-s)f(s)ds. \tag{21}$$

In the linear approximation,

$$\begin{aligned}&\varphi_0(x)=A\{|x|-1\}\psi_0(x)-[1-A\{|x|-1\}]x\\ &f_0(x)=0; \quad x>1\\ &\varphi_0(x)=-x; \quad x\leqslant 1\end{aligned} \tag{22}$$

and Eqs. (20) and (21) become

$$\begin{aligned}f_0(x)&=-x+\int_{-1}^{+1}k(x-s)f_0(s)ds; \quad x<1\\ \psi_0(x)&=-\int_{-1}^{+1}k(x-s)f_0(s)ds; \quad x>1.\end{aligned} \tag{23}$$

The first of Eqs. (23) determines $f_0(x)$ and the second determines the linear approximation $\psi_0(x)$ for $x>1$. In this approximation the determination of $g(x)$ thus reduces to the solution of a linear integral equation for $f_0(x)$ on the finite interval $-1<x<+1$, with the resolvent kernel $k(t, \lambda)$.

The resolvent kernel $k(t, \lambda)$ was calculated for a suitable range of the parameter, $\lambda=5$, 10, 20, 27.4, with the use of IBM equipment and the file of punched cards of $\sin ut$ employed in these laboratories for electron

[8] E. C. Titchmarsh, *Introduction to the Theory of Fourier Integrals* (Oxford University Press, London, 1948), pp. 303–305.

TABLE I.[a] Radial distribution functions for several values of parameter λ. $x[g(x)-1]$ as a function of x.

x \ λ	5	10	20	27.4	33
1.00	0.45	0.80	1.36	1.66	1.85
1.08	0.39	0.66	1.08	1.36	1.62
1.16	0.32	0.53	0.83	1.04	1.25
1.24	0.26	0.40	0.59	0.73	0.87
1.32	0.20	0.29	0.37	0.44	0.47
1.40	0.15	0.18	0.18	0.16	0.11
1.48	0.09	0.09	0.01	−0.08	−0.19
1.56	0.05	0.01	−0.12	−0.26	−0.41
1.64	0.01	−0.05	−0.22	−0.39	−0.56
1.72	−0.02	−0.10	−0.29	−0.46	−0.64
1.80	−0.04	−0.13	−0.31	−0.48	−0.63
1.88	−0.05	−0.13	−0.28	−0.41	−0.52
1.96	−0.05	−0.10	−0.18	−0.25	−0.29
2.04	−0.03	−0.05	−0.03	0.02	0.10
2.12	−0.02	−0.01	0.09	0.24	0.44
2.20	0.00	0.02	0.16	0.34	0.63
2.28	0.00	0.04	0.18	0.38	0.65
2.36	0.01	0.04	0.17	0.32	0.52
2.44	0.01	0.04	0.13	0.22	0.30
2.52	0.01	0.03	0.07	0.09	0.06
2.60	0.01	0.02	0.01	−0.03	−0.16
2.68	0	0.01	−0.04	−0.13	−0.32
2.76		0.00	−0.07	−0.20	−0.42
2.84		−0.01	−0.09	−0.24	−0.45
2.92		−0.01	−0.09	−0.21	−0.38
3.00		−0.01	−0.07	−0.15	−0.25
3.08		−0.01	−0.04	−0.06	−0.03
3.16		−0.01	0.00	0.03	0.14
3.24		0	0.02	0.09	0.29
3.32			0.04	0.15	0.41
3.40			0.05	0.17	0.36
3.48			0.05	0.14	0.28
3.56			0.04	0.09	0.14
3.64			0.02	0.03	0.00
3.72			0.00	−0.02	−0.12
3.80			−0.01	−0.06	−0.23
3.88			−0.02	−0.10	−0.28
3.96			−0.02	−0.11	−0.26
4.04			−0.02	−0.08	−0.20
4.12			−0.02	−0.05	−0.11
4.20			−0.01	−0.02	0.00
4.28			0.00	0.02	0.11
4.36			0.00	0.04	0.18
4.44			0.01	0.06	0.24
4.52			0.01	0.07	0.22
4.60			0.01	0.06	0.15
4.68			0.01	0.03	0.08
4.76			0.01	0.01	−0.01
4.84			0	−0.01	−0.09
4.92				−0.03	−0.15
5.00				−0.03	−0.19
5.08				−0.03	−0.18

TABLE I.—*Continued.*

x \ λ	5	10	20	27.4	33
5.16				−0.03	−0.13
5.24				−0.02	−0.06
5.32				0.00	0.01
5.40				0.01	0.07
5.48				0.02	0.12
5.56				0.02	0.16
5.64				0.02	0.14
5.72				0.02	0.10
5.80				0.01	0.05
5.88				0.00	−0.01
5.96				0.00	−0.06
6.04				0.00	−0.10
6.12				0.00	−0.13
6.20				−0.01	−0.12
6.28				−0.01	−0.08
6.36				−0.01	−0.03
6.44				−0.01	0.01
6.52				0	0.05
6.60					0.08
6.68					0.09
6.76					0.08
6.84					0.05
6.92					0.02
7.00					0.00
7.08					−0.02
7.16					−0.07
7.24					−0.07
7.32					−0.06
7.40					−0.05
7.48					−0.02
7.56					0.00
7.64					0.02
7.72					0.03
7.80					0.04
7.88					0.04
7.96					0.03
8.04					0.02
8.12					0.01
8.20					−0.01
8.28					−0.02
8.36					−0.02
8.44					−0.02
8.52					−0.02
8.60					−0.01
8.68					−0.01
8.76					0.00
8.84					0.00
8.92					0.00
9.00					0.01
9.08					0.01
9.16					0.01
9.24					0.01
9.32					0.01
9.40					0.01
9.48					0

[a] The solutions $g(x)$ were checked by direct iteration in Eq. (15) at intervals of 0.04 in x. The input $g(x)$ checked with the output $g(x)$ to ± 0.005 for $\lambda = 5$, 10, and 20, and to ± 0.02 for $\lambda = 27.4$ and 33.

diffraction calculation.[9] For these calculations it was transformed by partial integration in the following manner,

$$k(t) = -\frac{\lambda}{\pi t}\int_0^\infty \frac{3uG(u)+\sin u}{u^2[1-\lambda G(u)]^2}\sin utdu. \qquad (24)$$

Convolution operations with the kernel $k(x-s)$ involved in the solution of Eqs. (23) were then carried out on desk calculators.

Since, except for small values of λ, the kernel $k(t)$ possesses one or more eigenvalues less than unity,[10] solution of Eq. (23) by direct iteration fails to give convergent results (see Appendix). In order to overcome this difficulty, $k(t)$ is expressed in the form

$$k(t) = k_0(t) + k_1(t),$$
$$k_0(t) = A_0 + A_1\cos\gamma_1 t + A_2\cos\gamma_2 t, \qquad (25)$$

where the parameters A_0, A_1, A_2, γ_1, and γ_2 are chosen by trial to give $\int_0^2 k_1(t)^2 dt$ a sufficiently small value to raise all of the eigenvalues of $k_1(t)$, which may be shown

[9] Shaffer, Schomaker, and Pauling, J. Chem. Phys. **14**, 659 (1946).

[10] R. Courant and D. Hilbert, *Methoden der Mathematischen Physik* (Interscience Publishers, Inc., New York), Vol. I, pp. 104–110, 1943.

to be bounded below by $[2\int_0^2(2-t)k_1^2(t)dt]^{-\frac{1}{2}}$, above unity.[10] When this condition is fulfilled, $f_0(x)$ may be represented by the convergent sum

$$f_0(x)=\sum_{n=0}^{\infty} f_{0,n}(x), \tag{26}$$

where

$$f_{0,n}(x)=\sigma_{0,n}(x)+\int_{-1}^{+1} k_0(x-s)f_{0,n}(s)ds,$$

$$\sigma_{0,0}(x)=-x,$$

$$\sigma_{0,n}(x)=\int_{-1}^{+1} k_1(x-s)f_{0,n-1}(s)ds. \tag{27}$$

Since the approximate kernel $k_0(x-s)$ is chosen in degenerate form, the sequence of integral equations, Eq. (27), are solvable in closed form,

$$f_{0,n}(x)=\sigma_{0,n}(x)+2A_1M_{1,n}\sin\gamma_1x+2A_2M_{2,n}\sin\gamma_2x,$$

$$M_{1,n}=\int_0^1 f_{0,n}(s)\sin\gamma_1sds,$$

$$M_{2,n}=\int_0^1 f_{0,n}(s)\sin\gamma_2sds, \tag{28}$$

where the $M_{\alpha,n}$ are to be determined in each case by solving a set of two linear equations, following from their definition and the first of Eqs. (28). Several iterations, the number increasing with increasing values of λ, suffice to determine $f_0(x)$, which upon substitution in Eq. (23) yields the desired solution of the linearized problem.

In the non-linear case, $f(x)$ of Eqs. (20) and (21) no longer vanishes outside the interval $-1\leqslant x\leqslant+1$. Nevertheless, we write Eq. (21) in the form

$$f(x)=\sigma(x)+\int_{-1}^{+1} k(x-s)f(s)ds,$$

$$\sigma(x)=-x+\int_1^{\infty} k(x-s)f(s)ds+\int_{-\infty}^{-1} k(x-s)f(s)ds \quad x\leqslant 1, \tag{29}$$

and consider the sequence of integral equations,

$$f_n(x)=\sigma_n(x)+\int_{-1}^{+1} k(x-s)f_n(s)ds \quad x\leqslant 1,$$

$$\sigma_n(x)=-x+\int_1^{\infty} k(x-s)f_{n-1}(s)ds+\int_{-\infty}^{-1} k(x-s)f_{n-1}(s)ds,$$

$$f_n(x)=x[e^{[\psi_n(x)/x]}-1]-\psi_n(x) \quad x>1,$$

$$\psi_n(x)=-\int_{-1}^{+1} k(x-s)f_n(s)ds-\int_1^{\infty} k(x-s)f_{n-1}(s)ds-\int_{-\infty}^{-1} k(x-s)f_{n-1}(s)ds. \tag{30}$$

Starting with the solution of Eq. (23) as $f_0(x)$ with $\sigma_0(x)=-x$, and solving each of the linear integral equations, Eq. (30), by the method employed in the solution of Eq. (23), we find that the sequence $\psi_n(x)$ converges to the solution $\psi(x)$ of the non-linear integral equation, Eq. (18). All solutions are finally tested by direct iteration with the kernel $K_0(x-s)$ of Eq. (18).

For large values of the parameter λ, convergence is slow by the method of solution described here. However, when a moderately good approximation $\psi^0(x)$ has been obtained by this method, it may be refined by the following iterative procedure. If we linearize Eq. (18) with respect to the error $\omega(x)$, equal to $\psi(x)-\psi^0(x)$, we find,

$$\psi(x)=\psi^0(x)+\omega(x),$$

$$\omega(x)=L\omega+O(\omega^2),$$

$$L\omega=\nu(x)+\frac{\lambda}{4}\int_{-\infty}^{\infty} K_0(x-s)A\{|s|-1\}\times\exp\left[\frac{\psi^0(s)}{s}\right]\omega(s)ds$$

$$\nu(x)=\frac{\lambda}{4}\int_{-\infty}^{\infty} K_0(x-s)\varphi^0(s)ds-\psi^0(x) \tag{31}$$

where L is an inhomogeneous linear operator and $\nu(x)$ is the iterative defect of the trial function $\psi^0(x)$. Let us consider the sequence

$$\psi^{(n)}(x)=\psi^{(n-1)}(x)+\omega^{(n)}(x)$$

$$\omega^{(n)}(x)=L^{(n)}\omega^{(n)}$$

$$L^{(n)}\omega^{(n)}=\nu^{(n)}(x)+\frac{\lambda}{4}\int_{-\infty}^{\infty} K_0(x-s)A\{|s|-1\}\times\exp\left[\frac{\psi^{(n-1)}(s)}{s}\right]\omega^{(n)}(s)ds$$

$$\nu^{(n)}(x)=\frac{\lambda}{4}\int_{-\infty}^{\infty} K_0(x-s)\varphi^{(n-1)}(s)ds-\psi^{n-1}(x), \tag{32}$$

where $\omega^{(n)}$ exactly satisfies the linear equation, $L^{(n)}\omega^{(n)}=\omega^{(n)}$, and $\psi^0(x)$ is the first member of the sequence $\psi^{(n)}$. We now define a sequence

$$\omega_0{}^{(n)}=\nu^{(n)}(x),$$

$$\omega_1{}^{(n)}=L^{(n)}\omega_0{}^{(n)},$$

$$\omega_2{}^{(n)}=L^{(n)}\omega_1{}^{(n)},$$

$$\omega_3{}^{(n)}=\alpha^{(n)}\omega_1{}^{(n)}+(1-\alpha^{(n)})\omega_0{}^{(n)},$$

$$\Delta_{kk'}{}^{(n)}=\int_{-\infty}^{\infty}\chi_k{}^{(n)}\chi_{k'}{}^{(n)}dx;\ \chi_k{}^{(n)}=L^{(n)}\omega_k{}^{(n)}-\omega_k{}^{(n)}. \quad (33)$$

The value of α which minimizes $\Delta_{33}{}^{(n)}$ is given by

$$\alpha^{(n)}=(\Delta_{00}{}^{(n)}-\Delta_{01}{}^{(n)})/(\Delta_{11}{}^{(n)}+\Delta_{00}{}^{(n)}-2\Delta_{01}{}^{(n)})$$

$$\frac{\Delta_{33}{}^{(n)}}{\Delta_{00}{}^{(n)}}=1-\epsilon^{(n)} \quad \epsilon^{(n)}=\frac{1}{\Delta_{00}{}^{(n)}}\frac{[\Delta_{00}{}^{(n)}-\Delta_{01}{}^{(n)}]^2}{\Delta_{11}{}^{(n)}+\Delta_{00}{}^{(n)}-2\Delta_{01}{}^{(n)}}. \quad (34)$$

The denominator in the expression for $\epsilon^{(n)}$ is positive by the Schwarz inequality. Thus $\epsilon^{(n)}$ is positive and we have,

$$0\leqslant\Delta_{33}{}^{(n)}/\Delta_{11}{}^{(n)}\leqslant 1. \quad (35)$$

Repetition of this cycle will, except in singular cases, lead to a sequence $\omega_k{}^{(n)}(x)$ which converges in the mean to the solution $\omega^{(n)}(x)$ of the linear equation, $L^{(n)}\omega^{(n)}=\omega^{(n)}$, of Eq. (32). However, the most economical path to a solution of the non-linear problem is through the sequence

$$\psi_3{}^{(n)}=\psi_3{}^{(n-1)}+\omega_3{}^{(n)}, \quad (36)$$

where $\omega_3{}^{(n)}$ is given by Eqs. (33) and (34). Except in singular cases $\psi_3{}^{(n)}$ converges to the solution $\psi(x)$ of the non-linear equation Eq. (18).

III.

The methods described in Section II have been used to calculate $g(x,\lambda)$ for the fluid of rigid spheres for values of the parameter λ equal to 5, 10, 20, 27.4, and 33. The results of the calculations are presented in Table I and Fig. 1. In Fig. 2, the linear and non-linear solutions of Eq. (18) are compared for λ-27.4. It will be observed that they are appreciably different only in the neighborhood of $x=1$. A comparison of the linear solution for $\lambda=27.4$, with the approximate analytical solution of Kirkwood and Boggs,[7] shows the latter to be somewhat inaccurate in the neighborhood of $x=1$.

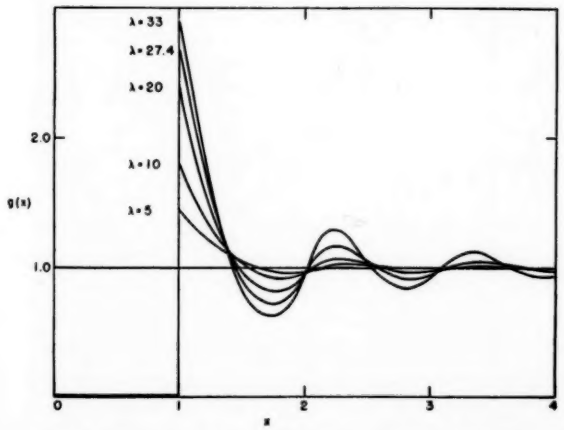

FIG. 1. Radial distribution functions for several values of the parameter λ.

All radial distribution functions exhibit their first peak at $x=1$, decreasing monotonically to the first minimum, which is followed by oscillations of diminishing amplitude resembling those of the experimentally determined radial distribution functions of real liquids.

From the values of $g_1(\lambda)$ obtained from the solutions presented in Table I, the densities corresponding to the family of distribution functions $g(x,\lambda)$ may be determined by means of Eq. (16) according to the Kirkwood theory and according to the Born and Green theory. The densities are presented as a function of λ for the two theories in Table II.

For values of λ equal to or exceeding 34.8, no solutions of Eq. (15) exist for which $x^2[g(x)-1]$ is integrable. This value of λ, corresponding to an expansion v/v_0 equal to 1.24 on the Kirkwood theory and 1.48 on the Born-Green theory evidently represents the limit of stability of a fluid phase of rigid spheres. For greater densities, a crystalline phase is the stable phase.[11] The transition between fluid and crystalline phases cannot be discussed quantitatively without an investigation of distribution functions in the crystalline phase itself. In the case of rigid spheres, it appears likely that the transition may be of second order rather than of first order, although at present this is no more than a surmise. It is also possible that the crystalline phase possesses some intrinsic disorder arising from the inability of rigid spheres to distinguish between next nearest neighbors and the likelihood of stacking errors leading to structures intermediate between the face-centered cubic and the hexagonal close-packed arrangements.

The equation of state, Eq. (3), becomes for rigid spheres,

$$\frac{pv}{NkT}-1=\frac{2\pi\sqrt{2}}{3}\frac{v_0}{v}g_1(\lambda), \quad (37)$$

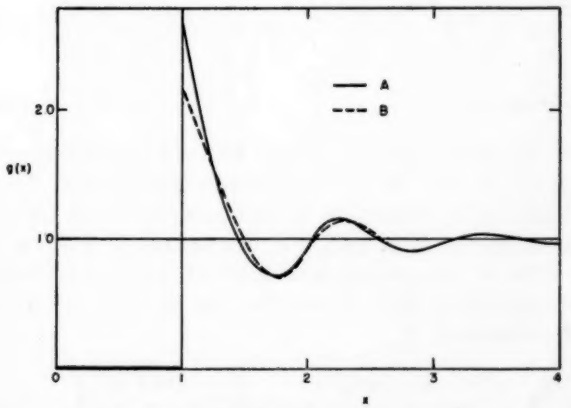

FIG. 2. Radial distribution functions for $\lambda=27.4$. A, solution of non-linear integral equation. B, solution of linear integral equation.

[11] J. G. Kirkwood and E. M. Boggs, J. Chem. Phys. 9, 514 (1941).

TABLE II. Fluid densities as function of λ.[a]

λ	$g_1(\lambda)$	v/v_0 (K)	v/v_0 (BG)
5	1.45	4.74	5.15
10	1.80	2.83	3.20
20	2.36	1.78	2.10
27.4	2.66	1.45	1.73
33	2.85	1.29	1.53
34.8	2.90	1.24	1.48

[a] v/v_0 = ratio of volume to close packed volume of spheres.

where $g_1(\lambda)$ is given as a function of density v/v_0 in Table II. In Table III, $pv/RT-1$ is presented as a function of v/v_0 for both the Kirkwood and the Born-Green theories. This function is also plotted in Fig. 3 together with the free volume[12] expression for rigid spheres,

$$\frac{pv}{RT}-1=\frac{1}{(v/v_0)^{\frac{1}{3}}-1}, \tag{38}$$

where v_0 is the close-packed volume of a face-centered cubic lattice rather than that of the simple cubic lattice originally used by Eyring and Hirschfelder.

The excess molal entropy, S^E, of a fluid phase is defined by the relation,

$$S=-R\log p+S^*(T)+S^E$$

$$S^E=\int_0^p\left[\frac{R}{p}-\left(\frac{\partial v}{\partial T}\right)_p\right]dp$$

$$S^*(T)=\lim_{p\to 0}[S+R\log p]. \tag{39}$$

For the fluid of rigid spheres,

$$\frac{S^E}{R}=\frac{-A^E}{RT}=-\frac{\mu^E}{RT}+\left[\frac{pv}{RT}-1\right],$$

$$\frac{S^E}{R}=\frac{2\pi\sqrt{2}}{3}\int_\infty^{v/v_0}\frac{g_1[\lambda(y)]}{y^2}dy+\log\left[1+\frac{2\pi\sqrt{2}}{3}\frac{v_0}{v}g_1\right],$$

$$y=v/v_0, \tag{40}$$

since the excess internal energy E^E vanishes. The excess entropy in the Born-Green approximation has been calculated by numerical integration, with the use of the second of Eqs. (40) and the values of $g_1(\lambda)$ as a function of v/v_0 presented in Table II. In the Kirkwood approximation, Eq. (5) and the first of Eqs. (40) yield the expression,

$$\frac{S^E}{R}=-\frac{\lambda}{3}+\frac{2\pi\sqrt{2}}{3}\frac{v_0}{v}g_1+\log\left[1+\frac{2\pi\sqrt{2}}{3}\frac{v_0}{v}g_1\right], \tag{41}$$

from which the excess entropy has been calculated with the aid of the data of Table II. The results of the two calculations are presented in Table IV.

It will be remarked that the agreement between the Kirkwood and the Born-Green approximations is moderately good both for the equation of state and for the entropy. In the case of the equation of state, the free volume theory yields a result which does not deviate greatly from either the Kirkwood or the Born-Green results, the departures becoming smaller as the density increases toward close-packing.

APPENDIX

1. The relation between the density Na^3/v and the parameter λ may be derived for the Kirkwood theory with the following thermodynamic equation, the equation of state, Eq. (37), and the expression for the chemical potential Eq. (34c) given by Kirkwood and Boggs,[7]

$$\frac{1}{RT}\left(\frac{\partial\mu}{\partial v}\right)_T=\frac{v}{RT}\left(\frac{\partial p}{\partial v}\right)_T, \tag{42}$$

$$\frac{\mu}{RT}=-\log v+\frac{\lambda}{3}+\frac{\mu^*(T)}{RT} \tag{34c}$$

$$\frac{p}{RT}=\frac{1}{v}+\frac{2\pi\sqrt{2}}{3}\frac{v_0}{v^2}g_1(\lambda), \tag{37}$$

where $g_1(\lambda)$ is $g(1+\epsilon)$ as $\epsilon\to+0$. By differentiating the last two equations with respect to v and equating their derivatives by the first expression, we get

$$-\frac{1}{v}+\frac{1}{3}\frac{d\lambda}{dv}=-\frac{1}{v}+\frac{2\pi\sqrt{2}}{3}v_0v\left[\frac{d}{dv}\left(\frac{g_1(\lambda)}{v^2}\right)\right]; \tag{43}$$

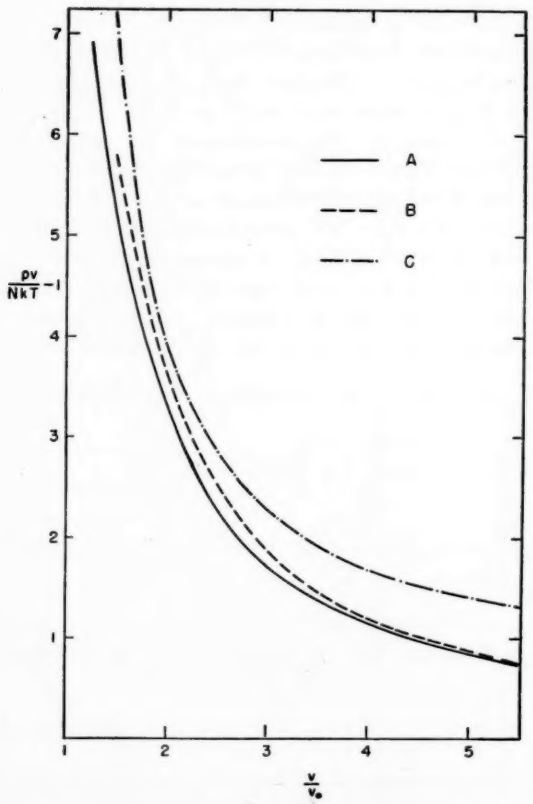

FIG. 3. Equation of state: $pv/RT-1$ as function of v/v_0. A, Kirkwood basis. B, Born and Green, C, free-volume theory. v = volume per mole, v_0 = volume per mole in close-packed arrangement.

[12] H. Eyring and J. O. Hirschfelder, J. Phys. Chem. 41, 249 (1937).

TABLE III. Equation of state of the fluid of rigid spheres.

v/v_0[a]	$pv/RT-1$ (K)	$pv/RT-1$ (BG)
8.38	0.44	0.44
4.74	0.91	0.93
3.48	1.39	1.46
2.83	1.89	2.04
2.42	2.40	2.65
2.15	2.91	3.21
1.94	3.43	3.75
1.78	3.93	4.33
1.64	4.44	4.96
1.53	4.95	5.54
1.44	5.46	
1.37	5.99	
1.30	6.50	
1.24	6.93	

[a] For values of the Kirkwood parameter $\lambda=2.5, 5.0, \cdots$, except for the last point, $\lambda=34.8$.

TABLE IV. Excess entropy of the fluid of rigid spheres as a function of density.

v/v_0	S^E/R (K)	S^E/R (BG)
8.38	−0.03	−0.03
4.74	−0.12	−0.11
3.48	−0.24	−0.23
2.83	−0.39	−0.37
2.42	−0.55	−0.56
2.15	−0.73	−0.76
1.94	−0.92	−1.00
1.78	−1.14	−1.23
1.64	−1.37	−1.49
1.53	−1.60	−1.77
1.44	−1.84	
1.37	−2.07	
1.30	−2.32	
1.24	−2.60	

hence, introducing $z=v/[g_1(\lambda)]^{\frac{1}{3}}$,

$$\frac{d\lambda}{[g_1(\lambda)]^{\frac{1}{3}}}=-4\pi Na^3\frac{dz}{z^2};\quad Na^3=\sqrt{2}v_0, \tag{44}$$

and integration with the limits (λ, v) and $(\lambda=0, v=\infty)$ yields Eq. (16, K).

2. The divergence of a direct iteration attempt to solve Eq. (23) may be seen by considering

$$f(x)=\sigma(x)+\int_a^b k(x,s)f(s)ds,$$

$$f^{(n)}(x)=\sigma(x)+\int_a^b k(x,s)f^{(n-1)}(s)ds; \tag{45}$$

hence, by subtraction,

$$\Delta f^{(n)}=f-f^{(n)}=\int_a^b k(x,s)\Delta f^{(n-1)}(s)ds, \tag{46}$$

where $f(x)$ is the exact solution of the linear integral equation whose inhomogeneous part is $\sigma(x)$, $f^{(n-1)}(x)$ is a trial solution, and $f^{(n)}(x)$ the iterate of the trial solution. Using a representation for the real symmetric kernel $k(x,s)$ in terms of its orthonormal set of eigenfunctions χ_i and its eigenvalues λ_i, and expanding $\Delta f^{(n-1)}$ in the form,

$$k(x,s)=\Sigma_i\frac{\chi_i(x)\chi_i(s)}{\lambda_i},$$

$$\Delta f^{(n-1)}(s)=\Sigma_j a_j^{(n-1)}\chi_j(s), \tag{47}$$

leads by substitution into Eq. (46) to

$$\Delta f^{(n)}(x)=\Sigma_j\frac{a_j^{(n-1)}\chi_j(x)}{\lambda_j}=\Sigma_j a_j^{(n)}\chi_j(x),$$

$$a_j^{(n)}=\frac{a_j^{(n-1)}}{\lambda_j}. \tag{48}$$

Thus $a_j^{(n-1)}$ is increased by $1/\lambda_j$ after each iteration, hence divergence occurs if for any $|\lambda_j|<1$ $a_j^{(n-1)}\neq 0$, because then

$$\left|\frac{a_j^{(n)}}{a_j^{(n-1)}}\right|>1$$

and $\Delta f^{(n)}$ increases in magnitude with each iteration.

Isotope Effect on Bond Rupture by Electron Impact on Hydrogen, Deuterium, and Tritium*

OLIVER A. SCHAEFFER AND JULIUS M. HASTINGS
Brookhaven National Laboratory, Upton, Long Island, New York
(Received March 27, 1950)

The relative yields by electron impact of atomic and molecular ions, x^+/x_2^+ ratios, from hydrogen, deuterium, and tritium have been measured with a 60° sector type mass spectrometer. It is shown that the major part of the previous disagreement between calculated and observed values can be understood on the basis of voltage discrimination by the ion source. By using magnetic scanning and a high ion accelerating voltage the experimental ratios are: $H^+/H_2^+=0.013$, $D^+/D_2^+=0.0070$, $T^+/T_2^+=0.0036$ for 30 volt electrons. These are to be compared with the calculated ratios: $H^+/H_2^+=0.016$, $D^+/D_2^+=0.0072$, $T^+/T_2^+=0.0038$.

THERE have been several experimental and theoretical estimates of the relative yields by electron impact of the atomic and molecular ions for hydrogen and deuterium.[1–3] The electronic energy levels and potential functions of hydrogen and deuterium are well known and when used in conjunction with the Franck-Condon principle provide a means for quantitatively interpreting the products formed by low velocity electron impact.

Although the ratio of the ratios of H^+/H_2^+ and D^+/D_2^+ as determined in a mass spectrometer is in satisfactory agreement with the calculated value, the discrepancy in the individual ratios, X^+/X_2^+, is large. It appears likely that this discrepancy is caused by voltage discrimination[4] in the mass spectrometer source. The investigation of this point together with the availability of a third hydrogen isotope, tritium, led us to undertake the present work.

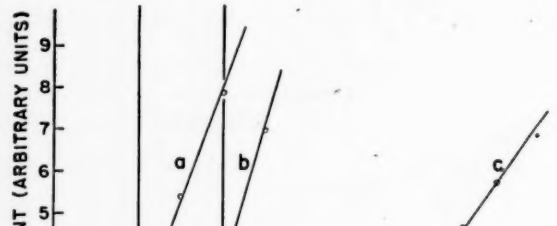

FIG. 1. Ion intensity as a function of electron energy, using a tungsten filament, (a) H^+, (b) D^+, (c) T^+.

EXPERIMENTAL ARRANGEMENT

The mass spectrometer used in this work was a conventional 60° sector type with a six-inch radius of curvature and 0.5 mm slit width. Accelerating voltage was obtained from an electronically regulated 5000 volt power supply which was stable to 0.1 percent. A tungsten filament whose emission was controlled to maintain a fixed trap current furnished the electron beam. The magnet was battery-operated. The positive ion current was measured with a Model 30 Applied Physics Corporation vibrating reed electrometer using a 2×10^{10} ohm input resistor. Except for a few of the early runs, the pressure in the tube before admitting a sample was of the order of 10^{-8} mm Hg. A "hairpin" type flattened copper tube leak was used. With a sample flowing into the tube the pressure never exceeded 10^{-6} mm Hg. The ionization gauge used to measure these pressures was placed in a remote position behind the mass spectrometer source. We believe these readings are valid measures of the pressure in the ionizing region since a close correlation has been found between these pressure readings and the collected ion currents of the mass spectrometer, all other conditions remaining constant. The voltage applied to the ionizing electrons was determined by a Rubicon precision potentiometer together with a precision voltage divider. In every case the masses were identified by a measurement of the magnetic field and accelerating voltage.

The source magnet was aligned by eye so that the electron beam coincided with the center line of the magnet and slight repositioning was made to obtain a maximum ratio of trap current to total emission current. In no case did this ratio fall below 40 percent. For all the measurements reported the ion repeller voltage was maintained constant. For each measurement the other gun voltages were adjusted for maximum positive ion current.

The hydrogen used was Linde tank hydrogen. The deuterium was 99.5 percent pure gas from the Stuart Oxygen Company. Both were used without further purification. A one cm³-atmosphere sample of 90 percent tritium was kindly supplied by the Argonne National Laboratory of the AEC. In order to increase the

* Research carried out under the auspices of the AEC.
[1] Bleakney, Condon, and Smith, J. Phys. Chem. **41**, 197 (1937).
[2] N. Bauer and J. Y. Beach, J. Chem. Phys. **15**, 150 (1947).
[3] D. Stevenson, J. Chem. Phys. **15**, 409 (1947). It should be noted that in this reference there is an error in the constant a of Eq. (4b). The correct value is $a=(2\pi^2\mu c^2\omega_e^2/D_e)^{\frac{1}{2}}$.
[4] N. D. Coggeshall, J. Chem. Phys. **12**, 19 (1944).

pressure of the sample and remove the He^3 decay product, the tritium was condensed into a smaller volume with liquid helium and pumped on for approximately five minutes. We were not, however, completely successful in removing all the He^3.

EXPERIMENTAL RESULTS

The positive ion currents for the atomic ions as a function of electron voltage are shown in Fig. 1. In the curves for H^+ and D^+ a distinct break is present at approximately 4.5 volts above the onset of the ion current. As this corresponds rather closely to the bond energy it appeared that this was caused by the formation of H^+ from hydrogen atoms, and D^+ from deuterium atoms. These atoms could arise either from electron impact or from thermal dissociation on the tungsten filament which operated at about 2500°K. By observing the variation of H^+ ions at 15 electron volts with both sample pressure and trap current it was shown that the positive ion current was proportional to the first power of both pressure and trap current. This indicates that the atoms arise by thermal dissociation. This was later shown to be the case when the mass spectrometer was operated using an oxide-coated cathode which operated near 1000°K. The dissociation constant is several orders of magnitude smaller than at the higher temperature. Figure 2 shows the variation of H^+ as a function of electron voltage using an oxide-coated cathode. Here the previously observed break is absent.

Figure 1c has a break which occurs at about 29 volts which is caused by the residual He^3 in the tritium. Although this curve was obtained with a tungsten filament, there is no break corresponding to the one observed in the hydrogen and deuterium runs. This is due to the fact that the pressure of tritium in the gun was much lower than that of hydrogen and deuterium. Indeed, this break was not observed in samples of deuterium run at pressures comparable to that at which the tritium was run.

Table I lists the observed ratios, X^+/X_2^+ for the three isotopes as well as the ratio of the ratios for various accelerating voltages. It is seen that although the individual ratios show a steady increase with accelerating voltage, the ratio of the ratios are about constant. The steady increase with accelerating voltage is caused by the voltage discrimination of the ion source.

The increased efficiency for the collection of positive ions with increased ion accelerating voltage arises from several sources. One of these is the decreased drift of ions out of the beam during transit of the region between the narrow accelerating and collimating slits. This drift is caused by the random velocities of the ions at the time of formation and by the magnetic acceleration of the ions in the magnetic field of the source magnet. Another, and perhaps the most important, factor in determining the collection efficiency is the increased penetration of the main accelerating field into

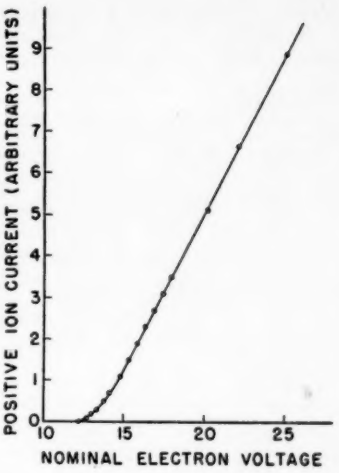

FIG. 2. Ion intensity of H^+ as a function of electron energy using an oxide coated cathode. It should be noted that the voltage scales for Figs. 1 and 2 do not correspond because of the different contact potentials for the two cathodes.

the ionizing region which has a large effect on the number of ions extracted.[5] The drift imposed by the source magnet is most pronounced for low masses. It is for this reason that the least reliance is placed on the H^+/H_2^+ ratio. From the data presented in Table I it is seen that at least 4000 volts must be used to eliminate a large discrimination effect.

A further check on the reliability of the tritium data was afforded by a measurement of the equilibrium constant for the reaction

$$T_2+H_2=2HT.$$

The sample of tritium was at isotopic equilibrium because of the radiation from the tritium decay. Bigeleisen[6] has calculated this equilibrium constant to be 2.56 at 25°C. The observed values listed in Table II are about 13 percent higher than this value after making a correction for the particular type of leak employed.[7] This deviation is not unexpected since the tritium sample contained less than 1 percent H_2 at equilibrium making an accurate measurement of the H_2 abundance difficult. As the ratios measured are also roughly 1 percent, this deviation may be used as a measure of the accuracy of the ratios in Table I.

Previous measurements of these ratios by Hipple[1] gave 0.0096 for H^+/H_2^+ and 0.0034 for D^+/D_2^+ using 22 volt electrons. Bauer and Beach[2] observed 0.0058 for the hydrogen ratio and 0.0038 for deuterium, using 30 volt electrons. Bauer and Beach's results were obtained with a Consolidated Mass Spectrometer. The low values obtained by them can be ascribed to voltage discrimination as they operated at relatively low voltages. Hipple's results were obtained on the 180° deflection mass spectrometer[8] described by Bleakney[9] which could have appreciable voltage discrimination also.

[5] K. T. Bainbridge, "Rapports et Discussions sur Les Isotopes" (Institut Internationale de Chimie Solvay, 1948), p. 97.
[6] J. Bigeleisen, J. Chem. Phys. **18**, 481 (1950).
[7] M. G. Inghram, *Advances in Electronics* (Interscience Publishers, Inc., New York, 1948), p. 235.
[8] J. A. Hipple, private communication.
[9] W. Bleakney, Phys. Rev. **40**, 496 (1932).

TABLE I. Effect of ion accelerating voltage on x^+/x_2^+ peak ratios for hydrogen, deuterium, and tritium with 30 volt electrons.

Ion accelerating voltage (volts)	H^+/H_2^+	D^+/D_2^+	T^+/T_2^+	$\frac{H^+/H_2^+}{D^+/D_2^+}$	$\frac{H^+/H_2^+}{T^+/T_2^+}$	$\frac{D^+/D_2^+}{T^+/T_2^+}$
2500	0.011	0.0057	0.0031	1.9	3.6	1.8
3000	0.012	0.0062	0.0031	1.9	3.9	2.0
3500	0.013	0.0067	0.0035	1.9	3.7	1.9
4200	0.013	0.0070	0.0036	1.8	3.6	1.9

TABLE II. Equilibrium constant for the reaction $H_2+T_2=2HT$. Theoretical value $K=2.56$.*

Ion accelerating voltage (volts)	$\frac{T^+}{T_2^+}$	$K^*=\frac{(HT)^2}{(H_2)(T_2)}$	K^{**}
2500	0.0031	2.9	2.5
3000	0.0031	3.3	2.8
4200	0.0036	3.4	2.9

K^* is calculated from the observed peak heights. K^{**} is corrected for fractionation by the type leak used.

The ratios X^+/X_2^+ for hydrogen and deuterium have been calculated[3] using both the harmonic and anharmonic oscillator approximation to the ground state wave function and assuming the applicability of the Franck-Condon principle to this type of transition. We have made the same calculation for the T^+/T_2^+ ratio. The comparison of this calculation with the observed results is presented in the first two rows of Table III. We believe that this difference, although much smaller than the previous results,[1,2] is still larger than our experimental error.

The calculation involves several approximations, among which are: (1) the use of the Franck-Condon principle rather than the calculation of the quantum mechanical transition probabilities; (2) the approximation to the wave function which is such that the wave function is too large for small internuclear distances and increases the calculated yield of X^+; (3) the assumption that the transition probabilities are independent of the voltage of the ionizing electrons.

It is not difficult to recalculate the ratios, X^+/X_2^+ assuming that the transition probability is linearly related to the excess energy of the electrons above the minimum energy required for the process.[10] The transition probability by impact with electrons of energy E for an internuclear separation r, is then given by

$$T(r, E)=k[E-V(r)], \tag{1}$$

where $V(r)$ is the minimum energy for the process and k is a proportionality constant. If the potential curve for the $^2\Sigma_g^+$ state of H_2^+ is approximated by a Morse curve, $V(r)$ is just

$$V(r)=D\{1-\exp[-a(r-r_e)]\}^2+U \tag{2}$$

where U is the energy difference between the minimum of the potential curve for H_2^+ and the ground vibrational state of H_2. The value of $f(<r_c)$ as defined by Stevenson[3] then becomes

$$f(<r_c)=\int_0^{r_c} T(r,E)\psi^2(r)dr. \tag{3}$$

Using the anharmonic oscillator approximation to ψ and $T(r, E)$ given by (1) and (2), the ratios X^+/X_2^+ are readily calculated and are listed in the third line of Table III. The agreement between these corrected values and the observed results is within experimental error. This may be fortuitous in that the calculated values are extremely sensitive to the value of r_c (all the above calculations were based on $r_c=0.586$A).

The agreement obtained between experimental and calculated ratios shows that, at least for the case of hydrogen, the process of bond rupture accompanying ionization by electron impact can be adequately described by means of the Franck-Condon principle.

We wish to thank the Electronics Group at Brookhaven National Laboratory for the design and construction of some of the electrical equipment used and to acknowledge the many helpful discussions with Dr. J. Bigeleisen and Dr. L. Friedman of this Laboratory.

TABLE III. Comparison between calculated and observed values of x^+/x_2^+ peak ratios for hydrogen, deuterium, and tritium.

	H^+/H_2^+	D^+/D_2^+	T^+/T_2^+	$\frac{H^+/H_2^+}{D^+/D_2^+}$	$\frac{H^+/H_2^+}{T^+/T_2^+}$	$\frac{D^+/D_2^+}{T^+/T_2^+}$
Observed value*	0.013	0.0070	0.0036	1.9	3.7	1.9
Anharmonic oscillator approximation	0.0187	0.0083	0.0044	2.3	4.3	1.9
Corrected value**	0.0159	0.0072	0.0038	2.2	4.2	1.9

* The observed value is for 30 volt electrons and an ion accelerating voltage of 4200 volts.
** These ratios are corrected for the dependence of the transition probabilities on the excess energy of the ionizing electrons.

[10] Coolidge, James, and Present, J. Chem. Phys. 4, 193 (1935).

Thermodynamic Properties of the Internal Rotation in Methyl Alcohol Vapor from 200 to 500°K

J. O. HALFORD
Chemistry Department, University of Michigan, Ann Arbor, Michigan
(Received April 14, 1950)

At ordinary and lower temperatures the thermodynamic properties of the methyl alcohol internal rotation are beyond the limits of available tabulations. For any internal rotator, of a given symmetry, with a fixed moment of inertia and potential barrier, two limiting values of each property can be calculated for any chosen temperature. Available tables are restricted to those cases for which the differences between the limiting values can be neglected. When, as with methyl alcohol, the differences are large, the representative values can be found by taking proper account of the symmetry and the dependence of the internal rotator energy levels upon the external rotations.

For methyl alcohol, the correct intermediate thermodynamic properties are obtained by using for the partition function and its derivatives the numerical mean of the limiting values of these sums obtained for the general rotator. This simple rule, however, is not necessarily applicable to other compounds.

Heat capacities and entropies, calculated from the spectroscopic potential barrier of 932 cal./mole and other molecular constants, are considered in relation to experimental data.

IN a recent paper[1] the height of the barrier to the internal rotation in methyl alcohol was recalculated from the difference between the third law entropy and the statistical entropy for free rotation. Substantially constant barrier calculations were obtained over a considerable temperature range, but deviations toward higher barriers were encountered both above and below the range of constancy. Such deviations are the expected result of inadequacy of the equation of state at the higher temperatures, but are probably due to other factors at lower temperatures. In particular, the low barrier and low moment of inertia cause this system to fall outside the limits of the entropy tables of Pitzer and Gwinn[2] at low temperatures, with the result that the barrier must be obtained by an extrapolation which becomes more doubtful with decreasing temperature.

To remove this uncertainty from the barrier calculation would require an extension of the entropy tables, but, although as will be shown, this can be done for any one compound like methyl alcohol, the results will not necessarily be useful for other compounds. Instead, it is simpler to undertake a direct comparison of the third law entropy with the entropy from molecular constants, using, in the latter, the newly determined spectroscopic barrier of 326 cm^{-1} or 932 cal./mole. The evidence of consistency with changing temperature will then have been shifted from constancy of the calculated barrier to constancy of the difference between the molecular and third law entropies.

The energy levels of the internal rotator occur in bands which permit the calculation of two extreme values of each thermodynamic property between which the correct properties of any rotator must lie. Available tables, and, in fact, any accurate general tables, are limited to those regions of the variables for which the extreme calculated properties are not appreciably different. Because the methyl alcohol system falls outside these limits there are appreciable differences, particularly in the heat capacity, between the extreme calculable properties, and a method must be found for establishing the valid intermediate values.

All of the necessary information about the energy levels is contained in the treatment of this system by Koehler and Dennison,[3] who show how the particular set of internal levels varies with K, the quantum number for rotation of the rigid molecule around the axis of the internal rotation. With their theory it is possible to calculate all the rotational levels, internal and external, and consequently, to obtain the correct thermodynamic properties. The implied detailed calculation for all the rotations would be extremely tedious. It is possible, however, to make simplifications which eliminate much of the detail.

The partition function for rotation, both external and internal, can be written as

$$Q=Q_J Q_K \bar{q}, \tag{1}$$

where Q_J refers to the external rotations with the large moments of inertia, Q_K to the external rotation about an axis approximately parallel to the CO bond and $\bar{q}$ is an effective average partition function for the internal rotation. Q_J and Q_K are equal to the classical partition functions at any temperature within the range of interest, and, further,

$$Q_K=\sum_K \exp(-K^2\beta), \tag{2}$$

with the summation taken over all integral values of K between minus and plus infinity, in spite of the fact that the actual range of K values is limited by J. It is therefore permissible to evaluate Q_J and the product $Q_K\bar{q}$ independently, thus eliminating Q_J from the present problem. There can be little doubt that for temperatures above 200°K the symmetry number approxima-

[1] J. O. Halford, J. Chem. Phys. **18**, 361 (1950).
[2] K. S. Pitzer and W. D. Gwinn, J. Chem. Phys. **10**, 428 (1942).
[3] J. S. Koehler and D. M. Dennison, Phys. Rev. **57**, 1006 (1940).

TABLE I. Energy ($\Delta E/V_0$) of the methyl alcohol internal rotation for $\alpha^2=6.0553$.

l \ θ	0	$\pi/8$	$\pi/4$	$3\pi/8$	$\pi/2$
0	0	0.008469	0.031159	0.058228	0.071306
1	1.014199	0.867439	0.711331	0.602615	0.562179
2	1.136431	1.317257	1.578233	1.872408	2.192515
3	3.788929	3.347544	2.934936	2.551397	2.201638
4	3.789210	4.2593	4.7588	5.2869	5.8423
5	8.3549	7.7840	7.0412	6.4275	5.8423
6	8.3549	9.0545	9.7823	10.5395	11.3487
7	14.7544	13.8532	12.9831	12.1385	11.3487
8	14.7544	15.6826	16.6398	17.6250	18.6395

tion is accurate. This means that for each symmetry class of energy levels the valid average partition function for internal rotation must be the same or nearly the same, and may be expected to lie somewhere near the mean of the extreme calculable values. Exactly what mean value to take, however, is not evident in advance.

For the levels within a single symmetry class, let

$$Q_K\bar{q}=\sum_{iK}\exp(-K^2\beta)\exp(-\epsilon_{iK}), \tag{3}$$

with β equal to $\hbar^2/8\pi^2CkT$ where C is the moment of inertia for external rotation, and ϵ_{iK} equal to E_{iK}/kT where E_{iK} is the excess of internal energy over that of the lowest possible internal rotation level. Since each K defines a specific set of internal levels and, therefore, a partition function, q_K, it is permissible to sum over i at constant K to obtain

$$\bar{q}=[\sum_K q_K\exp(-K^2\beta)]/Q_K. \tag{4}$$

Similarly

$$Q'=Q_K'\bar{q}+Q_K\bar{q}'$$
$$=\sum_{iK}(K^2\beta+\epsilon_{iK})\exp(-K^2\beta)\exp(-\epsilon_{iK}) \tag{5}$$

which leads to

$$\bar{q}'=[-Q_K'\bar{q}+\sum_K q_K K^2\beta\exp(-K^2\beta)$$
$$+\sum_K q_K'\exp(-K^2\beta)]/Q_K. \tag{6}$$

Finally,

$$Q''=Q_K''\bar{q}+Q_K\bar{q}''+2Q_K'\bar{q}'$$
$$=\sum_{iK}(K^2\beta+\epsilon_{iK})^2\exp(-K^2\beta)\exp(-\epsilon_{iK}) \tag{7}$$

with the result that

$$\bar{q}''=[-Q_K''\bar{q}-2Q_K'\bar{q}'+\sum_K q_K K^4\beta^2\exp(-K^2\beta)$$
$$+2\sum_K q_K'K^2\beta\exp(-K^2\beta)$$
$$+\sum_K q_K''\exp(-K^2\beta)]/Q_K. \tag{8}$$

Equations (4), (6), and (8) give the average effective sums for the internal rotation from which the mean thermodynamic properties follow as $-F/T=R\ln\bar{q}$, $H/T=R\bar{q}'/\bar{q}$, $S=R(\bar{q}'/\bar{q}+\ln\bar{q})$ and $C=R(\bar{q}''/\bar{q}-[\bar{q}'/\bar{q}]^2)$. The required calculation is straightforward but very detailed. At room temperature the total number of individual states involved is of the order of 600, divided equally among three symmetry classes. An approximation can be introduced, however, which is quite accurate down to very low temperatures and eliminates much of the detail.

The sums q, q', and q'' are required as functions of K. The energy levels are given by three periodic functions, one-third of them from each function. Each cycle is represented by three units on the scale $\sigma=-KC_1/C$ where C_1 is the moment of inertia of the OH group about the rotational axis. The three functions are the same except for a successive phase difference of one unit on the σ-scale. All the levels can be placed upon the same curve by the following device. Let $E_{iK}=P(\theta_K)$, where $\theta_K=\pi\sigma/3$ for one-third of the levels, $\pi(\sigma+1)/3$ for a second third, and $\pi(\sigma+2)/3$ for the rest. The θ-scale has been chosen, for convenience, so that the solutions repeat themselves at intervals of π-units, in order to avoid half-angles in the final expressions. The function

TABLE II. Partition function $q=\Sigma_i\epsilon^{-\epsilon_i}$ for $\alpha^2=6.0553$.

T \ θ	0	$\pi/8$	$\pi/4$	$3\pi/8$	$\pi/2$
200	1.16259	1.15711	1.14389	1.13066	1.12518
260	1.29146	1.28981	1.28582	1.28183	1.28018
300	1.37948				1.37453
340	1.46624				1.46410
380	1.55075				1.54983
420	1.63267				1.63229
460	1.71198				1.71182
500	1.78874				1.78868

TABLE III. First derivative, $q'=\Sigma_i\epsilon_i\epsilon^{-\epsilon_i}$ for $\alpha^2=6.0553$.

T \ θ	0	$\pi/8$	$\pi/4$	$3\pi/8$	$\pi/2$
200	0.40843	0.42973	0.48119	0.53260	0.55390
260	0.57235	0.58110	0.60225	0.62343	0.63224
300	0.65722				0.68812
340	0.72873				0.74407
380	0.79079				0.79827
420	0.84638				0.84992
460	0.89712				0.89880
500	0.94418				0.94498

TABLE IV. Second derivative $q''=\Sigma_i\epsilon_i^2\epsilon^{-\epsilon_i}$ for $\alpha^2=6.0553$.

T \ θ	0	$\pi/8$	$\pi/4$	$3\pi/8$	$\pi/2$
200	1.04052	1.00477	0.91864	0.83219	0.79642
260	1.17902	1.15138	1.08473	1.01832	0.99123
300	1.23759				1.11051
340	1.29211				1.21397
380	1.34710				1.30164
420	1.40200				1.37773
460	1.45162				1.44513
500	1.51265				1.50654

can be set up by solving for enough energy levels to define the curve from $\theta=0$ to $\theta=\pi/2$. Instead of outlining the function itself, it turns out to be simpler to set up q_K, q_K', and q_K'' in terms of θ_K.

In Table I, the internal energy levels are shown, for a sufficient number of the bands, at five points from $\theta=0$ to $\theta=\pi/2$. They are expressed as $\Delta E/V_0$ where ΔE is the excess of energy above the lowest real level and V_0 is the height of the potential barrier measured from the bottom of the potential valley. The energies are derived from the potential energy function $V=V_0(1-\cos 3\varphi)/2$ essentially by the methods described in an earlier paper,[4] using $V_0=932$ cal./mole, $C_1=1.01\times10^{-40}$, and, therefore, $\alpha=(9/4\pi)\,Q_f^2V/RT=(6.0553)^{\frac{1}{2}}$. In each column either four or five of the higher levels have been obtained by means of the old quantum theory approximation with the aid of a linear scale of fractional quantum numbers. For example, in the last row, at $l=8$, the successive quantum numbers are 4.0, 4.125, 4.250, 4.375, and 4.5.

The energies of Table I have been used to obtain the sums $q=\sum_i e^{-\epsilon_i}$ (Table II), $q'=\sum_i \epsilon_i e^{-\epsilon_i}$ (Table III) and $q''=\sum_i \epsilon_i^2 e^{-\epsilon_i}$ (Table IV).

Examinations of the sums at 200 and 260° in Tables II–IV reveals that, very closely,

$$\begin{aligned} q_K &= q_0 + a\sin^2\theta_K, \\ q_K' &= q_0' + b\sin^2\theta_K, \\ q_K'' &= q_0'' + c\sin^2\theta_K, \end{aligned} \tag{9}$$

where q_0, q_0' and q_0'' are obviously the sums for $\theta=0$, and a, b, and c are constants. Equations (9) effect a considerable simplification of the required summations, and have led to the omission from the tables of the sums at higher temperatures and intermediate values of θ, since these relations must become more accurate with increasing temperature and depend only upon the extreme values of the sums.

Equations (9) and the relations $Q_K'/Q_K=\frac{1}{2}$ and $Q_K''/Q_K=\frac{3}{4}$ are substituted into Eqs. (2), (4), and (6) to yield the results,

$$\bar{q}=q_0+a[\textstyle\sum_K(\sin^2\theta_K)\,\exp(-K^2\beta)]/Q_K \tag{10}$$

$$\begin{aligned} \bar{q}'=q_0'+(q_0-\bar{q})/2+[&a\textstyle\sum_K(\sin^2\theta_K)K^2\beta\,\exp(-K^2\beta) \\ &+b\textstyle\sum_K(\sin^2\theta_K)\,\exp(-K^2\beta)]/Q_K \end{aligned} \tag{11}$$

$$\begin{aligned} \bar{q}''=q_0''+3(q_0-\bar{q})/4+(q_0'-\bar{q}') \\ +[a\textstyle\sum_K(\sin^2\theta_K)K^4\beta^2\exp(-K^2\beta) \\ +2b\textstyle\sum_K(\sin^2\theta_K)K^2\beta\exp(-K^2\beta) \\ +c\textstyle\sum_K(\sin^2\theta_K)\,\exp(-K^2\beta)]/Q_K. \end{aligned} \tag{12}$$

In Eqs. (10)–(12) the sums are taken over all values of K from minus to plus infinity.

From Tables II–IV the constants of Eqs. (9)–(12) are found as shown in Table V.

The energy levels are now separated into individual symmetry classes, for which the above derived summations are made separately, on the ground that the different symmetry classes may have different statistical weights arising from nuclear spin degeneracy. As might be predicted, this separation proves to be unnecessary in the temperature range under consideration. It can be done, however, with very little additional labor, and its inclusion adds weight to the validity of the results. The symmetry classification can be made by examining the quantum numbers of the limiting free rotator, since the presence of the barrier can change neither the symmetry class nor the order of occurrence of the levels. For the free rotator, the energy in arbitrary units is $(m-KC_1/C)^2$, where m and K are integers, and the symmetry class is determined by $K-m$. It is easily shown that, within each of the groups of states distinguished by a particular definition of θ, each symmetry class will recur with each third value of K. If S is an integer one symmetry class (A) will have $K-m=3S$, a second class (E_1) will have $K-m=3S+1$, and, for the third class (E_2), $K-m=3S+2$.

For those states for which $\theta=\pi\sigma/3$, m is always a multiple of 3, and the symmetry is directly determined by K. At $K=0$, the symmetry is A; at $K=1$, it is E_1, and, throughout the series, starting with $K=0$, the order is $A\,E_1\,E_2\,A$ etc., within each of the bands of internal energy levels.

For the other two groups of levels, if $K=0$, $m=\pm1$, for two states, E_1 and E_2, at the same energy, and the correspondence between symmetry and θ classification is not determined. When $\theta=\pi(\sigma+1)/3$, the energy in the lowest band is greater for $K=1$ than for $K=0$, which is possible only if $m=-1$, and $K-m=2$, for symmetry E_2. If $K=2$, with still higher energy, $m=-1$

TABLE V. Constants in Eqs. 9–12.

T	a	b	c
200	−0.03741	0.14547	−0.24410
260	−0.01929	0.05989	−0.18779

TABLE VI. θ values and symmetry classes.

K	0	1	2	3	4
$\pi\sigma/3$	0°(A)	9.309(E_1)	18.618(E_2)	27.927(A)	37.236(E_1)
$\pi(\sigma+1)/3$	60°(E_1)	69.309(E_2)	78.618(A)	87.927(E_1)	97.236(E_2)
$\pi(\sigma+2)/3$	120°(E_2)	129.309(A)	138.618(E_1)	147.927(E_2)	157.236(A)

TABLE VII. Internal rotator thermodynamic properties for methyl alcohol with $C_1=1.01\times10^{-40}$, $V_0=932$ cal./mole. (cal./deg. mole).

T	$-F/T$	H/T	S	C
200	0.267	0.836	1.103	1.244
260	0.499	0.931	1.430	1.241
300	0.636	0.971	1.606	1.219
340	0.759	0.999	1.758	1.197
380	0.871	1.018	1.890	1.175
420	0.974	1.032	2.006	1.155
460	1.067	1.042	2.109	1.138
500	1.156	1.049	2.205	1.123

[4] J. O. Halford, J. Chem. Phys. **18**, 444 (1950).

TABLE VIII. Extreme values of the thermodynamic properties of the internal rotator $\alpha^2=6.0553$ at 200°K.

θ	$-F/T$	H/T	S	C
0	0.299	0.698	0.998	1.533
$\pi/2$	0.234	0.978	1.213	0.925

TABLE IX. Internal rotator thermodynamic properties for methyl alcohol with $C_1=1.353\times10^{-40}$, $V_0=932$ cal./mole. (cal./deg. mole).

T	$-F/T$	H/T	S	C
200	0.426	0.879	1.305	1.339
260	0.671	0.981	1.652	1.302
300	0.815	1.022	1.837	1.266
340	0.944	1.049	1.993	1.233
380	1.062	1.066	2.128	1.203
420	1.169	1.078	2.247	1.177
460	1.268	1.086	2.353	1.155
500	1.358	1.090	2.449	1.137

and $K-m=3$, for symmetry A. The symmetry order, starting with $K=0$, is therefore $E_1\,E_2\,AE_1$, etc. It is easily shown that for this definition of θ the same order holds for the higher internal energy bands.

By a like argument, or simply by inspection, the pattern of the states for which $\theta=\pi(\sigma+2)/3$ is $E_2AE_1\,E_2$, etc., at all internal levels. Within each of these groups, the separation of states on the θ scale is $\pi C_1/3C$ and the separation of states of like symmetry is $\pi C_1/C$. It follows from the above considerations that a set of internal rotator levels derived for a particular value of θ will all fall in the same symmetry class. Consequently, within each symmetry class, each K determines a value of θ which establishes a set of internal levels for which the sums q, q', and q'' can be evaluated as required by Eqs. (9).

For each value of K, there is then a value of θ for each symmetry class, and this value of θ leads to a complete set of internal rotator levels of the same symmetry, one state in each of the internal rotator bands. Within the limits of Eqs. (9), only the θ values are used as required by Eqs. (10)–(12). Otherwise, for greater accuracy, the summations q_K, q_K', and q_K'' could be evaluated individually and used as called for by Eqs. (4), (6), and (8).

Table VI illustrates the symmetry classification of the θ values and their association with K. The table is equally applicable to all the internal rotator bands. Within each of the three sets of levels, the interval between successive values of θ is $\pi C_1/3C=9.309$ degrees. The result, as shown below in Eqs. (13), is not sensitive to this interval, and would be obtained with a wide variety of intervals centered around the one used.

There is actually no need to distinguish between the E_1 and E_2 states, since there can never be any statistical difference between them. If a state at a given energy for $+K$ is an E_1 level, there will be an E_2 level at $-K$ with the same energy, with the result that the summations over all values of K will be the same for both symmetry classes. This follows from the energy of the free rotator, $(m-KC_1/C)^2$. If the signs of both m and K are reversed, the energy is invariant. If $K-m$ is a multiple of 3, then $m-K$ is also a multiple of 3 and the symmetry class (A) is unchanged. If, however, $K-m$ is $3S_1+1$, $m-K$ will be $3S_2+2$, for a change of symmetry from E_1 to E_2 by the reversal of signs. The situation is not changed by the presence of the barrier, with the result that the pattern of E_1 states for $+K$ is the same as that of the E_2 states for $-K$, with the two coinciding at $K=0$.

From Table VI, in an extended form, the θ values required by Eqs. (10)–(12) can be selected. When the indicated sums are evaluated at 200 and 260°K, it is found, independently for each symmetry class, that

$$\sum_K(\sin^2\theta_K)\exp(-K^2\beta)/Q_K=0.50000$$
$$\sum_K(\sin^2\theta_K)K^2\beta\exp(-K^2\beta)/Q_K=0.25000$$

and

$$\sum_K(\sin^2\theta_K)K^4\beta^2\exp(-K^2\beta)/Q=0.3750. \quad (13)$$

Consequently the thermodynamic properties do not vary with the symmetry class and are therefore calculable without knowledge of the actual spin degeneracies. The result obtained for any one symmetry class can be used to represent the whole system, or the summations could have been made over the whole set of states and subsequently adjusted by means of the symmetry number.

When the sums of Eqs. (13) are introduced into Eqs. (10)–(12), the results are

$$\bar{q}=q_0+a/2;\ \bar{q}'=q_0'+b/2 \text{ and } \bar{q}''=q_0''+c/2, \quad (14)$$

that is, the valid average sum is in each case the numerical mean of the sums for $\theta=0$ and $\theta=\pi/2$. It is evident that the thermodynamic properties will not be far from the numerical mean of the extreme calculable values.

It is of interest to inquire how general the result of Eqs. (13) and (14) may be. Further consideration reveals that, although there are a variety of geometrical situations for which the results would be at least fairly accurate, there are other situations for which the correct average results might be considerably different. If one of two coaxial rotators remains fixed while the other one is increased in size, it develops that, although the number of populated K states increases, the coverage of the cycle in θ or σ becomes less. Since the simple numerical results of Eqs. (13) and (14) can be obtained only with sufficient coverage of this cycle, it follows that a situation will eventually be reached in which the valid $\bar{q}$ for each symmetry class approaches the value of q for $K=0$. In a molecule like tert. butyl alcohol, where presumably only A states of the hydroxyl rotation could exist, the thermodynamic properties would approach those calculable for $\theta=0$, namely, those derived from q_0, q_0', and q_0''. In the extreme case of a small group rotating against an infinitely large one, this limit would actually be reached. It will be necessary to

TABLE X. Comparison with experimental heat capacities.

T	C_{t+r}	Cvib	C_{rr}	$C_v°$ (calc.)	$C_v°$ (E and F)
200	5.962	0.141	1.244, 1.339	7.347, 7.442	7.45±0.11
280	5.962	0.855	1.230, 1.284	8.047, 8.101	8.38±0.08
					$C_v°$ (Rowlinson)
338				8.95	8.9
351				9.18	9.2
362				9.37	9.7
383				9.75	10.0
406				10.19	10.3
448				11.01	11.7

take an average only when C_1 is small or T is very low, and the numerical mean sums validated here for methyl alcohol will be accurate only if C is also small so that C_1/C is appreciable.

The mean thermodynamic properties of the internal rotation are calculated from Tables II to V, inclusive, as shown in Table VII. At 200 and 260° the complete summations leading to the results of Eqs. (13) have been carried through, but at the higher temperatures only the extreme values of the sums have been used, in accordance with Eqs. (14).

As an example of the spread of the values for which the average has been found, the extreme thermodynamic properties at 200° are shown in Table VIII. Each range decreases with the temperature until at 500° the spread in each property has almost completely disappeared. At 200° the correct average heat capacity differs from the numerical mean of the extremes by 0.015, but is almost exactly equal to the result derived from a set of energy levels calculated for $\theta=\pi/4$, that is, to the result obtained from the mean θ for a half-cycle.

Because there is still some doubt about the correct value for C_1, the moment of inertia of the OH group, or, in other words, about the size of the COH angle, another set of properties has been calculated for $\alpha^2=10.0000$, which corresponds to a reduced internal moment of 1.0859, and to $C_1=1.353(\times10^{-40})$. For this case the COH angle would be slightly larger than the accepted internal angle of the water molecule. The required energy levels at $\theta=0$ and $\theta=\pi/2$, have been tabulated elsewhere.[4] The corresponding contributions to the thermodynamic properties appear in Table IX.

In the upper part of Table X heat capacities from molecular constants are compared with the low pressure experimental results of Eucken and Franck,[5] obtained from the thermal conductivity of the vapor at 200 and 280°K. Under C_{rr} and $C_V°$, two values are given which correspond, respectively, to the lower and higher moments of inertia which provide the bases for Tables VII and IX. In the lower part of Table X, the heat capacities of Rowlinson,[6] obtained from the velocity of supersonic waves, as read approximately from his plotted points, are compared with statistical heat capacities taken by linear interpolation from totals derived from the mean values of Tables VII and IX.

TABLE XI. Entropy of methyl alcohol, hypothetical perfect gas, with $C_1=1.01\times10^{-40}$, $V_0=932$ cal./mole. (cal./deg. mole).

T	$S(t+r)$	S(vib)	S_{rr}	$S°$ (1 atmos.)	S (third law)
200	52.142	0.019	1.103	53.264	51.286
260	54.282	0.103	1.430	55.815	55.511
300	55.365	0.223	1.606	57.194	56.944
340	56.360	0.405	1.758	58.523	58.273
380	57.244	0.644	1.890	59.778	59.489
420	58.040	0.937	2.006	60.983	60.578
460	58.763	1.274	2.109	62.146	61.381
500	59.429	1.652	2.205	63.282	61.079

The agreement between calculation and experiment is good enough to suggest that the molecular constants are nearly correct, but does not fully substantiate them and certainly provides no good basis for a choice between the alternative values of C_1. In addition, an attempt was made to reduce the calorimetric heat capacities of DeVries[7] and Collins to the limiting perfect gas values. The results obtained by using the equation of state proposed by Eucken and Meyer[8] were in fair agreement with calculated values only at the higher temperatures, but the over-all comparison with calculation was not instructive enough to justify separate tabulation.

In Table XI, the third law entropy, calculated as previously described,[1] is compared with the entropy from molecular constants obtained with $C_1=1.01\times10^{-40}$. At the extreme high and low temperatures there are evidently errors in the third law values due to extrapolation of the vapor pressures and heats of vaporization, and to the use of the equation of state beyond its range of validity. Between 260° and 380°K, however, there is a nearly constant difference between the molecular and third law values, which lies at the extreme limit of estimated errors. The substitution of $C_1=1.35\times10^{-40}$ adds approximately 0.30 entropy unit to this difference, and suggests that there is a residual entropy or at least a fairly large constant error. As compared with the earlier estimate of barrier height,[1] the elimination of the extrapolation of the tables of Pitzer and Gwinn has increased the range of consistency by about 50°.

From the above calculations, it appears that the required molecular constants are known well enough to determine the limiting low pressure heat capacity quite closely, and to fix the hypothetical perfect gas entropy at any one temperature within about 0.30 cal./deg. mole. Vapor densities, however, are not well enough established to give reliable properties of the

[5] A. Eucken and E. U. Franck, Zeits. f. Elektrochemie **52**, 195 (1948).
[6] J. S. Rowlinson, Nature **162**, 820 (1948).
[7] T. DeVries and B. T. Collins, J. Am. Chem. Soc. **63**, 1343 (1941).
[8] A. Eucken and L. Meyer, Zeits. f. physik. Chemie **5B**, 452 (1929).

real vapor over any considerable range of pressures. The third law entropy appears to contain a constant discrepancy between 0.25 and 0.55 cal./deg. mole, part of which, however, might be eliminated by more accurate vapor density data. Provisionally, the molecular constants used to obtain Tables I–VIII, X, and XI should give accurate enough limiting perfect gas thermodynamic properties for most purposes.

THE JOURNAL OF CHEMICAL PHYSICS VOLUME 18, NUMBER 8 AUGUST, 1950

On the Vibrational Spectra of Crystals

WAYNE A. BOWERS AND HERBERT B. ROSENSTOCK
University of North Carolina, Chapel Hill, North Carolina
(Received March 27, 1950)

In order to check the accuracy of distributions of characteristic vibration frequencies in crystals as calculated by approximate methods proposed by various workers, the frequency distribution is calculated rigorously for a lattice for which this is possible, *viz.*, a two-dimensional square lattice with vibrations perpendicular to the lattice plane. The calculation is then repeated by the use of the various approximate methods, and comparisons are drawn. The effect of using any of the approximate distributions in place of the exact one in the calculation of thermodynamic functions is illustrated by a calculation of the specific heat of this same crystal. Finally, an extension to three dimensions is discussed.

I. INTRODUCTION

IN order to calculate the specific heat and other thermodynamic functions of a crystalline solid, it is necessary to know the distribution of natural frequencies of the lattice vibrations. Although the fundamental equations for the natural frequencies were written down by Born and von Karman[1] in 1912, the mathematical complexities have prevented the actual calculation of frequency distributions except by laborious numerical procedures for particular values of the parameters involved. For this reason one has to rely on various approximations to the actual frequency distribution, of which the most famous one is, of course, the Debye theory, which approximates the crystal by a continuous medium and uses the distribution of elastic vibrations in a continuum, with a cut-off adjusted to give the correct total number of vibrations. The remarkable success of the Debye theory in explaining observed specific heat data put the question of rigorous calculation of frequency distributions in the background for a number of years, until Blackman,[2] in a series of papers, showed that certain anomalies in observed specific heat data could be at least qualitatively explained in terms of the deviation of the actual frequency distribution from the Debye distribution. Since that time a number of workers[3–5] have devoted themselves to working out approximate methods of calculating frequency distributions from the Born-von Karman equations.

The purpose of this paper is to compare the distributions obtained by various approximate methods with the actual one in a case for which an expression for it can be obtained in closed form, namely, the case of vibrations of a square two-dimensional lattice in a direction transverse to its own plane. Although this is a case of no direct physical significance (cf. Section V), the existence of an analytic solution makes possible a comparison with approximate methods and hence gives one some basis for evaluating these methods. Further, certain conclusions with regard to actual three-dimensional lattices may be drawn.

In Section II we formulate the two-dimensional problem mentioned above and derive the actual frequency distribution; in Section III we compare the actual distribution with the distributions of Debye, Montroll,[3] and Houston;[4] in Section IV we calculate the specific heat of the crystal, using both the exact and the approximate frequency distributions; and in Section V we discuss a three-dimensional problem for which a rigorous result can be obtained.

II. TRANSVERSE VIBRATIONS OF A SQUARE LATTICE

Consider a square lattice consisting of N rows and N columns of identical atoms. If the displacement, transverse to the plane of the lattice, of the atom in the lth row and mth column is denoted by $u_{l,m}$, we may write the Lagrangian function:

$$L=\tfrac{1}{2}M\sum_{l,m=1}^{N}\dot{u}_{l,m}^{2}$$
$$-\tfrac{1}{2}\alpha\{\sum_{l,m=1}^{N}(u_{l,m+1}-u_{l,m})^{2}+\sum_{l,m=1}^{N}(u_{l+1,m}-u_{l,m})^{2}\}$$
$$-\tfrac{1}{2}\gamma\{\sum_{l,m=1}^{N}(u_{l+1,m+1}-u_{l,m})^{2}$$
$$+\sum_{l,m-1}^{N}(u_{l+1,m-1}-u_{l,m})^{2}\}. \quad (1)$$

[1] M. Born and T. von Karman, Physik. Zeits. **13**, 297 (1912).
[2] M. Blackman, Proc. Roy. Soc. **148**, 365 (1935); **159**, 416 (1937).
[3] E. W. Montroll, J. Chem. Phys. **10**, 218 (1942); **11**, 481 (1943)
[4] W. V. Houston, Rev. Mod. Phys. **20**, 161 (1948).
[5] P. C. Fine, Phys. Rev. **56**, 355 (1939).

Here M is the mass of each atom, and α and γ are the force constants for nearest and next-nearest neighbors, respectively. This yields for the motion of each atom:

$$\begin{aligned} M\ddot{u}_{ij}=\alpha[&(u_{i+1,j}-2u_{ij}+u_{i-1,j})\\ &+(u_{i,j+1}-2u_{i,j}+u_{i,j-1})]\\ +\gamma[&(u_{i+1,j+1}-2u_{i,j}+u_{i-1,j-1})\\ &+(u_{i+1,j-1}-2u_{i,j}+u_{i-1,j+1})], \quad 1\leq i, j\leq N, \end{aligned} \tag{2}$$

and assuming solutions of the form

$$u_{ij}=e^{i\omega t}\sin\frac{ip\pi}{N+1}\sin\frac{jq\pi}{N+1}, \quad p, q=1, 2, \cdots, N, \tag{3}$$

corresponding to standing waves in the lattice, with dummy rows of atoms at $i, j=0, N+1$ which are held fixed, we find the N^2 natural frequencies of vibration:

$$M\omega_{pq}{}^2=2\alpha\left(2-\cos\frac{p\pi}{N+1}-\cos\frac{q\pi}{N+1}\right)+4\gamma\left(1-\cos\frac{p\pi}{N+1}\cos\frac{q\pi}{N+1}\right), \quad p, q=1, 2, \cdots, N. \tag{4}$$

Since N is a very large number (of the order 10^8), we may replace $p\pi/(N+1)$ and $q\pi/(N+1)$ by continuous variables x and y, respectively, which run from 0 to π. Then taking $M=1$, we have

$$\begin{aligned} \omega^2\equiv f(x, y)=&2\alpha(2-\cos x-\cos y)\\ &+4\gamma(1-\cos x\cos y), \quad 0<x, y<\pi. \end{aligned} \tag{5}$$

The curves of constant ω^2, in the $x-y$ plane, for several values of γ, are illustrated in Fig. 1.

The problem of finding the frequency distribution is now simply the problem of finding what fraction of the area π^2 of the square $0<x, y<\pi$ is bounded by the curves $f(x, y)=\omega^2$ and $f(x, y)=\omega^2+d\omega^2$. This gives directly the frequency distribution $g(\omega^2)d\omega^2$. It may be

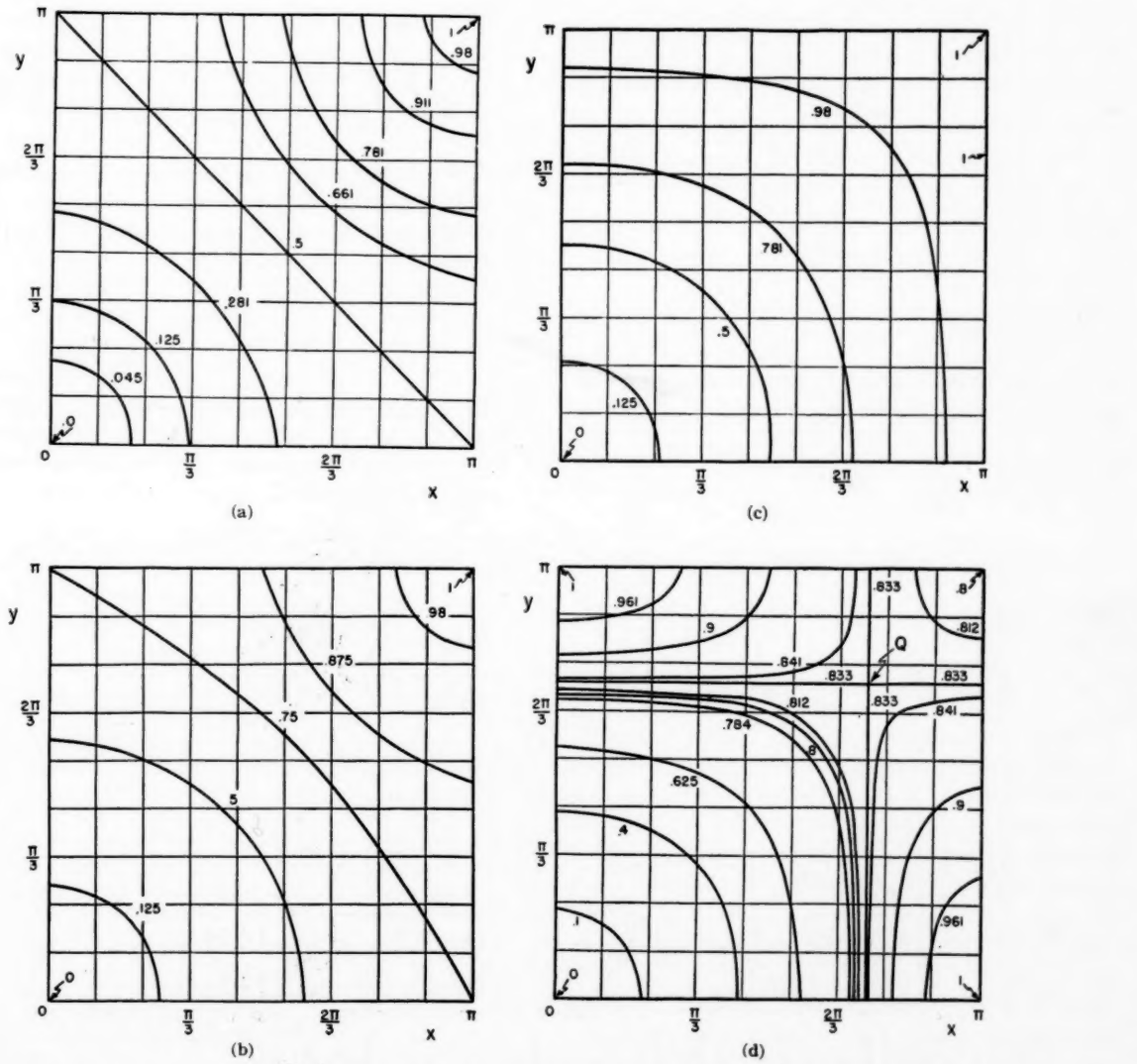

FIG. 1. Lines of constant $\bar{\omega}^2$ in $x-y$ space; $\bar{\omega}^2=\omega^2/\omega_{max}{}^2$. (a) $\gamma/\alpha=0$. (b) $\gamma/\alpha=\frac{1}{4}$. (c) $\gamma/\alpha=\frac{1}{2}$. (d) $\gamma/\alpha=\frac{3}{4}$.

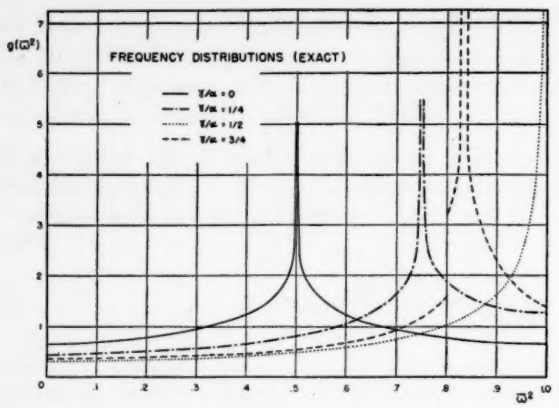

FIG. 2. Frequency distributions for a two-dimensional crystal (exact); $\bar{\omega}^2=\omega^2/\omega_{\max}{}^2$.

conveniently expressed as follows:

$$g(\omega^2)=\frac{1}{\pi^2}\int_0^\pi\int_0^\pi \delta(\omega^2-f(x,y))dxdy, \tag{6}$$

where δ is Dirac's delta-function.

Formula (6) is most simply verified as follows: letting

$$\Delta(x)\equiv\int_{-\infty}^{x}\delta(z)dz=\begin{cases}0 & x<0\\ 1 & x>0\end{cases},$$

we see that

$$\int_0^{\omega_0^2} g(\omega^2)d\omega^2,$$

which should represent the fractional number of frequencies with $\omega^2<\omega_0^2$, is, according to (6), equal to

$$\frac{1}{\pi^2}\int_0^\pi\int_0^\pi dxdy\int_0^{\omega_0^2}\delta(\omega^2-f(x,y))d\omega^2$$

$$=\frac{1}{\pi^2}\int_0^\pi\int_0^\pi \Delta(\omega_0^2-f(x,y))dxdy;$$

and since $\Delta(\omega_0^2-f(x,y))$ is unity when $f(x,y)<\omega_0^2$ and vanishes otherwise, the integral

$$\int_0^\pi\int_0^\pi \Delta(\omega_0^2-f(x,y))dxdy$$

does in fact represent the area of that part of the square for which $\omega^2<\omega_0^2$, and hence when divided by π^2 gives the fractional number of frequencies for which $\omega^2<\omega_0^2$.

The actual evaluation of the integral is conveniently carried out with the help of the change of variable $u=\cos x$, $v=\cos y$; we have then

$$g(\omega^2)=\frac{1}{\pi^2}$$

$$\times\int_{-1}^{1}\int_{-1}^{1}\frac{\delta(\omega^2-2\alpha(2-u-v)-4\gamma(1-uv))}{(1-u^2)^{\frac{1}{2}}(1-v^2)^{\frac{1}{2}}}dudv. \tag{7}$$

One integration can be carried out immediately using the properties of the delta-function; the remaining integration yields an elliptic integral. It is convenient to introduce $\bar{\omega}=\omega/\omega_{\max}$, where, from (5),

$$\omega_{\max}{}^2=\begin{cases}8\alpha & \gamma/\alpha\le\frac{1}{2}\\ 4\alpha+8\gamma & \gamma/\alpha\ge\frac{1}{2}\end{cases}.$$

In terms of $\bar{\omega}$, the distribution is then given by:

For $\gamma/\alpha\le\frac{1}{2}$

$$g(\bar{\omega}^2)=\frac{4K(k_1^2)}{\pi^2[(1+2\gamma/\alpha)^2-8(\gamma/\alpha)\bar{\omega}^2]^{\frac{1}{2}}},\quad k_1{}^2=\frac{4(1-\bar{\omega}^2)\bar{\omega}^2}{(1+2\gamma/\alpha)^2-8(\gamma/\alpha)\bar{\omega}^2},\quad 0<\bar{\omega}^2<1. \tag{8}$$

For $\gamma/\alpha\ge\frac{1}{2}$

$$g(\bar{\omega}^2)=\begin{cases}\dfrac{2K(k_2^2)}{\pi^2\left(1-\dfrac{4\gamma/\alpha}{1+2\gamma/\alpha}\bar{\omega}^2\right)^{\frac{1}{2}}}, & k_2{}^2=\dfrac{\left(\dfrac{2}{1+2\gamma/\alpha}-\bar{\omega}^2\right)\bar{\omega}^2}{1-\dfrac{4\gamma/\alpha}{1+2\gamma/\alpha}\bar{\omega}^2}, \quad 0<\bar{\omega}<\dfrac{2}{1+2\gamma/\alpha} & (9a)\\[2ex] \dfrac{4K(k_3^2)}{\pi^2(1-\bar{\omega}^2)}, & k_3{}^2=\dfrac{\left(\bar{\omega}^2-\dfrac{2}{1+2\gamma/\alpha}\right)\bar{\omega}^2}{(1-\bar{\omega}^2)^2}, \quad \dfrac{2}{1+2\gamma/\alpha}<\bar{\omega}^2<\dfrac{1+2\gamma/\alpha}{4\gamma/\alpha} & (9b)\\[2ex] \dfrac{4K(k_4^2)}{\pi^2\left[\left(\bar{\omega}^2-\dfrac{2}{1+2\gamma/\alpha}\right)\bar{\omega}^2\right]^{\frac{1}{2}}}, & k_4{}^2=\dfrac{(1-\bar{\omega}^2)^2}{\left(\bar{\omega}^2-\dfrac{2}{1+2\gamma/\alpha}\right)\bar{\omega}^2}, \quad \dfrac{1+2\gamma/\alpha}{4\gamma/\alpha}<\bar{\omega}^2<1. & (9c)\end{cases}$$

Here $K(k^2)$ denotes the complete elliptic integral of the first kind. These distributions are plotted, for $\gamma/\alpha=0, \frac{1}{4}, \frac{1}{2}, \frac{3}{4}$, in Fig. 2.

We notice the following features of these curves.

(a) In each case there is a frequency at which the density of natural frequencies becomes infinite. For $\gamma/\alpha<\frac{1}{2}$, this occurs for $\bar{\omega}^2=(1+2\gamma/\alpha)/2$, which corresponds to the point $(x, y)=(0, \pi)$ or $(\pi, 0)$, while for $\gamma/\alpha>\frac{1}{2}$, this occurs for $\bar{\omega}^2=(1+2\gamma/\alpha)/(4\gamma/\alpha)$, corresponding to the point $x=y=\cos^{-1}(-\alpha/2\gamma)$ [point Q in Fig. 1(d)]. At these points the surface $\bar{\omega}^2$ *vs.* (x, y) has a saddle point, and it can be shown that this always leads to a logarithmic divergence in the density. This divergence shows up in formulas (8) and (9) by the argument of the elliptic integral approaching unity. Of course the area under the curve remains finite, as it should.

(b) For $\gamma/\alpha>\frac{1}{2}$, there is a discontinuity in $g(\bar{\omega}^2)$ at $\bar{\omega}^2=2/(1+2\gamma/\alpha)$, where the density of frequencies is doubled. This, too, can be understood by considering Fig. 1(d), on which the discontinuity corresponds to $\bar{\omega}^2=0.8$: area elements corresponding to frequencies below $\bar{\omega}^2=0.8$ appear only near the lower left-hand corner of the square, whereas area elements corresponding to frequencies above $\bar{\omega}^2=0.8$ appear both near the lower left- and upper right-hand corners of the square.

(c) There is no qualitative difference between the distribution for $\gamma/\alpha=0$ and for small γ/α; only a shift of the peak to higher frequencies occurs. This is in contrast to the two-dimensional problem of Blackman[2] (vibrations in the plane of the lattice) where the distribution for $\gamma/\alpha=0$ reduces to that of a one-dimensional chain of atoms, which has a peak, at the maximum frequency, of inverse square root character in place of the logarithmic peak found for $\gamma/\alpha>0$.

(d) Equations (8) and (9) are quite similar to relations obtained by Montroll[6] for one special value of the force constant parameter in a square lattice with vibrations in the lattice plane; in fact, his distribution consists of two branches, which are identical with our distribution for $\gamma/\alpha=0$ and $\gamma/\alpha=1$, respectively. This suggests that the results obtained here may be carried over, at least qualitatively, to structures of more direct physical significance than the crystal considered here.

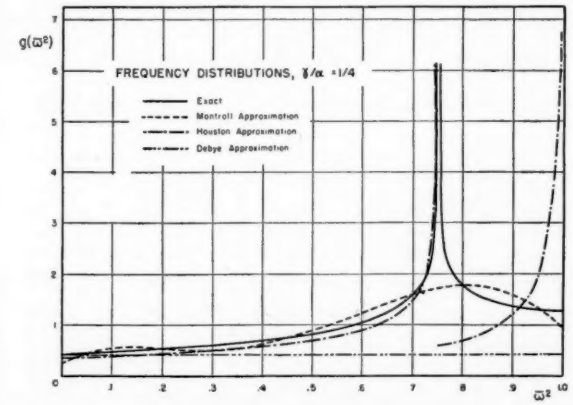

FIG. 3. Frequency distributions for a two-dimensional crystal ($\gamma/\alpha=\frac{1}{4}$). The exact curve is the same as the $\gamma/\alpha=\frac{1}{4}$ curve of Fig. 2. The exact Montroll and Houston curves are shown in their entirety; the Debye curve continues as a straight line up to $\bar{\omega}^2=2.36$, and is zero beyond that point.

[6] E. W. Montroll, J. Chem. Phys. **15**, 575 (1947).

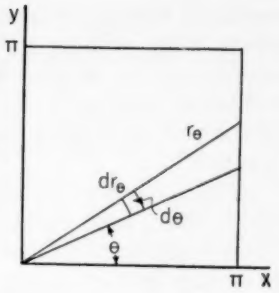

FIG. 4. Illustration of the Houston method in two dimensions. As in Fig. 1, the $x-y$ space is the reciprocal lattice of the crystal.

III. COMPARISON WITH APPROXIMATE METHODS

A. Montroll's Method

One form of Montroll's[3] method for approximating the frequency distribution of a crystalline solid may be summarized as follows.

Expand

$$g(\bar{\omega}^2)=\sum_{m=0}^{\infty} a_m\bar{\omega}^{2m}. \tag{10}$$

Defining the $(2n)$th moment μ_{2n} of $\bar{\omega}$ as

$$\mu_{2n}=\int_0^1 \bar{\omega}^{2n}g(\bar{\omega}^2)d\bar{\omega}^2, \tag{11}$$

we find, using (10),

$$\begin{aligned}\mu_{2n}&=\sum_{m=0}^{\infty} a_m/(m+n+1), \qquad n=0, 1, 2, \cdots\\ &=\sum_{m=0}^{\infty} T_{mn}a_m, \qquad T_{mn}=(m+n+1)^{-1}.\end{aligned} \tag{12}$$

The moments, being simply averages of the powers of $\bar{\omega}^2$, can be found from

$$\mu_{2n}=\frac{1}{\pi^2}\int_0^{\pi}\int_0^{\pi}[f(x, y)/\omega_{\max}{}^2]^n dxdy,$$

where $f(x, y)$ is given in (5); and by the use of the first k of the infinite set of equations (12), keeping k terms on the right side of each, we can solve for the first k of the coefficients a_m, which are so obtained as functions of the force constant parameter γ/α. The frequency distribution $g(\bar{\omega}^2)$ is thus approximated in (10) by a polynomial of degree k.

Even though Montroll[3] has given a formula* for the inverse of the matrix T_{mn} which facilitates solving equations of the form (12), the computation becomes

* *Note added in proof:* A general method for finding the inverse of a matrix of the type T_{mn} is given by A. R. Collar, Proc. Roy. Soc. (Edinburgh) **59**, 195 (1939).

exceedingly tedious for even rather low order approximations. Here, we have gone up to the fifth order; the results are shown, for $\gamma/\alpha=\frac{1}{4}$, in Fig. 3, where the exact distribution function is also plotted for the purpose of easy comparison. Similar curves are obtained for other γ/α-ratios.[7]

It appears that low order approximations by Montroll's method do not yield frequency distributions very close to the actual ones; and that approximations of an order high enough for fair agreement would involve excessive labor, as convergence is quite slow. (For instance, for $\gamma/\alpha=\frac{1}{4}$, the fourth- and fifth-order curves are almost indistinguishable in the physically significant range $\tilde{\omega}\equiv\omega/\omega_{\max}\leq 1$.) On the other hand, it should be remarked that the poor agreement, which is mainly due to our attempt to fit a low order polynomial to a curve with an infinite peak, should be improved when we deal with a distribution which is finite everywhere, such as the three-dimensional distribution discussed in Section V, and that even in the case at hand, the specific heat calculated by the Montroll distribution approximates the true specific heat very well (cf. Section IV).

B. Houston's Method

Houston's[4] method is based upon determining the frequency distribution along several special directions in the reciprocal lattice and summing over all directions. When applied to our two-dimensional lattice, it takes the following form.

Consider a line running from the origin through the $x-y$ plane in a direction making an angle θ with the x axis (cf. Fig. 4). Let $F(\omega^2, \theta)d\omega^2 d\theta$ be the fraction of frequencies between ω^2 and $\omega^2+d\omega^2$ corresponding to directions between θ and $\theta+d\theta$, so that

$$g(\omega^2)=\int_0^{\pi/2} F(\omega^2, \theta)d\theta. \tag{13}$$

If we now expand $F(\omega^2, \theta)$ in a Fourier series, we have

$$F(\omega^2, \theta)=\sum_{n=0}^{\infty} f_n(\omega^2)\cos 4n\theta; \tag{14}$$

all other terms must have zero coefficients as F is even and symmetric about $\pi/4$. [In the three-dimensional case that Houston treats,[4] the place of (14) is taken by an expansion in terms of combinations of associated Legendre polynomials of the proper cubic symmetry.] Substituting (14) in (13) we find

$$g(\omega^2)=(\pi/2)f_0(\omega^2). \tag{15}$$

The fractional number of points in an element of area in the reciprocal lattice space of width $d\theta$ and length dr_θ (cf. Fig. 4) is

$$(1/\pi^2)r_\theta dr_\theta d\theta=(1/\pi^2)r_\theta d\theta(dr_\theta/d\omega^2)d\omega^2.$$

But this is what $F(\omega^2, \theta)$ was defined to be. Hence

$$F(\omega^2, \theta)=(1/\pi^2)r_\theta(dr_\theta/d\omega^2),$$

where we must now express the right-hand side in terms of ω^2. This can be done for those few simple values of θ for which (5) is analytically solvable for $r_\theta=(x^2+y^2)^{\frac{1}{2}}$.

Once having obtained $F(\omega^2, \theta)$ for k different values of θ, we can write down k different equations (14), keeping k terms on the right side of each, and solve them for f_0 which, according to (15), is proportional to $g(\omega^2)$.

The approximation has here been carried out for $k=2$, the two angles used being $\theta=0$ and $\theta=\pi/4$. In that case, (15) yields

$$g(\omega^2)=1/4\pi[r_0(dr_0/d\omega^2)+r_{\pi/4}(dr_{\pi/4}/d\omega^2)]. \tag{16}$$

This equation, however, does not give the correct total number of frequencies; for proper normalization we must replace $1/4\pi$ by $2/3\pi^2$. Solution of (5) for r_θ gives in this case

$$r_0=2\sin^{-1}\left(\frac{2\tilde{\omega}^2}{1+2\gamma/\alpha}\right)^{\frac{1}{2}}$$

and

$$r_{\pi/4}=\sqrt{2}\cos^{-1}\left[\frac{-1\pm(1+4(\gamma/\alpha)\{1+(\gamma/\alpha)-2\tilde{\omega}^2\})^{\frac{1}{2}}}{2\gamma/\alpha}\right].$$

These expressions, together with their derivatives, enable us to get $g(\tilde{\omega}^2)$ from (16).

The approximate frequency distributions were computed[7] for several values of γ/α; for the typical case $\gamma/\alpha=\frac{1}{4}$, it is shown in Fig. 3. We find good agreement with the exact distribution for low frequencies, up to the infinite maximum at $\tilde{\omega}^2=0.75$, but gross discrepancies beyond, culminating in a spurious infinite peak at $\omega^2=1$.

By choosing, in addition to 0 and $\pi/4$, a third angle $\theta_3=\tan^{-1}\frac{1}{2}$ one may carry the approximation one step further ($k=3$). r_{θ_3} is found by solving an involved cubic equation, and $g(\tilde{\omega}^2)$ is obtained from an expression considerably more complicated than (16). To the left of the true peak $\tilde{\omega}^2=0.75$, its behavior is much the same as in

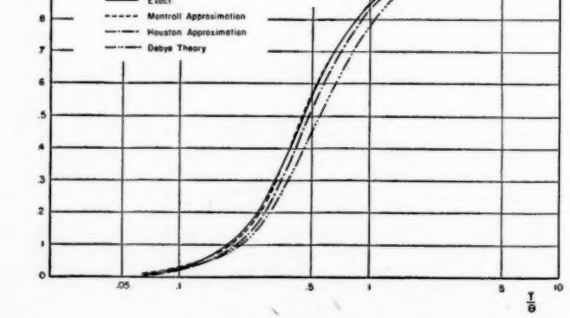

FIG. 5. Specific heat *vs.* temperature, two-dimensional crystal, $\gamma/\alpha=0$.

[7] H. B. Rosenstock, M.S. thesis, University of North Carolina (1949).

the $k=2$ case; to the right there appears, in addition to the spurious infinite peak at $\tilde{\omega}^2=1$, another steep, but finite, spurious maximum.

For angles other than these three, it appears impossible to obtain expressions for r_θ and $dr_\theta/d\tilde{\omega}^2$ in terms of $\tilde{\omega}^2$ by methods other than purely numerical ones. For this crystal model, Houston's method is therefore not useful beyond this point.

C. The Debye Approximation

The Debye theory approximates the frequency distribution by using the low frequency distribution for all frequencies, cutting it off at a value chosen to give the correct total number of frequencies. In our case this means that the Debye distribution is given by

$$g_D(\tilde{\omega}^2)=\begin{cases} g(0) & 0<\tilde{\omega}^2<1/g(0) \\ 0 & \tilde{\omega}^2>1/g(0) \end{cases},$$

i.e., the distribution as a function of $\tilde{\omega}^2$ is constant. If the distribution is expressed in terms of $\tilde{\omega}$ instead of $\tilde{\omega}^2$, we have $g(\tilde{\omega}^2)d\tilde{\omega}^2=[2\tilde{\omega}g(\tilde{\omega}^2)]d\tilde{\omega}$; hence the Debye approximation reads

$$g_D(\tilde{\omega}^2)d\tilde{\omega}^2=\begin{cases} [2\tilde{\omega}g(0)]d\tilde{\omega} & 0<\tilde{\omega}<1/[g(0)]^{\frac{1}{2}} \\ 0 & \tilde{\omega}>1/[g(0)]^{\frac{1}{2}} \end{cases}$$

which is linear in $\tilde{\omega}$, as it should be.

The Debye frequency distribution is also shown, for comparison, in Fig. 3.

IV. SPECIFIC HEATS

Vibrational frequency spectra are of interest primarily in connection with the calculation of thermodynamic functions. As a further check on the suitability of the approximate frequency distributions discussed in Section III, we therefore compute the specific heat of our crystal by the use of both the exact and the various approximate distributions.

By well-known methods[8] we find that the specific heat C_v per mole of a two-dimensional square lattice is given by

$$C_v=Nk\int_0^1\left[\frac{\tilde{\omega}(\theta/T)}{\sinh\tilde{\omega}(\theta/T)}\right]^2 g(\tilde{\omega}^2)d\tilde{\omega}^2, \qquad (19)$$

where N = Avogadro's number, k = Boltzman constant, $\theta=h\omega_{\max}/2k$, and h = Planck's constant$/2\pi$.

In the Debye case, the upper limit of integration is to be replaced by $1/g(0)$; expansions of the integrand are possible for both high and low temperatures.[8] Another series expansion, utilizing the moments defined in Section III-A, is possible for high temperatures for the exact and for the Montroll case. For the rest of the temperature range, and throughout it in the Houston case, integration of (19) must be numerical, except, of course, around infinite peaks, near which sufficiently rapidly converging series expansions of the integrand in terms of analytically integrable functions can be found.

The resulting, familiar-looking specific heat *vs.* temperature curves are exhibited in Fig. 5, for the case $\gamma/\alpha=0$. Results for $\gamma/\alpha>0$ will not be qualitatively different (cf. Section II). The following points should be noted.

(a) All curves are proportional to T^2 at very low temperatures, as they should be, and appear almost indistinguishable on the scale on which they are plotted here, although the proportionality constant, related to $g(0)$, is different in each case.

(b) The Montroll approximation is indistinguishable from the exact specific heat to the accuracy of this calculation (four significant figures) above $T/\theta=1$. Below this temperature, agreement becomes worse, with a discrepancy of 30 percent at zero temperature. In this connection, it may be remarked that Taylor[9] has proposed a modification of Montroll's method which gives the correct low temperature behavior.

(c) Comparison of the utter dissimilarity of the frequency distributions of Fig. 3 on the one hand with the rather close agreement of all specific heat curves of Fig. 5 on the other indicates that the specific heat is not very strongly sensitive to changes in the frequency distribution.

(d) The greatest deviations from the exact curve are found in the Debye curve; however, the simplicity of the theory enables one to perform numerical calculations that lead to qualitatively correct results with a considerable saving of labor.

V. "TRANSVERSE" VIBRATIONS OF A THREE-DIMENSIONAL CUBIC LATTICE

The lack of direct physical significance, previously referred to, of the transversely vibrating two-dimensional lattice, as compared to a two-dimensional lattice with vibrations in the lattice plane, results from the impossibility of generalizing it, even in an idealized way, into an observed three-dimensional structure; for if we generalize the lattice treated in this paper into three dimensions, we obtain a cubic lattice whose mass points oscillate in some fourth dimension to which we can ascribe no physical meaning. Comparison of the frequency spectrum of such a lattice with its two-dimensional analog may, nevertheless, give insight in the behavior of lattices describing observable structures; in this section we therefore calculate the frequency distribution of a "transversely" vibrating three-dimensional simple cubic lattice for one simple set of values of the force parameters.

The Lagrangian can be written down as a formal generalization of Eq. (1) without difficulty, and the equations of motion derived; proceeding exactly as in

[8] Cf. J. E. Mayer and M. G. Mayer, *Statistical Mechanics* (John Wiley and Sons, Inc., New York, 1941), Chapter 11.

[9] W. J. Taylor, Phys. Rev. **77**, 762 (1950).

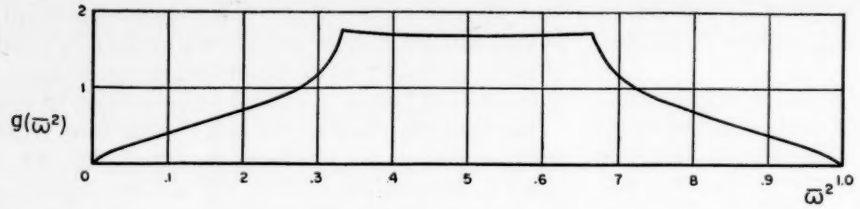

FIG. 6. Frequency distribution for a three-dimensional crystal, $\gamma=\beta=0$.

Section II, one obtains, corresponding to (5), for the natural frequencies

$$\omega^2\equiv f(x,y,z)=2\alpha(3-\cos x-\cos y-\cos z)+4\gamma(3-\cos x\cos y-\cos x\cos z-\cos y\cos z)+8\beta(1-\cos x\cos y\cos z), \quad (20)$$

where α, γ, x, and y are defined in Section II, β is the force constant for next-next-nearest neighbors and $z=r\pi/(N+1)$, $r=1, 2, \cdots, N$. Analogous to (6) the frequency distribution is given by

$$g(\omega^2)=\frac{1}{\pi^3}\int_0^\pi\int_0^\pi\int_0^\pi \delta(\omega^2-f(x,y,z))dxdydz. \quad (21)$$

The first two integrations can be done as before, and yield complete elliptic integrals with complicated arguments; the third integration must be done numerically. We have performed the numerical integration for the case $\beta=\gamma=0$, i.e., including only nearest-neighbor interaction, and the resulting distribution is shown in Fig. 6. This case is of interest in spite of the artificiality of the model for the following reasons.

(a) Since the two-dimensional "transverse" distribution for $\gamma/\alpha=0$ is identical with one branch of the two-dimensional "in-plane" distribution for Montroll's particular choice of parameters (cf. Section II and reference 6), we expect that the distribution of Fig. 6 likewise is identical with one branch of the distribution of a real three-dimensional lattice.

(b) We have seen in the two-dimensional case that the distribution is not changed qualitatively in going to the limit $\gamma/\alpha\to 0$, and this should also be true for our three-dimensional case.

Thus we expect Fig. 6 to give the general features of actual three-dimensional distributions correctly.*

We note that (a) for small $\bar{\omega}^2$, the distribution is proportional to $(\bar{\omega}^2)^{\frac{1}{2}}$; this is the usual result of the Debye approximation, since the distribution in terms of $\bar{\omega}$ will be proportional to $2\bar{\omega}(\bar{\omega}^2)^{\frac{1}{2}}$; (b) the distribution is everywhere finite, although it has logarithmically infinite slope at $\bar{\omega}^2=\frac{1}{3}$ and $\bar{\omega}^2=\frac{2}{3}$. Thus the Montroll method, which tries to approximate the distribution by polynomials, should yield better results in the three-dimensional than in the two-dimensional case. The Houston method will, however, still give spurious peaks and hence approximate the distribution poorly.

* It should be pointed out, for purposes of comparison with the distributions calculated by Blackman, Montroll, and others, that if plotted as a function of $\bar{\omega}$ instead of $\bar{\omega}^2$, our distribution has a fairly sharp maximum at $\bar{\omega}=(\frac{2}{3})^{\frac{1}{2}}=0.82$; hence its general appearance is similar to that of the approximate distributions of Blackman, etc.

Spectral Resemblances between Azulenes and Their Corresponding Six-Carbon Ring Isomers

H. B. KLEVENS
Division of Agricultural Biochemistry, University of Minnesota, St. Paul, Minnesota
(Received April 3, 1950)

The spectra of odd-ring compounds, azulene, 1,2-benzazulene, 2-phenyl azulene, and indeno-azulene are compared with those of their corresponding regular isomers, naphthalene, phenanthrene, phenylnaphthalene, and benzfluorene in part from 1730 to 7500A. The five band systems found in the azulenes seem to correspond with respect to intensity, vibrational structure, and sequence to the five found in their corresponding isomers except that the former are shifted to lower frequencies. The lowest frequency band is shifted some 17,000 cm^{-1} to the red in the azulenes, which accounts for the color observed in these compounds, whereas the four transitions at higher frequencies are shifted about 8000 to 9000 cm^{-1} as compared with the corresponding regular isomers. Decreases in total oscillator strengths with non-linearity of these planar molecules as compared with the linear compounds (a type of C_{2v} symmetry about the long axis) are noted as has previously been shown in the comparison of anthracene and phenanthrene, and tetracene and 1,2-benzanthracene and chrysene.

A DIRECT correlation between the spectra of naphthalene and its blue hydrocarbon isomer, azulene, has recently been shown[1] and this correspondence is shown in Fig. 1. The system of five absorption bands found in azulene corresponds, with respect to vibrational structure, intensity, and sequence, to the five found in naphthalene, except that the former are all shifted to lower frequencies. In Figs. 1 to 3, only the lowest vibrational level is shown, and the remaining structure of each electronic band is omitted for clearness. The lengths of the horizontal lines indicate $\log\epsilon_{max}$ for absorption from the ground state. There is a frequency difference of about 9000 cm^{-1} between corresponding states in these two hydrocarbons in all but the ^1L_b transition where this difference amounts to about 17,000 cm^{-1}. It is this ^1L_b transition in azulene which accounts for the blue color in this hydrocarbon. The ^1L_b transition in azulene has quite different properties from the lowest, 17,100 cm^{-1} ^1L_a band in the blue polycyclic pentacene for the character of the former transition is similar to that of 24,000 cm^{-1} ^1L_b band in the latter compound.[2]

Recently, the spectra of some phenyl substituted azulenes and of one annelated* (fusion of a ring) azulene, 1,2-benzazulene, have been reported.[3,4] The

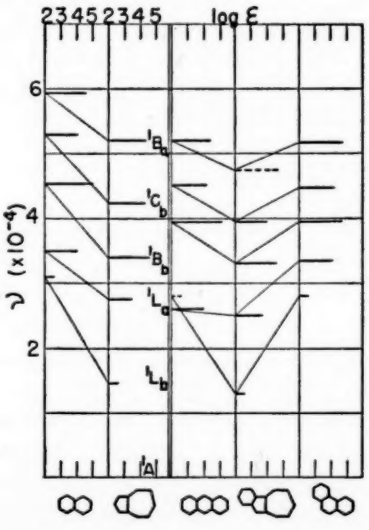

FIG. 1. Spectral resemblances between azulenes and their corresponding isomeric hydrocarbons. The frequency, ν, is that of the longest wave-length vibrational component of each particular electronic transition; the extinction coefficient, ϵ, is that of the most intense absorption in the particular transition. Data for naphthalene, azulene, anthracene and phenanthrene (see reference 2); for 1,2-benzazulene (see reference 3).

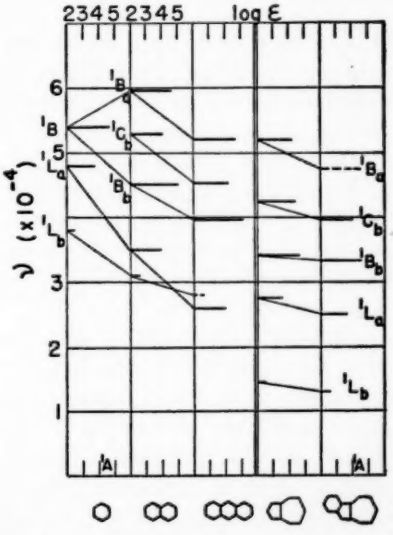

FIG. 2. Effect of annelation (fusion of a ring) on the spectra of polycyclic hydrocarbons. Data for benzene, naphthalene, anthracene, phenanthrene, and azulene (see reference 2); for 1,2-benzazulene (see reference 3).

[1] Mann, Platt, and Klevens, J. Chem. Phys. 17, 481 (1949).

[2] H. B. Klevens and J. R. Platt, J. Chem. Phys. 17, 470 (1949).

* Annelation is a term used to designate the fusion of a ring to a polycyclic compound. Thus 1,2-benzanthracene may be considered an annelated anthracene at the 1,2-position of the latter polycyclic.

[3] J. R. Nunn and W. S. Rapson, J. Chem. Soc., 825 (1949).

[4] Pl. A. Plattner and E. Heilbronner, Helv. Chim. Acta 31, 804 (1948).

TABLE I. Main features of spectra of condensed hydrocarbons.

	^1A–^1L_b	^1A–^1L_a	^1A–^1B_b	^1A–^1C_b	^1A–^1B_a	Total f-value
Naphthalene						
Onset of absorption (cm^{-1})	32000	34600				
Peak			45400	52500(?)	~59700	
ϵ_{max} ($mole^{-1}$ cm^{-1})	280	9300	133000	10000	~40000	
f	0.002	0.18	1.70	0.20	~0.8	
(To cut-off)	(34000)	(42500)	(49500)	(55000)	(63000)	~2.88
Azulene						
Onset of absorption (cm^{-1})	14400	25000				
Peak			37100	42300	51800	
ϵ_{max} ($mole^{-1}$ cm^{-1})	300	4000	47000	22000	18000	
f	0.009	0.08	1.10	0.38	0.65	
(To cut-off)	(25000)	(32700)	(40300)	(45000)	(60000)	2.22
Anthracene						
Onset of absorption (cm^{-1})		26400				
Peak			39000	45300	53700	
ϵ_{max} ($mole^{-1}$ cm^{-1})		9000	180000	14500	32000	
f		0.10	2.28	0.28	0.65	
(To cut-off)		(35000)	(44400)	(50800)	(59300)	3.31
Phenanthrene						
Onset of absorption (cm^{-1})	28300	33000				
Peak			39400	47100	53400	
ϵ_{max} ($mole^{-1}$ cm^{-1})	350	16000	65500	33000	31000	
f	0.003	0.18	1.09	0.60	0.59	
(To cut-off)	(32300)	(36300)	(44000)	(50800)	(56400)	2.46
1,2-Benzazulene[a]						
Onset of absorption (cm^{-1})	13000	24800				
Peak			33300	41000		
ϵ_{max} ($mole^{-1}$ cm^{-1})	320	5000	60000	10000		
f	0.007	0.10	1.95	~0.3		
(To cut-off)	(23800)	(29800)	(37000)	(44000)		2.36+

[a] Data calculated from curve of Nunn and Rapson (see reference 3).

spectra of these compounds are here shown to be related to their corresponding hydrocarbon isomers and have a correspondence similar to that proposed above. Thus the spectra of benzazulene is compared in Fig. 1 with that of its isomers anthracene and phenanthrene. Again there is this same similarity with respect to intensity, sequence and vibrational structure in the ^1B_a, ^1C_b, and ^1B_b bands in these isomers. It is evident that 1,2-benzazulene is a non-linear polycyclic, as is phenanthrene, and not one of the linear (C_{2v} symmetry about the long axis) polyacenes of which anthracene is typical. The fact, that the ^1L_a bands in 1,2-benzazulene and the other transitions at higher frequencies are on an average about 8000 cm^{-1} to the red of the corresponding bands in phenanthrene whereas only the higher frequency bands in anthracene show this correspondence, supports this concept of non-linearity. The ^1L_a band has been shown to shift most with increasing number of rings in the linear polyacenes and moves as much as 8000 to 10,000 cm^{-1} to the blue upon going from a linear to a non-linear polyacene.[2] The ^1L_a band in 1,2-benzazulene and in anthracene are both found at about the same wave-lengths. The intense blue color in the benzazulene solutions (deep green as crystalline plates) is due to the weak ^1L_b band which has its onset of absorption at about 13,000 cm^{-1} which is some 15,000 cm^{-1} to red of the corresponding band in phenanthrene. This transition is hidden by the more intense ^1L_a band in anthracene.[2,5]

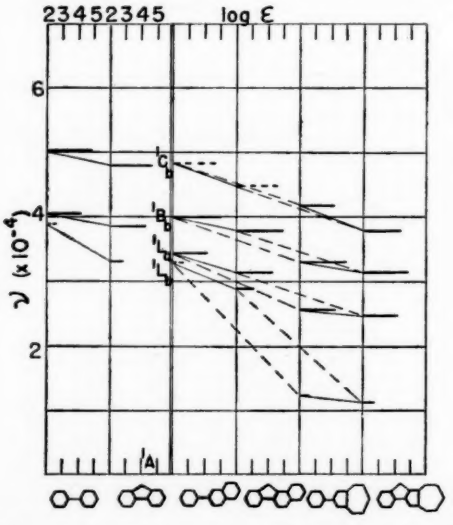

FIG. 3. Spectral resemblances between various phenyl substituted hydrocarbons. Date for biphenyl and fluorene (see reference 8); and 1- and 2-phenyl naphthalene and 1,2-benzfluorene (see reference c of Table II); and for 2-phenyl azulene and indenoazulene (see reference 4).

[5] H. Sponer and G. Nordheim, "Theoretical studies on the electronic levels of polynuclear hydrocarbons," ONR Contract N.6 ori-107, T.O. 1, Annual Report (June 1, 1948).

The spectral resemblances between these various compounds are noted when one considers the data in Fig. 2. Here the effect of annelation is seen from a comparison of the spectra of benzene, naphthalene, anthracene on the one hand with those of azulene and 1,2-benzazulene on the other. Similar types of shifts to the red in various bands are noted upon annelation in both series of compounds.

PHENYL-SUBSTITUTED COMPOUNDS

The spectra of various phenyl-substituted azulenes, 2-phenyl azulene and indeno-azulene, are compared with those of their regular isomers, 2-phenyl naphthalene and 1,2-benzfluorene in Fig. 3. The spectra of biphenyl and fluorene are added for comparison. The position of the ^1L_b band in biphenyl which is probably hidden by the more intense ^1L_a is indicated at 39,000 cm^{-1} by a dotted line. This band is seen to appear at 33,000 cm^{-1} when the two aromatic rings are twisted in the plane as occurs in fluorene.

This sequence of bands is repeated in the annelated biphenyl and fluorene, i.e., in 2-phenyl naphthalene and in 1,2-benzfluorene, and these bands are shifted some 7000 to 10,000 cm^{-1} in a regular manner to the red of those of the former compounds in a manner similar to the shift which is seen to occur in the case of benzene and naphthalene. Again the various corresponding band systems are similar with respect to vibrational structure, intensity and sequence, as can be seen from a study of the detailed spectra of these compounds.

When the naphthyl portion of the two last discussed compounds, 2-phenyl naphthalene and 1,2-benzfluorene, is replaced by its corresponding odd-ring isomer, azulene, one obtains 2-phenyl azulene and indeno-azulene, the spectra of which are included in Fig. 3. It is to be noted that again the sequence of bands in these azulene derivatives are similar and are shifted (except for ^1L_b) some 7000 cm^{-1} to the red of the regular isomers, 2-phenyl naphthalene and benzfluorene. The intense color of these azulene compounds may be accounted for by the presence of the ^1L_b band at about 12,500 cm^{-1}, some 17,000 cm^{-1} to the red of the corresponding band in the normal isomers.

DISCUSSION

The first five distinct band systems observed in azulene, labeled starting at longest wave-lengths, ^1L_b, ^1L_a, ^1B_b, ^1C_b, and ^1B_a according to a scheme of systematic nomenclature for condensed hydrocarbons which is described elsewhere[2,6] are seen to have their counterparts in the spectra of the various azulene derivatives described above. In peak intensity, the two sets of bands for each set of isomers agree within a factor of about two as is seen in the summary of the main features of the spectra in Tables I and II. If the integrated intensity over the whole spectrum, the oscillator strength,[7] f, is considered, the agreement is much better as is indicated by the total f-values. In position, the agreement between various transitions is within 2000 cm^{-1} for corresponding bands in each pair of compounds (the azulene derivative and its normal six-carbon ring isomer) when any one particular transition in the two compounds are allowed to overlap. This, of course, does not hold for the ^1L_b transition which is some additional 9000 cm^{-1} to the red in the various azulenes. It is seen that, for the spectra of each pair of compounds, there are the following differences. Two states have moved with respect to the higher singlet ^1B_a, ^1B_b, and ^1C_b states. The color of the azulenes is seen to result from the total 16,000 to 17,000 cm^{-1} shift of the ^1L_b band ($\log\epsilon \sim 2.4$–2.6) part of which shift is due to the fact that the ground state, ^1A, has moved upward by about 9000 cm^{-1} and the balance to the movement downward of about 7000 to 8000 cm^{-1} of the weak forbidden ^1L_b state.

In making a comparison of the spectra of fluorene

TABLE II. Main features of spectra of biphenyl-type compounds.

	^1A–^1L_b	^1A–^1L_a	^1A–^1B_b	^1A–^1C_b(?)	Total f-value
Biphenyl[a]					
Onset of absorption (cm^{-1})					
Peak		40500	50500	(62500)	
ϵ_{max} ($mole^{-1}$ cm^{-1})		18000	52000	(40000)	
f		0.47	1.70	~0.6	~2.77
(To cut-off)		(45000)	(55000)	(65000)	
Fluorene[a]					
Onset of absorption (cm^{-1})	33000				
Peak		38400	48000	(60500)	
ϵ_{max} ($mole^{-1}$ cm^{-1})	10500	21500	43000	(50000)	
f	0.08	0.41	1.37	~0.7	~2.56
(To cut-off)	(35600)	(42500)	(55000)	(63000)	
2-Phenyl naphthalene[b]					
Onset of absorption (cm^{-1})		35300			
Peak			40000	(48500)	
ϵ_{max} ($mole^{-1}$ cm^{-1})		17000	65000	(25000)	
f		0.40	1.10	~0.5	~2.0
(To cut-off)		(38000)	(44000)	(51000)	
1,2-Benzfluorene[c]					
Onset of absorption (cm^{-1})	28500	30600			
Peak			38000	45000	
ϵ_{max} ($mole^{-1}$ cm^{-1})	1100	15000	70000	30000	
f	0.005	0.28	1.02	0.6	1.9
(To cut-off)	(29500)	(35800)	(40800)	(47500)	
2-Phenyl azulene[d]					
Onset of absorption (cm^{-1})	12500	25700			
Peak			33100	42000	
ϵ_{max} ($mole^{-1}$ cm^{-1})	350	17500	85000	17500	
f	0.006	0.30	2.00	0.41	2.71
(To cut-off)	(25700)	(30700)	(40000)	(45500)	
Indeno-azulene[d]					
Onset of absorption (cm^{-1})	11700	25000			
Peak			31900	37900	
ϵ_{max} ($mole^{-1}$ cm^{-1})	300	14500	64000	26000	
f	0.005	0.29	1.35	0.55	2.20
(To cut-off)	(25000)	(29000)	(37000)	(41700)	

[a] See reference 8.
[b] Data calculated from curve of R. N. Jones, J. Am. Chem. Soc. 63, 1658 (1941).
[c] Data calculated from curve of Jacobs, Craig, and Lavin, J. Biol. Chem. 141, 51 (1941).
[d] See reference 4.

[6] J. R. Platt, J. Chem. Phys. 17, 484 (1949).

[7] J. R. Platt and H. B. Klevens, Chem. Rev. 41, 301 (1947).

and biphenyl to 1700A,[8] it is assumed that the introduction of a methylene bridge (fluorene is 2,2′-methylene-biphenyl) results in an approximately planar structure in which the phenyl groups are not symmetrical about an axis through the 4,4′-positions. This is in agreement with dipole moment measurements which favor this configuration.[9] The band positions change due to alkyl substitution (bathochromic shift) and the intensities of the ^1B_b bands decrease as is indicated by the decrease in f-values. It is to be noted that essentially the same occurs in the comparison of the spectra and the f-values of anthracene and phenanthrene.

Similar regularities (bathochromic shifts and decrease in f-values) are also observed in the spectra of 2-phenylnaphthalene and its methylene derivative, 1,2-benzfluorene, and in 2-phenylazulene and its methylene derivative, indeno-azulene, as can be seen from the data in Fig. 3 and Table II, although in these compounds the decreases are smaller due probably to less bending of the molecule. There is seen in these compounds only the normal bathochromic effect due to alkyl substitution and not the marked changes in intensity normally associated with twisting of double bonds and twisting of rings from planar positions. The ^1C_b band, transversely polarized to the long axis of the molecule, increases in intensity upon loss of C_{2v} symmetry about this long axis as is seen in a comparison of the f-values of 0.28 for anthracene and 0.60 for phenanthrene. A similar increase is observed for the same transition in 2-phenylazulene and indeno-azulene with f-values of 0.41 and 0.55, respectively, although this increase is also smaller than that observed in the case of the more highly bent polyacene, phenanthrene. The approximated f-values of this singlet $^1C_b(?)$ band in biphenyl and fluorene, and 2-phenylnaphthalene and 1,2-benzfluorene are to be expected to show a similar small increase in going from the linear to the slightly bent methylene derivative.

[8] J. R. Platt and H. B. Klevens (unpublished results).
[9] Hughes, LeFevre, and LeFevre, J. Chem. Soc., 202 (1937).

THE JOURNAL OF CHEMICAL PHYSICS VOLUME 18, NUMBER 8 AUGUST, 1950

On the Notion of Pressure in a Canonical Ensemble

R. J. RIDDELL, JR. AND G. E. UHLENBECK
University of Michigan, Ann Arbor, Michigan
(Received April 6, 1950)

Recently a controversy has arisen between J. De Boer and H. S. Green concerning the notion of pressure in a canonical ensemble. According to Green, only classically is the pressure as derived from the partition function equal to that obtained from the virial theorem, while at low temperatures, at which quantum effects become important, there will be considerable deviations between the two. De Boer attempts to prove that the two pressures are actually identical. We have come to the same conclusion, and shall show this in several ways; first, by considering a simple example (Section 2), and then in general using the energy representation (Section 3). We believe that the discrepancy between the two pressures which Green has found is in fact due to improper handling of the effect of the wall of the vessel in which the particles are contained. Finally, we are of the opinion that Green's criticism of De Boer's calculation is not justified, and in the last section arguments are given to show that the traces of all commutators of interest in quantum statistical mechanics are zero.

1. INTRODUCTION

RECENTLY a controversy has arisen between J. De Boer and H. S. Green[1] concerning the notion of pressure in a canonical ensemble. According to Green, the pressure as derived from the partition function Z:

$$p=1/\beta Z\cdot\partial Z/\partial V, \tag{1}$$

where $\beta=(kT)^{-1}$, is not necessarily equal to the pressure as derived from the virial theorem:

$$pV=\tfrac{2}{3}\langle K_n\rangle_{Av}+\tfrac{1}{3}\langle\Phi_n\rangle_{Av} \tag{2}$$

where K is the kinetic energy, Φ is the virial of the intermolecular forces, and where the $\langle\cdots\rangle_{Av}$ means an average over the canonical ensemble.* Green asserts that the first pressure (which he calls the thermodynamical pressure) is the one exerted by the system in the equilibrium state, while the second (kinetic pressure) is the one occurring in the hydrodynamical equations.[2] Only in classical statistical mechanics would these two pressures be identical. However, according to Green, as soon as quantum effects become important (as would be the case at very low temperatures) an

[1] J. De Boer, Physica XV, 843 (1949); Nuovo Cimento Supplement to the Statistical Mechanics Conference at Florence (May, 1949), p. 199 and discussion. H. S. Green, Physica XV, 882 (1949). Compare also J. Yvon, Comptes Rendus 227, 763 (1949).

* Compare, for instance, Tolman, *Principles of Statistical Mechanics*, Chapter IX. If F is any kind of operator then in the energy representation:

$$\langle F_n\rangle_{Av}=\frac{1}{Z}\sum_n F_n\exp(-\beta E_n),$$

where F_n is the average of F in a state of energy E_n.

[2] H. S. Green, Proc. Roy. Soc. A194, 244 (1949).

appreciable difference between the two pressures will occur.

On the other hand, De Boer has attempted to show that the two pressures as given by (1) and (2) are *always* identical. Since the argument does not seem to have been completely settled, and since Green's result is so different from the usual conception, a further analysis seems justified. In the following we will confirm De Boer's result using a slight modification of his method of proof. Green's criticism of De Boer's proof cannot, in our opinion, be justified. The origin of the discrepancy between Green's kinetic and thermodynamic pressures lies, in our opinion, in the treatment of the boundary conditions due to the potential of the wall of the vessel in which the system is enclosed. Green (and also De Boer) represents the vessel by a sudden infinite potential jump, and it is well known that with such potentials the formulas of the transformation theory have to be used with caution.

2. A SIMPLE EXAMPLE

In order to illustrate in an explicitly soluble case that with a non-singular wall potential the two pressures (1) and (2) are identical, consider the following simple example: two equal one-dimensional particles bound together by a harmonic potential, moving in a "vessel" represented by another, but very weak, harmonic potential. The Hamiltonian for the system is:

$$\mathcal{H}=(p_1^2+p_2^2)/2m+\tfrac{1}{2}m\omega^2(q_1^2+q_2^2)+\tfrac{1}{2}m\alpha^2(q_1-q_2)^2$$

or, introducing the center of gravity and relative coordinates Q, q:

$$\mathcal{H}=P^2/4m+p^2/m+m\omega^2Q^2+\tfrac{1}{4}m\omega_1^2q^2$$

where:

$$\omega_1^2=\omega^2+2\alpha^2.$$

Clearly the energy values are:

$$E_{N,n}=(N+\tfrac{1}{2})\hbar\omega+(n+\tfrac{1}{2})\hbar\omega_1.$$

To find the "pressure" from the partition function $Z=\sum_{N,n}\exp(-\beta E_{N,n})$ one has to identify the "volume" of the vessel with $1/\omega$. To prove, therefore, the equality of the thermodynamic and kinetic pressures, one has to show that:

$$-\omega^2/\beta Z\cdot\partial Z/\partial\omega=\omega\langle 2K_n+\Phi_n\rangle_{Av}. \tag{3}$$

The factor $\frac{1}{3}$ in (2) must be omitted since the problem is one dimensional.

Because of the harmonicity of the forces one has immediately:

$$2K_{N,n}=E_{N,n};$$

$$\Phi_{N,n}=-\sum_i\left(q_i\frac{\partial V_{\text{int}}}{\partial q_i}\right)_{N,n}=-m\alpha^2(q^2)_{N,n}$$

$$=-(n+\tfrac{1}{2})2\hbar\alpha^2/\omega_1.$$

On the other hand:

$$-\frac{\omega^2}{\beta Z}\cdot\frac{\partial Z}{\partial\omega}$$

$$=\frac{\omega^2}{Z}\sum_{N,n}\frac{\partial E_{N,n}}{\partial\omega}\exp(-\beta E_{N,n})$$

$$=\omega/Z\sum_{N,n}\{E_{N,n}-(n+\tfrac{1}{2})2\hbar\alpha^2/\omega_1\}\exp(-\beta E_{N,n})$$

so that (3) is evident.

3. THE GENERAL PROOF

To perform the differentiation of Z with respect to the volume in general, Green and also De Boer use the trick of measuring all coordinates with a unit L, which is characteristic of the vessel. In this way they were able to shift the differentiation with respect to the boundary to a differentiation of the operator $\exp(-\beta\mathcal{H})$. To show how this works, we will use as in Section 2 the energy representation of all operators. If $V=L^3$, then from (1):

$$p=-\frac{1}{3VZ}\sum_n L\frac{\partial E_n}{\partial L}\exp(-\beta E_n). \tag{4}$$

In order to determine $\partial E_n/\partial L$ we must go to the Schroedinger equation for the whole system:

$$\mathcal{H}\Psi_n\equiv[K+V_{\text{int}}+W(q_i/L)]\Psi_n=E_n\Psi_n, \tag{5}$$

where V_{int} is the potential of the intermolecular forces and where we have explicitly introduced the potential W due to the wall. It is best to consider W as a smooth, though nearly step-like, function near the boundary, becoming infinite for $q_i\to\pm\infty$. There is then no need to impose a boundary condition on Ψ_n (except for the usual one that $\Psi_n\to 0$ as $q_i\to\pm\infty$), and all the coordinates q_i can be taken from $-\infty$ to $+\infty$. Since W depends on L, Ψ_n and E_n are also functions of L. Now let us replace q_i by $L\bar{q}_i$, and then differentiate (5) with respect to L, considering the $\bar{q}_i$ as constant. Thus:

$$\frac{\partial\mathcal{H}}{\partial L}\Psi_n+\mathcal{H}\frac{\partial\Psi_n}{\partial L}=\frac{\partial E_n}{\partial L}\Psi_n+E_n\frac{\partial\Psi_n}{\partial L}.$$

Multiplying on the left by Ψ_n^* and integrating over all coordinates, one obtains:

$$\frac{\partial E_n}{\partial L}=\int\Psi_n^*\frac{\partial\mathcal{H}}{\partial L}\Psi_n d\tau, \tag{6}$$

since the terms in $(\partial\Psi_n/\partial L)$ cancel using the Hermitian property of $\mathcal{H}$. Since, in terms of the $\bar{q}_i$:

$$\mathcal{H}=-\frac{\hbar^2}{2mL^2}\sum_i\frac{\partial^2}{\partial\bar{q}_i^2}$$

$$+V_{\text{int}}(L\bar{q}_1,\cdots,L\bar{q}_N)+W(\bar{q}_1,\cdots,\bar{q}_N) \tag{7}$$

in $(\partial\mathfrak{H}/\partial L)$ the wall potential drops out and one verifies easily:

$$L(\partial\mathfrak{H}/\partial L)=-2K-\Phi, \tag{8}$$

where

$$\Phi=-\sum_i q_i\frac{\partial V_{\text{int}}}{\partial q_i}$$

is the virial of the intermolecular forces. From (6), therefore,

$$L(\partial E_n/\partial L)=-2K_n-\Phi_n$$

and substituting in (4) gives the virial theorem (2).

4. DISCUSSION OF GREEN'S CALCULATION

Green uses the coordinate representation of all operators, instead of the energy representation used in the previous section. The partition function is now written as:

$$Z=\int dq\langle q|\exp(-\beta\mathfrak{H})|q\rangle, \tag{9}$$

where q stands for the coordinates $q_1, \cdots, q_N$ of all the particles and where, if the wall potential is included in $\mathfrak{H}$, the integrals may be taken from $-\infty$ to $+\infty$. Introducing the reduced coordinates $\bar{q}_i=q_iL^{-1}$, one finds:

$$V\frac{\partial Z}{\partial V}=\frac{L}{3}\frac{\partial Z}{\partial L}=NZ$$
$$+\frac{L^{3N}}{3}\int d\bar{q}L\frac{\partial}{\partial L}\langle L\bar{q}|\exp(-\beta\mathfrak{H})|L\bar{q}\rangle. \tag{10}$$

To carry out the differentiation, one expands the matrix $\exp(-\beta\mathfrak{H})$ in its power series in $\mathfrak{H}$, and then differentiates term by term. Following Green, one obtains for the first term, going back to the original variables q_i after the differentiation is completed:

$$L\frac{\partial}{\partial L}\langle L\bar{q}|\mathfrak{H}|L\bar{q}'\rangle$$
$$=\left(q\cdot\frac{\partial}{\partial q}+q'\cdot\frac{\partial}{\partial q'}\right)\langle q|\mathfrak{H}|q'\rangle+\langle q|\Phi_{\text{wall}}|q'\rangle,$$

where

$$\Phi_{\text{wall}}=-\sum_i q_i\frac{\partial W}{\partial q_i}$$

is the virial of the wall potential. Analogously, one can proceed in the differentiation of the matrix elements of the higher powers of $\mathfrak{H}$, and one can show by induction:

$$L\frac{\partial}{\partial L}\langle L\bar{q}|\exp(-\beta\mathfrak{H})|L\bar{q}'\rangle$$
$$=\left(q\cdot\frac{\partial}{\partial q}+q'\cdot\frac{\partial}{\partial q'}\right)\langle q|\exp(-\beta\mathfrak{H})|q'\rangle$$
$$-\sum_{m=0}^{\infty}\frac{\beta^{m+1}}{(m+1)!}\langle q|\mu_m\exp(-\beta\mathfrak{H})|q'\rangle, \tag{11}$$

where $\mu_0\equiv\Phi_W$, and $\mu_m=[\mu_{m-1},\mathfrak{H}]$, and the square brackets indicate as usual the commutator. Introducing (11) in (10) and using (1), one easily verifies:

$$p=\frac{i}{3\beta\hbar VZ}\int dq\langle q|[p\cdot q,\exp(-\beta\mathfrak{H})]|q\rangle$$
$$-\frac{1}{3VZ}\sum_{m=0}^{\infty}\frac{\beta^m}{(m+1)!}\int dq\langle q|\mu_m\exp(-\beta\mathfrak{H})|q\rangle. \tag{12}$$

The first term in (12) is identical with Green's expression for the pressure. The reason that he does not obtain the second term in (12) is clearly due to the fact that he does not include the wall potential in the Hamiltonian, but instead restricts his coordinates q_i to the finite range $0\leqslant q_i\leqslant L$. Omitting the wall potential, the matrix element of $\exp(-\beta\mathfrak{H})$ in the coordinate representation is apparently a function of q, q' alone. Therefore with the reduced coordinates the differentiation operation $L(\partial/\partial L)$ is apparently equivalent to the differentiation operation $q\cdot(\partial/\partial q)+q'\cdot(\partial/\partial q')$ on the original matrix element. The second term in (11) would not be there and one would obtain Green's result for the pressure. We do *not* believe that this is correct, because the matrix element of $\exp(-\beta\mathfrak{H})$ besides being a function of q, q' is also implicitly a function of L because of the boundary condition imposed on the wave functions. One can see this, for instance, by going back to the energy representation. One has:

$$\langle q|\exp(-\beta\mathfrak{H})|q'\rangle=\sum_n\exp(-\beta E_n)\Psi_n^*(q)\Psi_n(q').$$

Following Green, one would neglect, for instance, the dependence of E_n on L. This, however, just gives, as shown in the previous section, De Boer's result. The other terms (including those of Green) obtained from the $L(\partial/\partial L)$ differentiation must, therefore, be zero. This is in fact, we think, the case. Contrary to Green, and in accordance with De Boer, we are of the opinion that the traces of the commutators which occur in the usual applications of quantum statistics and in particular in (12) are all zero,† so that (12) reduces to the trivial result:

$$pV=-\tfrac{1}{3}\langle(\Phi_{\text{wall}})_n\rangle_{\text{Av}}. \tag{13}$$

In order to obtain (2) from (9) one must carry out the L-differentiation more directly, essentially as De Boer does. Since

$$\langle q|\exp(-\beta\mathfrak{H})|q'\rangle=\exp(-\beta\mathfrak{H}_{\text{op}})\delta(q-q')$$

and

$$\delta(L\bar{q}-L\bar{q}')=1/L\delta(\bar{q}-\bar{q}'),$$

one can write for the partition function

$$Z=\int\int d\bar{q}d\bar{q}'\delta(\bar{q}-\bar{q}')\exp(-\beta\mathfrak{H}_{\text{op}})\delta(\bar{q}-\bar{q}').$$

† For some further comments on this point see Section 5. This is the main point of the criticism which Green made against De Boer's method of proof.

Now L appears only in $\mathfrak{H}_{op}$ (compare Eq. (7)), and one proves that

$$L\frac{\partial}{\partial L}\exp(-\beta\mathfrak{H}_{op})=-\sum_{m=0}^{\infty}\frac{\mu_m\beta^{m+1}}{(m+1)!}\exp(-\beta\mathfrak{H}_{op}), \quad (14)$$

where again $\mu_m=[\mu_{m-1},\mathfrak{H}]$, but where now

$$\mu_0\equiv L\frac{\partial\mathfrak{H}_{op}}{\partial L}=-2K-\Phi,$$

according to (8).†† Omitting the traces of all commutators, this leads immediately to (2).¶

5. ON THE TRACES OF COMMUTATORS IN QUANTUM STATISTICS

Green remarks that the trace of the commutator of two matrices A and B is not necessarily zero, since it depends on the convergence of the double integral (or double sum):

$$\int\int dq'dq''\langle q'|A|q''\rangle\langle q''|B|q'\rangle, \quad (15)$$

and this may not be the case if A and B are singular, as, for instance, p and q. However, in quantum statistics one of the matrices occurring is always the density matrix:

$$\rho(q,q')=\langle q|\exp(-\beta\mathfrak{H})|q'\rangle$$
$$=\sum_n\exp(-\beta E_n)\Psi_n^*(q)\Psi_n(q').$$

For the usual types of Hamiltonians $\rho(q,q')$ is an analytic function of q and q', vanishing exponentially for large values of q and q'. This follows from the fact that $\rho(q,q')$ is the fundamental solution of the parabolic differential equation:||

$$\frac{\partial\varphi(q,\beta)}{\partial\beta}=-\mathfrak{H}_{op}\varphi=\frac{\hbar^2}{2m}\Delta\varphi-V\varphi. \quad (16)$$

For instance, for the harmonic oscillator with

$$\mathfrak{H}=\tfrac{1}{2}(p^2+\omega^2q^2):$$

$$\rho(q,q')=\left\{\frac{\omega}{2\pi\hbar\sinh(\hbar\omega\beta)}\right\}^{\frac{1}{2}}\exp\left[-\frac{\omega}{2\hbar[1-\exp(-2\hbar\omega\beta)]}\right.$$
$$\left.\cdot\{(q^2+q'^2)(1+\exp(-2\hbar\omega\beta))-4qq'\exp(-\hbar\omega\beta)\}\right].$$

For such functions we believe that the integrals of the type (15) are always convergent, and therefore the order of integration may be interchanged, as is necessary in order to prove that the trace of the commutator is zero. For example:

$$Tr[p,\exp(-\beta\mathfrak{H})]=\frac{\hbar}{i}\int_{-\infty}^{\infty}dq\left(\frac{\partial\rho}{\partial q}+\frac{\partial\rho}{\partial q'}\right)_{q=q'}$$
$$=\frac{\hbar}{i}\int_C\left[\frac{\partial\rho}{\partial q}dq+\frac{\partial\rho}{\partial q'}dq'\right],$$

where C is the path $q=q'$ from $-\infty$ to $+\infty$. The line integral is clearly zero since ρ is zero at infinity. Analogously, one shows that the trace of the commutator of p^2 and of $p\cdot q$ with $\exp(-\beta\mathfrak{H})$ is zero. In general, the theorems:

$$Tr(AB)=Tr(BA)$$
$$Tr(ABC)=Tr(CAB)=Tr(BCA)$$

and so on, will be valid if only one of the matrices A, B, C, $\cdots$ is the density matrix. The other matrices may then be of the singular kind as, for example, the impulse and coordinate matrices are.

†† Equation (14) is equivalent to (*I*) in De Boer's paper after a slight error is corrected.

¶ (13) would result if one carries the L-differentiation out without introducing the reduced coordinates $\bar{q}_i$. One can then use (14) again, but now

$$\mu_0\equiv L(\partial W/\partial L)=+\Phi_{wall}.$$

|| This means that $\rho(q,q')$ is the solution of (16), which for $\beta=0$ becomes $\delta(q-q')$. Of course, certain regularity conditions are necessary for $V(q)$.

Molecular Orbitals for H_3^{+}*

J. M. WALSH, R. A. MOORE, AND F. A. MATSEN
Departments of Physics and Chemistry, The University of Texas, Austin, Texas
(Received April 24, 1950)

A somewhat more general concept of molecular orbitals than used heretofore is applied to H_3^+. It is shown to be superior to the Heitler-London approximation, but inferior to the HLSP-plus-ionic-terms treatment of Hirschfelder. Relations between the HLSP and molecular orbital approaches to wave functions are discussed.

IN the simplest LCAO molecular orbital treatment, the H_2 wave function[1] is

$$\psi=[a_1(1)+a_2(1)]\cdot[a_1(2)+a_2(2)] \quad (1)$$

which yields a relatively poor value of the binding energy. Coulson[2] has shown that if the electrons are allowed to separate to some extent, as with the orbitals

$$[a_1(1)+\lambda a_2(1)] \quad \text{and} \quad [\lambda a_1(2)+a_2(2)] \quad (2)$$

the binding energy calculation is greatly improved. For a two-electron singlet state, the orbital function must be symmetric with respect to electron interchange so that Coulson's final function is

$$\psi=[a_1(1)+\lambda a_2(1)][\lambda a_1(2)+a_2(2)]+[\lambda a_1(1)+a_2(1)][a_1(2)+\lambda a_2(2)]. \quad (3)$$

On expansion Coulson shows that this function actually is the Heitler-London-plus-ionic-term wave function as used by Weinbaum.

It was of interest in the light of the success of this analysis to examine the most general LCAO molecular orbital wave functions for a linear-symmetrical H_3^+ molecule. A simpler molecular orbital treatment for this system has been carried out by Pearson[3] and a complete HLSP-plus-ionic-terms analysis has been done by Hirschfelder, *et al.*[4]

First, it is instructive to consider the problem of one electron in the field of the nuclei, or H_3^{++}. The three orthogonal molecular orbitals which can be built for this linear symmetrical model are

$$\begin{aligned}&\text{(a)}\ a_1(k)+\lambda a_2(k)+a_3(k),\\ &\text{(b)}\ a_1(k)-a_3(k),\\ &\text{(c)}\ a_1(k)-\lambda' a_2(k)+a_3(k),\end{aligned} \quad (4)$$

where $\lambda'=[2(1+S_{13}+\lambda S_{12})]/[\lambda+2S_{12}]$ and S_{ij} are the overlap integrals

$$S_{ij}=\int a_i(k)a_j(k)d\tau_k.$$

The first of these is taken to represent the ground state since it contains no nodal surfaces.[5] A variation calculation was carried out using the H-like atomic orbitals $a_i(k)=(Z/a_0)^{\frac{3}{2}}1/\sqrt{\pi}\exp(-Zr_{ik}/a_0)$. The results show this symmetrical system unstable with respect to dissociation into two protons and a hydrogen atom, as shown in Fig. 1.

For the two-electron problem, the most general LCAO molecular orbital wave function is

$$\psi=[a_1(1)+\lambda_2 a_2(1)+\lambda_3 a_3(1)]\times[a_1(2)+\mu_2 a_2(2)+\mu_3 a_3(2)]+[(2)][(1)].$$

Expanding and regrouping

$$\begin{aligned}\psi=&\{(\mu_2+\lambda_2)[a_1(1)a_2(2)+a_2(1)a_1(2)]\\ &+(\lambda_2\mu_3+\lambda_3\mu_2)[a_2(1)a_3(2)+a_3(1)a_2(2)]\}\\ &+\{(\mu_3+\lambda_3)[a_1(1)a_3(2)+a_3(1)a_1(2)]\}\\ &+\{[2a_1(1)a_1(2)+2\lambda_3\mu_3 a_3(1)a_3(2)]\}\\ &+2\lambda_2\mu_2[a_2(1)a_2(2)].\end{aligned}$$

From

1. Symmetry of the molecule (requiring symmetry or antisymmetry with respect to a_1-a_3 nuclear interchange).

2. The condition that the lowest energy molecular orbitals will contain no nodal surfaces[5,6] (requiring λ-

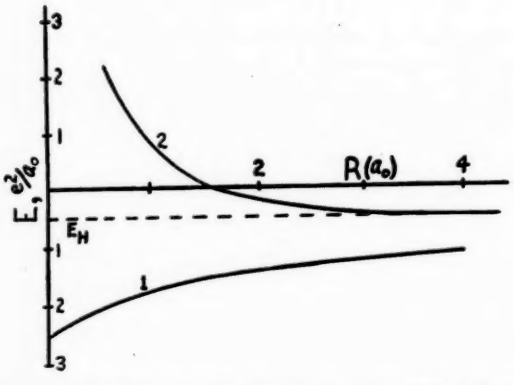

FIG. 1. H_3^{++} energy curves. 1. Electron energy. 2. Total energy.

* This research has been aided by funds made available under contract from the ONR.

[1] See L. Pauling and E. B. Wilson, *Introduction to Quantum Mechanics* (McGraw-Hill Book Company, Inc., New York, 1935), p. 347.

[2] C. A. Coulson and I. Fischer, Phil. Mag. **40**, 393 (1949).

[3] R. G. Pearson, J. Chem. Phys. **16**, 502 (1948).

[4] J. Hirschfelder, H. Eyring, and N. Rosen, J. Chem. Phys. **4**, 121–133 (1935).

[5] K. F. Herzfeld, Chem. Rev. **41**, 233 (1947); K. F. Herzfeld, Rev. Mod. Phys. **21**, 527 (1949). It is shown, for LCAO molecular orbitals built of similar atomic orbitals, that there will be 0, 1, 2, . . . nodal surfaces in the ground, first excited, second excited . . . energy states.

[6] Taken here to mean the λ- and μ-parameters are positive, eliminating from consideration values that are negative but nearly zero so that they produce no nodes.

and μ-parameters to be positive) it is necessary that

$$\mu_2+\lambda_2=\lambda_2\mu_3+\lambda_3\mu_2, \quad 1=\lambda_3\mu_3.$$

By straightforward algebra, these two relations are satisfied only if:

$$(A)\ \psi=[a_1(1)+\lambda a_2(1)+\lambda' a_3(1)] \times[\lambda' a_1(2)+\lambda a_2(2)+a_3(2)]+[(2)][(1)]$$

or,

$$(B)\ \psi=[a_1(1)+\lambda a_2(1)+a_3(1)] \times[a_1(2)+\mu a_2(2)+a_3(2)]+[(2)][(1)].$$

These two wave functions may be written in HLSP-plus-ionic-terms form:

$$(A')\ \psi=[a_1(1)a_2(2)+a_2(1)a_1(2) +a_2(1)a_3(2)+a_3(1)a_2(2)] +\frac{1+\lambda'^2}{\lambda(1+\lambda')}[a_1(1)a_3(2)+a_3(1)a_1(2)] +\frac{2\lambda'}{\lambda(1+\lambda')}[a_1(1)a_1(2)+a_3(1)a_3(2)] +\frac{2\lambda^2}{\lambda(1+\lambda')}[a_2(1)a_2(2)]$$

$$(B')\ \psi=[a_1(1)a_2(2)+a_2(1)a_1(2) +a_2(1)a_3(2)+a_3(1)a_2(2)] +\frac{2}{\lambda+\mu}[a_1(1)a_3(2)+a_3(1)a_1(2)] +\frac{2}{\lambda+\mu}[a_1(1)a_1(2)+a_3(1)a_3(2)] +\frac{2\mu\lambda}{\lambda+\mu}[a_2(1)a_2(2)].$$

Molecular orbitals forms (A) and (B) may be readily interpreted physically: The first of these (A) differs from the conventional molecular orbital treatment in that the λ' parameter, if different from unity, would cause one electron to shift toward atom a_3 because the other is on atom a_1. The second (B), if λ is unequal to μ, would cause one electron to have a greater affinity for the end nuclei because the other has a more central position. Thus the form of the one-electron molecular orbital as given above (Eq. (4a)) is altered to make allowance for electron repulsion effects. The electron permutation term in (A) and in (B) (required to satisfy the Pauli principle) introduces an orbital interchange resonance energy which will, in general, increase binding.

Several qualitative conclusions may be drawn without actual calculation:

1. Both functions (A') and (B') are less general than the HLSP-plus-ionic-terms wave function used by Hirschfelder *et al.*;[4] i.e.,

$$\psi=[a_1(1)a_2(1)+a_1(2)a_2(1)+a_2(1)a_3(2)+a_3(1)a_2(2)] +C_1[a_1(1)a_3(2)+a_3(1)a_1(2)] +C_2[a_1(1)a_1(2)+a_3(1)a_3(2)]+C_3[a_2(1)a_2(2)], \quad (5)$$

where C_1, C_2, and C_3 are independent. It follows from use of the variation principle that the binding energy with respect to dissociation into two H atoms and a proton, as obtained using functions (A) and (B), cannot exceed 108.6 kcal./mole obtained from (5).

2. If one lets $\lambda\rightarrow\infty$ and $\mu=0$, it is apparent that the (B') type wave function reduces to the Heitler-London wave function,

$$\psi=[a_1(1)a_2(2)+a_1(2)a_2(1)+a_2(1)a_3(2)+a_3(1)a_2(2)].$$

Hence the binding for the (B) wave function must not be less than 91.92 kcal./mole, as obtained in reference 4 for the above function. However, no particular choice of the λ, λ' parameters reduces (A') to a Heitler-London wave function, so there is no assurance that use of (A) will actually give greater binding than the Heitler-London wave function.

3. By setting $\lambda'=1$ in (A) or $\lambda=\mu$ in (B), these functions reduce to the conventional form in which both electrons occupy identical orbitals. This form, with a screening constant, was treated by Pearson.[3]

The integrals occuring in the variation treatments of H_3^+ are just those common to previous work on H_2, plus three-center integrals such as

$$\int\frac{a_1(1)a_2(1)}{r_{a3}1}d\tau_1 \quad \text{and} \quad \int\int\frac{a_1(1)a_2(1)a_2(2)a_3(2)}{r_{12}}d\tau_1 d\tau_2.$$

These integrals are discussed by Hirschfelder.[4] Values used here were taken from the tables of Hirschfelder and Weygandt,[7] which were compiled with the aid of a differential analyzer.

First will be presented the results obtained on setting $Z=1$. In the wave function of type (A) the binding energy was not affected to four significant figures by the variation of λ' away from unity. Thus this wave

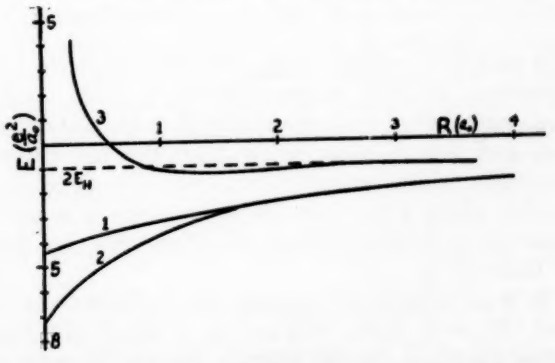

FIG. 2. H_3^+ energy curves. 1. Electron energy, $Z=1$. 2. Electron energy, $Z\neq1$. 3. Total energy.

[7] See J. Hirschfelder and C. Weygandt, J. Chem. Phys. 6, 806 (1938).

TABLE I. Wave function parameters and energy values.

	No screening ($Z=1$) Energy	No screening ($Z=1$) Parameters	With screening ($Z\neq1$) Energy	With screening ($Z\neq1$) Parameters
Conventional Molecular orbital (Equation (6))	88.90 kcal./mole	$\lambda=2.4$ $R=2.0a_0$	136.8 kcal./mole	$\lambda=1.8$ $Z=1.32$ $R=1.52a_0$
General Molecular orbital (Type (A))	88.90 kcal./mole	$\lambda=2.4$ $\lambda'=1.0$ $R=2.0a_0$	136.8 kcal./mole	$\lambda=1.8$ $\lambda'=1.0$ $Z=1.32$ $R=1.52a_0$
General Molecular orbital (Type (B))	97.96 kcal./mole	$\lambda=\infty$ $\mu=0.33$ $R=2.0a_0$	138.5 kcal./mole	$\lambda=\infty$ $\mu=0.25$ $Z=1.30$ $R=1.54a_0$
Heitler-London	91.92 kcal./mole	$R=2.0a_0$	130.9 kcal./mole	$R=1.55a_0$ $Z=1.30$
HLSP-plus-ionic-terms	108.6 kcal./mole	$C_1=1.0$ $C_2=0.54$ $C_3=0.70$ $C_4=-0.54$ $R=2.0a_0$	155.4 kcal./mole	$C_1\cdots$ $C_2\cdots$ $C_3\cdots$ $C_4\cdots$ $Z=1.31$ $R=1.52a_0$

function gives the same result as the conventional type molecular orbitals used for H_3^{++}; i.e.,

$$\psi=[a_1(1)+\lambda a_2(1)+a_3(1)]\cdot[a_1(2)+\lambda a_2(2)+a_3(2)]. \quad (6)$$

Variation of the λ-parameter to $\lambda=2.4$ gave a maximum binding of 88.90 kcal./mole for an internuclear separation of $2.0a_0$. Thus this two parameter wave function (A) (and also the conventional molecular orbital wave function above) give less binding than the 91.92 kcal./mole of the Heitler-London approximation.

With the wave function of type (B) considerable improvement was obtained. The values of the parameters that maximized the binding are $\lambda+\mu=\infty$, $\lambda\mu/(\lambda+\mu)=0.33$ corresponding to the molecular orbital picture

$$\psi=a_2(1)[a_1(2)+0.33a_2(2)+a_3(2)]+a_2(2)[a_1(1)+0.33a_2(1)+a_3(1)]$$

or in covalent-ionic resonance form

$$\psi=[a_1(1)a_2(2)+a_2(1)a_1(2)+a_2(1)a_3(2)+a_3(1)a_2(2)]+0.67[a_2(1)a_2(2)].$$

The associated energy value is 97.96 kcal./mole for a separation between adjacent nuclei of $2.0a_0$, some 6 kcal./mole better than the Heitler-London approximation and 9 kcal./mole better than the conventional molecular orbital representation (Eq. (6)). (The above results, along with those obtained when a screening constant is included in the wave functions, are listed in Table I).

It is of interest to compare the coefficients in (A') and (B') with those obtained by a HLSP-plus-ionic-terms approach, to see wherein the use of molecular orbitals has restricted the wave function. Values of the coefficients are listed in Table II. It is seen that the

TABLE II. Comparison of molecular orbital and HLSP-plus-ionic-terms coefficients (obtained from reference 4). All FCNS are for $Z=1$ (no screening).

Term	HLSP-plus-ionic terms	Ordinary M.O. (Equation (6))	(A') Type FCN	(B') Type FCN
$[a_1(1)a_2(1)+a_1(2)a_2(1)+a_2(1)a_3(2)+a_3(1)a_2(2)]$	1.0	1.0	1.0	1.0
$[a_1(1)a_3(2)+a_3(1)a_1(2)]$	0.54	0.42	0.42	0.00
$[a_1(1)a_1(2)+a_3(1)a_3(2)]$	0.70	2.4	2.4	0.67
$[a_2(1)a_2(2)]$	−0.54	0.42	0.42	0.00

ordinary molecular orbital treatment and the (A) type greatly overemphasize the $a_2(1)a_2(2)$ ionic term. Use of the (B) type wave function completely avoids the molecular orbital fault of overemphasis of ionic terms. It differs from the best combination (Eq. (5)) in that the first and third term coefficients (which are restricted to being equal by the use of M.O.'s) actually become zero upon variation.

If, in addition to the parameters discussed above, the screening constant (Z) of the atomic orbitals is also varied, considerable improvement is obtained in the binding energy. These results are given in Table II, with the $Z=1$ (no screening) values. The wave function of type (A) again gives maximum binding for $\lambda'=1$ and thus corresponds to the usual molecular orbital type wave function which was discussed by Pearson.[3,8] The $Z\neq1$ calculations differ notably from the $Z=1$ results in that:

(1) The conventional M.O. approximation, to which the type (A) function degenerates, is better here than the Heitler-London treatment (as pointed out by Pearson).[3]

(2) The (B) function gives only a slightly higher binding energy than the (A) function (and the conventional M.O.). This is surprising, since analogous separation-exchange functions gave considerable improvement for H_2 (mentioned above) and the helium atom.[9] The binding energy which is normally gained by the separation and exchange of the electrons is, in this case, very nearly offset by a change to a less favorable form of the one-electron orbitals, giving a rather interesting insight into the workings of the variation principle.

In conclusion, it seems probable that the above method of setting up the most general function and then equating certain parameters on the basis of molecular symmetry and nodal surfaces, should result in an improvement over the conventional molecular orbital treatment.

[8] The value reported in Table I of 136.8 kcal./mole is believed to be accurate to within 0.1 kcal./mole of the best obtainable with this function. There is a slight disagreement between this value and that reported by Pearson; i.e. 139.0 kcal./mole for $R=1.52a_0$, $\lambda=2$, $Z=1.31$.

[9] See reference 1, pp. 223–4, variation functions (2) and (4).

Substituted Methanes. II. Vibrational Spectra and Calculated Thermodynamic Properties of Deuterotribromomethane*

SALVADOR M. FERIGLE** AND FORREST F. CLEVELAND
Spectroscopy Laboratory, Department of Physics

AND

WILLIAM M. BOYER*** AND RICHARD B. BERNSTEIN
Department of Chemistry, Illinois Institute of Technology, Chicago, Illinois

(Received April 11, 1950)

Raman displacements, semiquantitative relative intensities, quantitative depolarization factors, and wave numbers and percent transmission for the infra-red bands in the region 400–5000 cm^{-1} have been obtained for CBr_3D. Details about the measurement of the depolarization factors are given. Thermodynamic properties—heat content, free energy, heat capacity, and entropy—have been calculated from the spectroscopic and molecular structure data for eight temperatures from 298.16° to 1000°K.

RAMAN displacements and relative intensities of deuterotribromomethane (deuterobromoform) have been published by Redlich and Stricks,[1] but no depolarization factors nor infra-red spectral data have been found in the literature. As a part of the work on substituted methanes and ethanes that is being carried out in this laboratory, Raman and infra-red spectral data have been obtained for this compound and thermodynamic properties for the ideal gaseous state have been calculated to a rigid rotator, harmonic oscillator approximation.

The deuterotribromomethane was prepared by the reaction of sodium deuteroxide with bromal in D_2O solution. The CBr_3D thus obtained was dried with anhydrous $CaSO_4$ and distilled in vacuum. A mass-spectrometric analysis showed it to contain approximately 4 percent CBr_3H.

RAMAN SPECTRUM OF CBr_3D

The Raman spectrum of CBr_3D has been redetermined and quantitative polarization data obtained. The spectrograms were obtained on Eastman 103-J plates with a Hilger E-518 spectrograph having a dispersion of 320 cm^{-1}/mm (64A/mm) at 4500A, and with a two-prism spectrograph having a dispersion of 144 cm^{-1}/mm (29A/mm) at 4500A, with Hg 4358A as the exciting line, by the experimental methods previously described.[2] The depolarization factors have been obtained by the single-exposure method given by Cleveland;[3] the densities of the two components have been measured with a Leeds and Northrup microphotometer equipped with a Speedomax pen recorder, instead of the Gaertner microdensitometer previously used. The depolarization factors have been measured as the ratio of the peak intensities for the weak and strong components. The correction for background has been made by taking the reading of the background density at the wave-length corresponding to the peak, on a smooth background curve drawn on the microphotometer tracing, transforming it into intensity from the calibration curve, and subtracting this background intensity value from the line intensity. Crawford and Horwitz[4] suggested taking the background minimum just in front of the line, but it seems that this "minimum adjacent background" correction is not adequate in all cases[5] and, as Lyons states,[6] "the method of taking background readings need not be necessarily arbitrary." Corrections for real or apparent polarization of the scattered beam in its optical path, for reciprocity failure of the plates, and for convergence errors have been made.[3] The present results are given in Table I, columns 2–4; the first column gives the Raman displacements reported by Redlich and Stricks.[1] The Raman displacements are, in general, in good agreement; however, some of the present values appear somewhat greater, in better agreement with our infra-red data.

INFRA-RED SPECTRUM OF CBr_3D

Infra-red absorption spectra have been obtained with both sodium chloride (12C Perkin-Elmer recording spectrometer) and potassium bromide (IR-2 Beckman spectrophotometer) optics. A continuous slit drive was used in both instruments to maintain the incident energy as constant as possible. The cell thicknesses were measured by the method of interference fringes.[7,8]

The results are given in Table I, columns 5 and 6, and the percent transmission curve is shown in Fig. 1.

* Presented at the Chicago meeting of the American Physical Society, November 1949; abstract in Phys. Rev. **77**, 740 (1950).

** One of the investigations carried out in partial fulfillment of the requirements for the Ph.D. Degree.

*** The preparation of the CBr_3D was part of a Master's thesis (1950).

[1] O. Redlich and W. Stricks, Sitz. Akad. Wiss. Wien, IIb, **145**, 192 (1936).

[2] F. F. Cleveland, J. Chem. Phys. **11**, 1, 227 (1943).

[3] F. F. Cleveland, J. Chem. Phys. **13**, 101 (1945).

[4] B. L. Crawford, Jr. and W. Horwitz, J. Chem. Phys. **15**, 268 (1947).

[5] B. L. Crawford, Jr. and W. Horwitz, J. Chem. Phys. **16**, 147 (1948).

[6] P. A. Lyons, Thesis, University of Wisconsin, 1948.

[7] D. C. Smith and E. C. Miller, J. Opt. Soc. Am. **34**, 130 (1944).

[8] G. B. B. M. Sutherland and H. A. Willis, Trans. Faraday Soc. **41**, 181 (1945).

All the infra-red bands can be interpreted as fundamentals or combination bands, allowed by the selection rules for the C_{3v} structure. The assignments are given at the right in Table I. In the numbering of the fundamentals, we have followed the procedure of the first paper of this series.[9] The broad infra-red band at 848 cm^{-1} was resolved in the gas into two components at 846 and 866 cm^{-1}. In carbon disulfide solution, this band also was resolved, the maxima of absorption appearing at 845 and 861 cm^{-1}; in chloroform solution the maxima exist at 848 and 866 cm^{-1}; this small difference can probably be accounted for in terms of a solvent effect. This doublet corresponds to a Fermi resonance between the fundamental ν_4 and the combination band $\nu_3+\nu_5=855$ cm^{-1}, both of symmetry *E*. The two components of the Fermi resonance doublet have been designated in Table I as ν_4' and ν_4''. The 1144 cm^{-1} band could be partly due to the small amount of CBr_3H present in the sample; however, since the other frequencies of this compound (especially the very strong C—H band) have not been observed, it seems reasonable to deduce that this band is due mainly to the combination $\nu_2+\nu_5$ of CBr_3D. All the bands for the gaseous state are weak because the vapor pressure was rather small.

THERMODYNAMIC PROPERTIES OF CBr_3D

The heat content, free energy, entropy, and heat capacity of CBr_3D have been calculated for temperatures from 298.16° to 1000°K, to a rigid rotator, harmonic oscillator approximation. Nuclear spins and the effect of the isotopic mixing have been neglected. The calculated values are for the ideal gaseous state at one atmosphere pressure. The moments of inertia have been calculated with C—Br=1.91A and with a Br—C—Br angle of 111°, as given by Lévy and Brockway,[10] and assuming C—D=1.09A, as in CD_4. The values obtained were $I_{zz}=792$ and $I_{xx}=I_{yy}=405$ Awv. A^2. The C—D distance is probably somewhat different in CBr_3D than in CD_4, but even if this is the case the error thus introduced would be quite small, since the contribution of the D atom to the moment of inertia is already only a fraction of the total. No microwave data are as yet available.

The values used for the fundamentals and their degeneracies are given in Table II; wave numbers for the gaseous state have been used when available. ν_4 has been taken as the mean value of the two components of the Fermi resonance doublet, so that the value 856 cm^{-1} is not very accurate, but it seems that this is the best possible choice with the available information. The symmetry number has been taken equal to 3 and Birge's 1941 values of the physical constants[11] have

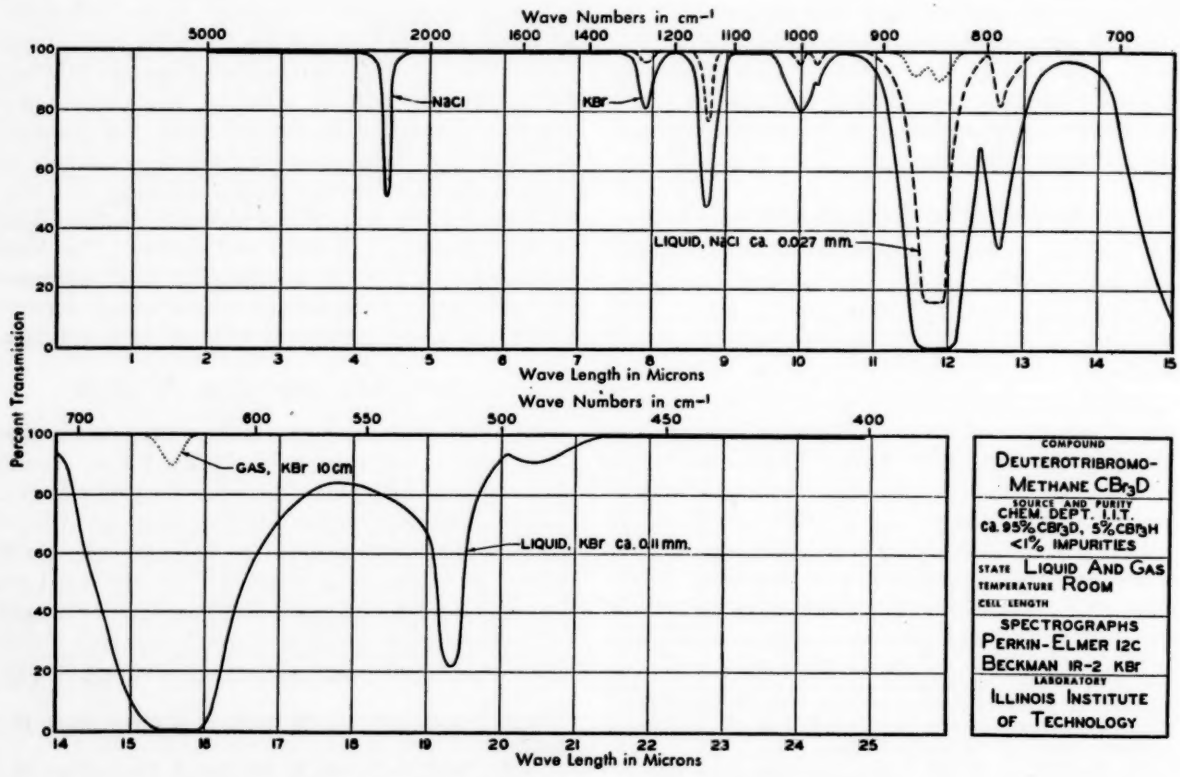

FIG. 1. Infra-red absorption bands for deuterotribromomethane.

[9] Meister, Rosser, and Cleveland, J. Chem. Phys. **18**, 346 (1950).
[10] H. A. Lévy and L. O. Brockway, J. Am. Chem. Soc. **59**, 1662 (1937).
[11] R. T. Birge, Rev. Mod. Phys. **13**, 233 (1941).

TABLE I. Raman and infra-red spectral data and assignments for deuterotribromomethane (CBr_3D).[a]

Raman (liquid)				Infra-red			
$\Delta\nu$ Redlich and Stricks	Present	I	ρ	$\nu_0 I_0$ gas	$\nu_0 I_0$ liquid	Assignments	Type
153.4	155	70	0.78			ν_6	E
221.6	222	100	0.26			ν_3	A_1
519.3	519	41	0.18		517 *S*	ν_2	A_1
628.5	633	16	0.77	644 *W*	634 *VS*	ν_5	E
					786 *S*	$\nu_5+\nu_6$	A_1+A_2+E
840	844			846 *W*		ν_4'	E
		9	0.83		848 *VS*		
856.5	858			866 *W*		ν_4''	E
					978 *W*	$\nu_4'+\nu_6$	A_1+A_2+E
					1003 *W*	$\nu_4''+\nu_6$	A_1+A_2+E
					1144 *S*	$\nu_2+\nu_6$	E
					1267 *M*	$2\nu_5$	A_1+E
2247	2251	11	0.28		2256 *S*	ν_1	A_1

[a] $\Delta\nu$ is the Raman displacement in cm^{-1}; I is the semiquantitative relative intensity; ρ is the depolarization factor of the Raman line; ν_0 is the wave number of the infra-red absorption band in cm^{-1}; and I_0 is the qualitative intensity of absorption (W=weak, M=medium, S=strong, V=very).

been used throughout the calculations. The results obtained for the thermodynamic properties are given in Table III.

Since 5 of the 9 fundamentals are liquid state frequencies, the values of the thermodynamic properties listed in the table may be slightly larger than the values for the ideal gaseous state. However, even if one assumes that the gaseous frequencies are 8 cm^{-1} higher than the liquid values—which is the mean of the two shifts which were observed—the thermodynamic properties listed in the first row of Table III for 298.16°K would decrease only by 0.09, 0.20, 0.29, and 0.05 cal. deg.$^{-1}$ mole^{-1}, respectively. These values are probably greater than the actual errors, since the greatest contributions to the thermodynamic properties are made by the low frequencies which are expected to have a smaller shift.

ACKNOWLEDGMENTS

The Hilger E-518 spectrograph used in this investigation was obtained, in part, with a grant from the Permanent Science Fund of the American Academy of Arts and Sciences; and the optical parts for the two-prism spectrograph were obtained with a grant from The Society of the Sigma Xi. The authors are grateful for this assistance. One of us (S. M. F.) wishes to thank the *Junta de Relaciones Culturales* of Spain for a scholarship that made it possible for him to carry out his part of this research. Thanks also are due to Dr. V. H. Dibeler of the National Bureau of Standards, who performed the mass-spectrometric analysis, and to Dr. Sidney Katz of the Institute of Gas Technology on our campus who kindly made available the Perkin-Elmer infra-red spectrometer. The D_2O was obtained through the courtesy of Dr. Martin Kilpatrick and the AEC.

TABLE II. Wave numbers and degeneracies corresponding to the fundamental frequencies of CBr_3D.

Designation	Wave number (cm^{-1})	Degeneracy
ν_1	2251	1
ν_2	519	1
ν_3	222	1
ν_4	[a]856	2
ν_5	[a]644	2
ν_6	154	2

[a] Gaseous state.

TABLE III. Heat content, free energy, entropy, and heat capacity of CBr_3D for the ideal gaseous state at one atmosphere pressure.[a]

T	$(H^0-H_0^0)/T$	$-(F^0-H_0^0)/T$	S^0	C_p^0
298.16	13.02	66.32	79.34	17.77
400	14.50	70.36	84.86	19.74
500	15.68	73.73	89.41	21.02
600	16.65	76.68	93.33	21.93
700	17.46	79.30	96.76	22.60
800	18.14	81.68	99.82	23.12
900	18.72	83.86	102.58	23.53
1000	19.21	85.85	105.06	23.86

[a] T is in degrees Kelvin and the other quantities in cal. deg.$^{-1}$ mole^{-1}.

Substituted Methanes. III. Raman Spectra, Assignments, and Force Constants for Some Trichloromethanes*

JAMES P. ZIETLOW,** FORREST F. CLEVELAND, AND ARNOLD G. MEISTER
Spectroscopy Laboratory, Department of Physics, Illinois Institute of Technology, Chicago, Illinois
(Received April 19, 1950)

Raman displacements, semiquantitative relative intensities, and precise depolarization factors for trichloromethane, fluorotrichloromethane, and bromotrichloromethane were obtained in the liquid state. Several overtones and combination bands hitherto unreported are given and frequency assignments are made. The Raman data in the literature for CCl_3H, CCl_3D, CCl_3F, CCl_4, and CCl_3Br in the liquid state have been collected and the probable values ascertained. Force constants in modified valence force potential functions containing all possible interaction constants were calculated for the five molecules.

IN the first paper[1] of this series, Raman and infra-red spectral data, assignments, and force constants were given for some tribromomethanes. The present paper gives similar results for the trichloromethanes.

The experimental methods were the same as in the previous work.[1] Depolarization factors were measured only when the densities of both components of the line fell on the straight portion of the *density-log intensity* curve, except for the most highly polarized line of CCl_3H and CCl_3F where this was impossible.

RESULTS AND ASSIGNMENTS

The Raman spectral data, calculated frequencies, and assignments are given in Tables I–VI. The relative intensities obtained by the photoelectric method are probably more accurate than for other methods in general use and are given as the probable values where available. Otherwise, those obtained by the semiquantitative method used in this laboratory are preferred over the visual estimates of others. Evaluation of the depolarization data in the literature is difficult because the various methods used differ in their reliability. Hence, all the depolarization data are presented in the tables rather than an average value, and a decision was made finally as to whether the line is polarized (P) or depolarized (D) under the heading PS. The probable values of the fundamentals, their degeneracies, and the description of the normal vibrations are given for comparison and ready reference in Table VII. The selection rules for the present molecules are the same as for the tribromomethanes[1] and have been taken into account in all of the assignments.

Trichloromethane (Chloroform, CCl_3H)

The trichloromethane used in the investigation was classified "chemically pure;" further purification was undertaken by mixing with H_2SO_4, removal of the acid with sodium bicarbonate, water washings, and several distillations. No evidence of CCl_3H decomposition was found. The spectra had very little continuous background.

Twenty-six investigators[2–25] have reported Raman displacements for CCl_3H, and eight[20–26,13b] have measured the depolarization factors. The present results and the previous data for CCl_3H are summarized and compared in Table I. The calculated values for the fundamentals are more reliable than those for the combinations and overtones; this has been emphasized in Table I and the other tables by using **bold face type** for the fundamentals and *italics* for the combinations and overtones. For the chloroform data, no reasonable assignment could be made for the 1442.3 cm^{-1} band, which was found in six separate investigations in India, five before 1931 and one by Sirkar[15] in 1936. Ethyl alcohol has a band at 1455 cm^{-1} of medium intensity; another possible impurity is acetone whose Raman spectrum

* Presented at the Chicago meetings of the American Physical Society, November, 1948 and November, 1949; abstracts in Phys. Rev. **75**, 333 (1949); **77**, 739 (1950).

** This paper is based upon an investigation carried out by Mr. James P. Zietlow in partial fulfillment of the requirements for the M.S. and Ph.D. degrees at Illinois Institute of Technology.

[1] Meister, Rosser, and Cleveland, J. Chem. Phys. **18**, 346 (1950).

[2] J. Rud Nielsen and N. E. Ward, J. Chem. Phys. **10**, 81 (1942).
[3] M. de Hemptinne, Ann. Soc. Sci. Bruxelles **B52**, 185 (1932).
[4] M. V. Rao, Proc. Indian Acad. Sci. **24A**, 510 (1946).
[5] A. Dadieu and K. W. F. Kohlrausch, Phys. Zeits. **31**, 514 (1930); Sitz. Akad. Wiss. Wien **138**, 635 (1929).
[6] C. D. Cleeton and R. T. Dufford, Phys. Rev. **37**, 362 (1931).
[7] M. de Hemptinne and A. Peters, Bull. Acad. Roy. de Belgique **5**, 1107 (1931).
[8] R. W. Wood and D. H. Rank, Phys. Rev. **48**, 63 (1935).
[9] R. Truchet, Comptes Rendus **202**, 1997 (1936).
[10] O. Redlich and F. Pordes, Sitz. Akad. Wiss. Wien **IIb**, **145**, 67 (1936).
[11] A. S. Ganesan and S. Venkateswaran, Indian J. Phys. **4**, 195 (1929).
[12] S. Bhagavantam and S. Venkateswaran, Proc. Roy. Soc. London **A127**, 360 (1930).
[13] S. Bhagavantam, (a) Indian J. Phys. **5**, 35 (1930); (b) **5**, 59 (1930).
[14] J. T. Dhar, Indian J. Phys. **9**, 189 (1934).
[15] S. C. Sirkar, Indian J. Phys. **10**, 189 (1936).
[16] R. W. Wood, Phil. Mag. **6**, 729 (1928).
[17] R. M. Langer and W. F. Meggers, J. Research. Nat. Bur. Stand. **4**, 711 (1930).
[18] W. M. Dabadghao, Indian J. Phys. **5**, 207 (1930).
[19] P. Pringsheim and B. Rosen, Zeits. f. Physik **50**, 741 (1928).
[20] M. de Hemptinne and J. Wouters, Nature **138**, 884 (1936).
[21] D. H. Rank, J. Opt. Soc. Am. **37**, 798 (1947).
[22] L. Simons, Soc. Sci. Fenn. Comm. Phys. Math. **6**, No. 13 (1932).
[23] A. V. Rao, Zeits. f. Physik **97**, 154 (1935).
[24] S. Venkateswaran, Phil. Mag. **15**, 263 (1933).
[25] J. Cabannes and A. Rousset, Ann. de Phys. **19**, 229 (1933).
[26] B. L. Crawford, Jr. and W. Horwitz, J. Chem. Phys. **15**, 268 (1947).

TABLE I. Raman spectral data, calculated frequencies, and assignments for liquid trichloromethane (CCl_3H).*

PR	N	$\Delta\nu$ PV	AD	I (21)	Depolarization factors (24)	(13b)	(23)	(20)	(26)	(25)	(22)	(21)	PR	PS	ν_c	Assignment	Type
262	26	261.1	1.4	100	0.8	0.73	0.95	0.7	0.86	0.70	0.87	0.86	0.86	D	**258.4**	ν_6	E
369	26	366.4	1.4	70	0.2	0.22	0.18	0.22	0.18	0.22	0.19	0.19	0.25	P	**371.8**	ν_3	A_1
	1	497	—												*500*	$\nu_5-\nu_6$	A_1+A_2+E
	1	622	—												*627*	$\nu_3+\nu_6$	E
667	27	667.4	1.3	80	0.1	0.13	0.06	0.06	0.08	0.06	0.07	0.082	0.07	P	**669.2**	ν_2	A_1
759	26	761.5	2.7	56	0.8	0.5	0.80	0.68	0.92	0.68	0.86	0.93	0.87	D	**772.0**	ν_5	E
	1	1027	—												*1023* *1034*	$\nu_5+\nu_6$ $\nu_2+\nu_3$	A_1+A_2+E A_1
1214	24	1215.6	2.0	15	0.8	0.5	0.60	6/7	0.9	~6/7	0.87	0.83	0.89	D	**1210.0**	ν_4	E
	1	1420	—												*1429*	$\nu_2+\nu_5$?	E
	6	1442.3	1.8														
1501	1	1501	—	2											*1494*	$2\nu_3+\nu_5$	E
1518	1	1518	—												*1523*	$2\nu_5$	A_1+E
(1888)	1	(1888)	—												*1883* *1889*	$\nu_2+\nu_4$ $\nu_3+2\nu_5$	E A_1+E
3020	24	3018.2	2.2	30	0.2	0.22	0.31	0.32	0.4	0.32	0.20	0.24	0.38	P	**3017.2**	ν_1	A_1
	1	3072.4	—												*3099*	$\nu_2+2\nu_4$	A_1+E

* $\Delta\nu$ is the Raman displacement in cm^{-1}; I is the relative intensity; ν_c is the calculated frequency in cm^{-1}; PR = present results; N = number of times the band has been observed in independent investigations; PV = the probable value of the Raman displacement (mean of the N values, including the present value); AD = the average deviation of the individual value from the mean; PS = polarization state (P = polarized, D = depolarized); an uncertain frequency is enclosed in parentheses. Numbers in parentheses at head of columns are reference numbers.

contains a broad band of medium intensity reported variously from 1423 cm^{-1} to 1438 cm^{-1}. Thus, the 1442 cm^{-1} band and the 1420 cm^{-1} band reported by Rao[4] may not be part of the Raman spectrum of chloroform. Dabadghao[18] reported the 3072.4 cm^{-1} band in 1930 but there has been no confirmation. However, this band was measured by him from three different excitation frequencies and the assignment can be readily made as $2\nu_4+\nu_2$. The 1501 cm^{-1} and 1518 cm^{-1} bands were clearly resolved in the present investigation. Other investigators[4, 8, 21] report a single band between these two values.

Deuterotrichloromethane (CCl_3D)

Table II contains the Raman spectral data,[8–10, 27] calculated frequencies, and assignments for CCl_3D. The only depolarization data[27] available for this molecule were obtained using the method described before.[1]

Fluorotrichloromethane (Freon 11, CCl_3F)

The fluorotrichloromethane used was kindly provided by Kinetic Chemicals, Inc. of Wilmington, Delaware. Purification was accomplished simply by several distillations. No evidence of photochemical decomposition was apparent. The boiling point of CCl_3F is 23.7°C. Spectra were obtained by means of a sealed Raman tube and also by using a condensing tube attachment through which ice water was circulated. The temperatures at the Raman tube in these cases were about 28°C and 23°C, respectively.

Table III contains the present results and previous data[28, 29] and the calculated frequencies and assignments. The appreciable intensity of the 1079 cm^{-1} band may be due to resonance of $\nu_4+\nu_6$ with the 1068.1 cm^{-1} fundamental. Two broad bands at 1645 and 1659 cm^{-1} appeared after an exposure of 73 hrs. These bands can correspond to the combination $\nu_1+\nu_2=1604$ and the overtone $2\nu_4=1671$ cm^{-1}, respectively. Since the bands are so broad, however, it is quite possible that they are caused by the superposition of these and $3\nu_2=1607$, $\nu_4+2\nu_5=1631$, $\nu_2+\nu_4+\nu_6=1616$, $\nu_1+\nu_4-\nu_6=1659$, and $\nu_1+\nu_3+\nu_6=1663$ cm^{-1}.

TABLE II. Raman spectral data, calculated frequencies, and assignments for liquid deuterotrichloromethane (CCl_3D).*

N	$\Delta\nu$ PV	AD	I (27)	$(27)^\rho$	PS	ν_c	Assignment	Type
4	262.5	1.3	100	0.87	D	**257.5**	ν_6	E
4	365.1	0.5	92	0.10	P	**368.1**	ν_3	A_1
4	651.3	1.8	72	0.03	P	**641.1**	ν_2	A_1
4	737.7	1.4	14	0.84	D	**734.1**	ν_5	E
4	908.8	1.3	3	0.87	D	**914.7**	ν_4	E
4	2256.0	2.0	15	0.26	P	**2259.0**	ν_1	A_1

* ρ = depolarization factor; other symbols have the same meaning as in Table I.

Tetrachloromethane (Carbon Tetrachloride, CCl_4)

This compound was included in the present investigation as still another molecule of the type CCl_3X, despite the fact that it represents the very special case in which X = Cl. Thirty-eight investigations[11–19, 21–24, 26, 30–48, 55] have yielded Raman displacements for CCl_4, and twenty-one[13b, 21–26, 43–54] have yielded

[27] Madigan, Cleveland, Boyer, and Bernstein, Phys. Rev. **77**, 740 (1950).
[28] M. L. Delwaulle and F. Francois, Comptes Rendus **214**, 828 (1942).
[29] G. Glockler and G. R. Leader, J. Chem. Phys. **7**, 278 (1939).
[30] C. V. Raman and K. S. Krishnan, Nature **122**, 278 (1928); Proc. Roy. Soc. London **A122**, 23 (1929).
[31] R. Ananthakrishnan, Proc. Indian Acad. Sci. **2A**, 452 (1935).
[32] P. Daure, Ann. de Phys. **12**, 375 (1929); Comptes Rendus **187**, 940 (1928).
[33] K. Venkateswarlu, Proc. Indian Acad. Sci. **21A**, 126 (1945).
[34] L. Guilotto, Nuovo Cimento **17**, 436 (1940).
[35] N. B. Reynolds and J. W. Williams, J. Franklin Inst. **210**, 41 (1930).
[36] Morino, Watanabe, and Mizushima, Sci. Papers Inst. Phys. Chem. Research (Tokyo), No. 1083, **39**, 348 (1942).

TABLE III. Raman spectral data, calculated frequencies, and assignments for liquid fluorotrichloromethane (CCl_3F).*

PR	N	$\Delta\nu$ PV	AD	I PR	(28)	ρ PR	PS	ν_c	Assignment	Type
247	3	244.6	1.6	25	0.82	0.83	D	**244.6**	ν_6	E
352	3	350.5	1.0	30	0.2	0.42	P	**350.5**	ν_3	A_1
399	3	397.8	0.8	15	0.82	0.81	D	**397.8**	ν_5	E
538	3	535.8	1.5	100	0.05	0.11	P	**535.8**	ν_2	A_1
837	3	835.4	1.5	5	0.88	0.88	D	**835.4**	ν_4	E
1066	3	1068.1	2.0	1	0.60	0.66	P	{**1068.1**	{ν_1	{A_1
1079	1	1079	—	~0.7				{*1080*	{$\nu_4+\nu_6$	{A_1+A_2+E
1645	1	1645	—	*vw*				*1604*	$\nu_1+\nu_2$	A_1
1659	1	1659	—	*vw*				*1671*	$2\nu_4$	A_1+E

* The symbols are defined below Table I.

TABLE IV. Fundamental frequencies for liquid tetrachloromethane (CCl_4).

N	$\Delta\nu$ PV	AD	I (21)	(43)	(13b)	(24)	Depolarization factors (46)	(47)	(44)	(23)	(22)	(25)	(49)	(45)	(47)	(26)	(50)	(52)	(51)	(51)	(54)	(21)	(53)	PS	ν_c	Assignment	Type
36	217.0	1.3	66	0.8	0.75	0.8		0.80	0.81	0.89	0.88	0.83	0.83	0.86	0.82	0.83	0.899	0.83	0.854	0.84	0.853	0.89	0.85	D	**217.0**	ν_2	E
36	313.5	1.1	88	0.8	0.8	0.8		0.81	0.82	0.83	0.93	0.79	0.83	0.78	0.83	0.82	0.913	0.81	0.872	0.87	0.867	0.88	0.86	D	**313.5**	ν_4	F_2
36	458.7	1.0	100	0.04	0.1	0.04		0.29	0.40	~0	0.05	0.05	0.02	0.05	0.08	0.044	0.450	0.03	0.045	0.04	0.072	0.064	0.042	P	**458.7**	ν_1	A_1
28	761.7	2.1	37		0.75	0.8				0.79		~6/7		0.86				0.84	0.742	0.89	0.847	0.86		D		{ν_3'	{F_2
				0.8			0.89		0.85		0.87		0.86		0.80	0.88	0.952						0.73		**776.0**		
28	790.4	1.5	37		0.75	0.8				0.78		~6/7		0.86				0.82	0.777	0.84	0.832	0.86		D		ν_3''	F_2

TABLE V. Combinations and overtones for liquid tetrachloromethane (carbon tetrachloride, CCl_4).

N	$\Delta\nu$ PV	AD	(48)	ρ PS	ν_c	Assignment	Type
1	94		0.8	(D)	*96*	$\nu_4-\nu_2$	F_1+F_2
2	144.0	1.0	0.9	(D)	*145*	$\nu_1-\nu_4$	F_2
1	434				*434*	$2\nu_2$	A_1+E
2	536.5	1.5	1.3	(D)	*530*	$\nu_2+\nu_4$	F_1+F_2
2	587.0	7.0			*573*	$\nu_3''-\nu_2$	F_1+F_2
1	630		0.8	(D)	*627*	$2\nu_4$	A_1+E+F_2
1	673		1.1	(D)	*676*	$\nu_1+\nu_2$	E
1	915				*917*	$2\nu_1$	A_1
1	989				{*979*	{$\nu_2+\nu_3'$	{F_1+F_2
					{*989*	{$\nu_1+\nu_2+\nu_4$	{F_1+F_2
1	1072				*1075*	$\nu_3'+\nu_4$	$A_1+E+F_1+F_2$
1	1110				*1104*	$\nu_3''+\nu_4$	$A_1+E+F_1+F_2$
1	1221				{*1220*	{$\nu_1+\nu_3'$	{F_2
					{*1224*	{$2\nu_2+\nu_3''$	{F_1+2F_2
1	1250				*1249*	$\nu_1+\nu_3''$	F_2
14	1538.1	2.3	0.5*	P	{*1544*	{$2\nu_1+2\nu_4$	{A_1+E+F_2
					{*1552*	{$\nu_3'+\nu_3''$	{A_1+E+F_2
1	1749				*1740*	$\nu_2+2\nu_3'$	$A_1+A_2+2E+F_1+F_2$
1	1860				*1866*	$\nu_3'+\nu_3''+\nu_4$	$A_1+E+2F_1+3F_2$
1	1995				{*1982*	{$\nu_1+2\nu_3'$	{A_1+E+F_2
					{*2011*	{$\nu_1+\nu_3'+\nu_3''$	{A_1+E+F_2

* Additional ρ values have been reported for this line: they are 0.33, 0.3, 0.41, 0.58; see references 13b, 24, 46, and 50, respectively.

depolarization factors. Tables IV and V contain Raman spectral data, calculated frequencies, and assignments for tetrachloromethane. Fermi resonance between the 776 cm^{-1} fundamental and the $\nu_1+\nu_4$(=772 cm^{-1}) combination leads to the splitting into the 761.7 and 790.4 cm^{-1} bands as is well known.

[37] B. Trumpy, Zeits. f. Physik **66**, 790 (1930).
[38] G. B. B. M. Sutherland, Proc. Roy. Soc. London **A141**, 535 (1933).
[39] D. L. Mesnage, J. de Phys. et le Rad. **2**, 403 (1931).
[40] A. Dadieu and K. W. F. Kohlrausch, Wien Ber. **138**, 41 (1929), or Monatshefte f. Chem. **52**, 220 (1929).
[41] A. Carelli and J. J. Went, Zeits. f. Physik **76**, 236 (1932).
[42] A. Dadieu and K. W. F. Kohlrausch, Phys. Zeits. **30**, 384 (1929).
[43] S. Bhagavantam, Indian J. Phys. **7**, 79 (1932).
[44] L. S. Ornstein and P. Stoutenbeck, Zeits. f. Physik **85**, 754 (1933).
[45] B. K. Chaudhuri, Indian J. Phys. **11**, 203 (1937).
[46] B. P. Rao, Proc. Indian Acad. Sci. **11A**, 1 (1940).
[47] G. Glockler and H. T. Baker, J. Chem. Phys. **10**, 404 (1942); **11**, 446 (1943).
[48] H. L. Welsh and M. F. Crawford, J. Chem. Phys. **16**, 97 (1948).
[49] A. Rousset, Comptes Rendus **202**, 654 (1936).
[50] G. Placzek and W. R. van Wijk, Zeits. f. Physik **67**, 582 (1931).
[51] A. W. Reitz, Zeits. f. phys. Chemie **B33**, 368 (1936); **B38**, 275 (1937).
[52] O. Paulsen, Zeits. f. phys. Chemie **B28**, 123 (1935).
[53] Susz, Papazian, Berenstein, and Briner, Helvetica Chimica Acta **31**, 1133 (1948).
[54] Forrest F. Cleveland, J. Chem. Phys. **13**, 101 (1945).
[55] A. Langseth, Zeits. f. Physik **72**, 350 (1931).

TABLE VI. Raman spectral data, calculated frequencies, and assignments for liquid bromotrichloromethane (CCl_3Br).*

PR	N	$\Delta\nu$ PV	AD	I PR	(56)	ρ PR	PS	ν_c	Assignment	Type
193	3(4)	193.3	1.1	40	7/8**	0.84	D	**193.3**	ν_6	E
247	3(4)	247.3	0.4	50	0.35	0.57	P	**247.3**	ν_3	A_1
295	3(4)	295.0	0.0	25	7/8**	0.84	D	**295.0**	ν_5	E
420	3(4)	422.3	1.8	100	0.05	0.15	P	**422.3**	ν_2	A_1
718	3(4)	716.3	1.1	15	0.7	0.75	P	**716.3**	ν_1	A_1
774	3(4)	775.3	1.8	5	0.7	0.82	D	**775.3**	ν_4	E
1438	1	1438	—	*vw*				*1433*	$2\nu_1$	A_1
1542	1	1542	—	*vw*				*1551*	$2\nu_4$	A_1+E

* *vw* = very weak; other symbols are defined below Table I.
** Given as 6/7 in a later paper: M. L. Delwaulle and F. Francois, J. de phys. et rad. **7**, 15 (1946).

TABLE VII. Probable values of the fundamental vibrational frequencies of the trichloromethanes (liquid).

Description	Type	Degeneracy	CCl_3H	CCl_3D	CCl_3F	CCl_3Br	CCl_4	Degeneracy	Type
CCl_3 Deformation	E	2	261.1	262.7	244.6	193.3	217.0	2	E
CCl_3 Deformation	A_1	1	366.4	365.2	350.5	247.3	313.5	3	F_2
C—Cl Stretching	A_1	1	667.4	652.1	535.8	422.3	458.7	1	A_1
C—Cl Stretching	E	2	761.5	738.5	835.4	775.3	776.0*	3	F_2
Bending	E	2	1215.6	909.1	397.8	295.0			
C—X Stretching	A_1	1	3018.2	2256.3	1068.1	716.3			

* Mean of the resonance doublet.

Bromotrichloromethane (CCl_3Br)

The bromotrichloromethane was kindly furnished by the Dow Chemical Company of Midland, Michigan. The compound was purified by distillation; the CCl_3Br came over slowly at 104.0°C. The compound is photochemically unstable and became light brown after an exposure of 50 min. to two Pyrex mercury arcs. It was necessary to remove the colored sample from the Raman tube and to refill it with fresh CCl_3Br every 45 min. In this way a good spectrogram of the pure compound was obtained after $2\frac{1}{2}$ hr. For further spectra, one part of *n*-amylene was added to approximately 15 parts of bromotrichloromethane by volume; this kept the mixture clear indefinitely.[55] Comparison of the spectra obtained with this mixture with that of the spectrum of the pure compound showed that the presence of the *n*-amylene had no noticeable effect upon the spectrum of CCl_3Br. A separate investigation of *n*-amylene reveals it to be a weak scatterer; its strongest line did not appear in the Raman spectrum of the mixture. Further, in no case is there a coincidence of any *n*-amylene frequency with a frequency of bromotrichloromethane.

The present results and the previous data[56, 57] are compared in Table VI. The depolarization factor for the 716.3 cm^{-1} fundamental may be too high because of coincidence with the combination band (295+422=717 cm^{-1}). Since this combination has the same symmetry as the 775.3 cm^{-1} fundamental, Fermi resonance may lead to sufficient intensity of the combination to account for the high depolarization factor obtained for the 716.3 cm^{-1} band. The data of Lecomte, Volkringer, and Tchakirian[58] were not used in obtaining the probable displacements, since their values all seem too low by more than would be expected from random experimental error.

The depolarization data are sufficient to permit the designation of the 247.3 cm^{-1} band rather than the 295.0 cm^{-1} band as the one corresponding to the symmetrical $C-Cl_3$ deformation vibration; Wu[59] has these bands reversed in his assignments which were made on the basis of frequencies and relative intensities only.

In general, the continuous backgrounds for the three spectra studied were very light. The broadest and most diffuse bands by far were those corresponding to the degenerate C—Cl stretching vibration, that is, 761.5 cm^{-1} in CCl_3H, 738.5 cm^{-1} in CCl_3D,[8,10] 835.4 cm^{-1} in CCl_3F, and 775.3 cm^{-1} in CCl_3Br.

CALCULATION OF FORCE CONSTANTS

Force constants were determined in the present investigation, even though sets of constants already existed for all the molecules except CCl_3F, because of significant differences in the fundamental frequencies used by the other investigators and the omission by them of several terms in the potential function which this analysis indicates are important. It also seemed desirable to make another attempt to better the agreement of calculated and observed frequencies and to obtain a set of constants which may be tested for transferability to other substituted methanes and to more complicated molecules, such as the halogenated ethanes. The method, potential energy functions, and

[56] M. L. Delwaulle and F. Francois, Comptes Rendus **214**, 226 (1942).
[57] J. Wouters, Bull. Acad. Roy. de Belgique **20**, 782 (1934).
[58] Lecomte, Volkringer, and Tchakirian, Comptes Rendus **204**, 1927 (1937).
[59] Ta-You Wu, *Vibrational Spectra and Structure of Polyatomic Molecules* (J. W. Edwards, Ann Arbor, Michigan, 1946), p. 243.

TABLE VIII. Force constants for some trichloromethanes (10^5 dynes/cm).

Type	CCl_3H and CCl_3D Present	CCl_3H and CCl_3D Decius	CCl_3H and CCl_3D Simanouti	CCl_3H and CCl_3D Stepanov	CCl_3F Present	CCl_3Br Present	CCl_3Br Simanouti	CCl_4 Present	CCl_4 Decius	CCl_4 Simanouti	CCl_4 Stepanov
k_D	4.8002	5.04	5.04	5.02	4.9447	2.8976	2.55	—	—	—	—
k_d	3.4580	3.383	3.19	3.59	3.4580	3.4580	2.91	3.4580	3.383	2.975	3.65
k_{dd}	0.30760	0.332	0.467	0.265	0.30760	0.30760	0.470	0.31207	0.332	0.470	0.265
k_{dD}	0.088000	0.000	0.527	0.088	0.90713	0.37782	0.412	—	—	—	—
$*k_{D\gamma}$	0.36071	0.000	−0.215	−0.218	−0.077586	−0.30971	−0.249	—	—	—	—
$k_{d\alpha}$	0.20584	0.193	0.259	0.363	0.20584	0.20584	0.2635	0.20584	0.193	0.2635	0.417
$k_{d\alpha}'$	−0.15413	−0.142	0.000	0.000	−0.15413	−0.15413	0.000	−0.15617	−0.142	0.000	0.000
$k_{d\beta}$	0.10509	0.194	0.298	0.363	0.17480	0.24085	0.229	—	—	—	—
$k_{d\beta}'$	−0.092655	−0.0937	0.000	0.000	−0.12752	−0.12042	0.000	—	—	—	—
k_α	0.37094	0.3709	0.480	0.362	0.37094	0.37094	0.458	0.39512	0.3709	0.460	0.364
$k_{\alpha\alpha}$	0.027140	0.0300	0.0647	0.031	0.027140	0.027140	0.0629	0.025819	0.030	0.0647	0.031
$k_{\alpha\beta}$	0.0090124	0.0000	0.0647	0.022	0.019904	0.042852	0.0629	—	—	—	—
$k_{\alpha\beta}'$	0.00000	0.0000	0.000	0.000	0.00000	0.00000	0.000	—	—	—	—
k_β	0.29406	0.224	0.299	0.250	0.52922	0.41617	0.398	—	—	—	—
$k_{\beta\beta}$	0.087157	0.0029	0.0647	0.038	0.070440	0.038757	0.0629	—	—	—	—
$k_{\alpha\alpha}'$	—	—	—	—	—	—	—	−0.012082	−0.012	0.0000	0.000
$k_{D\alpha}$	—	0.0000	0.0000	0.000	—	—	0.000	—	—	—	—
$k_{D\beta}$	—	0.0000	0.215	0.218	—	—	0.249	—	—	—	—

$*k_{D\gamma}=k_{D\alpha}-k_{D\beta}$.

symbols are the same as in the tribromomethane paper,[1] except now D refers to the C−X bond (X=H, D, F, Br); d always indicates a C−Cl bond, α a Cl−C−Cl angle, and β a Cl−C−X angle. Tetrahedral angles were assumed and the values used for the reciprocals of the masses of the atoms were the same as before.[1] The equilibrium values of the bond distances[60] were taken as C−Cl=1.77, C−H=C−D=1.093, C−Br=1.91, and C−F=1.40A. The C−Br bond distance in the bromomethanes is reported as 1.91A by some electron diffraction workers and about 2.01A by others even for the same molecule; *e.g.*, for CBr_4 Lévy and Brockway[61] give 1.91A and Wierl[62] gives 2.05A. Although Maxwell lists 2.01A as the C−Br length in CCl_3Br, this is the report of only one investigator.[63] In the present calculation, 1.91A was used because it is the sum of the normal covalent radii and because Lévy and Brockway chose this value after discussing the discrepancies for several bromomethanes.

For the molecules considered $k_{\alpha\beta}'$ was set equal to zero, while $k_{D\alpha}$ and $k_{D\beta}$ could not be obtained except as the combination $k_{D\gamma}=(k_{D\alpha}-k_{D\beta})$. For chloroform and deuterochloroform the value of k_{dD} was taken from the work of Stepanov;[64] and k_α was obtained from a paper by Decius.[65] The C−Br stretching force constant (k_D) was transferred from the set given in the tribromomethane paper.[1] The method of "splitting out" frequencies[1] was used to obtain the value of the C−F constant (k_D). Even though the C−F stretching frequency is not very high, comparison with the same constant obtained for CBr_3F[1] by this method shows close agreement (4.9447×10^5 dynes/cm in CCl_3F and 4.9531×10^5 dynes/cm in CBr_3F). All the constants of the CCl_3 group were transferred from the CCl_3H and CCl_3D molecules to CCl_3Br and CCl_3F. For CCl_4, the value of $k_{\alpha\alpha}'$ was taken from Decius.[65] Table VIII contains the force constants for the five molecules as determined in the present investigation, and for comparison the force constants determined for the trichloromethanes by Decius, Simanouti,[66] and Stepanov also are given.

A study of Table VIII shows that $k_{D\gamma}$ has a fairly large positive value for CCl_3H but takes on a negative value for CCl_3F and CCl_3Br, having the largest negative value for CCl_3Br. The same change in sign was observed for the corresponding constant for the tribromomethanes, where it was found that as the atomic weight of the halogen increased, the constant assumed a larger negative value, having its greatest negative value for CBr_3Cl. However, k_{dD} behaves differently since it was always positive and had its lowest value for CCl_3H, the highest value for CCl_3F, and a smaller value for CCl_3Br. The same pattern was found for the corresponding constants for the tribromomethanes. The C−H stretching force constant for CCl_3H (4.8002×10^5 dynes/cm) is in good agreement with the same constant for CBr_3H (4.8828×10^5 dynes/cm). Also one notices that when the H or D atom is replaced by a halogen, most of the interaction and bending constants involved usually increase considerably.

ACKNOWLEDGMENTS

The Hilger E-518 spectrograph was obtained, in part, with a grant from the Permanent Science Fund of the American Academy of Arts and Sciences, and the optical parts for the two-prism spectrograph were obtained with a grant from the Society of the Sigma Xi. The authors are grateful for the above mentioned assistance and to the Dow Chemical Company and Kinetic Chemicals, Inc. for furnishing some of the compounds. Thanks also are due Mr. James E. Lamport of this laboratory for the use of his Raman spectrograms of *n*-amylene.

[60] L. R. Maxwell, J. Opt. Soc. Am. **30**, 374 (1940).
[61] H. A. Lévy and L. O. Brockway, J. Am. Chem. Soc. **59**, 1662 (1937).
[62] R. Wierl, Ann. Physik **8**, 521 (1931).
[63] P. Capron and M. de Hemptinne, Ann. Soc. Sci. de Bruxelles **56**, 342 (1936).
[64] B. I. Stepanov, Acta Physicochimica URSS **20**, 174 (1945).
[65] J. C. Decius, J. Chem. Phys. **16**, 214 (1948).
[66] T. Simanouti, J. Chem. Phys. **17**, 245 (1949).

Substituted Methanes. IV. Vibrational Spectra and Calculated Thermodynamic Properties of Deuterotrichloromethane*

JOHN R. MADIGAN† AND FORREST F. CLEVELAND
Spectroscopy Laboratory, Department of Physics,

AND

WILLIAM M. BOYER† AND RICHARD B. BERNSTEIN
Department of Chemistry, Illinois Institute of Technology, Chicago, Illinois

(Received April 20, 1950)

Raman displacements, semiquantitative relative intensities, quantitative depolarization factors, and wave numbers and percent transmission for the infra-red bands in the region 400–5000 cm^{-1} have been obtained for CCl_3D. Thermodynamic properties—heat content, free energy, entropy, and heat capacity—have been calculated from the spectroscopic and molecular structure data, to a rigid rotator, harmonic oscillator approximation, for nine temperatures from 298.16° to 1000°K.

RAMAN displacements and visual estimates of the relative intensities of the Raman lines for deuterotrichloromethane (deuterochloroform) have been obtained previously[1–3] in three investigations, but only one report[3] has been made regarding the polarization state of the lines and that gave only qualitative information. No previous infra-red spectral data could be found for this molecule.

As a part of the work on substituted methanes and ethanes that is being carried out in this laboratory, Raman and infra-red spectral data have been obtained for this compound, and thermodynamic properties for the ideal gaseous state have been calculated to a rigid rotator, harmonic oscillator approximation. No previous observed or calculated thermodynamic properties were found in the literature for this molecule.

EXPERIMENTAL

The Raman displacements, semiquantitative relative intensities, and quantitative depolarization factors were obtained with previously described instruments and methods[4] at 30°C. Eastman 103-J plates were used and excitation was by Hg 4358A. The relative intensities are only semiquantitative, since no correction was made for variation of the sensitivity of the plate with wavelength, and since calibration marks were not placed upon each plate but only upon a master calibration plate with the same type of emulsion. The depolarization factors were obtained by the well-tested single exposure method.

The infra-red absorption spectra were obtained both with a Beckman IR-2 spectrophotometer (KBr optics) and with a Perkin-Elmer 12-C spectrometer (NaCl optics). A continuous slit drive was used with both instruments to maintain the deflection of the recorder as constant as possible. Records were obtained for the vapor, liquid, and CS_2 solutions at 30°C. The gas and liquid cells were 10 cm and 0.11 mm in length, respectively, for the Beckman instrument and the liquid cell was 0.027 mm thick for the Perkin-Elmer records. The thickness for the liquid cells was determined by the method of interference fringes.[5,6] The spectrum was scanned from 400–10000 cm^{-1}, but bands were found only in the region 600–2300 cm^{-1}.

The CCl_3D was prepared by the reaction of sodium deuteroxide with chloral in D_2O solution. The product thus obtained was dried with anhydrous $CaSO_4$, then distilled in vacuum into the Raman tube. A mass spectrometric analysis showed it to contain approximately 10 percent CCl_3H, but probably less than 0.1 percent of other impurities.

SPECTRAL DATA AND ASSIGNMENTS

The present Raman data are compared with the previous data in Table I, columns 1–8. As indicated in column 2, $\Delta\nu$ values have been obtained in 4 separate investigations; however, values from only 3 of these were averaged to obtain the "probable values" in column 3, since Truchet's values[3] seem to be generally too large.

The infra-red data obtained in the present investigation also are given in Table I, columns 9–14. Only two bands were observed for the vapor since the vapor pressure at 30°C was rather small. The percent transmission curve is shown in Fig. 1. The bands at 3.31, 8.22, and 13.16μ for the liquid and the band at 12.94μ for the gas are caused by the 10 percent CCl_3H present in the sample, as indicated in the figure.

In column 15 of Table I are given—in **bold face type**—the wave numbers for the fundamentals calculated in paper III[7] of this series, and—in *italics*—the combina-

* Presented at the Chicago meeting of the American Physical Society (November, 1949); abstract in Phys. Rev. **77**, 740 (1950).

† Based upon investigations carried out in partial fulfillment of the requirements for the degree of Master of Science.

[1] R. W. Wood and D. H. Rank, Phys. Rev. **48**, 63 (1935).

[2] O. Redlich and F. Pordes, Sitz. Akad. Wiss. Wien IIb, **145**, 67 (1936).

[3] M. Rene Truchet, Comptes Rendus **202**, 1997 (1936).

[4] F. F. Cleveland, J. Chem. Phys. **11**, 1, 227 (1943); **13**, 101 (1945).

[5] D. C. Smith and E. C. Miller, J. Opt. Soc. Am. **34**, 130 (1944).

[6] G. B. B. M. Sutherland and H. A. Willis, Trans. Faraday Soc. **41**, 181 (1945).

[7] Zietlow, Cleveland, and Meister, J. Chem. Phys. **18**, 1076 (1950).

tion and overtone wave numbers calculated from the probable values of the fundamentals listed in column 3. The calculated values of the fundamentals are of course much more reliable than for the overtones and combinations. The numbering of the fundamentals in column 16 follows the procedure given in Paper I.[8]

THERMODYNAMIC PROPERTIES FOR CCl_3D

The heat content, free energy, entropy, and heat capacity of CCl_3D were calculated for temperatures from 298.16° to 1000°K, to a rigid rotator, harmonic oscillator approximation. Nuclear spins and the effect of isotopic mixing were neglected. The calculated values are for the ideal gaseous state at one atmosphere pressure.

The bond distances and interbond angles required for the calculation of the moments of inertia were taken from the microwave data[9] for CCl_3H; they were: C−H=C−D=1.090±0.005A, C−Cl=1.761±0.004A, and Cl−C−Cl=112° 0′±40′. From these, the moments

TABLE I. Raman and infra-red spectral data and assignments for deuterotrichloromethane (CCl_3D).[a]

Raman								Infra-red							
PR	N	Δν PV	AD	I PR	T	ρ PR	PS	ν vapor	I_e	ν CS_2 soln.	I_e	ν liquid	I_e	ν_c	Assignments	Type
262	3(4)	261.7	0.3	100	D	0.87	D							**257.5**	ν_6	E
365	3(4)	365.5	0.5	90	P	0.10	P							**368.1**	ν_3	A_1
649	3(4)	650.1	0.8	69	P	0.03	P			648	M			**641.1**	ν_2	A_1
735	3(4)	736.9	1.5	12	D	0.84	D	747	VS	735	VS			**734.1**	ν_5	E
										743	(VS)			*731*	$2\nu_3$	A_1
908	3(4)	908.4	0.4	3	D	0.87	D	909	VS	904	VS	910	VS	**914.7**	ν_4	E
												(1095)	W, b	*1102*	$\nu_2+\nu_5$	E
										1400	M			*1387*	$\nu_2+\nu_5$	E
1463	1	1463		VW										*1474*	$2\nu_5$	A_1+E
1642	1	1642		VW										*1645*	$\nu_4+\nu_5$	A_1+A_2+E
1796	1	1796		VW										*1817*	$2\nu_4$	A_1+E
2255	3(4)	2254.7	1.0	15	P	0.26	P			[b]		2245	M	**2259.0**	ν_1	A_1

[a] $\Delta\nu$ is the Raman displacement in cm^{-1}; I is the semiquantitative relative intensity; ρ is the depolarization factor; ν is the wave number of the infra-red absorption band in cm^{-1}; I_e is the estimated intensity of absorption (W=weak, M=medium, S=strong, V=very); b=broad; PR=present results; N=number of times $\Delta\nu$ has been measured in separate investigations; PV=probable value (mean of the N values, including the present value); AD is the average deviation of the individual values from the mean; T=Truchet, reference 3; PS=polarization state of the line (P=polarized, D=depolarized); ν_c=calculated frequencies (see reference 7); and uncertain data are enclosed in parentheses.

[b] Unresolved from solvent band.

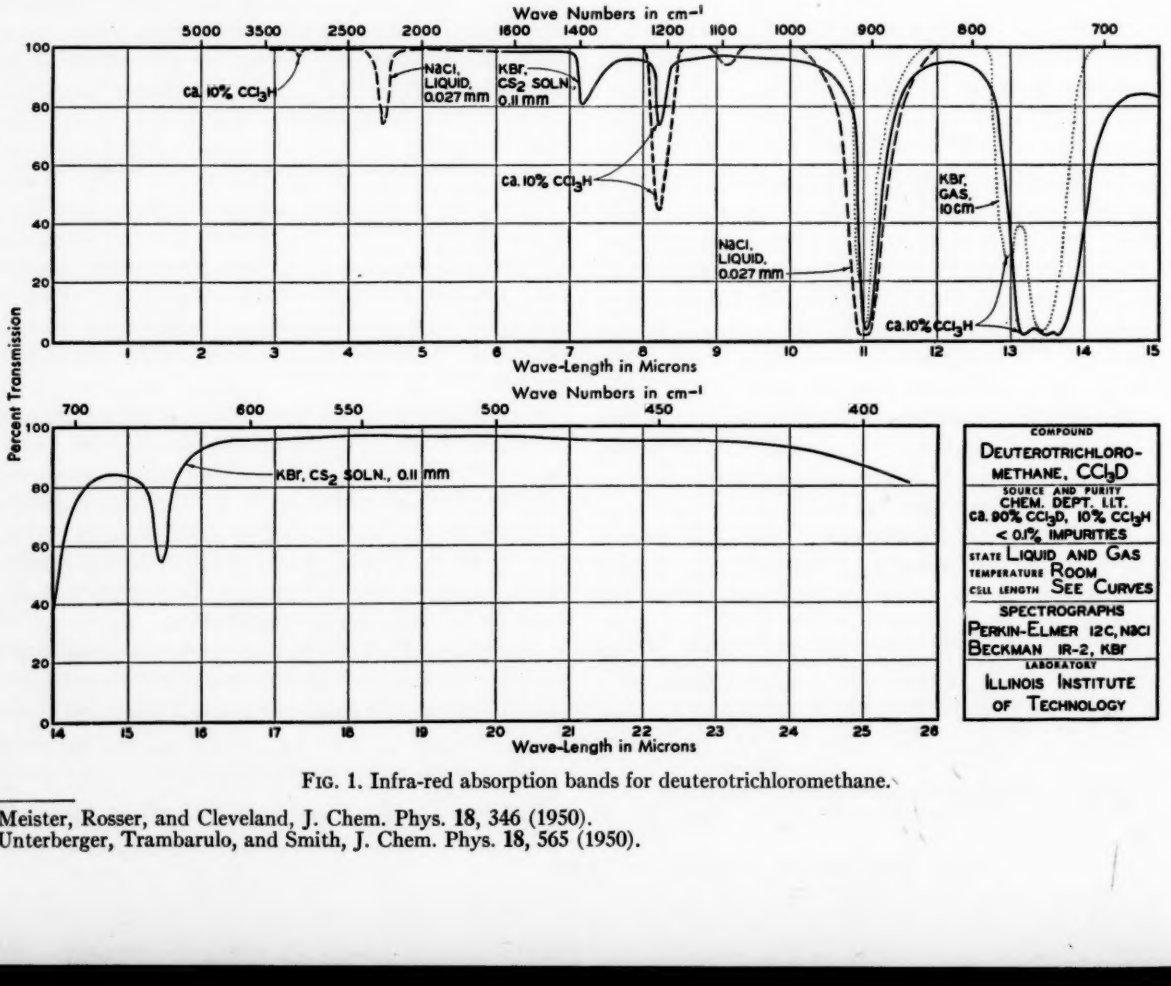

FIG. 1. Infra-red absorption bands for deuterotrichloromethane.

[8] Meister, Rosser, and Cleveland, J. Chem. Phys. **18**, 346 (1950).
[9] Unterberger, Trambarulo, and Smith, J. Chem. Phys. **18**, 565 (1950).

TABLE II. Wave numbers and degeneracies corresponding to the fundamental frequencies of CCl_3D.

Designation	Wave number (cm^{-1})	Degeneracy
ν_1	2255	1
ν_2	650	1
ν_3	365	1
ν_4	[a]909	2
ν_5	[a]747	2
ν_6	262	2

[a] Gaseous state.

of inertia were found to be: $I_{zz}=302$ Awu. A^2 ($501\cdot10^{-40}$ g cm^2), and $I_{xx}=I_{yy}=159$ Awu. A^2 ($264\cdot10^{-40}$ g cm^2). The symmetry number was 3 and Birge's 1941 values[10] of the physical constants were used throughout the calculations. The values used for the fundamentals and their degeneracies are given in Table II.

The results obtained for the thermodynamic properties are given in Table III.

Since 5 of the 9 fundamentals are liquid state frequencies, the values of the thermodynamic properties listed in the table may be slightly larger than the values for the ideal gaseous state. However, even if one assumes that the gaseous frequencies are 6 cm^{-1} higher than the liquid values—which is the mean of the two observed shifts—the values listed in the first row of Table III for 298.16°K would decrease only by 0.07, 0.06, 0.13, and 0.09 cal. $deg.^{-1}$ $mole^{-1}$, respectively. These are probably greater than the actual errors, since the greatest contributions to the thermodynamic properties are made by the low frequencies which are expected to have a smaller shift.

[10] R. T. Birge, Rev. Mod. Phys. **13**, 233 (1941).

TABLE III. Heat content, free energy, entropy, and heat capacity of CCl_3D for the ideal gaseous state at one atmosphere pressure.[a]

T	$(H^0-H_0^0)/T$	$-(F^0-H_0^0)/T$	S^0	C_p^0
298.16	11.55	59.40	70.95	16.37
300	11.58	59.47	71.05	16.42
400	13.09	63.02	76.11	18.68
500	14.37	66.08	80.45	20.22
600	15.44	68.79	84.23	21.32
700	16.34	71.25	87.59	22.13
800	17.11	73.49	90.60	22.75
900	17.76	75.54	93.30	23.23
1000	18.33	77.44	95.77	23.61

[a] T is in degrees Kelvin and the other quantities are in cal. $deg.^{-1}$ $mole^{-1}$.

ACKNOWLEDGMENTS

The Hilger E-518 spectrograph used in this investigation was obtained in part with a grant from the Permanent Science Fund of the American Academy of Arts and Sciences, and the optical parts of the two-prism spectrograph were obtained with a grant from the Society of the Sigma Xi. The authors are grateful for this assistance. Thanks also are due Dr. V. H. Dibeler, of the National Bureau of Standards, who performed the mass-spectrometric analysis, and Dr. Sidney Katz of the Institute of Gas Technology on our campus who kindly made available the Perkin-Elmer infra-red spectrometer. The D_2O was obtained through the courtesy of Dr Martin Kilpatrick and the AEC.

THE JOURNAL OF CHEMICAL PHYSICS VOLUME 18, NUMBER 8 AUGUST, 1950

The Conductance of Potassium Chloride, Potassium Bromide and Potassium Iodide in Aqueous Solutions from 5 to 55°*

BENTON BROOKS OWEN AND HENRY ZELDES†
Sterling Chemistry Laboratory, Yale University, New Haven, Connecticut

(Received May 3, 1950)

The equivalent conductivities of dilute solutions of potassium chloride, potassium bromide, and potassium iodide have been measured at various temperatures, and extrapolated to infinite dilution. These results, when combined with those of A. R. Gordon and others, yield limiting equivalent conductivities of each of the three potassium salts at 10° intervals between 5 and 55°C.

INTRODUCTION

In recent years accurate values of the conductivities[1,2] and transport numbers[3,4] of some simple salts have been reported at temperatures between 15 and 45°, and of hydrochloric acid[5,6] from 0 to 60°. The work reported in this paper extends the range of these results by conductivity measurements at 5 (25) and 55° on potassium chloride and bromide solutions, and at 10° intervals from 5 to 55° on solutions of potassium iodide.

In subsequent papers from this laboratory, measure-

* This communication embodies part of the thesis presented by Henry Zeldes to the Graduate School of Yale University, in partial fulfillment of the requirements for the degree of Doctor of Philosophy (1947).

† Present address: Oak Ridge National Laboratory, Oak Ridge, Tennessee.

[1] G. C. Benson and A. R. Gordon, J. Chem. Phys. **13**, 473 (1945); **13**, 470 (1945).

[2] H. E. Gunning and A. R. Gordon, J. Chem. Phys. **11**, 18 (1943); **10**, 126 (1942).

[3] R. W. Allgood and A. R. Gordon, J. Chem. Phys. **10**, 124 (1942).

[4] Allgood, LeRoy, and Gordon, J. Chem. Phys. **8**, 418 (1940).

[5] B. B. Owen and F. H. Sweeton, J. Am. Chem. Soc. **63**, 2811 (1941).

[6] H. S. Harned and E. C. Dreby, J. Am. Chem. Soc. **61**, 3113 (1939).

TABLE I. Potassium chloride.

5°			25°			55°		
1000 C	Λ	δ	1000 C	Λ	δ	1000 C	Λ	δ
0.8700	92.64	−1	0.5506	147.74	−5	3.2512	236.75	−10
2.1374	91.73	+2	1.5636	146.26	−3	5.6633	233.99	−5
4.0694	90.84	0	3.7404	144.35	+2	8.4251	231.70	−6
7.3332	89.79	+1	7.0663	142.49	+1	11.6256	229.52	−4
11.4479	88.82	+1	9.2057	141.57	−1	16.8195	226.75	−4
14.5221	88.25	0	13.0101	140.23	−1	19.1899	225.66	−3
19.9284	87.41	−1	17.7312	138.88	+1	22.9392	224.17	−9
27.3940	86.50	0				2.2774	238.08	−4
1.3633	92.23	0				4.2395	235.41	+4
2.7962	91.39	+1				6.6311	233.04	+8
4.8599	90.54	+2				10.9499	229.86	+8
6.9114	89.91	+1				13.7269	228.21	+9
11.0372	88.90	+1				19.5238	225.43	+5
14.6232	88.23	−1				25.7958	222.99	+2
19.2367	87.51	0						

TABLE II. Potassium bromide.

5°			25°			55°		
1000 C	Λ	δ	1000 C	Λ	δ	1000 C	Λ	δ
1.1480	94.13	0	1.3949	148.27	−1	1.2891	241.37	−5
2.2559	93.41	0	2.7881	146.91	+1	2.6802	238.86	+3
3.8367	92.68	−1	4.2183	145.88	+2	4.2678	236.85	+5
6.0580	91.90	0	5.9269	144.90	+1	7.0329	234.21	+4
7.5932	91.47	−1	7.1696	144.30	−1	8.8795	232.80	+2
						11.0850	231.35	0
						13.2244	230.16	−7

ments on other alkali halide solutions will be reported in an effort to build up a considerable body of data from which self-consistent values of the limiting mobilities of simple spherical ions, and their temperature coefficients, may be calculated. The present paper will, therefore, be confined to the experimental determination of conductivities and their extrapolation. Consideration of limiting ionic mobilities will be deferred to the next paper of this series where additional data will permit establishing the mobility of the chloride ion from the conductivities of four different chlorides and a variety of transport data.

MATERIALS AND TECHNIQUE

The potassium chloride was a sample purified by Dr. E. J. King in this laboratory for determining cell constants. It was a reagent grade product, repeatedly recrystallized from conductivity water, dried over sodium hydroxide in vacuum at room temperature, then air-dried at slowly increasing temperatures, and finally, fused and cooled in platinum boats. The fused salt was clear, water-white, and produced no color with phenolphthalein.

The potassium bromide was a sample purified by Dr. L. Foering[7] in this laboratory for determining standard electrode potentials. It was prepared from carefully purified samples of bromine and potassium oxalate according to the method of Baxter and Grover[8] which eliminates traces of chloride and iodide, and recrystallized three times from conductivity water. The salt was dried in vacuum, then heated to constant weight at 120°, and finally fused in platinum in an atmosphere of nitrogen. The fused salt was clear, water-white, and produced no color with phenolphthalein.

The potassium iodide was a reagent grade product, twice recrystallized from conductivity water, and dried in vacuum over sodium hydroxide at room temperature. Further drying of this salt raised the question as to whether it could withstand fusion without some decomposition. Two stock solutions were prepared, one from salt heated at 60° for twenty-four hours in air, and another from salt fused in an atmosphere of nitrogen. For equal concentrations calculated from weights of salt and solvent, the conductivities of these two solutions differed by 0.05 percent, the fused salt giving the higher result. A careful analysis of the solution prepared from the unfused salt was made by differential potentiometric titration[9] against silver nitrate, and showed that the difference in conductivity was not due entirely to moisture in this salt. The end point in the titration was corrected for the adsorption of potassium iodide by the precipitate.[10] The silver nitrate solution was made up by weight from a fused, recrystallized reagent grade product, and its titre was checked exactly by differential potentiometric titration against our fused sample of potassium chloride. Unfortunately, we were not able to analyze the stock solution of fused potassium iodide because, at the time that the difference in conductivities became evident, we had exhausted our supplies of both fused and unfused salt. All of the results reported in the tables to follow are based upon concentration determined by analysis.

All conductances reported are referred to the Jones and Bradshaw[11] demal standards. The cell constant was measured in two ways. One determination made use of the 0.1 demal standard potassium chloride solution, and yielded the value 4.6422 at 25°. The other determination consisted in making a series of measurements at six concentrations between 0.0016 and 0.018 normal, and calculating the cell constant at each concentration from values of Λ reported by Shedlovsky, Brown, and MacInnes,[12] which were in turn based upon the Jones and Bradshaw[11] standards. The value of Λ required at each concentration was interpolated from the results of Shedlovsky, Brown, and MacInnes by employing their empirical equation (7) and a plot against concentration of the deviations of their observed values of Λ from the equation. In this way, we obtained the average value 4.6424 ± 0.0004 for the cell constant at 25°. The values at other temperatures were calculated from the geometry of the cell and the co-

[7] L. Foering, Thesis, Yale University (1936).
[8] G. P. Baxter and F. L. Grover, J. Am. Chem. Soc. **37**, 1027 (1915).
[9] D. A. MacInnes, *Principles of Electrochemistry* (Reinhold Publishing Corporation, New York, 1939), p. 306.
[10] I. M. Kolthoff and J. J. Lingane, J. Am. Chem. Soc. **58**, 1524 (1936).
[11] G. Jones and B. C. Bradshaw, J. Am. Chem. Soc. **55**, 1780 (1933).
[12] Shedlovsky, Brown, and MacInnes, Trans. Electrochem. Soc. **66**, 165 (1934).

TABLE III. Potassium iodide.

5°			15°			25°		
1000 C	Λ	δ	1000 C	Λ	δ	1000 C	Λ	δ
0.9822	93.60	0	0.9068	119.67	0	1.3835	147.00	−1
1.6750	93.09	+1	2.0018	118.68	−1	3.8674	144.95	−3
2.7735	92.50	+1	3.8038	117.57	0	5.8982	143.78	−1
4.8149	91.69	+1	5.7454	116.68	0	7.2957	143.13	−1
6.8829	91.06	0	7.4005	116.08	0	8.9114	142.47	0
8.7610	90.60	0	9.2226	115.50	0	11.7214	141.50	−2
13.2357	89.71	0	12.6652	114.59	0	15.9940	140.27	−1
18.3163	88.92	+2	16.9408	113.68	−2	1.9682	146.38	0
						3.9858	144.85	0
						6.6355	143.42	0
						8.9277	142.45	+1
35°			45°			55°		
1.2633	176.63	−2	1.6373	206.70	−2	1.3527	238.84	−1
2.4626	175.13	0	2.9458	204.92	+3	3.2462	235.83	+1
3.9050	173.83	+1	3.7024	204.15	+1	4.9941	233.90	+1
5.9058	172.42	+1	5.7514	202.37	+2	6.9704	232.17	−1
7.4725	171.51	+3	9.1338	200.17	+2	8.6627	230.89	+1
9.3285	170.61	+1	13.3067	198.10	+2	10.6530	229.61	+1
13.2222	169.02	−1	17.3469	196.52	−1	12.8409	228.39	−2
17.8220	167.51	−2				16.1548	226.75	−0

efficients of expansion of platinum[13] and of Jena 16^{III} glass,[14] and could be represented by the equation

$$K=4.6424\{1-0.82\times10^{-5}(t-25)\}. \quad (1)$$

Each temperature was established by a pair of Beckman thermometers set against a freshly calibrated bridge and platinum resistance thermometer. Regulation of the oil thermostat was better than ±0.005°C.

The conductivity measurements were made on a Dike[15] bridge built after the design of Jones and Josephs,[16] and carefully re-calibrated.

The specific conductivity of the water used fell within the range 2.5×10^{-7} and 1.06×10^{-6} mhos, and never exceeded 0.6 percent of the specific conductivity of the most dilute salt solutions studied. Carbon dioxide was swept out of the cell by a stream of air or nitrogen (hydrogen, in the potassium iodide runs) which had been freed from traces of ammonia by passage through a scrubber containing sulfuric acid. A presaturator located in the thermostat prevented loss of water vapor from the cell to the gas stream. Each run consisted of resistance measurements on a series of solutions of increasing concentrations made up by adding increments of four grams, or more, of stock solution.

The electrodes were lightly platinized according to the directions of Jones and Bollinger.[17] Since the measured resistance of various solutions differed less than 0.01 percent at 1000 and 4000 cycles per second, the correction for Parker effect was negligible[18] at 1000 cycles, and this latter frequency was used throughout without correction.

[13] *International Critical Tables* (McGraw-Hill Book Company, Inc., New York, 1927), II, p. 461.
[14] G. W. Morey, *Properties of Glass* (Reinhold Publishing Corporation, New York, 1938), p. 23.
[15] P. H. Dike, Rev. Sci. Inst. **2**, 379 (1931).
[16] G. Jones and R. C. Josephs, J. Am. Chem. Soc. **50**, 1049 (1928).
[17] G. Jones and D. M. Bollinger, J. Am. Chem. Soc. **57**, 280 (1935).
[18] G. Jones and G. M. Bollinger, J. Am. Chem. Soc. **53**, 411 (1931).

TABLE IV. Parameters of Eq. (2).

	5°	15°	25°	35°	45°	55°
$100\alpha^*$	22.15	22.49	22.89	23.34	23.86	24.43
β^*	35.08	46.78	60.19	75.22	91.48	108.53
Λ°, KCl	94.26		149.88			245.69
B	88.3		145.0			177.3
D	20		30			0
Λ°, KBr	96.00		151.68			247.15
B	92.3		91.8			184.0
D	20		0			0
Λ°, KI	95.32	121.83	150.34	180.60	212.13	244.73
B	103.7	108.0	121.1	148.0	184.0	217.6
D	20	10	0	0	0	0

EXPERIMENTAL RESULTS AND EXTRAPOLATION

Tables, I, II, and III contain the experimental results. Concentrations are expressed as moles of salt per liter of solution at the temperature of the measurements. Equivalent conductivities are expressed in reciprocal ohms. In order to make full use of the data over the entire concentration range, we employed the equation

$$\frac{\Lambda+\beta^*(C)^{\frac{1}{2}}}{1-\alpha^*(C)^{\frac{1}{2}}}\equiv\Lambda^{\circ\prime}=\Lambda^\circ+BC+DC\log C \quad (2)$$

which is an extension of the Onsager[19] equation employed by Shedlovsky, Brown and MacInnes,[12] and by Gordon,[1,2] for extrapolation of their results. Values of the empirical parameters, obtained by fitting this equation to the data, are given in Table IV, together with the theoretical Onsager[19] coefficients[20] α^* and β^*. The deviations of Eq. (2) from the experimental data are recorded as the difference

$$\delta\equiv100(\Lambda^{\circ\prime}_{\text{calc.}}-\Lambda^{\circ\prime}_{\text{obs.}}) \quad (3)$$

immediately following values of Λ in Tables I, II, and III.

At 25°, comparison may be directly made between values of Λ° given in Table IV and modern values reported in the literature. Thus, for potassium chloride Λ° is given as 149.86 by Shedlovsky, Brown, and MacInnes.[12] The value of Benson and Gordon,[3] reduced by 0.021 percent to adjust it to the Jones and Bradshaw[11] standard, is 149.85. For potassium bromide Λ° is given as 151.63 by Jones and Bickford,[21] and the adjusted value of Benson and Gordon[1] is 151.64. For potassium iodide the value 150.38 for Λ° is attributed[2] to Longsworth.

[19] L. Onsager and R. M. Fuoss, J. Phys. Chem. **36**, 2681 (1932); Eq. (1.1.2).
[20] These coefficients were calculated from the physical constants of R. T. Birge [Rev. Mod. Phys. **13**, 233 (1941)], viscosities from *International Critical Tables* [**5**, 10], and dielectric constants reported by J. Wyman [Phys. Rev. **35**, 623 (1930)].
[21] G. Jones and C. F. Bickford, J. Am. Chem. Soc. **56**, 602 (1934).

Statistical Mechanics of Dilute Polymer Solutions. II*,[1]

P. J. FLORY AND W. R. KRIGBAUM**
Department of Chemistry, Cornell University, Ithaca, New York
(Received May 1, 1950)

New thermodynamic relationships applicable to dilute solutions of heterogeneous high polymers are derived. The function previously given to express the interaction between two polymer molecules of equal size is modified to include chemically similar polymer molecules differing in size. With the aid of this more general pair partition function the mutually excluded volume for a pair of polymer molecules is easily computed. The osmotic pressure for a dilute solution of a heterogeneous polymer may be expressed in virial form through the application of conventional methods for treating imperfect gases. The second virial coefficient in the series expansion for the osmotic pressure is readily obtained but it is necessary to resort to the hard sphere approximation for estimation of the third coefficient. The third coefficient is much larger than was indicated by earlier theories now known to be inapplicable to dilute solutions, and plots of π/c *vs.* c must be appreciably curved if the slope is great. Similar expressions are derived for Hc/τ obtained from light scattering measurements.

For a dilute solution of a homogeneous polymer the value of the second coefficient in either the osmotic pressure or light scattering expression is not entirely independent of molecular weight, as predicted by earlier theories. The effect of heterogeneity on the second coefficient in these expressions is investigated for the special case of a dilute solution of two polymers differing only in molecular weight, from which it follows that the ratio of the second coefficients in the light scattering and osmotic pressure relations may be either equal to two, or greater or less than that value, depending on the heterogeneity ratio.

At the critical miscibility temperature Θ, the excluded volume vanishes and the present treatment becomes identical with previous theories. The latter should be valid for all concentrations only at the unique temperature $T=\Theta$. The primary parameters κ_1 and ψ_1 governing the heat and entropy of interaction between polymer segments and solvent molecules are difficult to evaluate solely from thermodynamic measurements on dilute solutions except at $T=\Theta$.

INTRODUCTION

THE statistical mechanical theories of polymer solutions currently in use do not conform with observed thermodynamic data at high dilutions.[1–4] These various theories[5–9] are essentially equivalent; they differ principally only in methods of derivation. All of them involve an implicit assumption which usually has escaped notice. In one way or another it is assumed that the interactions of the segments of a given polymer molecule with the segments of all other polymer molecules are the same as would be realized if these latter segments were randomly distributed over the entire volume. A relatively inconsequential correction has been included[5,7–9] for the slightly decreased probability of occupancy of a lattice cell immediately adjacent to a cell known to be vacant (this increase arising from the contiguous relationship of consecutive segments in the chain), but the far more important decrease in the number of intermolecular segment-segment interactions resulting from longer range deviations from a random distribution of segments usually has been ignored.

It was pointed out several years ago by one of us[3] that the implicit assumption mentioned above, though justified at high concentrations where the polymer domains overlap extensively, will not in general be acceptable at low concentrations where these domains are well separated from one another. At high dilutions the solution may be considered to consist of two more or less distinct regions: the one, comprising regions between polymer molecules, is occupied by pure solvent; and the other, representing the regions within polymer domains, contains a segment concentration averaging about a percent or two. If the net thermodynamic interaction between segments causes them to be repellent, only intermolecular interactions between segments near the peripheries of the polymer domains are realized, and the magnitude of the previously calculated chemical potentials, relative to the standard state, is therefore too large. A treatment was given in the 1945 paper[3] referred to above which avoids the unrealistic assumption of a random distribution of segments. It was restricted, however, to the calculation of entropies in systems with low heats of interaction between polymer segments and solvent. Consequently, this theory has been of limited value in quantitative application to experimental data, although it succeeded in demonstrating the source of the discrepancy between previous theories and experiment.

The derivation of the partition function for a pair of equivalent polymer molecules from simple formulation of the segment-segment (or segment-solvent) interactions was presented in a recent note.[1] Thermodynamic properties of the dilute polymer solution were calculated from this partition function according to the well-

* Presented before the High Polymer Forum at the 117th Meeting of the American Chemical Society, Detroit, Michigan, April 18, 1950.

** National Research Fellow in Chemistry.

[1] For the previous paper on this subject see J. Chem. Phys. **17**, 1347 (1949).

[2] Ferry, Gee, and Treloar, Trans. Faraday Soc. **41**, 340 (1945); G. Gee and W. J. C. Orr, *ibid.* **42**, 507 (1946).

[3] P. J. Flory, J. Chem. Phys. **13**, 453 (1945).

[4] For a comparison of experimental data with previous theories, see A. R. Miller, *The Theory of Solutions of High Polymers* (Oxford University Press, London, 1948), Chapter IV.

[5] M. L. Huggins, J. Phys. Chem. **46**, 151 (1942); Ann. N. Y. Acad. Sci. **43**, 1 (1942).

[6] P. J. Flory, J. Chem. Phys. **10**, 51 (1942); **12**, 425 (1944).

[7] A. R. Miller, Proc. Camb. Phil. Soc. **39**, 54, 131 (1943); see also reference 4.

[8] E. A. Guggenheim, Proc. Roy. Soc. **183**, 203, 213 (1944); Trans. Faraday Soc. **41**, 107 (1945).

[9] W. J. C. Orr, Trans. Faraday Soc. **40**, 320 (1944).

established procedures used in the treatment of imperfect gases. The results obtained are applicable for any value of the heat of mixing. In the present paper the statistical mechanics of dilute polymer solutions will be examined from this point of view in somewhat greater detail, and the treatment will be extended to include heterogeneous polymers consisting of chemically similar molecules differing in chain length. The procedure resembles in some respects that of Zimm,[10] who also sought to apply methods formally equivalent to those of imperfect gas theory. However, Zimm calculated segment-segment interactions on the assumption that they are the same as would be found if the segments were cut loose from the chain and allowed to distribute themselves independently of one another. As a consequence of this assumption, which was shown previously[3] to be in error and which is equivalent to the one discussed above, he obtained results which differ from previous theories[5–9] only through contributions from terms of higher order.

THE PARTITION FUNCTION FOR A PAIR OF POLYMER MOLECULES

For the purpose of computing the interaction between two polymer molecules with indices k and l, we first consider the interaction between segments of k and those of l occurring within a volume element $\delta\mathcal{U}$. It has been pointed out elsewhere[11] that the exclusion of a polymer segment from the space occupied by other segments may be treated directly as a spatial interference, or the interaction between segments may be taken into account through the entropy of mixing; these two procedures differ only in the words used to describe them. The latter approach will be pursued here. This permits immediate introduction of parameters which occur also in the related theories concerned with the influence of intramolecular interactions on molecular configuration and intrinsic viscosity[11,12] and with solubility and the thermodynamic behavior of more concentrated solutions. The net energy of mixing polymer segments with solvent must also be taken into account.

We first express the factor in the partition function arising from interactions within the volume element $\delta\mathcal{U}$ between polymer segments of k and those of l when the centers of gravity of the two molecules are separated by a distance a_{kl}. For this purpose, we make use of the theory developed by Huggins[5] and the writer[6] according to which the entropy of mixing n_1 solvent molecules with n_2 polymer molecules to form a solution containing a volume fraction v_2 of polymer is given by

$$\Delta S=-k[n_1\ln(1-v_2)+n_2\ln v_2], \tag{1}$$

where k is Boltzmann's constant. In the present application the centers of gravity of the polymer molecules (e.g., molecules k and l) are fixed at preassigned positions, hence the second term in Eq. (1) must be omitted, giving

$$\Delta S=-kn_1\ln(1-v_2). \tag{1'}$$

It has been shown[3] that Eq. (1) is inapplicable to the dilute polymer solution as a whole, owing to the nonuniform distribution of polymer segments over the entire volume (see above). Within a limited region of space over which the segment expectancy is uniform, this objection is inoperative and it is therefore permissible to apply Eq. (1′) within the volume element $\delta\mathcal{U}$. In one respect, however, Eqs. (1) and (1′) appear to contain a rather serious over simplication: they make no allowance for the specific nature of the given solvent-polymer pair. Recent results[13] give evidence that the entropy of dilution is by no means the same for different solvent-polymer pairs, even among athermal mixtures. On the assumption that Eq. (1′) affords a suitable *form* for the concentration dependence of the entropy of mixing segments with solvent in dilute solutions, although in general it may not correctly represent the *magnitude* of the entropy of mixing, we write

$$\Delta S=-k[n_1\ln(1-v_2)-(\Psi_1-\tfrac{1}{2})n_1v_2] \tag{2}$$

where the parameter ψ_1 is considered to be characteristic of a given polymer-solvent pair;[14] ψ_1 assumes the value $\frac{1}{2}$ in the ideal case represented by Eq. (1).

Assuming for convenience a lattice model of cell size V for the liquid mixture, let the polymer molecules consist of linear sequences of segments, each having a volume V. If the expected densities of segments in the initially separate volume elements $\delta\mathcal{U}$ are represented by ρ_k and ρ_l, then $V\rho_k$ and $V\rho_l$ are their volume fractions. The numbers (n_1) of solvent molecules in these volume elements are $(1-\rho_kV)\delta\mathcal{U}/V_1$ and $(1-\rho_lV)\delta\mathcal{U}/V_1$, respectively, where V_1 is the molecular volume of the solvent. From Eq. (2), the entropy change within this volume element when molecule l is brought into proximity with k is therefore given by

$$\begin{aligned}\delta(\Delta S)=&-(k\delta\mathcal{U}/V_1)\{(1-\rho_kV-\rho_lV)\ln(1-\rho_kV-\rho_lV)\\&-(1-\rho_kV)\ln(1-\rho_kV)-(\Psi_1-1/2)\\&\times[(1-\rho_kV-\rho_lV)(\rho_kV+\rho_lV)\\&-(1-\rho_kV)\rho_kV-(1-\rho_lV)\rho_lV]\}.\end{aligned}$$

Expanding the logarithms and discarding higher terms in ρV, thereby limiting the expression to dilute regions,

$$\delta(\Delta S)=-2k\psi_1(V^2/V_1)\rho_k\rho_l\delta\mathcal{U}. \tag{3}$$

The heat of mixing of x' polymer segments with solvent to form a solution of volume fraction v_2 in polymer

[10] B. H. Zimm, J. Chem. Phys. **14**, 164 (1946).
[11] P. J. Flory, J. Chem. Phys. **17**, 303 (1949).
[12] T. G. Fox, Jr., and P. J. Flory, J. Phys. Coll. Chem. **53**, 197 (1949).
[13] Shick, Doty, and Zimm, J. Am. Chem. Soc. **72**, 530 (1950). Also T. G. Fox, Jr., and P. J. Flory, unpublished.
[14] It is sufficient for the purposes of the present treatment merely to assume that the partial molal entropy of dilution is satisfactorily represented by $\Delta\bar{S}_1=R\psi_1v_2^2$, where ψ_1 remains constant for a given polymer-solvent combination at concentrations not exceeding those occurring in regions encompassed jointly by two polymer molecules.

may be expressed as the product of the expected number of near neighbor polymer-to-solvent contacts times the energy change in the formation of such a contact from the pure components. Thus, ΔH may be written as a minor variant of the usual form

$$\Delta H = \kappa_1 kT x'(V/V_1)(1-v_2), \tag{4}$$

where

$$\kappa_1 = [\epsilon_{12} - (\epsilon_{11}+\epsilon_{22})/2](\gamma-2)V_1/VkT = BV_1/kT. \tag{5}$$

Here ϵ_{11}, ϵ_{22}, and ϵ_{12} are the interaction energies for solvent-solvent, polymer-polymer, and solvent-polymer contacts, respectively, γ is the lattice coordination number, and B is the parameter, often used in previous theories, expressing interaction energy per unit volume. κ_1 corresponds *formally* to the "energy" part of μ_1 of former theories.[5] In assigning numerical values to κ_1, however, it should not be confused with the semi-empirical μ_1 widely used in the past in the treatment of dilute solution thermodynamic data. Actual values of κ_1 may differ considerably from those of μ_1.

The energy change in the volume element $\delta\mathcal{U}$ due to the partial superposition of the two polymer molecules is readily obtained from Eq. (4) by setting $x' = (\rho_k+\rho_l)\delta\mathcal{U}$ in the final state, and $x' = \rho_k\delta\mathcal{U}$ and $\rho_l\delta\mathcal{U}$ in the initially separate volume elements, and by introducing corresponding values for the final and initial volume fractions, v_2. Thus,

$$\delta(\Delta H) = -2kT\kappa_1(V^2/V_1)\rho_k\rho_l\delta\mathcal{U}, \tag{6}$$

which is similar in form to Eq. (3) for the entropy.

The contribution to the partition function from the volume element $\delta\mathcal{U}$ as obtained from these expressions is

$$f^{\delta v} = \exp[-2\rho_k\rho_l(V^2/V_1)(\psi_1-\kappa_1)\delta\mathcal{U}]. \tag{7}$$[15a]

The total partition function for the pair of molecules with centers of gravity separated by a distance a_{kl} is given by the product of the $f^{\delta v}$ for all volume elements, or

$$\ln f(a_{kl}) = -2\int_0^\infty\int_0^\pi JV^2\bar{v}^{-2}\rho_k\rho_l 2\pi r^2 \sin\theta dr d\theta, \tag{8}$$

where r and θ represent cylindrical coordinates which it will be convenient to take from an origin midway between the centers of the two molecules; $\bar{v}$ is the specific volume of the polymer, and

$$J = (\psi_1-\kappa_1)\bar{v}^2/V_1 \tag{9}$$

The spatial distributions of segments of the two molecules are assumed to be Gaussian:[15b]

$$\rho_k = x_k(\beta_k'^2/\pi)^{\frac{3}{2}}\exp(-\beta_k'^2 s_k^2),$$
$$\rho_l = x_l(\beta_l'^2/\pi)^{\frac{3}{2}}\exp(-\beta_l'^2 s_l^2),$$

where x_k and x_l represent the numbers of segments in the respective molecules k and l and s_k and s_l are distances of the volume element from the respective centers of gravity.

$$s_k^2 = a_{kl}^2/4 + a_{kl}r\cos\theta + r^2,$$
$$s_l^2 = a_{kl}^2/4 - a_{kl}r\cos\theta + r^2.$$

The parameters β' are defined[11] by expressions (subscripts omitted)

$$\beta' = 3/\alpha l Z^{\frac{1}{2}}, \tag{10}$$

where Z is the number of configurational segmants of length l in the equivalent flexibly-jointed chain[16] and α is the factor by which the linear dimensions of the molecule are increased due to intramolecular interactions equivalent in nature to those responsible for intermolecular interactions. Thus, α is a function of ψ_1 and κ_1, and also of the chain length Z.[17]

Substituting the Gaussian distributions in (8), and introducing the above expressions for s_k and s_l in cylindrical coordinates, there is obtained through suitable combination of factors

$$\ln f(a_{kl}) = -(4J/\pi^2)V^2\bar{v}^{-2}(\beta_k'\beta_l')^3 x_k x_l \times \int_0^\infty\int_0^\pi \exp[-(\beta_k'^2+\beta_l'^2)(r^2+a_{kl}^2/4) - (\beta_k'^2-\beta_l'^2)a_{kl}r\cos\theta]\times r^2\sin\theta dr d\theta$$
$$= -(4J/\pi^2)(\beta_k'\beta_l')^3 m_k m_l \exp[-(\beta_k'^2+\beta_l'^2)a_{kl}^2/4]\int_0^\infty \exp[-(\beta_k'^2+\beta_l'^2)r^2] \times\left\{\frac{2\sinh[a_{kl}r(\beta_k'^2-\beta_l'^2)]}{a_{kl}r(\beta_k'^2-\beta_l'^2)}\right\} r^2 dr \tag{11}$$

where $m_k = x_k V\bar{v}^{-1}$ and $m_l = x_l V\bar{v}^{-1}$ are the weights of the respective molecules.

The integration may be performed by expanding the factor in braces and integrating term by term. The series obtained after integration is the expansion of an exponential, and the final result reduces to the closed form

$$\ln f(a_{kl}) = -(J/2^{\frac{1}{2}}\pi^{\frac{3}{2}})\tilde{\beta}_{kl}'^3 m_k m_l \exp(-\tilde{\beta}_{kl}'^2 a_{kl}^2/2) \tag{12}$$

[15a] Eq. (7) differs from the expression previously published[1] for $f^{\delta v}$ only through the introduction of ψ_1 instead of $\frac{1}{2}$ in the factor (ψ_1-K_1).

[15b] P. Debye and I. M. Krieger have shown that the distribution of segments about the center of gravity is Gaussian in the case of a random chain devoid of long range interactions. Our assumption that the spatial distribution also is Gaussian for actual chains in which these interactions are by no means negligible (see reference 11) represents a minor approximation. We are indebted to Professor Debye and Dr. Krieger for making their results available to us.

[16] For a more precise description of the definitions and significance of Z and l see reference 11, in particular footnote 5 and Eqs. (28) and (29). Z depends on the average bond configuration for the structural units, in general varying with chain flexibility, and l denotes the length of an equivalent segment such that the product Zl gives the contour length of the chain.

[17] In the first paper (see reference 11) dealing with intramolecular interactions κ_1 is represented by μ_1 and the value $\frac{1}{2}$ has been employed in place of ψ_1. These and other minor revisions in the intramolecular theory will be presented in a later paper.

where

$$\bar{\beta}_{kl}'=[2\beta_k'^2\beta_l'^2/(\beta_k'^2+\beta_l'^2)]^{\frac{1}{2}}. \quad (13)$$

Thus, the partition function for a pair of dissimilar molecules assumes a form corresponding to that for molecules of equal size. For identical polymer molecules $\bar{\beta}_{kl}'=\beta_k'=\beta_l'$ and $m_k=m_l$, so that Eq. (12) reduces to Eq. (5) of reference 1. It should be noted that the partition function does not depend on any parameter of the lattice.

For purposes of the further development it is convenient to replace Eq. (12) with the following simplified expression for the pair partition function

$$\ln f(a_{kl})=-J\xi_{kl}^3\exp(-y^2), \quad (14)$$

where

$$\xi_{kl}=\bar{\beta}_{kl}'(m_km_l)^{1/3}/2^{1/6}\pi^{1/2} \quad (15)$$

and

$$y=\bar{\beta}_{kl}'a_{kl}/2^{1/2}=\xi_{kl}a_{kl}\pi^{1/2}/(2m_km_l)^{1/3}. \quad (16)$$

THE PARTITION FUNCTION FOR THE SOLUTION AND THE SECOND VIRIAL COEFFICIENT IN THE OSMOTIC PRESSURE RELATIONSHIP

The excluded volume for the k, l pair is given by

$$u_{kl}=\int_0^\infty[1-f(a_{kl})]4\pi a_{kl}^2da_{kl}$$

$$=2Jm_km_lF(J\xi_{kl}^3) \quad (17)^{18}$$

where

$$F(X)=(4/\pi^{\frac{1}{2}})X^{-1}\int_0^\infty \times\{1-\exp[-X\exp(-y^2)]\}y^2dy \quad (18)$$

which can be transformed through integration by parts to the more convenient form

$$F(X)=(8/3\pi^{\frac{1}{2}})\int_0^\infty\exp[-y^2-X\exp(-y^2)]y^4dy \quad (18.1)$$

or by series expansion and term by term integration to

$$F(X)=(1-X/2\,!2^{3/2}+X/3\,!3^{3/2}-\cdots). \quad (18.2)$$

u_{kl} represents an effective volume of either polymer molecule with respect to the other. Depending on the parameters ψ_1 and κ_1 and the chain length Z, it may be as much as a hundred or more times the actual molecular volume of either polymer molecule. Direct integration of Eq. (18) or (18.1) does not appear to be possible. The series (18.2) is rapidly asymptotic only for small values of X, whereas the series obtained from Eq. (18.1) on expanding the factor in square brackets in a Taylor's series about its minimum absolute value and integrating term by term is rapidly asymptotic only for values of X which are larger than those of interest here. $F(X)$ has been evaluated by graphical integration of Eq. (18.1) with the results shown in Fig. 1. Here $F(X)$ is plotted against X, using a logarithmic scale of the abscissa for convenience. For lower values of X than are included in Fig. 1, $F(X)$ is readily calculated from the series expansion (18.2).

The partition function for a dilute solution of the heterogeneous polymer may be deduced in standard fashion by considering the volume available to each successive polymer molecule added to the solution, which will be assumed to be sufficiently dilute to justify neglect of ternary and higher interactions. Letting the molecules be numbered in the order of their addition to the solution, the partition function can be written

$$Q=\mathcal{V}(\mathcal{V}-u_{21})(\mathcal{V}-u_{31}-u_{32})\cdots$$

$$=\mathcal{V}^N\prod_{k=2}^{N}\left(1-\sum_{l=1}^{k-1}u_{kl}/\mathcal{V}\right), \quad (19)$$

where $\mathcal{V}$ is the total volume of the solution and N is the total number of polymer molecules. The solution is assumed to be sufficiently dilute so that all factors in the above product are near unity (i.e., it is assumed that $\sum u_{kl}\ll\mathcal{V}$). Then,

$$\ln Q\cong N\ln\mathcal{V}-(\tfrac{1}{2})\textstyle\sum_k\sum_l u_{kl}/\mathcal{V}.$$

Letting N_i and N_j represent the numbers of molecules of molecular weight M_i and M_j, respectively, the partition function may be rewritten

$$\ln Q=N\ln\mathcal{V}-(\tfrac{1}{2})\textstyle\sum_i\sum_j N_iN_ju_{ij}/\mathcal{V}. \quad (20)$$

Since the osmotic pressure π is equal to $kT(\partial\ln Q/\partial\mathcal{V})$, we obtain from Eq. (20)

$$\pi=kT(N/\mathcal{V})+(kT/2\mathcal{V}^2)\textstyle\sum_i\sum_j N_iN_ju_{ij}. \quad (21)$$

This equation holds only at very high dilutions, for we have considered only binary interaction between molecules. Expressing the osmotic pressure as a power series in the concentration analogous to the virial expansion for a gas, we may adopt the convenient form

$$\pi=RT[A_1c+A_2c^2+A_3c^3+\cdots], \quad (22)^{19}$$

where c expresses the concentration of polymer in g. per unit volume. Noting that $N/\mathcal{V}=c\mathbf{N}/\bar{M}_n$ where $\mathbf{N}$ is Avogadro's number, and $\bar{M}_n=\mathbf{N}\sum_i m_iN_i/N$ is the number average molecular weight, comparison of Eqs. (21) and (22) yields values for the first and second coefficients as follows

$$A_1=1/\bar{M}_n$$

$$A_2=(\mathbf{N}/2N^2\bar{M}_n^2)\textstyle\sum_i\sum_j N_iN_ju_{ij}. \quad (23)^{20}$$

Introducing Eq. (17) for u_{ij}

$$A_2=(\mathbf{N}J/N^2\bar{M}_n^2)\textstyle\sum_i\sum_j m_iN_im_jN_jF(J\xi_{ij}^3). \quad (24)$$

[18] In the case of a homogeneous polymer, $J\xi_{kl}^3$ corresponds to K of reference 1, if $\psi_1=\frac{1}{2}$.

[19] This is the form used by W. G. McMillan and J. E. Mayer, J. Chem. Phys. 13, 276 (1945), and by B. H. Zimm, *ibid.*, 14, 164 (1946).

[20] A_2 corresponds to B'/M^2 in the preceding paper (see reference 1) on homogeneous polymers.

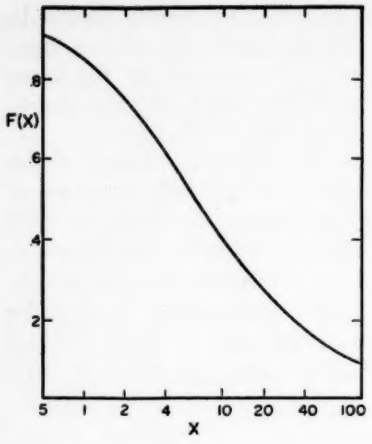

FIG. 1. The function $F(X)$ *vs.* X.

Or

$$A_2=J\Upsilon/\mathbf{N}, \tag{25}$$

where

$$\Upsilon=\sum_i\sum_j w_i w_j F(J\xi_{ij}{}^3), \tag{26}$$

and w_i and w_j are the weight fractions of components i and j, i.e., $w_i=m_iN_i/\sum m_iN_i$, where the summation is taken over all polymer species. According to the definition of J,

$$A_2=(\bar{v}^2/V_1)(\psi_1-\kappa_1)\Upsilon, \tag{27}$$

where V_1 is the *molar* volume of the solvent. Or

$$A_2=(\bar{v}^2/V_1)\psi_1(1-\Theta/T)\Upsilon, \tag{28}$$

where

$$\Theta=\kappa_1 T/\psi_1=BV_1/R\psi_1. \tag{29}$$

As has been pointed out previously,[1] Θ represents the critical temperature for complete miscibility (κ_1 assumed positive) in the limit of infinite molecular weight. For polymers of finite molecular weight at $T=\Theta$, $A_2=0$ and the dilute solution should obey Van't Hoff's law.

For many purposes it is preferable to use the series expression

$$\pi/c=(RT/\bar{M}_n)(1+\Gamma_2 c+\Gamma_3 c^2+\cdots). \tag{30}$$

Comparing with Eq. (22)

$$\Gamma_2=A_2/A_1=J\bar{M}_n\Upsilon/\mathbf{N} \tag{31}$$

and

$$\Gamma_3=A_3/A_1.$$

The approximate evaluation of Γ_3 will be discussed below.

Expressions for the partial molal heats and entropies of dilution, derived from the osmotic pressure expansion (22) and A_2 as given by Eq. (28), are as follows

$$\Delta\bar{H}_1=RT\kappa_1(\bar{v}c)^2[\Upsilon+\psi_1(1-\Theta/T)\mathbf{N}\Upsilon'\bar{v}^2/V_1] \tag{32}$$

and

$$T\Delta\bar{S}_1=RTV_1c/\bar{M}_n+RT\kappa_1(\bar{v}c)^2[\Upsilon(T/\Theta)+\psi_1(1-\Theta/T)\mathbf{N}\Upsilon'\bar{v}^2/V_1]. \tag{33}$$

where

$$\Upsilon'=\partial\Upsilon/\partial J.$$

HOMOGENEOUS POLYMERS AND THE THIRD VIRIAL COEFFICIENT

The form of the quantity $J\xi^3$ for homogeneous polymers is particularly important in relation to the theory of intramolecular interactions.[11] If the polymer is homogeneous β_{kl}' reduces to β', so that

$$\xi=\beta' m^{2/3}/2^{1/6}\pi^{1/2} \tag{15.1}$$

and from Eqs. (9), (10), (29), and (15.1)

$$J\xi^3=4C_M\psi_1(1-\Theta/T)M^{1/2}/\alpha^3, \tag{34}$$

where

$$C_M=(3^3\bar{v}^2/2^{5/2}\pi^{3/2}V_1)(M/Z\bar{l}^2\mathbf{N}^{2/3})^{3/2}. \tag{35}$$

The parameter C_M differs by the factor $(Z/M)^{\frac{1}{2}}$ from C_1 first introduced in the intramolecular theory.[11,21] The latter theory yielded a relationship between the intramolecular deformation α and the thermodynamic parameters. When modified through the introduction of ψ_1 in place of $\frac{1}{2}$, this relationship may be written

$$\alpha^5-\alpha^3=2C_M\psi_1(1-\Theta/T)M^{\frac{1}{2}}. \tag{36}$$

On comparing Eqs. (32) and (34),

$$J\xi^3=2(\alpha^2-1). \tag{37}$$

Now α may be evaluated from measurements of the intrinsic viscosity in various solvents and/or at different temperatures.[12] It appears at present that the absolute value of $J\xi^3$ determined in this way probably would be uncertain to some extent owing to uncertainty in the coefficient expressing the elastic response of the polymer molecule to deformation. This would alter the numerical factor in Eq. (36). Relative values for $J\xi^3$ in different solvents and at different temperatures estimated in this manner should be realistic, however.

The excluded volume for the interaction of a pair of molecules equal in size reduces to

$$u=2Jm^2F(J\xi^3) \tag{38}$$

or

$$u=2\psi_1(1-\Theta/T)(\bar{v}^2m^2/V_1)F(J\xi^3). \tag{38.1}$$

Thus, the excluded volume depends on the thermodynamic parameters principally through $\psi_1(1-\Theta/T)$, but also, though less critically, through $F(J\xi^3)$.

For the dilute solution of homogeneous polymer we take $A_1=1/M$, and since $\Upsilon=F(J\xi^3)$

$$A_2=(J/\mathbf{N})F(J\xi^3) \tag{39}$$

$$=(\bar{v}^2/V_1)\psi_1(1-\Theta/T)F(J\xi^3). \tag{39.1}$$

The connection between A_2 and the excluded volume is shown by comparing (38) and (39), whence

$$A_2=u/2\mathbf{N}m^2=\mathbf{N}u/2M^2. \tag{40}$$

Similarly

$$\Gamma_2=u/2m=\mathbf{N}u/2M. \tag{41}$$

[21] The numerical factor in the preceding paper (see reference 1) on intramolecular interactions was expressed in approximation only.

As was noted in the discussion of heterogeneous polymers in the preceding section, A_2 and Γ_2 vanish at $T=\Theta$, and Van't Hoff's law is obeyed. The excluded volume is then zero, which signifies that the molecules overlap freely in the solution.

According to the earlier theories of polymer solutions[5,6] modified with the proposed entropy factor $2\psi_1$

$$\pi=-\Delta\bar{F}_1/V_1=-(RT/V_1)[\ln(1-v_2)+(1-V_1/M\bar{v})v_2 -(\psi_1-\kappa_1-\tfrac{1}{2})v_2^2] \quad (42)$$

$$=RT\{c/M+[(\psi_1-\kappa_1)\bar{v}^2/V_1]c^2 +(\bar{v}^3/3V_1)c^3+\cdots\}, \quad (42.1)$$

whence

$$A_2=(\bar{v}^2/V_1)(\psi_1-\kappa_1) =(\bar{v}^2/V_1)\psi_1(1-\Theta/T), \quad (43)$$

which differs from Eq. (39.1) only in the omission of $F(J\xi^3)$. Failure of these relationships when applied to dilute solutions arises because of the non-random distribution of polymer segments when the solution is sufficiently dilute to permit the polymer molecules to occupy separate regions of space.[3] More specifically, in the dilute solution all segments of polymer molecules are not equally available for interaction with segments of other molecules. When the excluded volume is zero, this is no longer true; the polymer molecules then interpenetrate one another freely and the total number of segment-segment interactions is the same as if the segments were uniformly distributed throughout the space. Thus, the earlier theories should be valid at the unique temperature $T=\Theta$. Examination of the various equations shows that the new and the older theories do indeed converge as $T\to\Theta$. When $T=\Theta$, $J\xi^3=0$ and $F(J\xi^3)=1$.

This deduction may appear to be trivial inasmuch as both theories give $A_2=0$ at $T=\Theta$. However, it must be borne in mind that the present theory is necessarily restricted to dilute solutions as a consequence of the retention of only the first term in the series expansion of the primary entropy of dilution expression (see Eq. (3)). No such approximation was required in the former theories, and we may conclude that, within the limits of other approximations common to all existing theories, Eq. (42) or (42.1) may be appropriate for *all* concentrations when $T=\Theta$. Regardless of the value of Θ/T, complications arising from non-uniformity in the distribution of segments over the volume must become trivial as the concentration is increased owing to the forced overlapping of polymer molecules. Hence, Eq. (42) would appear to be generally acceptable at higher concentrations. In conclusion, in a good solvent the previous theories of polymer solutions should be applied only where the concentration is great enough to assure intense overlapping of molecules; the present theory may be applied only to solutions so dilute that overlapping of the excluded volumes u is slight (cf. following); at intermediate concentrations neither theory is appropriate. In a poor solvent at $T=\Theta$, the former theory (i.e., Eq. (42)) should apply at all concentrations.

The partial molal heats and entropies of dilution for dilute solutions of homogeneous polymers assume forms only slightly less formidable than Eqs. (32) and (33); Υ' is merely replaced by $F'=\partial F(J\xi^3)/\partial J$. When $T=\Theta$, however,

$$\Delta\bar{H}_1=R\Theta\psi_1\bar{v}^2c^2\equiv R\Theta\kappa_1(\bar{v}c)^2 \quad (44)$$

and

$$\Delta\bar{S}_1=RV_1c/M+R\psi_1(\bar{v}c)^2 \quad (45)$$

which are equivalent to the expressions given by the earlier theory. Whereas Eqs. (32) and (33) are too cumbersome to be of much use, the temperature coefficient of π, or of A_2, at $T=\Theta$ readily yields the value of ψ_1, which is also equal to κ_1 at this temperature.

If the series expression (30) is re-written in powers of the reciprocals of the volume per mole of solute, i.e., in powers of $N/\mathbf{N}\mathcal{V}=c/M$

$$\pi/c=(RT/M)[1+(\Gamma_2M)(c/M) +(\Gamma_3M^2)(c/M)^2+\cdots]. \quad (30.1)$$

The coefficient of the second term is half of the excluded volume for all of the molecules or

$$\Gamma_2M=\mathbf{N}u/2=(\mathbf{N}/2)\int[1-f(a_{kl})]d\omega_l, \quad (46)$$

where ω_l represents the space coordinates of molecule l, and the integration is to be performed over all values of those coordinates for a fixed location of molecule k. This result is familiar from the theory of imperfect gases.

The third coefficient, which in the present notation is Γ_3M^2, depends on interactions involving three molecules. In particular, it is necessary to consider the regions of the space from which the center of gravity of molecule k is "repelled" by both of the molecules l and m. In a general treatment of the problem, Kirkwood[22] has shown that

$$\Gamma_3M^2=(\mathbf{N}^2/3)\int\int[1-f(a_{kl})][1-f(a_{km})] \times[1-f(a_{lm})]d\omega_l d\omega_m \quad (47)$$

where $f(a_{kl})$, $f(a_{km})$, and $f(a_{lm})$ are the partition functions for the respective pairs of molecules. Accurate evaluation of these integrals appears to be prohibitively difficult, but an approximate procedure may be applied as follows. It will be assumed that each $f(a)$ is defined by

$$f(a)=0 \quad \text{for} \quad a<d_s.$$
$$f(a)=1 \quad \text{for} \quad a>d_s.$$

In other words, the molecules are treated as impenetrable non-interacting spheres of diameter d_s, this

[22] J. G. Kirkwood, J. Chem. Phys. **3**, 300 (1935).

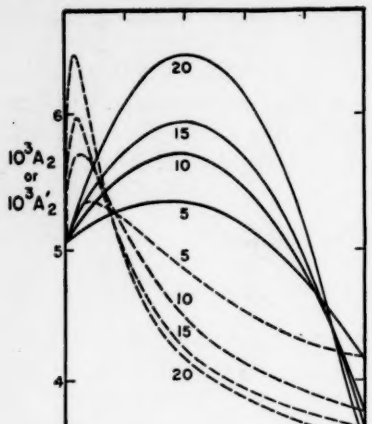

FIG. 2. A_2 and A_2' for ternary mixtures consisting of a solvent and two polymers of molecular weights M_j and M_i *vs.* the weight fraction w_j of polymer consisting of the component of higher molecular weight. Numbers above the curves represent the ratio of the molecular weights, M_j/M_i. Solid curves represent A_2; dashed curves, A_2'.

diameter being so chosen as to give the correct second coefficient in accordance with Eq. (46), i.e., we will let

$$d_s^3=(3/4\pi)u.$$

The integration over ω_m in Eq. (47) amounts merely to the evaluation of the volume common to the spheres k and l, each of diameter d_s, their centers being separated by a distance a_{kl}. It remains to integrate the value of this volume for all positions of l relative to k. The final result is

$$\Gamma_3M^2=(\mathbf{N}^2/3)(5\pi^2d_s^6/6)=(5/32)\mathbf{N}^2u^2. \quad (48)$$

Comparing this equation with (46), we finally obtain

$$\Gamma_3=(\tfrac{5}{8})\Gamma_2^2. \quad (49)$$

In other words, in the hard sphere approximation the coefficient of the third term in Eq. (30.1) is $\frac{5}{8}$ of the square of the second coefficient. This result was obtained in an equivalent manner many years ago by Boltzmann,[23] for a gas composed of hard sphere molecules. A value for the coefficient of the next higher term may be obtained similarly, but in light of the limitations of the hard sphere approximation (i.e., the spherical domains are not actually impenetrable, and interpenetrations must occur as the concentration is increased), this further extension does not seem justified.

Introducing the approximate third virial coefficient from Eq. (49)

$$\pi/c=(RT/M)[1+\Gamma_2c+(\tfrac{5}{8})\Gamma_2^2c^2+\cdots], \quad (50)$$

or

$$\pi/c=RT[A_1+A_2c+(\tfrac{5}{8})(A_2^2/A_1)c^2+\cdots], \quad (51)$$

where $A_1=1/M$. According to these equations, at concentrations such that π/c is appreciably greater than its limiting value, RT/M, curvature in the plot of π/c *vs.* c should be appreciable. Such curvature has been observed experimentally, and was predicted by a previous related theoretical treatment.[3]

The above expressions are necessarily limited to quite low concentrations. The effective volume of a polymer molecule may be taken as one-eighth of u. Somewhat arbitrarily we suggest that the three terms of the series in Eq. (50), or (51), are sufficient only at concentrations such that the total effective volume of all the molecules amounts to no more than one-fourth of the volume of the solution, i.e.,

$$Nu/8\leqslant\mathcal{V}/4=NM/4\mathbf{N}c$$

or

$$\mathbf{N}u/2M\leqslant 1/c.$$

Recalling Eq. (41), this condition requires that

$$\Gamma_2c\leqslant 1.$$

Hence, the three terms which have been evaluated may be expected to be adequate only for concentrations such that

$$(\pi/c)/(\pi/c)_0<ca.\ 2\text{ or }3.$$

The hard sphere approximation doubtless makes the third term somewhat too large. Consequently, omission of the fourth term (also positive in the hard sphere approximation[23]) and the error in the third term provide partially compensating errors. For this reason, Eqs. (50) and (51) with higher terms omitted may apply at somewhat higher concentrations than one would otherwise expect.

The deduction of the third virial coefficient for heterogeneous polymers from the present theory seems beyond hope. We therefore offer the plausible postulate that the third coefficient is related to the second just as in the homogeneous polymer case. Thus, corresponding to Eqs. (50) and (51), we suggest

$$\pi/c=(RT/\bar{M}_n)[1+\Gamma_2c+(\tfrac{5}{8})\Gamma_2^2c^2+\cdots] \quad (50.1)$$

or

$$\pi/c=RT[1/\bar{M}_n+A_2c+(\tfrac{5}{8})A_2^2\bar{M}_nc^2+\cdots], \quad (51.1)$$

where Γ_2 and A_2 are defined by equations of the preceding section. The actual validity of the third coefficients in these expressions may be established by experiments on heterogeneous polymers.

LIGHT SCATTERING OF HETEROGENEOUS POLYMERS AND THE THIRD COEFFICIENT FOR HOMOGENEOUS POLYMERS

The turbidity of multi-component systems, first given a theoretical treatment by Zernicke,[24] has been

[23] L. Boltzmann, *Vorlesungen über Gastheorie* (V. Abschnitt, Verlag von Johann Ambrosius Barth, Leipzig, 1898), Vol. II, p. 138. This derivation of the third virial coefficient is outlined here in order to bring out the significance of the hard sphere approximation with reference to the present problem. See also, R. H. Fowler and E. A. Guggenheim, *Statistical Thermodynamics* (Cambridge University Press, London, 1939), p. 289.

[24] F. Zernicke, *L'Opalescence critique*, Dissertation, Amsterdam, 1915; Archives Neerland (3A) **4**, 74 (1918).

the subject of several recent papers.[25–27] All of these treatments demonstrate that the turbidity of such a system is not the sum of the turbidities of the components, as had been assumed until recently. Brinkmann and Hermans[25] show that the coefficients in the light scattering expression are independent of the molecular weight distribution whenever the free energy of dilution is of the form

$$\Delta\bar{F}_1=RT[f(v_2)-(1/\bar{M}_n)(V_1/\bar{v})v_2-(v_2^2/2)-\cdots] \quad (52)$$

where $f(v_2)$ is an arbitrary function of the volume fraction of total polymer. This differs from the free energy of dilution as given by combining Eqs. (32) and (33) principally through the omission of the molecular weight dependent parameter Υ in the third term. Stockmayer[27] also gives a treatment for a dilute solution consisting of solvent and a series of polymers differing only in molecular weight. His relation for τ, the excess turbidity over that of the solvent, may be written

$$\tau/H=\sum_i c_iM_i-\sum_i\sum_j \beta_{ij}c_ic_j, \quad (53)$$

where

$$\beta_{ij}=(1/RT)(\partial^2F/\partial n_i\partial n_j)_{T,\,p}. \quad (54)$$

In these equations H is the usual light scattering constant, F is the Gibbs free energy, n_i is the number of moles per cc, and c_i the concentration in grams per cc, of the component having molecular weight M_i. Expressing the osmotic pressure in the form

$$\pi=RT[\textstyle\sum_i(c_i/M_i)+A_2\sum_i\sum_j c_ic_j+\cdots] \quad (55)$$

he makes the assumption, based on previous theories, that A_2 is independent of molecular weight to obtain

$$Hc/\tau=1/\bar{M}_w+2A_2c+\cdots. \quad (56)$$

In dilute solution the free energy of dilution is not in the form of Eq. (52), nor is A_2 of Eq. (55) independent of molecular weight. According to the partition function as given by Eq. (20), the Gibbs free energy in dilute solutions is

$$F=-kT[N\ln\mathcal{V}-(1/2\mathcal{V})\textstyle\sum_k\sum_l N_kN_lu_{kl}+\cdots]. \quad (57)$$

Omitting terms of order higher than those shown in Eq. (57)

$$\beta_{ij}\cong\mathbf{N}u_{ij}/\mathcal{V}. \quad (58)$$

Substituting the value of u_{ij} from Eq. (17)

$$\beta_{ij}\cong 2(J/\mathbf{N})M_iM_jF(J\xi_{ij}^3). \quad (59)$$

In place of Eq. (56) there is obtained

$$Hc/\tau=1/\bar{M}_w+2A_2'c+\cdots, \quad (60)$$

where

$$A_2'=(J/\mathbf{N})(1/\bar{M}_w)^2\textstyle\sum_i\sum_j F(J\xi_{ij}^3)w_iM_iw_jM_j. \quad (61)$$

It therefore appears that for heterogeneous polymers the second coefficient in the light scattering expression, and presumably higher coefficients as well, will be dependent to some extent on the molecular weight distribution. An indication of the magnitude of this dependence will be given in the next section.

If the polymer is homogeneous, the light scattering expression can be obtained from the corresponding osmotic pressure expansion by use of

$$Hc/\tau=(1/RT)(\partial\pi/\partial c). \quad (62)$$

From the osmotic pressure of a homogeneous polymer in dilute solution as given by Eqs. (50) or (51) there are obtained

$$Hc/\tau=(1/M)[1+2\Gamma_2c+(15/8)\Gamma_2^2c^2+\cdots] \quad (63)$$

$$Hc/\tau=[A_1+2A_2c+(15/8)(A_2^2/A_1)c^2+\cdots] \quad (64)$$

where

$$A_1=1/M,\quad A_2=(J/\mathbf{N})F(J\xi^3),\quad \text{and}\quad \Gamma_2=A_2/M.$$

These equations predict curvature in the plot of Hc/τ *vs.* c. Comparison with Eqs. (50) or (51) reveals that the predicted ratio of curvature to slope for the Hc/τ curve is half again as large as that of the π/RTc curve.

CALCULATIONS FOR TERNARY MIXTURES CONTAINING POLYMERS OF TWO MOLECULAR WEIGHTS

In order to evaluate the coefficients occurring in the osmotic pressure and light scattering expressions for any given molecular weight distribution, values of J and Υ must be obtained. At present it appears impossible to obtain $F(J\xi_{ij}^3)$ in closed form, which precludes evaluation of these coefficients for a distribution of molecular weights. To investigate the effect of heterogeneity on the coefficients of Eqs. (22) and (60), calculations were carried out for hypothetical ternary mixtures containing polymers of two molecular weights. The values assumed were: $\psi_1=\frac{1}{2}$, $\bar{v}=1$, $\mathbf{N}V=V_1=100$, and $M_i=50{,}000$, so that $2(J/\mathbf{N})=0.01$. Values of $J\xi_{ij}^3$ were calculated from Eqs. (9) and (15), and the corresponding $F(J\xi_{ij}^3)$ taken from Fig. 1. For a ternary mixture containing polymers of molecular weight M_i and M_j, the coefficients A_2 and A_2' were obtained from Eqs. (25), (26), and (61), the required summations being evaluated numerically. The results are plotted in Fig. 2 as functions of the weight fraction w_j of the higher molecular weight component when the ratio M_j/M_i assumes the values 5, 10, 15, and 20. The second coefficient in the osmotic pressure expression (22) is RTA_2, and in the light scattering expression (60) it is $2A_2'$.

It can be seen that A_2 and A_2' are neither constant nor linear in w_j. The second coefficient in both expressions exhibits a maximum, that in the osmotic pressure

[25] H. C. Brinkmann and J. J. Hermans, J. Chem. Phys. **17**, 574 (1949).
[26] J. G. Kirkwood and R. J. Goldberg, J. Chem. Phys. **18**, 54 (1950).
[27] W. H. Stockmayer, J. Chem. Phys. **18**, 58 (1950).

relation occurring at $w_j=0.04$ for the mixtures investigated, whereas the light scattering second coefficient appears to be most sensitive to traces of high molecular weight material. It has frequently been pointed out that the light scattering second coefficient is twice that occurring in the osmotic pressure relation; however, this will only be the case in general for well fractionated polymers. The ratio of $2A_2'$ to A_2 varies with heterogeneity. For normal degrees of heterogeneity this ratio will not differ much from two, but for an extreme heterogeneity the ratio may be appreciably greater or less than this value.

THE JOURNAL OF CHEMICAL PHYSICS VOLUME 18, NUMBER 8 AUGUST, 1950

Migration of Lithium and Several Multicharged Ions through Quartz Plates in an Electric Field. II

GEORGE GIBSON* AND RICHARD C. VOGEL**
Department of Chemistry, Illinois Institute of Technology, Chicago, Illinois
(Received May 4, 1950)

The kinetics of the migration of lithium ions through crystalline quartz plates has been studied. The migration is induced by an electric field and probably takes place through tunnels inherent in the crystal structure and parallel to the principal axis of the quartz. It was shown that the rate-determining step is not the migration with in the quartz plate, but is some step associated with the passage of the lithium ions into or out of the quartz plate. A previous investigation showed that the migration within the quartz plate is the rate-determining step for sodium ions.

It was demonstrated that neither magnesium, zinc, cadmium, nor bismuth ions will migrate through quartz plates under our experimental conditions. Copper ions migrated through the quartz plates but caused the plate to crack in each experiment.

I. INTRODUCTION

IT has been demonstrated[1] that lithium and sodium ions in an electric field will migrate through crystalline quartz plates cut perpendicular to the Z or principal crystallographic axis. Gibbs,[2] in investigations of alpha-quartz, has indicated the existence of tunnels about an Angstrom in radius which are parallel to the principal axis. It has been suggested[3] that this tunnel-like structure is responsible for the anisotropic ease of sodium and lithium ion migration in quartz plates.

In the first paper of this present series[4] the authors have presented a kinetic study of the migration of sodium ions through quartz plates in an electric field. Liquid sodium amalgam anodes against one face of the plate served as the ion source, while pure mercury against the opposite face of the quartz plate was used as the cathode. A comparison of the behavior of lithium with that of sodium would be of interest. One might expect the smaller lithium ion to migrate more readily. Harris and Waring[3] studied the migration of lithium ions using fused lithium nitrate as the anolyte and fused ammonium bisulfate or mercury as the catholyte. Their system and apparatus were sufficiently different from that which we used in the study of sodium that it seemed desirable to carry out the present investigation using lithium amalgams instead of fused lithium nitrate in the anode compartment.

Apparently, no studies have been made on the migration of the smaller multicharged ions. If such migration were to occur, some interesting correlations of ion charge and ionic radius might be observed. The results of an attempt to study the migration of magnesium, zinc, copper, cadmium, and bismuth ions through quartz plates are given below.

II. APPARATUS AND EXPERIMENTAL PROCEDURE

The apparatus and experimental procedure were modified from those used in the sodium studies[4] in two ways found necessary during observations made during orientation runs with lithium. The Pyrex glass of the anode compartment of the cell used in the orientation runs with the lithium amalgam became dark red-brown throughout. In order to obviate this questionable behavior a quartz cell was substituted for the Pyrex one. The area of the plate exposed in the quartz cell was 3.048 cm^2.

In order to prevent the formation of lithium nitride, an inert atmosphere of helium was used in preference to the atmosphere of nitrogen used in the sodium studies.

The lithium amalgams were prepared by adding small pieces of metal to purified hot mercury (160°C) in sufficient quantity to form a solid amalgam on cooling. The solid amalgam was then diluted with additional mercury to the desired concentration. The lithium

* Present address: On leave of absence to the Chemistry Division, Argonne National Laboratory, Chicago 80, Illinois.
** Present address: Chemical Engineering Division, Argonne National Laboratory, Chicago 80, Illinois.
[1] E. Warburg and F. Tegetmeier, Ann. Physik **35**, 455 (1888).
[2] R. E. Gibbs, Proc. Roy. Soc. (London) **A110**, 443 (1926).
[3] P. M. Harris and C. E. Waring, J. Phys. Chem. **41**, 1077 (1937).
[4] R. C. Vogel and G. Gibson, J. Chem. Phys. **18**, 490 (1950).

metal (Metalloy Corp., Minneapolis, Minnesota) contained 0.6 percent sodium, 0.02 percent calcium, 0.01 percent potassium, and 0.001 percent iron. The lithium amalgams were analyzed in the same manner as the sodium amalgams.

The amalgams of the other metals were prepared by adding weighed quantities of the pure metals directly to a weighed quantity of mercury. These amalgams were used without further analysis. All amalgams were prepared and stored in a helium atmosphere.

In the lithium runs, currents were measured for applied potentials of 20, 16, 12, 8, and 4 volts at four different temperatures between 200 and 170°C. It was necessary to lower the temperatures and the voltages from those used in the sodium studies. Under the sodium conditions (100 to 20 volts; 240 to 210°C) lithium gave such high currents that the lithium amalgam (whose concentration had a practical upper limit of about 0.014 mole fraction, the room temperature solubility) would be depleted before the end of a run. In addition to this difficulty, the high currents apparently caused cracks to form in the quartz plates on several occasions.

The quartz plates were 2.54 cm² and varied in thickness from 0.0492 to 0.1257 cm. They were the same plates that were used in the sodium studies. It was found in the sodium work that satisfactory reproducibility could not be obtained unless each plate was etched with a concentrated sodium amalgam. The etched surface was kept against the lithium amalgam. Before lithium runs were made, however, the crystals were pretreated by running a lithium ion current of about 1000 microamperes through the crystal for about sixteen hours.

III. DATA

Since the current passing through the quartz plate was used to determine the amount of lithium migrating, it was necessary to show that all current passing through the cell was carried by lithium ions. To establish this a quartz plate, 0.0925 cm thick, was used with a concentrated two phase lithium amalgam in an extended run at 180°C with an applied voltage of 93 volts. The current was plotted against time and graphically integrated. The mercury in the cathode compartment was analyzed for lithium. Graphical integration showed that 5.95×10^{-4} mole of lithium was transferred while analysis of the cathode contents indicated that 5.81×10^{-4} mole of lithium had migrated. Thus, apparently all but 2.3 percent of the current was carried by migration of the lithium ions. This difference, also noted in the case of sodium, probably exists because of mechanical difficulties in quantitatively transferring the catholyte from the cell.

To further verify the anisotropic behavior of quartz, one run was made with a 0.0787-cm thick plate, cut with major faces parallel to the principal axis. At 140 volts and 200°C, the equilibrium current was less than 0.01 microampere cm⁻².

TABLE I. Kinetic data for migration of lithium ions through quartz plates. (Mole fraction of lithium 0.0140.)

Run no.	Plate thickness (cm)	Potential gradient (volts cm⁻¹)	Activation energy (kcal. mole⁻¹) "a"	"b"	Average percent deviation of calculated i from experimental i
1	0.0492	407	4651.62	21.3 10.5276	0.9
		325	4616.62	21.1 10.2963	0.9
		244	4598.11	21.0 10.0536	0.7
		163	4658.49	21.3 9.9050	0.6
		81.3	5075.66	23.2 10.3750	0.9
2[a]	0.0498	402	3883.46	17.8 9.1200	0.4
		321	3873.12	17.7 8.9231	0.5
		241	3859.93	17.7 8.6713	0.7
		161	3837.18	17.6 8.3118	0.7
		80.3	3922.73	17.9 7.9881	1.0
3	0.0744	269	4692.10	21.5 10.6702	1.2
		215	4780.58	21.9 10.7497	1.7
		161	4836.00	22.1 10.7244	1.4
		108	4874.58	22.3 10.6075	1.4
		53.8	4925.04	22.5 10.3926	1.3
4	0.0744	269	4695.19	21.5 10.6121	0.5
		215	4723.02	21.6 10.5394	0.3
		161	4771.28	21.8 10.4781	0.1
		108	4837.72	22.1 10.4002	0.2
		53.8	4876.33	22.3 10.1373	0.5
5[b]	0.0744	269	4561.98	20.9 10.0955	0.5
		215	4566.19	20.9 9.9659	0.6
		161	4601.72	21.0 9.8719	0.7
		108	4689.51	21.4 9.8321	0.3
		53.8	4886.04	22.3 9.8897	0.1
6	0.0744	269	4708.10	21.5 10.7417	1.0
		215	4704.98	21.5 10.5916	0.9
		161	4734.50	21.7 10.4774	0.9
		108	4786.60	21.9 10.3508	0.7
		53.8	4877.13	22.3 10.1666	0.7
7	0.0925	216	3882.07	17.8 9.0943	1.3
		173	3861.76	17.7 8.8864	1.3
		130	3878.10	17.7 8.7081	1.3
		86.5	3994.60	18.3 8.6700	1.2
		43.2	4346.47	19.9 8.9515	0.5
8	0.1257	159	3771.27	17.2 8.7717	0.7
		127	3786.02	17.3 8.6510	0.3
		95.5	3871.37	17.7 8.6396	0.5
		63.6	4033.31	18.4 8.7235	0.6
		31.8	4485.77	20.5 9.2864	1.1
9	0.1257	159	3846.59	17.6 8.9190	0.5
		127	3869.06	17.7 8.8183	0.9
		95.5	3982.99	18.2 8.8757	0.6
		63.6	4126.02	18.9 8.9303	0.5
		31.8	4554.85	20.8 9.4513	1.3

[a] Crystal not etched with sodium amalgam before use.
[b] Lithium amalgam in both anode and cathode compartments of cell.

The kinetic data for the lithium ion migration were treated in much the same manner as in the sodium work. In each run five current readings were made at each of five potential gradients for a particular temperature. This procedure was repeated for four temperatures. The temperature dependence of the data for a given potential gradient and plate thickness is well represented by the Arrhenius equation,

$$\log_{10} i = -(a/T)+b, \qquad (1)$$

TABLE II. Current in microamperes per cm² at 190°C and a potential of 20 volts. (Mole fraction of lithium 0.0140.)

Run no.	Crystal thickness (cm)	Potential gradient (volts cm^{-1})	Current (microamperes cm^{-2})	Activation energy kcal. $mole^{-1}$ at 20 volts
2[a]	0.0498	402	5.42	17.8
7	0.0925	216	5.15	17.8
8	0.1257	159	4.25	17.2
9	0.1257	159	4.10	17.6
6	0.0744	269	3.76	21.5
3	0.0744	269	3.45	21.5
1	0.0492	407	3.04	21.3
4	0.0744	269	2.97	21.5
5[b]	0.0744	269	1.76	20.9

[a] Crystal not etched with sodium amalgam before use.
[b] Lithium amalgam in both anode and cathode compartments of cell.

where i is the current in microamperes per square centimeter of exposed plate face, T is the absolute temperature and "a" and "b" are constants. By the method of least squares the best values of the constants were found for a particular potential gradient and quartz plate thickness. The data are presented in Table I. The mole fraction of lithium in the anode compartment was 0.0140. Column 3 gives the potential gradient calculated on the basis of plate thickness in volts cm^{-1}, column 5 gives the activation energy for the process and column 7 gives the average percent deviation of the experimentally determined currents at the four different temperatures from the corresponding currents calculated using Eq. (1). The data for a particular potential gradient generally fit Eq. (1) to about one percent.

The currents flowing through the quartz plates at 190°C with an applied potential of 20 volts are given in Table II. These currents are calculated from the data given in Table I. In the right column of Table II the activation energies at 20 volts are given.

The amalgams of the other metals used had the following mole fraction concentrations: magnesium 0.019, zinc 0.045, cadmium 0.018, bismuth 0.0096; the copper amalgam used was saturated at the temperature of the run. These latter runs were all exploratory in nature and were made using a 0.049 cm crystal, a temperature of about 260°C and an applied potential of 140 volts. With the exception of copper all the species studied showed no indication of ion migration. The currents observed were less than 0.01 microampere cm^{-2}.

When copper was studied, very interesting results were obtained. When the cell was brought up to temperature and the 140 volts applied, no current was observed for about an hour. Then the current rose erratically. Steady current readings were very difficult to obtain. When the cell was disassembled copper-colored stains and minute cracks were found which seemed to be beneath the surface of the crystal. The stains did not disappear on prolonged boiling of the plate with concentrated nitric acid or *aqua regia*. The experiment was repeated using a 0.0762 cm plate. With this crystal the current rose smoothly to 440 microamperes over a period of twenty minutes and then became very erratic. The same type of copper-colored stains were found in the crystal. It is suspected that copper will diffuse through quartz plates but that it cracks the plates in the process.

IV. DISCUSSION OF DATA AND CONCLUSIONS

A very striking difference in the behavior of sodium and lithium ions diffusing through quartz plates is that the rate for lithium is considerably greater. For example, with a potential of twenty volts across a plate 0.1257 cm thick at 200°C, the current due to lithium ions would be about thirty times greater than that in a similar experiment using sodium. This can be reasonably explained on the basis of the smaller ion size of lithium. The activation energies observed for lithium are also lower than those observed for sodium.

The data in Table II show that the current does not seem to depend upon the potential gradient. The currents vary from 1.76 to 5.42 microamperes cm^{-2} with no correspondence between current and potential gradient. This behavior is entirely different from that observed with sodium. In the case of sodium, the curves of current *versus* potential gradient at constant temperature and amalgam concentration for all different plate thicknesses almost superimpose upon one another.[4] The lithium data indicate that the diffusion within the quartz plate is not the rate-determining step. Since the diffusion rate is independent of the plate thickness, it appears reasonable that the rate-determining step is associated with the transfer of ions either into or out of the plate. This also would explain the fact that the data for lithium are not as reproducible from run to run as that for sodium. This irreproducibility can be seen in Table II, which gives data for four runs using the 0.0744 cm plate. The currents under presumably similar conditions vary by a factor of about two. When sodium was used in two similar runs, the maximum deviation was less than ten percent. The difficulty of reproducibility would be expected if the diffusion through a film or surface layer, either on the crystal face or within the amalgam, were the controlling factor since surface conditions are often difficult to reproduce from experiment to experiment.

The data in Table II are arranged in the order of decreasing currents rather than potential gradients to illustrate two important points. At high currents the activation energy is low as might be expected. The values of the activation energies fall into two groups. The activation energies from 17.2 to 17.8 kcal. $mole^{-1}$ are for three plates, the 0.0498, 0.0925 and the 0.1257 cm and the activation energies from 20.9 to 21.5 kcal. $mole^{-1}$ are for two plates, 0.0744 and 0.0492 cm thick. In no case does one plate give both a high and a low activation energy. This suggests that the slow step of the diffusion process is determined by the surface condition of the plate itself. It is not believed that this surface condition resulted from using the plates first

in the sodium studies. This is implied by Run 2 which was made with a plate (0.0498 cm) which had not been used (or etched) with sodium amalgam. It can be calculated from Table II that the resistance of this plate is only five percent less than that of the much thicker 0.0925 cm plate which was used in a number of sodium runs.

It is worth while to compare our data for lithium with that obtained by Harris and Waring.[3] The activation energies which they obtained using fused lithium nitrate in the anode compartment and ammonium bisulfate in the cathode compartment are around 17 kcal. mole^{-1}. These values are in reasonable agreement with our lower set of activation energies. Their currents were much higher since they were not concerned with either lithium depletion or plate damage due to the high current. Thus, they were able to use temperatures from 250 to 300°C and applied potentials up to 125 volts. When their data were examined by plotting current against potential gradient for five runs using five different plates, a closely grouped family of curves was obtained similar to our results obtained for sodium.

We conclude that the surface effect which appears to be the slow step in the lithium diffusion process in our experiments may be a property of amalgams not possessed by fused salts. There is a possibility that the surface effect would become negligible at temperatures higher than those we used although no such trend was observed in our temperature range.

The lack of diffusion shown by magnesium, zinc, cadmium, and bismuth suggests that these ions of higher charge interact with the oxygen atoms of the quartz and thus do not diffuse under the potentials which we applied. The cuprous ion (radius 0.96A) is about the same size as that of the sodium ion (radius 0.95A) so that the observed diffusion is reasonable; however, the plate damage by these ions is difficult to explain.

THE JOURNAL OF CHEMICAL PHYSICS VOLUME 18, NUMBER 8 AUGUST, 1950

The Reactions of Methyl Radicals. I. The Photolysis of Acetone

A. F. TROTMAN-DICKENSON* AND E. W. R. STEACIE
Division of Chemistry, National Research Council, Ottawa, Canada

(Received May 2, 1949)

The photolysis of acetone has been investigated between 100°C and 300°C. The rates of production of carbon monoxide, methane and ethane have been measured over a range of acetone pressures from 3.9 to 100 mm and with a thirty-fold variation of light intensity. The methane and ethane formed can be quantitatively accounted for by the equations

$$CH_3+CH_3=C_2H_6, \quad CH_3+CH_3COCH_3=CH_4+CH_2COCH_3.$$

It is found that $E_3-\frac{1}{2}E_2=9.7$ kcal., where E_2 and E_3 are the activation energies of the above reactions. The photolysis of deuterated acetone has also been investigated, here $E_3'-\frac{1}{2}E_2'=10.3$ kcal. The collision theory "steric" or "P" factor for the second reaction is less than 10^{-3} in each case.

INTRODUCTION

THIS paper is the first of a series which we hope to present on the quantitative study of the reactions of methyl radicals. Here is described the preliminary work which had to be carried out on the photolysis of acetone alone before it could be used as a source of methyl radicals for reaction with other hydrogen-containing compounds at high temperatures.

Acetone was chosen as the source of methyl radicals because its photolysis and the mechanism of the subsequent reactions are better understood than those of any of the alternative substances such as mercury dimethyl, acetaldehyde, or azomethane. This is largely owing to the very careful work of Noyes and his school, whose recent reviews[1,2] of the subject obviate the need for detailed discussion here.

The photolysis of acetone above 100°C may be fully described by the scheme,

$$CH_3COCH_3+h\nu=2CH_3+CO \quad (1)$$

$$CH_3+CH_3=C_2H_6, \quad (2)$$

$$CH_3+CH_3COCH_3=CH_4+CH_2COCH_3, \quad (3)$$

$$CH_3+CH_2COCH_3=C_2H_5COCH_3, \quad (4)$$

$$2CH_2COCH_3=(CH_2COCH_3)_2, \quad (5)$$

which has been proposed by Noyes. Ferris and Haynes[3] have shown that ketene is a product at high temperatures and hence step (6) must be included above 250°C. This is also evident from the present

$$CH_3COCH_2=CH_3+CH_2CO \quad (6)$$

work. For the present purpose the important feature

* National Research Council (Canada) Postdoctoral Fellow.

[1] W. A. Noyes, Jr. and L. M. Dorfman, J. Chem. Phys. **16**, 788 (1948).

[2] W. Davis, Jr., Chem. Rev. **40**, 201 (1947).

[3] R. C. Ferris and W. S. Haynes, J. Am. Chem. Soc. **72**, 893 (1950).

TABLE I. The photolysis of acetone.

Run	Temp. (°K)	Acetone pressure (mm)	Time (sec.)	Products (micromoles) CO	CH_4	C_2H_6	$\frac{\frac{1}{2}CH_4+C_2H_6}{CO}$	$k_3/k_2^{\frac{1}{2}}$ $\times 10^{13}$	$13+\log\frac{k_3}{k_2^{\frac{1}{2}}}$	$13+\log\frac{k_3}{k_2^{\frac{1}{2}}}$ from Eq. (2)	Diff.
					Mean acetone pressure 24 mm						
15	404	23.0	7500	11.38	1.52	11.70	1.09	5.24	0.72	0.70	+0.02
10	438	22.4	11150	10.27	3.48	7.92	0.94	13.2	1.12	1.11	+0.01
11	470	24.3	12000	11.95	7.15	6.53	0.85	28.5	1.45	1.44	+0.01
16	483	24.5	8100	11.70	7.86	6.08	0.85	40.6	1.61	1.56	+0.05
14	526	25.0	7620	12.01	11.00	3.00	0.71	88.9	1.95	1.92	+0.03
12	572	24.1	11400	10.98	12.60	0.72	0.64	191	2.28	2.25	+0.03
					Mean acetone pressure 45 mm						
22	411	43.9	4920	14.20	2.86	11.60	0.81	6.47	0.81	0.79	+0.02
25	444	45.6	4800	14.78	5.45	9.21	0.81	14.6	1.17	1.17	—
21	473	45.3	5400	15.59	9.48	7.06	0.76	29.2	1.47	1.47	—
37	491	43.3	4500	15.32	10.60	5.99	0.74	42.2	1.63	1.64	−0.01
24	504	42.1	4260	10.81	9.34	2.72	0.69	60.2	1.78	1.76	+0.02
26	543	45.9	5100	13.17	15.20	1.70	0.71	111	2.05	2.05	—
23	573	46.2	4500	12.81	16.80	0.98	0.73	183	2.26	2.25	+0.01
					Mean acetone pressure 100 mm						
132	394	92.2	4750	17.50	3.57	13.20	0.86	3.52	0.55	0.57	−0.02
33	404	95.5	1920	12.55	2.77	10.10	0.92	4.88	0.69	0.70	−0.01
27	423	93.6	2760	17.68	5.67	12.80	0.89	7.89	0.90	0.94	−0.04
133	440	103.4	5390	22.20	12.62	10.20	0.74	13.2	1.10	1.12	−0.02
32	449	96.6	2340	15.10	8.22	8.14	0.81	16.0	1.20	1.23	−0.03
29	471	96.5	2400	15.67	11.20	6.30	0.76	25.8	1.41	1.45	−0.04
31	507	96.6	1860	11.70	12.20	2.46	0.73	54.6	1.74	1.77	−0.03
134	536	122.4	5520	23.40	32.70	1.46	0.77	92.0	1.96	1.99	−0.03
30	544	96.8	2400	15.13	19.70	1.47	0.75	108	2.03	2.06	−0.03
28	573	101.0	2220	14.73	20.70	0.85	0.76	158	2.20	2.25	−0.05

of this mechanism is that ethane and methane are produced only by steps (2) and (3).

Acetone has many intrinsic advantages as a source of methyl radicals. Between 100° and 250°C it has a quantum yield of unity so that the formation of carbon monoxide provides a convenient internal actinometer and check on the number of methyl radicals released. The acetonyl radical is considerably stabilized by resonance, when it does decompose it forms ketene and a methyl radical and does not provide an alternative source of methane or ethane. Acetone is convenient experimentally because it is thermally stable, chemically inert, has a vapor pressure of 15 to 20 cm at room temperature and does not readily attack stopcock grease. Acetone absorbs radiation over a very wide range of wave-lengths but has a moderate extinction coefficient so that only about 40 percent of the incident radiation of 2537A is absorbed under the conditions holding in these experiments when the acetone pressure is 5 cm. Therefore corrections for the effective reaction volume being smaller than the size of the cell are much less important than if mercury alkyls were used. Furthermore fully deuterated acetone is readily prepared.

EXPERIMENTAL

Apparatus

The light source was a Hanovia S-500 medium pressure arc. After a preliminary period for warming up, the current in the primary circuit of the lamp transformer was manually adjusted to a constant value. The nearly parallel beam of light produced by a system of three quartz lenses and two stops passed through a 5-cm filter of chlorine at one-third of an atmosphere pressure and within about 3 mm of the longitudinal walls of the reaction vessel. The volume of the light beam within the cell was approximately 140 cc. The light intensity was varied by the progressive decline in the output of the lamp, by the use of a drilled plate and by a neutral density filter of chromel deposited on quartz.

The reaction cell was placed in an aluminum block furnace with one-inch walls, whose over-all temperature was manually controlled to ±0.5°C during each run. The variation of the temperature along the length of the reaction cell did not exceed 1°C.

The glass apparatus was of the conventional type used for studying gas reactions. It consisted of a double pumping system, eight storage vessels for acetone and other reagents and two analysis systems of the modified Ward type[4] one with two traps the temperature of which could be controlled and the other with four such traps, to deal with mixtures of different complexities. A copper oxide tube was used to analyze for the carbon monoxide in the "non-condensable" fraction of the products and a combustion tube to find the hydrogen and carbon numbers of the methane and ethane fractions. With such a system 0.5 percent each of carbon

[4] Savelli, Seyfried, and Filbert, Ind. Eng. Chem. Anal. Ed. 13, 868 (1941).

TABLE II. The effect of the variation of light intensity in the photolysis of acetone.

All runs done at 422°K, average values from Eq. (5)

Run	Light absorbed (quanta/sec.)	Acetone pressure (mm)	Time (sec.)	Products (micromoles) CO	CH_4	C_2H_6	$k_3/k_2^{\frac{1}{2}}$ $\times 10^{13}$
—	38.6×10^{14}	Average of runs 27, 28, 29, 30, 31, 32, 33					7.8
—	19.8×10^{14}	Average of runs 132, 133 and 134					7.8
159	7.9×10^{14}	96.3	10280	13.42	8.56	6.24	8.6
158	3.8×10^{14}	96.3	15420	9.85	8.05	3.68	8.6
160	1.2×10^{14}	96.3	29250	5.79	6.56	1.66	7.6

The amount of light absorbed has been calculated on the assumption that the quantum yield of carbon monoxide formation is unity.

TABLE III. The effect of the variation of pressure in the photolysis of acetone.

All runs done at 420°K, average values obtained from Eqs. (3), (4), and (5)

Run	Acetone pressure (mm)	Time (sec.)	Products (micromoles) CO	CH_4	C_2H_6	$k_3/k_2^{\frac{1}{2}}$ $\times 10^{13}$
—	100	Average of runs 27, 28, 29, 30, 31, 32, 33, 132, 133, 134				7.4
—	45	Average of runs 21, 22, 23, 24, 25, 26 and 37				8.1
—	24	Average of runs 10, 11, 12, 14, 15, 16				8.5
162	11.3	23000	11.13	2.16	9.40	10.0
161	5.7	35800	9.47	1.13	8.00	10.3
163	3.9	47000	6.76	0.94	5.78	11.2

TABLE IV. The photolysis of deuterated acetone.

Run	Temperature (°K)	Acetone pressure (mm)	Time (sec.)	Products (micromoles) CO	CD_4	C_2D_6	$\frac{CD_4}{CO}+\frac{C_2D_6}{CO}$	$k_3'/k_2'^{\frac{1}{2}}$ $\times 10^{13}$
176	411	93.0	7650	14.35	2.10	12.35	0.93	1.75
173	449	100.9	6130	13.41	4.68	9.45	0.88	5.01
175	483	107.2	5860	12.15	7.95	5.85	0.81	11.2
177	519	114.0	7970	16.70	16.60	3.68	0.72	25.4
174	565	126.7	6230	15.00	19.10	1.32	0.72	53.5

monoxide, methane, and ethane may be determined in a 50-cc sample of acetone at N.T.P. An accuracy of ±3 percent is readily obtained for each constituent. The total volume of the reaction system with connecting tube and manometer was 320 cc. The system was isolated by a mercury cut-off. The volume of the quartz reaction vessel, which was 10 cm long, was 195 cc.

Materials

Three different samples of Mallinckrodt Analytical Reagent acetone were used, two of which were simply distilled; the third was first refluxed over potassium permanganate. No difference could be detected in their behavior. The deuterated acetone which contained on the average about one light hydrogen atom in three molecules of acetone was made for us by Dr. L. C. Leitch in this laboratory. The acetone was stored over a mercury cut-off.

Results

In Tables I, II, and III are given the results of runs carried out to determine the activation energy of the reaction of methyl radicals with acetone, the effect of the variation of light intensity and the effect of the variation of acetone pressure. No trace of hydrogen or ethylene was found in the products. In Table IV are given the results of runs done to determine the activation energy of the reaction of heavy methyl radicals with acetone.

DISCUSSION

If k_2 and k_3 are the rate constants of reactions (2) and (3) then

$$R_{CH_4}=k_3[CH_3][Ac]$$

and

$$R_{C_2H_6}=k_2[CH_3]^2,$$

where $[CH_3]$ and $[Ac]$ are the concentrations of methyl and acetone and R_{CH_4} and $R_{C_2H_6}$ are the rates of formation of methane and ethane. Hence

$$k_3/k_2^{\frac{1}{2}}=R_{CH_4}/R_{C_2H_6}^{\frac{1}{2}}[Ac]$$
$$=P_3Z_3\exp(-(E_3-\tfrac{1}{2}E_2)/RT)/P_2^{\frac{1}{2}}Z_2^{\frac{1}{2}}, \quad (7)$$

where E_2 and E_3 are the activation energies of reactions (2) and (3), Z_2 and Z_3 the number of collisions occurring between methyl and methyl radical and methyl and acetone molecule at unit concentration in unit time, P_2 and P_3 are the steric factors for the two reactions. In Fig. 1 the logarithm of $k_3/k_2^{\frac{1}{2}}$ is plotted against the reciprocal of the absolute temperature; all rate constants are expressed in molecules, cc, and sec. The best line through all the points has been found by the method of least squares to be

$$13+\log k_3/k_2^{\frac{1}{2}}=5.96-2.124\cdot10^3/T. \quad (8)$$

However, the deviations of the points from this line, given in Table I, show that the results are better expressed by three separate lines corresponding to the three different mean pressures of acetone. These lines are

$$13+\log k_3/k_2^{\frac{1}{2}}=5.99-2.124\cdot10^3/T \text{ at 24 mm} \quad (9)$$

$$13+\log k_3/k_2^{\frac{1}{2}}=5.97-2.124\cdot10^3/T \text{ at 45 mm} \quad (10)$$

$$13+\log k_3/k_2^{\frac{1}{2}}=5.93-2.124\cdot10^3/T \text{ at 100 mm.} \quad (11)$$

The slopes of the lines give a value of 9.7 kcal. for $E_3-\frac{1}{2}E_2$, as it is probable that $E_2=0$, 9.7 kcal. may be taken as the activation energy for the abstraction of a hydrogen atom from acetone by a methyl radical.

It has been suggested that the combination of methyl radicals takes place on the wall of the reaction vessel and/or is subject to a third body restriction. To determine whether the combination of methyl radicals behaved as a second-order reaction under the conditions of our experiments we investigated the photolysis over a range of light intensities and over a range of pressures. Within the probable limits of experimental error $k_3/k_2^{\frac{1}{2}}$ is shown in Table II to be constant over a thirty-two-fold variation of light intensity. The results in Table

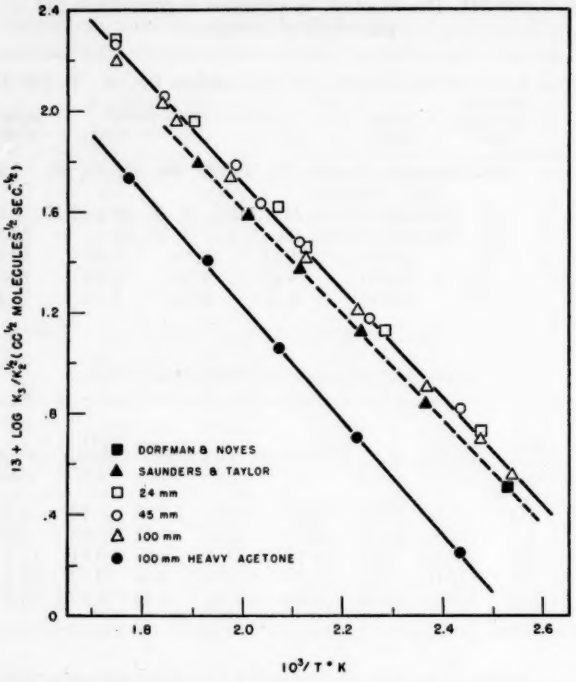

FIG. 1. Arrhenius plot for the reaction of methyl radicals with acetone.

III show that $k_3/k_2^{\frac{1}{2}}$ drifts very slightly with pressure from 3.7 to 100 mm, the change is however not of the type which would be expected if the combination of radicals took place only at the wall or which would result from a third body restriction. Probably, in so far as the change is real, it is due to a slight alteration in the effective reaction volume as the light absorption increases with increasing pressure. Dorfman and Noyes[5] also found that $k_3/k_2^{\frac{1}{2}}$ was independent of the light intensity at 26° and 122°C. Thus all the available facts are explained by the supposition that the only source of ethane is the combination of methyl radicals which obeys a kinetic equation for a second-order reaction.

In Fig. 1 are plotted also the value of $k_3/k_2^{\frac{1}{2}}$ at 122°C given by Dorfman and Noyes[5] and the values obtained by recalculating the results of Saunders and Taylor[6] on the basis of the mechanism used here. The agreement between the three sets of results is very satisfactory. The work of Allen[7] and of Taylor and Rosenblum[8] is less reliable because Allen's results were not very full and Taylor and Rosenblum carried the photolysis to a very high percentage conversion.

The value of 6.1 kcal. for $E_3-\frac{1}{2}E_2$ found by Dorfman and Noyes[5] from results at 26° and 122°C differs far too much to be ascribed to experimental error, but until more facts are known it is not profitable to speculate on the cause of this phenomenon. As we were concerned with the photolysis of acetone above 100°C where there is no sign of curvature in the Arrhenius plot and our apparatus was not suitable for studying the photolysis at low temperatures we did not pursue the matter further.*

Since $E_3-\frac{1}{2}E_2$ has been determined and Z_3 and Z_2 may be calculated, it is possible from Eq. (1) to obtain a value of $P_3/P_2^{\frac{1}{2}}$. Values of 3.5 and 5.5A have been adopted as the diameters of the methyl radical and the acetone molecule, respectively. Then if allowance is made for the temperature coefficients of the collision frequencies $P_3/P_2^{\frac{1}{2}}=1\times10^{-3}$. We have shown elsewhere [9] that this is of the usual order of magnitude of $P/P_2^{\frac{1}{2}}$ for the abstraction of a hydrogen atom from a paraffin hydrocarbon by a methyl radical. Thus $P_3<10^{-3}$; this conclusion is interesting in view of the contrary suggestion on theoretical grounds by Evans and Szwarc[10] that the steric factors of such reactions lie in the range 1 to 10^{-2}. Furthermore recent work in this laboratory by Dr. D. M. Miller has shown that the collision yield for reaction (2) is probably not greater than 10^{-4}. If $E_2=0$ then P_3 is probably less than 10^{-5}.

The rate of the reaction of deuterated methyl radicals with deuterated acetone is slower than that for the normal species, as may be seen from Fig. 1. The Arrhenius plot is given by the equation

$$13+\log k_3'/k_2'^{\frac{1}{2}}=5.73-2.257(10^3/T).$$

The difference in the rates is due to the difference in the activation energies, that for the heavy methyl radical being 10.3 kcal. Within the limits of experimental error the steric factor is unchanged.

[5] L. M. Dorfman and W. A. Noyes, Jr., J. Chem. Phys. **16**, 557 (1948).
[6] K. W. Saunders and H. A. Taylor, J. Chem. Phys. **9**, 616 (1941).
[7] A. O. Allen, J. Am. Chem. Soc. **63**, 708 (1941).
[8] H. S. Taylor and C. Rosenblum, J. Chem. Phys. **6**, 119 (1938).
* Professor Noyes tells us that further work in his laboratory has confirmed both his and our values for the activation energy in the different temperature ranges and that he is seeking the cause of this anomaly.
[9] A. F. Trotman-Dickenson and E. W. R. Steacie, J. Am. Chem. Soc. **72**, 2310 (1950).
[10] M. G. Evans and M. Szwarc, Trans. Faraday Soc. **46**, 940 (1949).

The Infra-Red Spectrum of Borine Carbonyl and a Normal Coordinate Analysis of Axial $WXYZ_3$ Molecules*

R. D. COWAN**
Physics Department, University of Chicago, Chicago, Illinois
(Received May 9, 1950)

The infra-red spectrum of borine carbonyl has been investigated in the region 2 to 25μ. Two perpendicular-type bands have been partially resolved, and indicate that the molecule is a symmetric top with symmetry C_{3v}. A normal coordinate analysis of axial $WXYZ_3$ molecules has been carried out and applied to H_3BCO, the following values having been obtained for the force constants: $k_{CO}=17.3$, $k_{BC}=2.97$, $k_{BH}=3.21$, $k_{BCO}=0.142$, $k_{HBC}=0.333$, $k_{HBH}=0.363$, all in units of 10^5 dynes/cm.

INTRODUCTION

THE structure of the borine carbonyl molecule has, until recently, remained in some doubt. The two most likely alternatives are H_3BCO, in which all three hydrogen atoms are bonded to the boron atom, and H_2BCHO, with two hydrogen atoms bonded to the boron and the third hydrogen and one oxygen bonded to the carbon. The fact that borine carbonyl is unstable at room temperature and dissociates rather rapidly into diborane (B_2H_6) and carbon monoxide favors the former structure,[1] as does an electron-diffraction investigation of the molecule.[2] However, the electron-diffraction results are not conclusive, and the dissociation of borine carbonyl could be the result of the transitory existence of H_3BCO or an equilibrium mixture of H_3BCO and H_2BCHO. A decision between these two possible structures is easily made from the infra-red spectrum of the compound, since the characteristic absorption of a C—H bond lies at about 3000 cm^{-1} whereas that of a B—H bond lies in the region 2400 to 2600 cm^{-1}. Since the completion of the experimental work on which this paper is based but before publication of preliminary results,[3] Gordy, Ring, and Burg[4] reported proof of the structure H_3BCO with symmetry C_{3v} from observations of the microwave spectrum.

EXPERIMENTAL

The borine carbonyl was prepared by the method described by Burg and Schlesinger[1] from diborane and commercial carbon monoxide. It was purified by discarding those vapors which did not pass through a trap at −125°C and those which did pass through one at −150°C. The remaining vapor was frozen into a 10-cm Pyrex absorption cell with KBr windows. (It was sufficient in quantity to give a pressure in the cell of about 120 mm at room temperature.) To retard the decomposition of the borine carbonyl, carbon monoxide was added to a partial pressure of 200 mm; in addition, whenever spectra were not being run, a side-tube connected to the cell was kept in a liquid nitrogen bath to freeze out the H_3BCO.

Spectra of the vapor were run with a Perkin-Elmer model 12B recording spectrometer, using LiF, NaCl, and KBr prisms. Spectra were obtained at pressures below 120 mm by connecting the cell to a vacuum line and allowing a portion of its contents to expand into the line. (The vapor in the line was then pumped through a trap at liquid nitrogen temperature, thus separating the H_3BCO from the CO, and the borine carbonyl was later frozen back into the cell and new carbon monoxide added ready for the next run.)

Over a period of eleven days, during which the borine carbonyl sample was kept in an excess of carbon monoxide, no appreciable decomposition of the former was noted. This is in contrast to later observations made after removing the CO: a measurable decrease in intensity of the borine carbonyl bands and an appreciable increase in intensity of the diborane bands was observed within fifteen minutes, and half of the carbonyl dissociated in two or three hours. (According to Burg and Schlesinger,[1] the half life of H_3BCO is about $3\frac{1}{2}$ hours when starting with pure H_3BCO at a pressure of 105 mm.)

The fundamental band of carbon monoxide (2143 cm^{-1}) nearly coincided with one of the borine carbonyl bands, but the latter was so extremely strong that the interference was not serious. Most of the absorption bands of diborane were also observed, but there was only one case of overlapping and that again involved a very strong band of borine carbonyl (2440 cm^{-1}) so that no difficulty was experienced.

In addition to the diborane and carbon monoxide which were unavoidably present in the absorption cell, a third (unidentified) impurity was also detected. In the course of the observations which were made on the borine carbonyl spectrum with no added CO, it was found that two bands—one at 2015 cm^{-1} showing about ten percent absorption, and one at 2057 cm^{-1} showing essentially 100 percent absorption at its center—remained constant in intensity while the borine carbonyl was decomposing. These bands were thus not due to

* Work supported by Contract N6ori-20, T. O. IX, with the ONR.
** Present address: Friends University, Wichita, Kansas.
[1] A. B. Burg and H. I. Schlesinger, J. Am. Chem. Soc. **59**, 780 (1937).
[2] S. H. Bauer, J. Am. Chem. Soc. **59**, 1804 (1937).
[3] R. D. Cowan, J. Chem. Phys. **17**, 218L (1949).
[4] Gordy, Ring, and Burg, Phys. Rev. **74**, 1191L (1948).

H_3BCO (nor to its decomposition products), as had been suspected also from the fact that they were only about half as wide as the other observed bands. Unfortunately, the observations on the dissociation of borine carbonyl were made with a rock salt prism, and so no check was obtained on the authenticity of the bands observed at 622 and 423 cm^{-1}. The 423 cm^{-1} band is probably also due to the impurity, since it is rather narrow. The compound responsible for the extraneous bands remains unidentified—the bands cannot be attributed to any of the impurities likely to be present in diborane, and no impurities were detected spectroscopically in the carbon monoxide used (run at a pressure of 70 cm in a 10 cm cell). It was considerably less volatile than borine carbonyl, as it was found to pass fairly readily through a trap at −85°C whereas most of it was caught in a trap at −95°C. It may have been produced by a side reaction in the absorption cell, or may have been present in the originally prepared sample and not completely removed during the purification process, which was carried out only once due to the fear that borine carbonyl was more unstable than it actually proved to be.

RESULTS

A general view of the spectrum is shown in Fig. 1. The percent absorption plotted there was obtained with the aid of estimated background curves (such as the dashed line in Fig. 2); actual background runs with an empty cell were not made since they would not have allowed for absorption by the carbon monoxide and diborane anyway. The frequencies of the absorption maxima are given in Table I. It will be noticed that there are no strong bands in the vicinity of 3000 cm^{-1}, which indicates that at least the great majority of borine carbonyl molecules do not have the structure H_2BCHO.

In Figs. 2 and 3 are shown photographs of original records of the bands at 809 cm^{-1} and 2440 cm^{-1}. The structure of these bands is typical of perpendicular bands of a symmetric top molecule, and the maxima produced by successive Q branches show a distinct intensity alternation of the type *strong, weak, weak, strong* . . . , which indicates the presence of a threefold symmetry axis.[5] The observed intensity ratio agrees well with the value 2:1 to be expected for one set of three off-axis hydrogen atoms.[5] The infra-red evidence thus very strongly favors the structure H_3BCO (or H_3BOC) with symmetry C_{3v} for borine carbonyl, in agreement with the microwave results.[4]

The positions and probable assignments of the maxima of the 809 and 2440 cm^{-1} perpendicular bands are given in Tables II and III, respectively. (The assignments have been based on the requirement[5] that the strong maxima should correspond to values of K'' of 0, 3, 6, ... It may be noted that there are some irregularities in the 2440 cm^{-1} band—due perhaps to interference from the corresponding band of $H_3B^{10}CO$.)

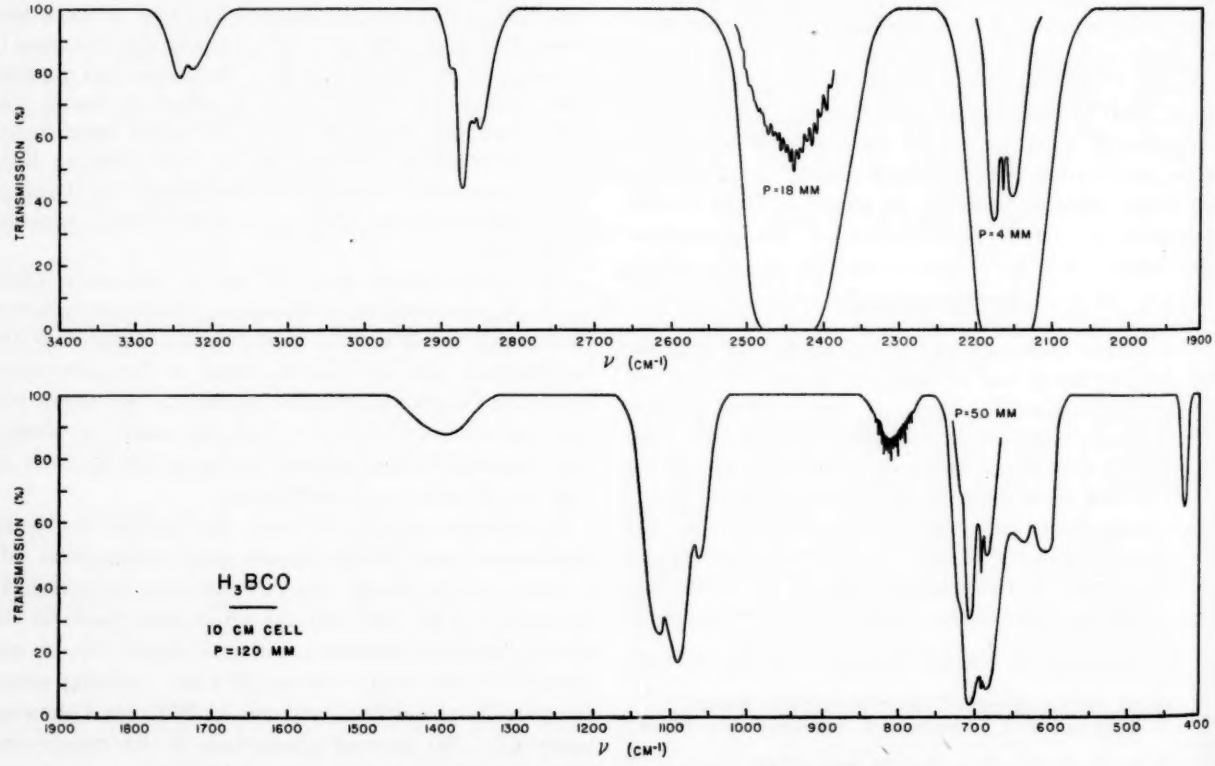

FIG. 1. The infra-red absorption spectrum of borine carbonyl.

[5] G. Herzberg, *Infrared and Raman Spectra of Polyatomic Molecules* (D. Van Nostrand Co., Inc., New York, 1945), p. 432.

The average spacing between Q-maxima is 3.1 cm^{-1} for the 809 cm^{-1} band and 6.7 cm^{-1} for the other, the difference being attributable to Coriolis coupling between vibration and rotation. Since there should be four perpendicular bands and these have not all been resolved (nor even observed?), it is not possible to draw any conclusions regarding the moments of inertia of the borine carbonyl molecule. However, accurate values of the moments are available, and from these an estimate can be made of the spacings which should be observed in the other two perpendicular bands:

A straightforward extension of the calculation of Johnston and Dennison[6] for axially symmetric XYZ_3 molecules has been carried out by the present author, the result obtained being that for axial $WXYZ_3$ molecules, the sum of the ζ-values for the fundamental vibrations of species E is

$$\zeta_5+\zeta_6+\zeta_7+\zeta_8=(I_A/2I_B)+1=(B/2A)+1,$$

where I_A and I_B are the moments of inertia about axes along and perpendicular to the symmetry axis respectively, and $A(=h/8\pi^2cI_A)$ and B are the corresponding rotational constants. The structure of borine carbonyl has been determined from the microwave spectra of the normal and deuterated compounds (for both B^{10} and B^{11}) by Gordy, Ring, and Burg.[7] From their results, the calculated values of A and B are 4.17 and 0.29 cm^{-1}, respectively. This gives $\sum\zeta=1.03$. From the theoretical expression $\Delta\nu=2(A-B)-2A\zeta$ for the separation of successive Q maxima, one obtains $\zeta=0.13$ for the 2440 cm^{-1} band and $\zeta=0.56$ for the 809 cm^{-1} band, leaving 0.34 as the sum of the ζ-values for the other two perpendicular bands. Thus, if the two unknown ζ-values were about equal ($=0.17$), the spacings of the corresponding bands would be about 6.3 cm^{-1}, and therefore rather easily resolvable.

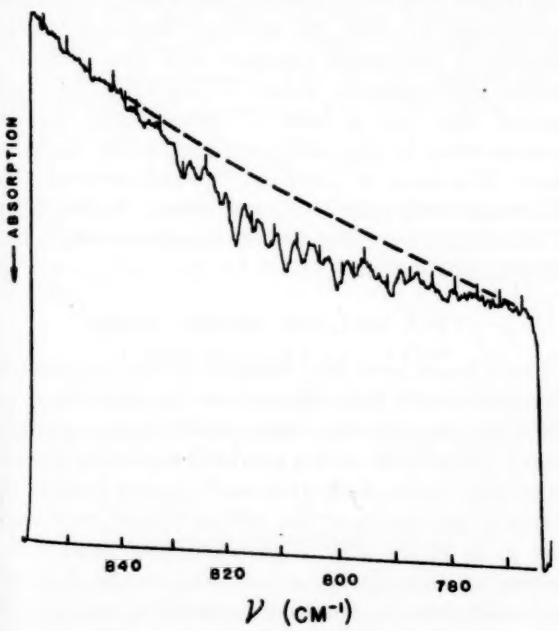

FIG. 2. Record of the 809 cm^{-1} band.

TABLE I. Absorption bands of borine carbonyl.

ν_{vac}	Type	Intensity[a]	Effective slit width
423 cm^{-1}	(impurity?)	35	4.5 cm^{-1}
609, 635	∥?	45	4.5
681, 692, 706	∥	230	1.8
809	⊥	20	1.7
1062, 1091, 1114	∥?	230	2.6
c.1392	⊥? (interf. H_2O)	10	4.5
2152, 2164, 2176	∥	3300	2.5
2440	⊥	500	2.6
2851, 2860, 2872	∥?	65	4.4
3226, (3231 min.), 3242	∥?	20	7.1

[a] The intensities given are rough values of the peak-absorption-coefficient β as calculated from the expression $\ln(I_0/I)=10^{-6}\beta lp$, where l is the path length of the absorbing gas in centimeters, p is its pressure in millimeters of mercury, and the 10^{-6} is an arbitrary factor.

VIBRATIONAL ASSIGNMENTS

Borine carbonyl, being a six-atomic molecule, has twelve normal vibration modes. Assuming the molecule

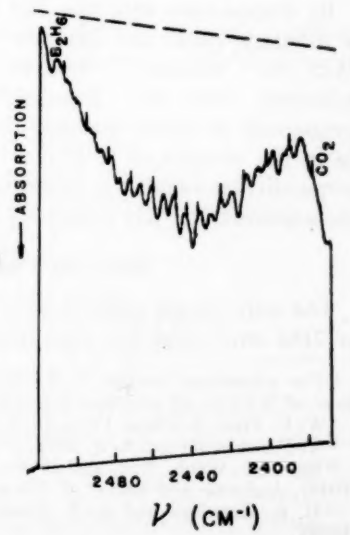

FIG. 3. Record of the 2440 cm^{-1} band.

[6] M. Johnston and D. M. Dennison, Phys. Rev. 48, 868 (1935).
[7] Gordy, Ring, and Burg, Phys. Rev. 78, 512 (1950). A copy of their manuscript was very kindly sent to the present author by Professor Gordy prior to publication.

TABLE II. Positions of the maxima of the 809 cm^{-1} band.

Assignment	ν_{vac}	$\Delta\nu$	Assignment	ν_{vac}	$\Delta\nu$
$^PQ_9$	782.1* cm^{-1}		$^RQ_1$	812.0	
		2.5			3.4
$^PQ_8$	784.6		$^RQ_2$	815.4	
		3.4			3.1
$^PQ_7$	788.0		$^RQ_3$	818.5*	
		2.7			3.0
$^PQ_6$	790.7*		$^RQ_4$	821.5	
		2.9			3.5
$^PQ_5$	793.6		$^RQ_5$	825.0	
		3.3			3.3
$^PQ_4$	796.9		$^RQ_6$	828.3*	
		3.0			3.5
$^PQ_3$	799.9*		$^RQ_7$	831.8	
		3.0			3.4
$^PQ_2$	802.9		$^RQ_8$	c835.2	
		3.0			3.7
$^PQ_1$	805.9		$^RQ_9$	c838.9*	
		3.3			
$^RQ_0$	809.2*				
		2.8			

TABLE III. Positions of the maxima of the 2440 cm^{-1} band.

Assignment	ν_{vac}	$\Delta\nu$	Assignment	ν_{vac}	$\Delta\nu$
$^PQ_7$	2389.5 cm^{-1}		$^RQ_1$	2446.9	
		7.3			6.3
$^PQ_6$	2396.8*		$^RQ_2$	2453.2	
		8.4			5.6
$^PQ_5$	2405.2		$^RQ_3$	2458.8*	
		5.1			6.7
$^PQ_4$	2410.3		$^RQ_4$	2465.5	
		6.3			5.8
$^PQ_3$	2416.6*		$^RQ_5$	2471.3	
					5.8
$^PQ_2$	2423.5		$^RQ_6$	2477.1*	
					3.7
$^PQ_1$	2428.7			2480.8	
					5.7
	2433.4			2486.5	
					4.8
$^RQ_0$	2440.2*			2491.3	
		6.7			

* The asterisks mark the strong lines.

to have asymmetry C_{3v}, the usual group-theoretical analysis indicates that four of these are totally symmetric and of species A_1, while the other eight correspond to four doubly degenerate vibrations of species E, both species being infra-red (and Raman) active. The A_1 modes give rise to parallel bands, and may be described as a symmetrical BH stretching, a symmetrical BH bending (BH_3 deformation), a BC stretching, and a CO stretching. The E modes produce perpendicular bands; and consist of an asymmetrical BH stretching, an asymmetrical BH_3 deformation, a BH_3 rocking, and a BCO bending.[8]

Tentative assignments of the observed bands are given in Table IV, where ν_1, ν_2, ν_3, ν_4 represent the totally symmetric vibrations and ν_5, ν_6, ν_7, ν_8 the degenerate vibrations, in the order of decreasing frequency in each case. A discussion of these assignments follows.

2440 cm^{-1} band

By comparison with the BH stretching frequencies of diborane (2522 and 2614 cm^{-1} infra-red;[9] 2489 and 2523 cm^{-1} Raman[10])[11] and of borazole (2519 cm^{-1} infra-red; 2535 cm^{-1} Raman),[12] the BH stretching frequencies of borine carbonyl may also be expected to lie in the vicinity of 2500 cm^{-1}. Thus the 2440 cm^{-1} perpendicular band can immediately be attributed to the asymmetrical BH stretching frequency.

2164 cm^{-1} band

The only strong parallel band above 1100 cm^{-1} lies at 2164 cm^{-1}, and has here been assigned to the CO stretching rather than to the symmetrical BH stretching vibration. According to Gordy, Ring, and Burg,[7] the CO distance in borine carbonyl is 1.13A, which is the same as the internuclear distance in carbon monoxide and nearly as short as the triple bond distance (1.11A). Thus borine "carbonyl" does not contain the carbon-oxygen double bond (internuclear distance about 1.24A) of a true carbonyl, and it is to be expected that the CO frequency will lie in the vicinity of 2100 cm^{-1} rather than near the double-bond frequency 1740 cm^{-1}.

The question remains as to the whereabouts of the symmetrical BH stretching frequency ν_1. Ordinarily, a hydrogen vibration would be associated with quite a strong band; however, the electronic structure of borine carbonyl is sufficiently complex that it is difficult to predict what intensity should be expected. It is quite possible that the ν_1 band is rather weak, and was masked either by the 2440 cm^{-1} band or by the atmospheric CO_2 band at 2349 cm^{-1} (which showed about 60 percent absorption at its maximum). If this is true, an investigation of the Raman spectrum might be of value in locating ν_1.

1392, 1091, and 809 cm^{-1} bands

These bands have been assigned to the asymmetrical and symmetrical BH_3 deformation and the BH_3 rocking vibrations, respectively, which should produce a perpendicular, a parallel, and a perpendicular band, in that order. The width of the 1392 cm^{-1} band is intermediate between the widths of the 809 and 2440 cm^{-1} bands, and so is presumably a perpendicular band with a spacing of roughly 5 cm^{-1}. (Compare the comments on ζ-values at the end of the preceding section.) The fact that this band has not been resolved can be laid to the rather wide effective slit width of 4.5 cm^{-1}, interference from the atmospheric water vapor band (which, though the latter showed only about seven percent maximum absorption, was still serious with a

[8] The vibrational modes of H_3BCO may be compared with those of H_3CCN; cf. reference 5, p. 332.
[9] W. C. Price, J. Chem. Phys. **16**, 894 (1948).
[10] T. F. Anderson and A. B. Burg, J. Chem. Phys. **6**, 586 (1938).
[11] See also: Webb, Neu, and Pitzer, J. Chem. Phys. **17**, 1007 (1949); Anderson and Barker, J. Chem. Phys. **18**, 698 (1950).
[12] B. L. Crawford and J. T. Edsall, J. Chem. Phys. **7**, 223 (1939).

weak band), and possibly also interference from the B^{10} isotopic molecule.

The envelope of the absorption in the vicinity of 1091 cm^{-1} is rather peculiar, and has a width about twice the proper value for a parallel band. The boron isotope shift could well be sufficient to account for the width, but not for the fact that the high frequency maximum has a greater intensity than the low frequency one. Several combination frequencies can be found which lie close to 1100 cm^{-1}, but none of these seems a very satisfactory explanation. If this absorption includes the ν_3 band as assumed, it seems likely that the center of the band lies at about 1100 cm^{-1} rather than 1091 cm^{-1}. This frequency might be compared with that of a somewhat analogous BH_2 deformation vibration in diborane (1175 cm^{-1}).[9]

692 cm^{-1} band

As the only possibility left for a strong parallel band, this is assigned to the boron-carbon stretching vibration ν_4. This frequency is not excessively low in spite of the weak bond which might be expected from the instability of borine carbonyl.

622 cm^{-1} band

No central Q branch was observed for this band, due presumably to the low available resolution, but the separation of the two observed maxima is about right for a parallel band. For lack of anything better, it has been assigned to the second harmonic of the BCO bending vibration ν_8, with intensity perhaps borrowed from the 692 cm^{-1} band by Fermi resonance. If this assignment is correct, ν_8 is placed at about 315 cm^{-1}, which may be compared with the frequencies 380 and 290 cm^{-1} in H_3CCN and H_3CNC, respectively.[8]

423 cm^{-1} band

This band is too narrow to be either a parallel or perpendicular band of borine carbonyl, and is probably due to an impurity, as mentioned in the experimental section.

2860 and 3231 cm^{-1} bands

These are obviously combination bands. The assignments $\nu_2+\nu_4$ (=2856 cm^{-1}) and $\nu_2+\nu_3$ (=3255 cm^{-1}) fit fairly well and involve the strongest bands in the spectrum.

NORMAL COORDINATE ANALYSIS

On the basis of a valence-force field, the potential energy of a $WXYZ_3$ molecule of symmetry C_{3v} can be written.

$$2V=k_a(\Delta a)^2+k_b(\Delta b)^2+k_c\Sigma(\Delta c_i)^2+k_{\alpha}ab(\Delta\alpha)^2+k_{\beta}c^2\Sigma(\Delta\beta_i)^2+k_{\gamma}c^2\Sigma(\Delta\gamma_{ij})^2$$

where a, b, and c are the internuclear distances r_{WX}, r_{XY}, and r_{YZ}, respectively; α is the angle WXY; β is the supplement of the angle XYZ; and γ is the angle ZYZ.

TABLE IV. Tentative vibrational assignments.

ν_{vac}	Type	Intensity	Assignment
423 cm^{-1}		35	impurity
622	∥?	45	$2\nu_8$?(BCO bending)
692	∥	230	ν_4(BC)
809	⊥	20	ν_7(BH_3 rock.)
1091	∥?	230	ν_3(BH_3 def.)
1392	⊥?	10	ν_6(BH_3 def.)
2164	∥	3300	ν_2(CO)
2440	⊥	500	ν_5(BH)
2860	∥?	65	$\nu_2+\nu_4$
3231	∥?	20	$\nu_2+\nu_3$

A normal vibration analysis using such a potential function has been carried out by expressing the various changes in bond lengths and angles in terms of a set of eighteen orthogonal mass-adjusted displacement symmetry coordinates. The five coordinates of symmetry A_1 led in the usual manner to a fifth-order secular determinant with one zero root (corresponding to translation parallel to the z [symmetry] axis); the coordinate of symmetry A_2 to a first-order determinant with zero root (rotation about the z-axis); and the twelve coordinates of species E to two identical sixth-order determinants, each having two zero roots (translation parallel to and rotation about the x or y axis). Thus from each of the A_1 and E determinants there resulted a fourth-degree equation in $\lambda=(2\pi\nu)^2$, the solutions giving the fundamental vibration frequencies ν_1, ν_2, ν_3, ν_4 in the one case and ν_5, ν_6, ν_7, ν_8 in the other.

If these equations are written

$$A_1:\ \lambda^4-A\lambda^3+B\lambda^2-C\lambda+D=0$$

and

$$E:\ \lambda^4-F\lambda^3+G\lambda^2-H\lambda+I=0$$

then the results obtained for the various coefficients are as follows, where the following abbreviations have been used:

$$k_{\gamma}'=k_{\gamma}/\cos^2(\gamma/2)$$
$$1/m_1=1/m_W+1/m_X$$
$$1/m_2=1/m_X+1/m_Y$$
$$1/m_3=1/m_Z+3\cos^2\beta/m_Y$$
$$1/m_4=1/m_Z+3\sin^2\beta/m_Y$$
$$1/m_5=1/m_Z+3/m_Y$$
$$1/m_6=1/m_Z+3\cos^2\beta/2m_Y$$
$$1/m_7=1/m_Z+3\sin^2\beta/2m_Y$$
$$1/m_8=1/m_Z+3/2m_Y$$
$$1/m_9=b/am_W+b(1+a/b)^2/am_X$$
$$f=1+\cos^2\beta.$$

$$A=\lambda_1+\lambda_2+\lambda_3+\lambda_4=k_a/m_1+k_b/m_2+k_c/m_3+(k_{\beta}+3\cos^2\beta k_{\gamma}')/m_4. \quad (1)$$

$$B=\lambda_1\lambda_2+\lambda_1\lambda_3+\lambda_1\lambda_4+\lambda_2\lambda_3+\lambda_2\lambda_4+\lambda_3\lambda_4$$
$$=k_ak_b\{1/m_1m_Y+1/m_Wm_X\}$$
$$+k_ak_c/m_1m_3+k_a(k_\beta+3\cos^2\beta k_\gamma')/m_1m_4$$
$$+k_bk_c\{1/m_3m_X+1/m_Ym_Z\}$$
$$+k_b(k_\beta+3\cos^2\beta k_\gamma')\{1/m_4m_X+1/m_Ym_Z\}$$
$$+k_c(k_\beta+3\cos^2\beta k_\gamma')/m_5m_Z. \quad (2)$$

$$C=\lambda_1\lambda_2\lambda_3+\lambda_1\lambda_2\lambda_4+\lambda_1\lambda_3\lambda_4+\lambda_2\lambda_3\lambda_4$$
$$=k_ak_bk_c\{1/m_1m_Ym_Z+1/m_3m_Wm_X\}$$
$$+k_ak_b(k_\beta+3\cos^2\beta k_\gamma')\{1/m_1m_Ym_Z+1/m_4m_Wm_X\}$$
$$+k_ak_c(k_\beta+3\cos^2\beta k_\gamma')/m_1m_5m_Z$$
$$+k_bk_c(k_\beta+3\cos^2\beta k_\gamma')\{1/m_5m_Xm_Z+1/m_Ym_Z^2\}. \quad (3)$$

$$D=\lambda_1\lambda_2\lambda_3\lambda_4$$
$$=k_ak_bk_c(k_\beta+3\cos^2\beta k_\gamma')\{1/m_1m_Ym_Z^2$$
$$+1/m_5m_Wm_Xm_Z\}. \quad (4)$$

$$F=\lambda_5+\lambda_6+\lambda_7+\lambda_8$$
$$=k_c/m_7+k_a\{1/m_9+a/bm_Y\}$$
$$+k_\beta\{3c^2/2b^2m_2+1/m_6+3c\cos\beta/bm_Y\}$$
$$+k_\gamma'\{9\sin^4\beta/8m_Y+3f/4m_Z\}. \quad (5)$$

$$G=\lambda_5\lambda_6+\lambda_5\lambda_7+\lambda_5\lambda_8+\lambda_6\lambda_7+\lambda_6\lambda_8+\lambda_7\lambda_8$$
$$=k_ck_a\{1/m_7m_9+a/bm_Ym_Z\}+k_ck_\beta\{1/m_8m_Z$$
$$+(3c^2/2b^2)(1/m_7m_X+1/m_Ym_Z)+3c\cos\beta/bm_Ym_Z\}$$
$$+k_ck_\gamma'\{9\sin^2\beta/4m_Ym_Z+3f/4m_Z^2\}$$
$$+k_ak_\beta\{1/m_6m_9+3c\cos\beta/am_1m_Y+a/bm_Ym_Z$$
$$+(3c^2/2ab)(1/m_1m_Y+1/m_Wm_X)+3c\cos\beta/bm_Xm_Y\}$$
$$+k_ak_\gamma'\{9\sin^4\beta/8m_9m_Y+3f/4m_9m_Z+3af/4bm_Ym_Z\}$$
$$+k_\beta k_\gamma'\{9c^2f/8b^2m_2m_Z+27c^2\sin^4\beta/16b^2m_Xm_Y$$
$$+9(f+4c\cos\beta/b)/8m_Ym_Z+3/4m_Z^2\}. \quad (6)$$

$$H=\lambda_5\lambda_6\lambda_7+\lambda_5\lambda_6\lambda_8+\lambda_5\lambda_7\lambda_8+\lambda_6\lambda_7\lambda_8$$
$$=k_ck_ak_\beta\{(3c^2/2ab+3c\cos\beta/a)/m_1m_Ym_Z$$
$$+3c^2/2abm_7m_Wm_X+1/m_8m_9m_Z$$
$$+3c\cos\beta/bm_Xm_Ym_Z+a/bm_Ym_Z^2\}$$
$$+k_ck_ak_\gamma'\{3f(1/m_9+a/bm_Y)/4m_Z^2$$
$$+9\sin^2\beta/4m_9m_Ym_Z\}$$
$$+k_ck_\beta k_\gamma'\{9c^2f/8b^2m_2m_Z^2+3/4m_5m_Z^2$$
$$+27c^2\sin^2\beta/8b^2m_Xm_Ym_Z+9\cos\beta/2bm_Ym_Z^2\}$$
$$+k_ak_\beta k_\gamma'\{(9c^2f/8abm_Z)(1/m_1m_Y+1/m_Wm_X)$$
$$+9c\cos\beta/2am_1m_Ym_Z+9f/8m_9m_Ym_Z$$
$$+3(1/m_9+a/bm_Y)/4m_Z^2$$
$$27c^2\sin^4\beta/16abm_Wm_Xm_Y+9c\cos\beta/2bm_Xm_Ym_Z\}. \quad (7)$$

$$I=\lambda_5\lambda_6\lambda_7\lambda_8$$
$$=k_ck_ak_\beta k_\gamma'\{9c^2f(1/m_1m_Y+1/m_Wm_X)/8abm_Z^2$$
$$+9c\cos\beta/2am_1m_Ym_Z^2+3/4m_5m_9m_Z^2$$
$$+27c^2\sin^2\beta/8abm_Wm_Xm_Ym_Z$$
$$+9c\cos\beta/2bm_Xm_Ym_Z^2+3a/4bm_Ym_Z^3\}. \quad (8)$$

In addition to the internal checks in the calculations afforded by the occurrence of zero roots, the absence of any terms which were not linear in each of the force constants, etc., the above equations have been partially checked as follows:

The expressions for A, B, C, and D have been compared with the corresponding ones given by Glockler and Wall[13] for methylacetylene ($HCCCH_3$)—the appropriate special cases having been taken in each instance, and complete agreement having been obtained.

Since Glockler and Wall do not give expressions for the degenerate frequencies, partial checks on the expressions for F, G, H, and I were obtained by comparison with equations given by Herzberg[14] for linear WXY molecules, by Wagner[15] for axial XYZ_3 molecules, and by Slawsky and Dennison[16] for axial XCH_3 molecules—the appropriate special cases again being used. The following discrepancies were noted:

(1) In place of the k_β in Eqs. (1) to (8) above, the corresponding expression in Wagner's results is ck_β/b. Since this difference is present in the non-degenerate as well as the degenerate equations, it is probably due to a mistake in Wagner's expression for the potential energy of the molecule.

(2) A single term in the coefficient of k_ck_β in Eq. (6) above disagrees completely with the corresponding term given by Wagner, but agrees with that given by Slawsky and Dennison; hence it is presumably Wagner's which is in error.

(3) Slawsky and Dennison appear to have made a typographical error in their potential energy function, omitting what corresponds to the c^2 coefficient of k_γ in the potential function given above.

The numerical calculations described below have provided further checks on the algebra.

APPLICATION TO BORINE CARBONYL

The equations given above have been used to calculate force constants of the $H_3B^{11}CO$ molecule, the values used for the various parameters being those obtained by Gordy, Ring and Burg:[7] $a=1.131$A, $b=1.540$A, $c=1.194$A, $\beta=75°\ 23'$, $\gamma=113°\ 52'$.

On the surface, it would appear that Eqs. (1)–(8) could be used with the known values of ν_2, ν_3, $\cdots\nu_7$ to calculate the six force constants and the unknown values of ν_1 and ν_8. However, due to the approximations involved in using a valence-force potential (and in neglecting anharmonicities), the eight equations cannot be expected to make up a consistent set of functions of the six force constants. Correspondingly, an attempt to solve these equations exactly in the manner just mentioned would most likely lead to highly erroneous values of ν_1 and ν_8 and to values of the force constants which had little physical significance. It was therefore felt that it would be better to assume values for ν_1 and ν_8 and then determine values of the force constants which would satisfy all eight equations as closely as possible. The resulting indeterminacy in the values for the force constants (except possibly for k_α) is probably no greater than the errors inherent in the use of a valence-force treatment.

The frequencies used in the calculations were those

[13] George Glockler and F. T. Wall, J. Chem. Phys. **5**, 813 (1937).

[14] See reference 5, p. 173.

[15] J. Wagner, Zeits. f. physik. Chemie **B40**, 36 (1938).

[16] Z. I. Slawsky and David M. Dennison, J. Chem. Phys. **7**, 522 (1939).

given in Table V. By more or less trial and error procedures the following set of values of the force constants was found to satisfy each of Eqs. (1)–(8) to within an error of 1.2 percent or less: CO stretching: $k_a=17.3\times10^5$ dynes/cm, BC stretching: $k_b=2.97\times10^5$, HB stretching: $k_c=3.21\times10^5$, BCO bending: $k_\alpha=0.142\times10^5$, HBC bending: $k_\beta=0.333\times10^5$, HBH bending: $k_\gamma=0.363\times10^5$ dynes/cm.

The frequencies calculated from these force constants and Eqs. (1)–(8) are given in Table V, along with the percent difference between observed and calculated values. The agreement is probably as good as can be expected with a simple valence-force potential function. (The close agreement between observed and calculated values of ν_8 does not of course imply that the assumed value 315 cm^{-1} is accurate, since ν_8 is determined primarily by the value of k_α, and the latter has little effect on the other frequencies. Any future revision in the value of ν_8 will entail a corresponding change in k_α.)

The CO stretching force constant, 17.3×10^5 dynes/cm, may be compared with that of the CO molecule (18.5) and with the CN force constant[17] in the isoelectronic molecule H_3CCN (17.5). The author is aware of no other available values of the BC force constant; however, the internuclear distances calculated with the aid of Badger's rule[18] from the values $k_a=17.3\times10^5$ and $k_b=2.97\times10^5$ are $a=1.15$A and $b=1.54$A, respectively, and the latter especially is in good agreement with the microwave data.

The BH stretching force constant, 3.21×10^5 dynes/cm, is about six percent smaller than the value 3.42×10^5 given by Crawford and Edsall for borazole[12] and by Bell and Longuet-Higgins for diborane.[19] This can probably be ascribed to the difference between an H−B− bond in the former case and an H−B= bond in the latter ones, analogous to the corresponding CH bonds where the difference in force-constant values (4.79 and 5.1×10^5)[20] is also 6 percent. A point of some interest in connection with the HBC and HBH bending force constants is the fact that k_β is smaller than k_γ, whereas the opposite is the case with methyl radicals;[20] this may correspond to the relatively weak boron-carbon bond in borine carbonyl.

In summary, it may be said that although k_c and especially k_α may require some revision when ν_1 and ν_8 are determined more accurately, the values of the force constants which have been calculated appear to be quite reasonable, and a valence-force function seems to represent the potential energy of the borine carbonyl molecule with fair accuracy.

[17] J. W. Linnett, J. Chem. Phys. **8**, 91 (1940).
[18] R. M. Badger, J. Chem. Phys. **3**, 710 (1935).
[19] R. P. Bell and H. C. Longuet-Higgins, Proc. Roy. Soc. **A183**, 357 (1945).
[20] See reference 5, p. 193.

TABLE V. Calculated frequencies of borine carbonyl.

Mode	ν_{obs} (cm^{-1})	ν_{calc} (cm^{-1})	Difference
A_1: ν_1	(2360 est.)	2350	−0.4 percent
ν_2	2164	2135	−1.3
ν_3	1105	1152	+4.2
ν_4	692	674	−2.6
E: ν_5	2440	2479	+1.6
ν_6	1392	1346	−3.3
ν_7	809	822	+1.6
ν_8	(315 est.)	316	+0.3

ELECTRONIC STRUCTURE

A very good discussion of the electronic structure of borine carbonyl has been given by Gordy, Ring, and Burg[7] on the basis of resonance among the following five structures: I. $H_3B^--C\equiv O^+$; II. $H_3B^--C^+=O$; III. $H_3^+B^-=C=O$; IV. $H_3^+B^-=C^+-O^-$; V. $H_3B\ CO$; the latter being essentially free BH_3 and CO. They conclude that the departure of the angle HBC from the tetrahedral value, the known internuclear distances, and the small permanent dipole moment of borine carbonyl (1.80 debye)[21] can be accounted for by assuming the ground state to consist of a resonant mixture of these five structures in the following order of importance: V, II, III, I, and IV—the contributions being about 50 percent structure V, about 30 percent I and II combined, and about 20 percent III and IV combined. The predominance of V (which provides no formal BC bond) explains the chemical instability of the molecule; at the same time, the reasonably large value of the BC force constant obtained from the infra-red data is understandable from the contribution of the double-bond structures III and IV.

ACKNOWLEDGMENTS

The author wishes to express his appreciation to Dr. G. W. Schaeffer of the Chemistry Department, who suggested this investigation of borine carbonyl and supplied much helpful advice concerning its preparation and purification. He is also indebted to Mr. Riley Schaeffer of the Chemistry Department for the sample of diborane used, and to Prof. R. S. Mulliken for helpful discussions regarding the interpretation of the spectrum.

[21] Strandberg, Pearsall, and Weiss, J. Chem. Phys. **17**, 429 (1949).

On a Distillation Theorem by Schreinemakers

O. REDLICH AND A. T. KISTER
Shell Development Company, Emeryville, California
(Received June 5, 1950)

CONCLUSIONS of Schreinemakers are usually accepted without question, perhaps not only because he was extremely careful but also because his derivations are not easy to follow. One theorem of Schreinemakers,[1] which has been generally accepted in the literature,[2,3] would if true lead to the important practical consequence that of two impurities one is always *much* more easily removed by distillation. Although we shall discuss only ternary systems and assume a perfect vapor, the results can be immediately extended to the isothermal or isobaric distillation of any mixture.

According to Schreinemakers the distillation lines, describing the composition of the contents of the kettle in a distillation without reflux, are at the end points tangent to one boundary line of the phase triangle (Fig. 1). The slope of a distillation line at the point (x_1, x_2, x_3) is

$$dx_2/dx_1=(y_2-x_2)/(y_1-x_1), \tag{1}$$

where x_1, x_2, x_3 are the mole fractions of the liquid and y_1, y_2, y_3 those of the vapor. The mole fractions are related through the activity coefficients γ_1 etc., the vapor pressures p_1^0 etc. of the components and the total pressure P

$$y_1=x_1\gamma_1p_1^0/P \text{ etc.} \tag{2}$$

By means of

$$P=x_1\gamma_1p_1^0+x_2\gamma_2p_2^0+x_3\gamma_3p_3^0 \tag{3}$$

and the abbreviation

$$r=x_3/x_2, \tag{4}$$

the slope (1) of a distillation line can be represented by

$$dx_2/dx_1=-(P-\gamma_2p_2^0)/x_1[\gamma_1p_1^0-\gamma_2p_2^0+r(\gamma_1p_1^0-\gamma_3p_3^0)]. \tag{5}$$

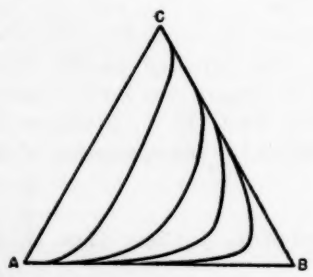

FIG. 1. Distillation lines according to Schreinemakers. (The lines are tangent to the boundaries in A and C.)

Approaching the corner point 1 we have

$$x_1=1; \quad x_2=x_3=0; \quad \gamma_1=1; \quad P=p_1^0, \tag{6}$$

so that

$$dx_2/dx_1=-(p_1^0-\gamma_2p_2^0)/[p_1^0-\gamma_2p_2^0+r(p_1^0-\gamma_3p_3^0)]. \tag{7}$$

The ratio r indicates on which distillation line we approach the corner point. It assumes all values between 0 (approach along the boundary from corner 2 to corner 1) and ∞ (from corner 3 to corner 1). The values of dx_2/dx_1 for the two limiting binary systems are, of course, -1 and 0.

But dx_2/dx_1 assumes other values for finite r. If we identify the subscript 1 with the most volatile component (A in Fig. 1) we have

$$p_1^0>\gamma_2p_2^0; \quad p_1^0>\gamma_3p_3^0, \tag{8}$$

so that dx_2/dx_1 according to (7) assumes *all values* between -1 and 0. In other words, the distillation lines originate from A in *all* directions (Fig. 2). A similar result is obtained for the corner C of the least volatile component.

If we identify the subscript 1 with component B, subscript 2 with C, and subscript 3 with A, we have

$$p_1^0>\gamma_2p_2^0 \quad \text{but} \quad p_1^0<\gamma_3p_3^0. \tag{9}$$

Now the denominator in (7) decreases with increasing r from a finite positive value to zero. The value zero is reached for a definite value of r, indicated by a broken line in Fig. 2, namely,

$$r=-(p_1^0-\gamma_2p_2^0)/(p_1^0-\gamma_3p_3^0). \tag{10}$$

On passing the broken line, we obtain

$$dx_2/dx_1=\mp\infty, \tag{11}$$

so that the distillation lines there are parallel to the line AC.

The discussion of azeotropic points is similar to that of the corner points. The slope of the distillation lines in the vicinity, for instance, of a binary azeotrope with the mole fractions x_{1az}, x_{2az}, 0 can be represented as a

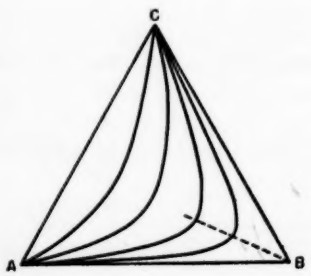

FIG. 2. Distillation lines.

[1] F. A. H. Schreinemakers, Zeits. f. physik. Chemie **36**, 449 (1901).
[2] W. Reinders and C. H. de Minjer, Rec. Trav. Chim. Pays Bas (a) **59**, 369 (1940), Table V. (b) **59**, 207 (1940). (c) **59**, 392 (1940), Fig. 1.
[3] R. Haase, Zeits. f. Naturforschung **4a**, 342 (1949).

function of the quotient

$$(\gamma_1 p_1^0 - \gamma_2 p_2^0)/x_3 \qquad (12)$$

in which both numerator and denominator approach zero. Any reasonable representation of activity coefficients shows that the numerator can be developed with respect to $x_2 - x_{2az}$ and x_3. The slope of the distillation lines again turns out to be a continuous function of the ratio $(x_2 - x_{2az})/x_3$.

It may be concluded that, contrary to Schreinemakers assertion, the distillation lines in the vicinity of corner points and azeotropic points are *not* tangent to the boundary lines.

The careful measurements of Reinders and de Minjer[2a] fully confirm this conclusion although these authors accepted[2b] Schreinemakers' theorem and, not quite successfully, attempted[2c] to represent their results in accord with Schreinemakers.

THE JOURNAL OF CHEMICAL PHYSICS VOLUME 18, NUMBER 8 AUGUST, 1950

The Microwave Spectra and Molecular Structure of Phosphorus and Arsenic Trichloride*

P. KISLIUK AND C. H. TOWNES
Columbia University, New York, New York

(Received May 25, 1950)

The pure rotational spectra of PCl_3 and $AsCl_3$ have been observed in the microwave region, and the observed fine structure has been partially explained. The distance P—Cl is 2.043±0.003A and the angle Cl—P—Cl is 100° 6′±20′. The distance As—Cl is 2.161±0.004A and the angle Cl—As—Cl is 98° 25′±30′.

THE pure rotational spectra of phosphorus and arsenic trichloride have been observed in the microwave region with all possible combinations of the chlorine isotopes. The results are listed in Tables IA, B and C.

Because J is large (4—6) and a number of different K values occur, the quadrupole interactions of the three chlorine nuclei split each transition into several hundred lines, even after selection rules and the degeneracies due to the symmetry of the molecule are taken into account. The case of $AsCl_3$ is further complicated by the quadrupole interaction of the arsenic nucleus. These lines were not resolved, although the lines appeared broader than those of the majority of molecules which have been investigated by microwave spectroscopy. The main $AsCl_3$ line, for example, was about 20 megacycles wide at about 0.05 mm pressure, and showed a double peak at reduced pressures and Stark voltages.

From the frequencies of the $J=4-5$ transition of PCl_3^{35} and PCl_3^{37}, and the $J=5-6$ transitions of $AsCl_3^{35}$ and $AsCl_3^{37}$, the bond angles and internuclear distances were calculated† (method I of Table II), and are compared with other determinations in Table II. Using these parameters the expected spectrum of $PCl_2^{35}Cl^{37}$ was calculated and compared with the observed spectrum (Fig. 2). Agreement was satisfactory, and it was decided to calculate the two structural parameters of PCl_3 from the frequency of the PCl_3^{35} line and the separation between the two lines of $PCl_2^{35}Cl^{37}$ corresponding to $K=1$ in the limiting (oblate) symmetric rotor (method II of Table II). Since zero-point vibrations enter in a different way into the calculation of molecular structure by the two above methods, the difference between the results obtained (see Table II) probably indicate roughly the magnitude of errors due to zero-point vibrations. Method II, using an asymmetric isotopic species, should be particularly helpful in eliminating uncertainties due to zero-point vibrations in symmetric tops containing three hydrogens and is being applied in this laboratory to CH_3Cl.

The angle Cl—As—Cl is found to be slightly smaller than the angle Cl—P—Cl in keeping with the tendency

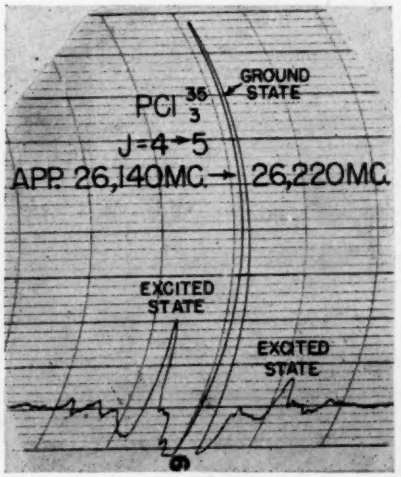

FIG. 1. PCl_3^{35}, $J=4-5$ at dry ice temperature.

* Work supported jointly by the Signal Corps and the ONR.
† Thanks are due to Mr. Henry Friedman for most of the computations.

TABLE IA. Microwave absorption lines of phosphorus trichloride.

Molecule	Transition	Frequency (megacycles/sec.)
PCl_3^{35}	$J=4\rightarrow5$, ground state	26,171[a]
	$J=4\rightarrow5$ excited vibrational states	26,190 26,152 26,210
$PCl_2^{35}Cl^{37}$	$J=4\rightarrow5$	
	$4_{31}-5_{41}$	25,552[a]
	$4_{22}-5_{32}$	25,649
	$4_{13}-5_{23}$	25,716
	$4_{04}-5_{14}$, $4_{14}-5_{24}$, $4_{23}-5_{33}$	25,725
	$4_{32}-5_{42}$	25,748
	$4_{41}-5_{51}$	25,971[a]
	Several more weak lines were observed, attributable to excited vibrational states.	
$PCl^{35}Cl_2^{37}$	$J=4\rightarrow5$	25,306
PCl_3^{37}	$J=4\rightarrow5$	24,875[a]

[a] These frequencies are subject to an error of ±1 mc. All others are only correct to within 10 Mc.

TABLE IB. Microwave absorption lines of arsenic trichloride.

Molecule	Transition	Frequency
$AsCl_3^{35}$	$J=4\rightarrow5$, ground state	21,472
	$J=4\rightarrow5$, excited vibrational state	21,426
	$J=5\rightarrow6$ ground state	25,767[a]
	$J=5\rightarrow6$ excited vibrational states	25,724 25,675
$AsCl_2^{35}Cl^{37}$	$J=5\rightarrow6$	25,308 25,354 25,381 25,393 25,411
	Several more weak lines were observed, attributable to excited vibrational states.	
$AsCl^{35}Cl_2^{37}$	$J=5\rightarrow6$	24,932 24,973
$AsCl_3^{37}$	$J=5\rightarrow6$	24,536[a]

[a] These frequencies are subject to an error of ±2 mc. All others are only correct to within 10 Mc.

TABLE IC. Rotational constants of PCl_3 and $AsCl_3$.

PCl_3^{35}	PCl_3^{37}
$B_0=2617.1\pm0.1$	2487.5±0.2
$AsCl_3^{35}$	$AsCl_3^{37}$
$B_0=2147.2\pm0.2$	2044.7±0.3

TABLE II.

	Internuclear distance $M-X$ in Angstroms	Bond angle $X-M-X$
PCl_3		
Method I	2.044±0.003	99° 56′±20′
Method II	2.041±0.003	100° 17′±20′
Swingle[a]	2.03 ±0.02	100° 30′±90′
Pauling and Brockway[b]	2.00 ±0.02	101°±2°
Brockway and Wall[c]	2.02 ±0.02	100°±2°
Wierl[d]	2.04 ±0.06	102°
Sum of covalent radii	2.09	
$AsCl_3$		
Method I	2.161±0.004	98° 25′±30′
Swingle[a]	2.17 ±0.02	99°±2°
Pauling and Brockway[b]	2.16 ±0.03	103°±3°
Brockway and Wall[c]	2.18 ±0.03	101°±40′
Sum of covalent radii	2.20	

[a] S. M. Swingle, quoted by P. W. Allen and L. E. Sutton, Acta Crystallographica **3**, pt. 1, 46 (1950).
[b] L. Pauling and L. O. Brockway, J. Am. Chem. Soc. **57**, 2684 (1935).
[c] L. O. Brockway and F. T. Wall, J. Am. Chem. Soc. **56**, 2373 (1934).
[d] R. Wierl, Ann. d. Physik **8**, 521 (1931).

noted by Pauling[1] for heavier elements to have smaller bond angles. Previous measurements on these molecules had reversed the relative size of these angles, but there is reasonable agreement with the electron diffraction measurements on the whole. The P−Cl distance is found to be somewhat longer than the previously accepted value, indicating less drastic shortening of the bond by double bond and ionic character, but it is still shortened relatively more than the As−Cl bond. It is to be expected that the double bond character would shorten the P−Cl bond relatively more than the As−Cl bond,[2] as was observed but ionic character would produce more shortening of the As−Cl bond.

Both PCl_3 and $AsCl_3$ have several normal vibrational

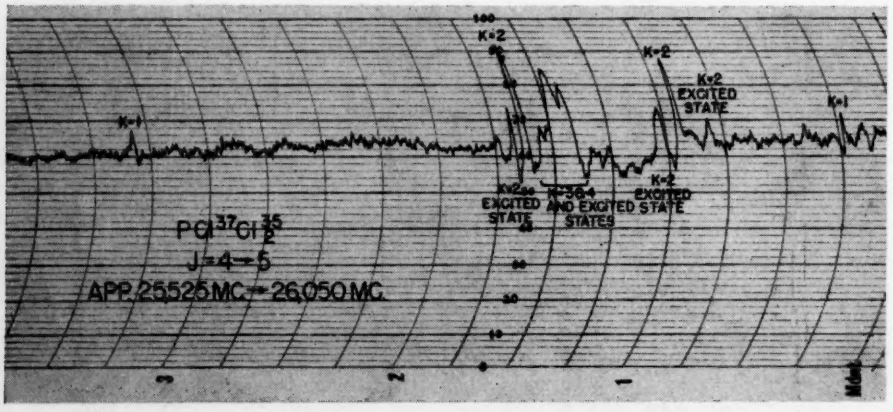

FIG. 2. $PCl_2^{35}Cl^{37}$, $J=4-5$ at dry ice temperature.

[1] L. Pauling, *The Nature of the Chemical Bond* (Cornell University Press, Ithaca, New York, 1940), p. 80.
[2] See reference 1, p. 235.

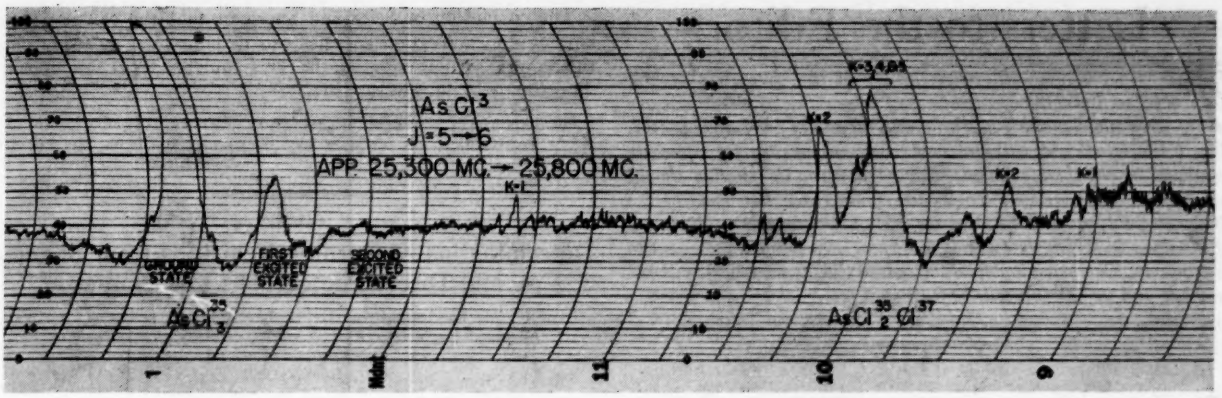

FIG. 3. $AsCl_3^{35}$ and $ClsCl_2^{35}Cl^{37}$, $J=5-6$ at room temperature.

modes of frequency sufficiently low to make observable lines due to the excited states. Several of these were measured as listed in Tables IA and B. These were shown not to be hyperfine structure in PCl_3 by the effect of temperature changes on their relative intensity. This was also supported by the frequency spacing and relative intensity in the two cases where more than one excited state of the same vibration was observed. The remaining expected vibrational states apparently have such a small vibration-rotation interaction that they were observed as part of the rather broad ground state line. From the relative intensities at room and at dry ice temperature, the two lines of higher frequency than the ground state line of PCl_3 (see Fig. 1) are tentatively assigned to the vibration of frequency ω_4,[3] and the single one of lower frequency than the ground state line to ω_2. The observed excited states in $AsCl_3$ (Fig. 3) are assigned to ω_2. These assignments are not completely satisfactory because the observed intensity ratios indicate somewhat higher vibrational frequencies in all three cases.

[3] Following the nomenclature of G. Herzberg, *Molecular Spectra and Molecular Structure, II. Infrared and Raman Spectra* (D. Van Nostrand Company, Inc., New York, 1945), p. 164.

Letters to the Editor

THIS section will accept reports of new work, provided these are terse and contain few figures, and especially few half-tone cuts. The Editorial Board will not hold itself responsible for opinions expressed by the correspondents. Contributions to this section should not exceed 600 words in length and must reach the office of the Managing Editor not later than the first of the month preceding that of the issue in which the letter is to appear. No proof will be sent to the authors. The usual publication charge ($8.00 per page) will not be made and no reprints will be furnished free.

The Lowest Energy of Symmetric Configurations

S. KRUYER
Central Laboratory of Staatsmijnen, Geleen, The Netherlands
June 5, 1950

FOR different cases it was shown by Seitz and Sherman[1] that the lowest state of a symmetric configuration is determined by the wave functions invariant under the group which expresses the symmetry of the atomic configuration; they expected that this will always be so.

In Steam *et al.*[2] a case is given where this expectation is not fulfilled.

I found another exception to this rule when calculating the activation energy for the addition of a diatomic molecule to a linear triatomic molecule. If we consider only plain configurations with a twofold rotation axis of symmetry A, approaching with the

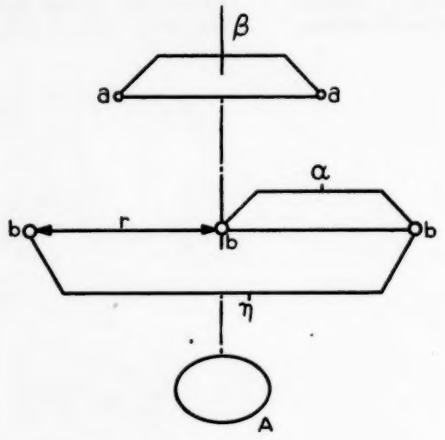

FIG. 1.

center of the diatomic molecule along the vertical through the middle of the triatomic molecule, the secular equation of the general 5-electron problem can be factorized in an equation of the third degree for the symmetric and in a quadratic for the antisymmetric wave functions. When the molecules are so far spaced that the Coulomb and the exchange integrals between a and b atoms may be neglected, the lowest root for the symmetric wave functions gives $E_2=Q-\alpha+\beta+\eta$ if $(\beta+\eta)>\alpha$ or $E_3=Q+\alpha-\beta-\eta$ if $(\beta+\eta)<\alpha$, where α stands for the exchange integral between the b atoms at a distance r and η for the exchange integral between b atoms at a distance $2r$. But the lowest root for the symmetric wave functions is higher than the lowest root for the antisymmetric wave functions $E=Q+\alpha+\beta-\eta$ because $(\alpha)>(\eta)$.

Numerical calculations on the adsorption of nitrogen on iron, where three iron atoms on a line were substituted for the actual surface, showed also for finite distances of the normal nitrogen that the lowest energy was given by the antisymmetric functions. The conclusion of Seitz and Sherman that the calculation of binding and activation energies can be simplified by using only the reduced secular equation for the symmetric wave functions is, unfortunately, not always true.

[1] F. Seitz and A. Sherman, J. Chem. Phys. **2**, 11 (1934).
[2] A. E. Steam, C. H. Lindsley, and E. Eyring, J. Chem. Phys. **2**, 410 (1934).

Determination of Burning Velocities from Shadow and Direct Photographs of a Flame

G. K. ASHFORTH, R. LONG, AND F. H. GARNER
Chemical Engineering Department, University of Birmingham, Birmingham, England
June 6, 1950

A METHOD of measuring the normal burning velocity of propane-air flames from shadow photographs has recently been reported by Andersen and Fein.[1] The observation that the area of the shadow cone varies with the distance from the flame to the film and the claim that the area to be used in the Gouy relationship is that obtained by entrapolation to the diametral plane of the flame, has led us to examine the method which we proposed for the determination of burning velocities.[2]

Our method possesses the advantage that the measurement of cone areas is not employed and consequently the effects of disturbances at the tip and base of the flame are avoided, since it is generally accepted that the cone area method gives only an average value of the burning velocity. The determination of burning velocity from measurements on a stationary flame involves the choice of a suitable part of the flame zone on which the measurements must be made, since combustion takes place in a zone of measurable thickness. Smith and Pickering[3] and Garside, Forsyth, and Townend[4] based their measurements upon the outer edge of the luminous cone, while Sherratt and Linnett[5] and Andersen and Fein[1] have preferred to use the zone revealed by shadow photographs of the flame.

The present authors consider that both outer and inner edges of the flame zone must be taken into consideration and in an attempt to do this, use has been made of both shadow and direct photographs of the flame. This method is based upon an imaginary surface developed as shown in Fig. 1 from a consideration of the over-all effect of the flame zone so that all the assumptions upon which the relationship $V_B=U\sin\alpha$ are based, apply to this surface. Using this relationship, the apparent burning velocity at different points on the shadow and luminous cones is measured

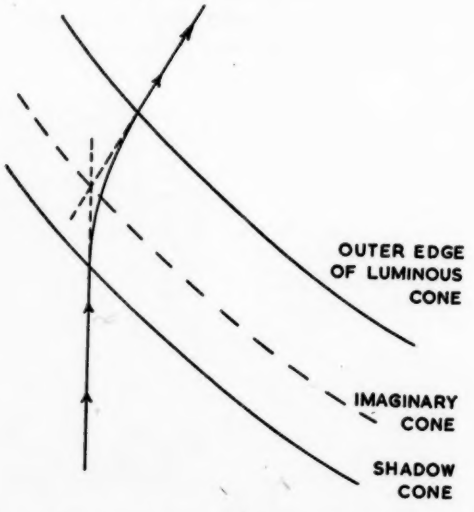

FIG. 1. Path of a gas flow line through the flame zone showing the development of the imaginary surface.

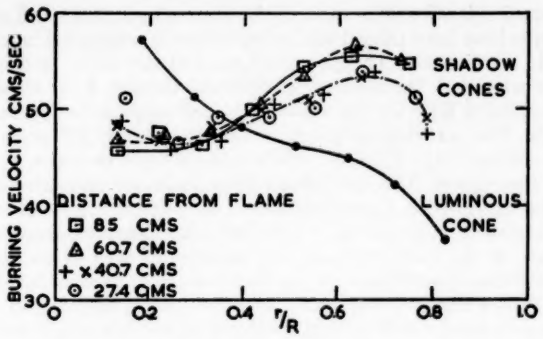

FIG. 2. Variation of the apparent burning velocity over the cone from measurements of the luminous and shadow cones.

and plotted against r/R where r is the radius of the flame cone at which the determination of α is made and R is the burner radius (Fig. 2). It has been shown[2] that the value at the point of intersection of the shadow and luminous curves is a true value of the burning velocity, this point corresponding to one value of r/R at which the shadow, luminous and imaginary cones are parallel and where the relationship $V_B = U \sin\alpha$ applies to all three surfaces.

Further experiments have been made in which the distance between the flame and film has been varied and the results are shown in Fig. 2. The apparent burning velocity over the shadow cone for a stoichiometric *n* heptane-air flame (with the mixture at 50°C and 740 mm Hg pressure) is plotted against r/R. While the curves are not independent of the distance between the flame and the screen, in the neighborhood of the point of intersection with the luminous curve, the agreement is such as to allow the above method to be applied. Normally the shadow cone is photographed with the flame midway between the light source and the screen for in this position the sensitivity of the shadow process is a maximum while the defocusing effects of diffraction and of the extension of the light source are not too great.

[1] J. W. Andersen and R. S. Fein, J. Chem. Phys. **18**, 441 (1950).
[2] Garner, Long, and Ashforth, Fuel **28**, 272 (1949).
[3] F. A. Smith and S. F. Pickering, J. Research Nat. Bur. Stand. **17**, 7 (1936).
[4] Garside, Forsyth, and Townend, J. Inst. Fuel **18**, 175 (1945).
[5] S. Sherratt and J. W. Linnett, Trans. Faraday Soc. **44**, 596 (1948).

Nuclear Magnetic Resonance Absorption in Hygroscopic Materials

T. M. SHAW AND R. H. ELSKEN
Western Regional Research Laboratory, Albany, California*
May 29, 1950

EXPERIMENTS have been performed to measure the magnetic absorption[1] by the hydrogen nuclei in a number of hygroscopic substances. The materials studied are primarily of biological origin and include proteins, carbohydrates, and vegatable tissue. The main interest in these experiments was the form of the relationship between the peak intensity of the absorption (I_p) and water content of the material. The present note summarizes the results obtained on vegetable materials studied.

The absorption in such materials is due, of course, to hydrogen nuclei in the aqueous and in the non-aqueous (mostly solid) constituents of the tissue. The theory of nuclear magnetic phenomena leads to an expectation of a linear relation between I_p and the water content of the tissue providing the magnetic environment of the hydrogen nuclei is independent of the water content.[2] One source of variation from linearity might be the specific orientation of the initial water absorbed.[3]

The experimental arrangement used to measure the nuclear magnetic absorption is based upon designs described in the literature.[4] A magnetic field of 3500 gauss was provided by a permanent magnet. Small coils on the pole pieces were energized with 60-cycle current in order to sweep the magnetic field through the resonance value and enable the absorption signal to be displayed on an oscilloscope. Means were provided to maintain the r-f magnetic field intensity at a fixed level during observations. I_p was determined by measurement of the maximum height of the absorption curve displayed on the oscilloscope. The r-f coil used to contain the sample under investigation was a solenoid of 0.5 cm internal diameter by 3.5 cm long. The specimens of tissue investigated were in the form of cylinders 0.3 cm in diameter by 5 cm long. Observations were made at room temperature (about 25°C).

The experimental results for apple and potato are summarized in Figs. 1 and 2. The graphs show I_p for the tissue at its original water content and for a number of water contents obtained by progressive dehydration. Early stages in the dehydration were performed in air under an infra-red lamp and the final dehydration was completed in a vacuum oven. The precision of the moisture determinations is about one percent. Both apple and potato shrank markedly during dehydration. Since shrinkage resulted in a significant change in the amount of material contributing to the magnetic absorption, the observed absorption signals were corrected to allow for shrinkage. The figures show the value of I_p as observed and after correction. Despite the rather large variations shown for different specimens of the same kind of tissue, the figures establish that I_p varies linearly with the amount of water in the tissue.

Since effects due to changes in the state of the water caused by interaction with the absorbent should be more pronounced when the water content is small,[5] the nuclear absorption was measured for maple wood. Wood was chosen for preliminary work because it is typical of many interesting hygroscopic materials, provides a system that is mechanically self-supporting, and is thus easily handled in the nuclear resonance apparatus. The results of ex-

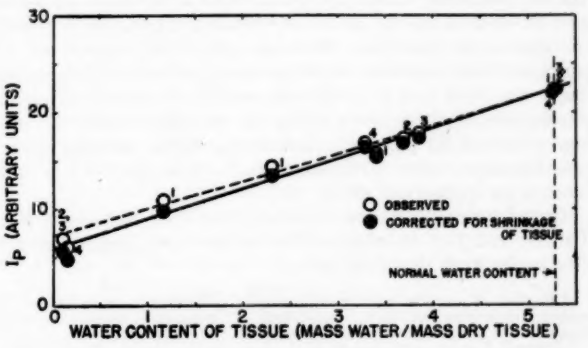

FIG. 1. Relation between peak intensity of nuclear absorption (I_p) and water content of apple tissue. The numbers near plotted points denote different samples of tissue. Zero absorption level uncertain because of noise.

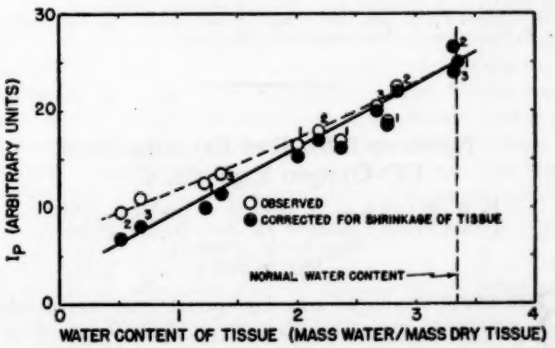

FIG. 2. Relation between peak intensity of nuclear absorption (I_p) and water content of potato tissue. The numbers near plotted points denote different samples of tissue. Zero absorption level uncertain because of noise.

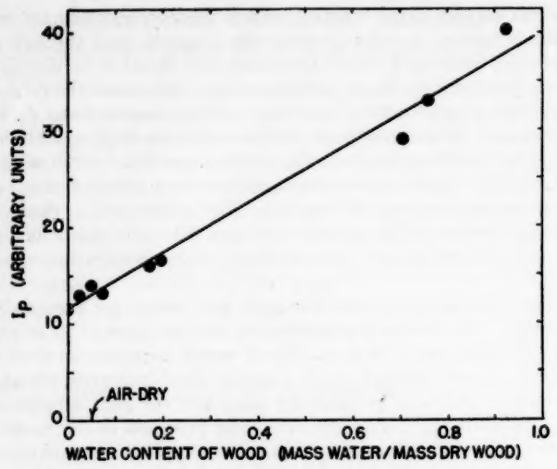

FIG. 3. Relation between peak intensity of nuclear absorption (I_p) and water content of maple wood. Each point denotes a different sample of wood. Zero absorption level uncertain because of noise.

periments for wood containing amounts of water ranging from zero (oven dry) up to about 1 gram of water per gram of dry wood, are shown in Fig. 3. I_p varied linearly with the water content of the material and showed no significant departures from linearity such as might be ascribed to interaction between the water and the non-aqueous components of the wood. Absorption line width[2] measurements may possibly provide a better method for investigating the interaction between water and the non-aqueous constituents of hygroscopic materials. Exploration of the possible utility of line width measurements awaits the completion of improved apparatus.

The present observations appear to establish the feasibility of the use of nuclear absorption phenomena as the basis for an improved method for the rapid determination of the water content of hygroscopic materials. Methods now widely used[5] for this purpose utilize variations in the electrical properties of hygroscopic materials. As is well known, such methods are useful only when the amount of water contained in the material is relatively small (up to about 20 percent). A moisture meter utilizing nuclear phenomena is under development and will be described in detail later in an appropriate place.

Grateful acknowledgment is made to C. H. Kunsman, K. J. Palmer, and J. J. Windle for their interest and suggestions relative to the work described above.

* Bureau of Agricultural and Industrial Chemistry, Agricultural Research Administration, U. S. Department of Agriculture. Report of a study made under the Research and Marketing Act of 1946.

[1] Purcell, Torrey, and Pound, Phys. Rev. **69**, 37 (1946); Block, Hansen, and Packard, Phys. Rev. **70**, 474 (1946).

[2] Bloembergen, Purcell, and Pound, Phys. Rev. **73**, 679 (1948).

[3] R. A. Gortner, *Outlines of Biochemistry* (John Wiley and Sons, Inc., New York, 1938), second edition, Chapter 9, p. 278.

[4] R. V. Pound, Phys. Rev. **72**, 527 (1947); A. Roberts, Rev. Sci. Inst. **18**, 845 (1947); N. J. Hopkins, Rev. Sci. Inst. **20**, 401 (1949).

[5] L. Hartshorn, J. Inst. Elec. Eng. **92**, 403 (1945); W. C. Dunlap, Jr. and B. Makower, J. Phys. Chem. **49**, 601 (1945).

Notes on Infra-Red Emission from CO-Oxygen Explosions* †

B. W. BULLOCK, G. A. HORNBECK, AND S. SILVERMAN
Applied Physics Laboratory, The Johns Hopkins University, Silver Spring, Maryland

May 29, 1950

RECENTLY a rapid scanning spectrometer was developed for use in the near infra-red,[1] primarily for studying the radiation accompanying rapid combustion processes such as occur in explosions. Some of the preliminary results of investigations of the CO-O_2 reaction are reported although as yet no definitive explanation is offered for some of the observed phenomena. Experiments have been carried out on explosions in a spherical bomb of ~15 cm diameter. The gases are ignited at the center by a spark discharge and the radiation is observed through $\frac{7}{8}$ in. diameter windows of KRS for the region 4–15μ and sapphire for the region 1–5μ. The scanning spectrometer was operated at 125 scans per second and with PbSe and PbTe cells covered the region 1–5.5μ in two ranges. This instrument gives radiation intensity *versus* time curves with a resolving power of ~25 cm^{-1} at 4.4μ while sweeping an interval of ~2.0μ per scan. Measurements were made of the rate or rise of the radiation as well as its decay. Additional observations on the decay of radiation were taken on a Perkin-Elmer spectrometer equipped with thermocouple of time constant ~0.05 sec. used with a G-M breaker type amplifier. At a given wave-length the radiation intensity *versus* time for the CO-O_2 explosion was recorded on a DuMont 247 oscilloscope with a synchronized single sweep circuit. A sample trace of the early portion of an explosion, taken on the scanning spectrometer in the 4.4μ region is shown in Fig. 1. The observations for the explosion of CO and O_2 in stoichiometric proportions (the mixture

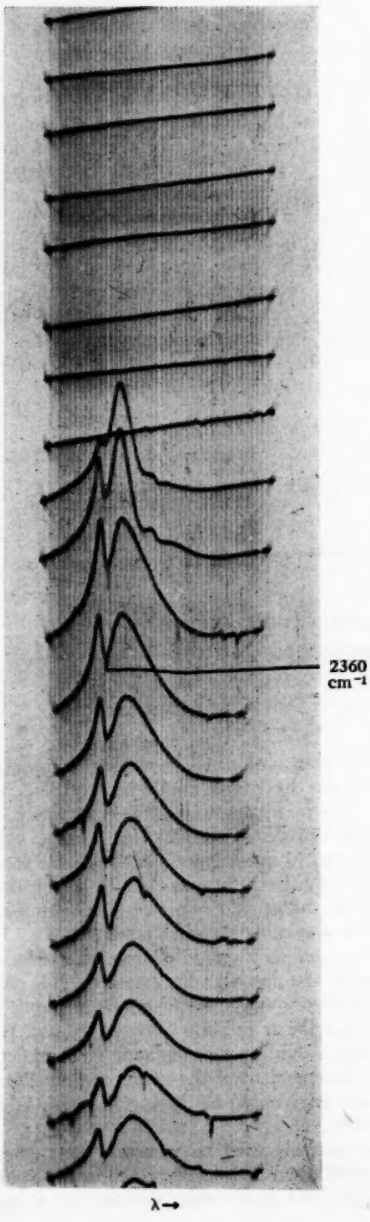

FIG. 1. This illustrates the radiation from a spherical bomb explosion of CO+O_2 (stoichiometric mixture) at 4.4μ. A scanning rate 125 frames per sec. was maintained, and in the first two frames of the explosion proper, the absorption of unburned CO is evident.

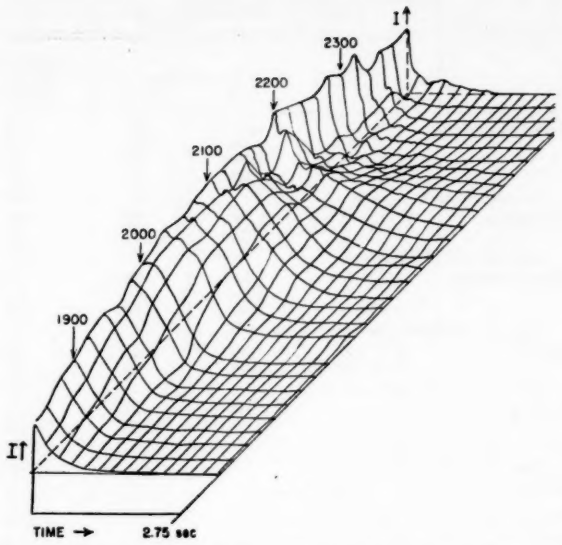

FIG. 2. This figure shows the intensity-time-frequency decay curves in the 4.4μ region for a $CO+O_2$ explosion (stoichiometric mixture) in a spherical bomb. The "afterglow" phenomenon is evident in the region of 2000–2400 cm^{-1}.

contained about one percent of H_2 as an impurity) may be summarized as follows.

The fundamental 4.4μ band with its overtones reaches peak intensity in approximately 0.02 sec. while the combination bands at 2.8μ reach peak intensity in about 0.03–0.04 sec. The long wave portion of the 4.4μ band reaches peak intensity earlier than the high frequency side and decays more slowly. The wave-length spread of all the bands observed are considerably greater relative to the same bands observed in the ordinary CO-O_2 flame.

The radiation decay process is quite complicated and shows repeated "afterglows" in those regions of the spectrum where there is considerable self-absorption. This is seen in the frequency, time, intensity plot of Fig. 2 for the 4.4μ region. The pulsating "afterglow" seems to have a period of about 0.2 sec.; a standing wave of this frequency in a vessel of 15 cm diameter should have a velocity of approximately 1.5 cm/sec. which is in fair agreement with the expected flame velocity of this sort of reaction. However, it is not yet clear how a subsonic wave could be maintained for so long in a burned mixture nor is it yet clear why the afterburning seems to be limited to frequencies near the center of the stronger absorption bands.

Further work is now underway on the propagation of essentially plane flames along cylindrical tubes. This we feel will present a better geometry than the spherical flame front. Observations are being made on this new vessel at right angles to the direction of propagation, and studies of the contour of the flame front and pressure front for various gaseous mixtures will be reported on in detail at a later date.

* This work was supported by ONR and Navy Bureau of Ordnance under Contract NO-rd 7836.

† A preliminary account for some of these results was given at the February, 1950 ONR conference on spectroscopy.

The Theoretical Treatment of the Monosilan Molecule

J. I. HORVÁTH
Department of Theoretical Physics, University of Debrecen, Debrecen, Hungary
May 29, 1950

IN a previous paper[1] we have described a method, derived in his original form by Neugebauer,[2] for the theoretical treatment of hydrid molecules with spherical symmetry and we have solved the binding problem of the ammonium molecule-ion. This method is generalizable for hydrid molecules which contain more protons spaced spherically,[3] for molecules which have an atom with higher atomic number in their center (such as SiH_4, GeH_4, etc.),[4] and also for complex molecules, or radicals with spherical symmetry ($Co(NH_3)_6^{+++}$, etc.).[5] It is useful for the discussion of the binding and of the constants of the molecules such as the above-mentioned type. Now we have determined the binding energy of the monosilan (SiH_4) which is a 18-electron problem. This is a case whose satisfactory theoretical treatment has some interest.

The general idea of our method is that the molecule is divided by a spherical surface which contains the four protons and it is supposed in our first approximation that the charge of the protons is distributed uniformly on this surface. Now we have inside our sphere a silicon nucleus, the charge of which is overcompensated by the electrons of the hydrogens and so a Si^{4-} ion is formed. The whole formation can be regarded from the outside of the sphere similar to an argon atom, because the charge of the four protons has been added to the charge of the Si nucleus. In a second approximation we pay attention to the fact, that the charge of the protons are not exactly uniformly distributed on the surface of the sphere, but are concentrated on the points of a tetrahedron. We have taken into consideration the inhomogeneous field of the protons in a perturbation calculation. The solution of the binding problem of the monosilan has, compared to the previously discussed cases, an essential novelty namely that the silicon, in addition to its four valence electrons, has two closed shells, therefore we must pay attention to the interaction between the protons and electrons in these shells.

We have used as wave functions of the molecule inside of the sphere of the protons the wave functions of the Si^{4-} ion and outside of which the wave functions of the Ar atom determined by the Slater's method.[6] Naturally the introduced two wave functions are not equal on the surface of the sphere of the protons, therefore we determine a parameter of equalization, as we have described this process in our previous paper, which solves this difficulty satisfactorily. Now the difference is only that we introduce for every different wave function a proper parameter of equalization. The normalizations must be defined also separately for the different shells. When determining energy terms we take the mutual effects into consideration as follows: the mutual effect among the proton, between the protons and the silicon nucleus, between protons and the closed shells, between protons and the valence electrons, between the central nucleus and the valence electrons, between the valence electrons and the closed shells, and finally must be considered the mutual effect among the valence electrons. The energy terms explicitly are the same as were described in the cited paper, introduced in our previous formulas the proper density of the electrons in the different shells in place of the density of the electrons. The parameter of variation of the energy is the radius of the above-mentioned sphere, which can be found explicitly in our formulas and the calculation can be carried out by machine.

We have found the minimum of the energy at $R=1.58$A distance of protons from the silicon nucleus and the calculated energy is 0.77 ev, which gives the energy necessary to carry out the four protons and the eight electrons from our molecule into infinity. The experimental value for R is given by Tindal, Stranly and Nielsen[7] as 1.5A. The difference is also 5.86 percent, which is satisfactory enough. For the binding energy we have no experimental value, but the smallness of the calculated energy is in very good agreement with the well-known fact, that the monosilan molecule is unstable at normal temperature and pressure.

[1] J. I. Horváth, J. Chem. Phys. **16**, 851 (1948).
[2] Th. Neugebauer, Zeits. f. Physik **98**, 638 (1936).
[3] Th. Neugebauer, Mat. Term. Tud. Ért. Budapest **56**, 450 (1937); **57**, 182 (1938).
[4] J. I. Horváth, Hung. Acta Physica, Budapest (to be published).
[5] J. I. Horváth, Acta Physica et Chemica Segediensis, Szeged (to be published).
[6] J. C. Slater, Phys. Rev. **38**, 1109 (1931).
[7] Tindal, Stranley and Nielsen, Proc. Nat. Acad. Sci. U. S. A. **27**, 208 (1941).

Bond Energy and Bond Order

GEORGIO NEBBIA
University of Bologna, Bologna, Italy
May 1, 1950

RECENTLY Kavanau[1] has compared the relations between bond order, bond energy and interatomic distance for carbon-carbon bonds. Concerning his paper I should observe that bond energy and interatomic distance may be related in a rather different way from those reviewed by Kavanau, considering that all the C−C bonds do vary with continuity either in bond energy and in interatomic distance, the "pure" double bond of ethylene being but a particular case of the series of the bonds of organic chemistry, each with a certain grade of hybridization of the four binding electrons, starting from ethane and ending with acetylene.

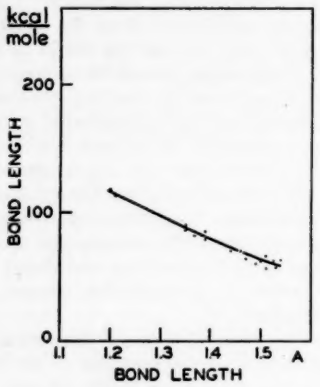

FIG. 1. C−C bond.

TABLE I.

		Bond length in A	Bond energy kcal/mole	Dissociation energy Q_a kcal/mole
Diamond	π C−C	1.54	62.5	125
Q_a obs. following Bichowski and Rossini and Pauling = 125 kcal/mole				125
Ethylene	1 C−C	1.35	90	90
	4 C−H	1.09	88	352
Q_a obs. = 444 kcal/mole				442
Acetylene	1 C−C	1.20	118	118
	2 C−H	1.09	88	176
Q_a obs. = 300 kcal/mole				294
Allene	2 C−C	1.33	92	184
	4 C−H	1.09	88	352
Q_a obs. = 537 kcal/mole				536
Ethane	1 C−C	1.55	62	62
	6 C−H	1.09	88	528
Q_a obs. = 583 kcal/mole				590
Carbon monoxide	1 C−O	1.13	211	211
Q_a obs. = 211 kcal/mole				211
Carbon dioxide	2 C−O	1.16	169	338
Q_a obs. = 338 kcal/mole				338
Formaldehyde	1 C−O	1.21	145	145
	2 C−H	1.09	88	176
Q_a obs. = 317 kcal/mole				321
Acetaldehyde	1 C−O	1.22	145	145
	4 C−H	1.09	88	352
	1 C−C	1.50	62	62
Q_a obs. = 561 kcal/mole				559
Glyoxal	2 C−O	1.20	153	306
	2 C−H	1.09	88	176
	1 C−C	1.47	64	64
Q_a obs. = 547 kcal/mole				546
Dimethyl ether	2 C−O	1.42	70	140
	6 C−H	1.09	88	528
Q_a obs. = 668 kcal/mole				668
Hydrogen cyanide	1 C−H	1.09	88	88
	1 C−N	1.15	168	168
Q_a obs. = 259 kcal/mole				256
Cyanogen	1 C−C	1.37	82	82
	2 C−N	1.16	160	320
Q_a obs. = 404 kcal/mole				402

TABLE I.—(*Continued*)

		Bond length in A	Bond energy kcal/mole	Dissociation energy Q_a kcal/mole
Methyl acetylene	1 C−C	1.21	113	113
	1 C−C	1.46	70	70
	1 C−H	1.057	90	90
	3 C−H	1.09	88	261
Q_a obs. = 536 kcal/mole				537
Cycloexane	12 C−H	1.09	88	1056
	6 C−C	1.53	57	342
Q_a obs. = 1397 kcal/mole				1398
Methyl cyanide	1 C−C	1.49	60	60
	1 C−N	1.16	148	148
	3 C−H	1.09	88	264
Q_a obs. = 470 kcal/mole				472
Benzene	6 C−C	1.39	85	510
	6 C−H	1.09	88	528
Q_a obs. = 1039 kcal/mole				1038
Pyridine	5 C−H	1.09	88	440
	4 C−C	1.39	85	340
	2 C−N	1.37	79	158
Q_a obs. = 938 kcal/mole				939
Pyrrole	1 N−H		84	84
	4 C−H	1.09	88	352
	2 C−N	1.42	65	130
	2 C−C	1.35	87	174
	1 C−C	1.44	70	70
Q_a obs. = 811 kcal/mole				810
Pyrazine	2 C−C	1.39	79	158
	4 C−N	1.35	81	324
	4 C−H	1.09	88	352
Q_a obs. = 833 kcal/mole				834
Acetamide	1 C−C	1.51	66	66
	1 C−N	1.38	89	89
	1 C−O	1.28	120	120
	3 C−H	1.09	88	264
	2 N−H		84	168
Q_a obs. = 708 kcal/mole				707
Urea	1 C−O	1.25	118	118
	2 C−N	1.37	83	166
	4 N−H		84	336
Q_a obs. = 620 kcal/mole				620
Furan	1 C−C	1.46	70	70
	2 C−C	1.35	86	172
	2 C−O	1.40	88	176
	4 C−H	1.09	88	352
Q_a obs. = 770 kcal/mole				770

To a C−C bond is therefore associated an energy and an interatomic distance related between them by the curve shown in Fig. 1 and drawn with the data of Table I, from which has been drawn also the curves of Figs. 2 and 3 for the C−O and the C−N bonds, respectively.*

The dissociation energy of a molecule is given directly by the sum of the various bond energies present in the molecule itself and, in any way, avoiding the concept of single, double and triple bond energy, the resonance energy is "lost." Furthermore the following picture, apparently more physically correct, could be used instead of that of bond order. The interatomic distance could be related to the sum of the π-electron charges upon the bonded

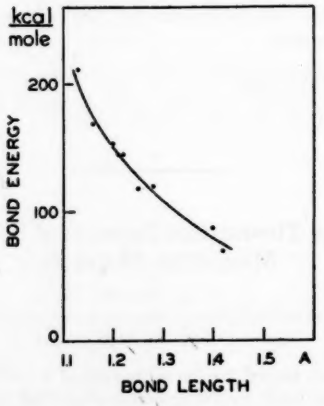

FIG. 2. C−O donb.

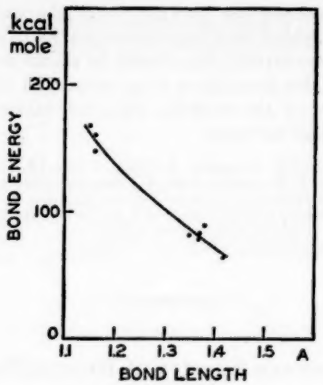

FIG. 3. C−N bond.

atoms, obtainable with the molecular orbital treatment.[2] There exist many uncertainties for a relation of this type since we know but little about the true charges in π-electrons near the linked atoms and about the C−C distance in many conjugated systems. We know, e.g., that the 2 and 3 atoms of butadiene have low charge and that their distance is high (1.46A), and that the meso-phenanthrene-type atoms have high charge and short bond (1.35A in pyrene, 1.38A in dibenzanthracene and coronene, following Robertson).[3]

On the other hand the calculations give (1.00+1.00) π-electrons both for the ethylene carbon atoms and for two carbon atoms linked together in benzene, the interatomic distances being 1.35 and 1.39A, respectively. This may be due to our too rough calculations of charge densities. The limiting cases should be acetylene with 4 π-electrons upon its two carbon atoms (1.20A) and ethane with zero π-electrons upon his two carbon atoms and with C−C distance 1.54A.

* In such curves the heat of vaporization of carbon has been assumed, for an easier comparison with the well-known data of Pauling (L. Pauling, *The Nature of the Chemical Bond* (Cornell University Press, Ithaca, New York, 1939)), as 125 kcal/mole, following the old data of Bichowski and Rossini (F. R. Bichowski and D. R. Rossini, *The Thermochemistry of the Chemical Substances* (Reinhold Publishing Corporation, New York, 1936). In any way the data may be transformed, assuming a new heat of vaporization (see reference 1 and also K. S. Pitzer, J. Am. Chem. Soc. **20**, 2140 (1948)), by a simple shifting of the curves. All the heats of dissociation have been recalculated from the heats of combustion, corrected to the gaseous state of the molecules, referred to by Wheland (G. W. Wheland, *The Theory of Resonance* (John Wiley and Sons, Inc., New York, 1944). From the same author have been obtained the interatomic distances.

[1] J. L. Kavanau, J. Chem. Phys. **17**, 738 (1949).
[2] C. A. Coulson and H. C. Longuet-Higgins, Proc. Roy. Soc. (London) **A191**, 39 (1947).
[3] J. M. Robertson, Acta Crystall. **1**, 101 (1948).

Electronic Kinetic Energy in Gases at High Pressures

T. L. COTTRELL
Research Department, I. C. I. Ltd., Nobel Division, Stevenston, Ayrshire, Scotland
May 31, 1950

APPLICATION of the virial theorem to a substance of volume V and pressure p gives

$$\Delta\bar{T}=3\Delta(pV)-\Delta U, \qquad (1)$$

where $\bar{T}$ is the average kinetic energy of electrons and nuclei and U is the total energy.[1] Michels *et al.*[2] have used this result to calculate changes in average kinetic energy brought about by compression of gases; $\Delta(pV)$ was directly measured and ΔU was calculated from the observed P-V-T relationships. $\Delta\bar{T}$ was found to increase with pressure, and it was pointed out that this must be due to an increase in electronic kinetic energy. It was shown that a change of the correct order of magnitude in electronic kinetic energy could be demonstrated by solving the wave equation for the hydrogen atom with the boundary condition that $\Psi=0$ at $r=r_0$.[2,3] It is of interest to try to interpret these results on a molecular basis, particularly because such an interpretation may enable one to discuss the effects of pressures greater than those used by Michels (3×10^3 atmos.).

Slater[4] has pointed out that, for a diatomic molecule,

$$\bar{T}=-E-R(dE/dR), \qquad (2)$$

where E is the electronic energy, as a function of the internuclear distance R. This shows that as the nuclei are moved closer together than the equilibrium distance, there is a sharp rise in kinetic energy, and a relatively flat rise in total energy. Thus, if the compression of a gas composed of diatomic molecules could be regarded as pushing the nuclei a little closer together, the qualitative explanation of the effect is clear. The large effect of compression on the kinetic energy is very striking, but it is notable that a compression which increases the kinetic energy by an amount as great as the dissociation energy of the molecule leads to only a small increase in total energy. Using the $E(R)$ function and constants given by Linnett,[5] we may use (2) to calculate how E and $\bar{T}$ vary with R for nitrogen:

R(A)	E(kcal./mole)	ΔT(kcal./mole)
1.094	0.00	0.00
1.092	0.01	6.9
1.050	3.45	172.

The force required to bring about a given change in R and hence in $\bar{T}$ can thus be obtained from spectroscopic data; moreover, the corresponding pressure required can be obtained from Michels' experimental work. From this force and pressure the "effective area" of the molecule can be calculated. This "effective area" should be about the same as that of the van der Waals sphere, but close agreement is not to be expected: Michels' results on the hydrogen atom suggest that the area might be greater. The results for nitrogen are of the correct order, and their approximate constancy with increasing pressure suggests that this viewpoint is justifiable. They are as follows:

$\Delta\bar{T}$(kcal.)	1	2	3	4	5	6
Area (A^2)	143	151	152	149	145	142.

The "effective area" seems to be decreasing at high pressures; thus $\Delta\bar{T}$ calculated from it for still higher pressures is likely to be an upper limit. In nitrogen at 10^5 atmospheres, for example, 180 kcal. is an upper limit to the change in kinetic energy, and 4 kcal. to the change in energy. Dissociation should take place at about 10^6 atmospheres.

[1] Schottky, Physik. Zeits. **21**, 232 (1920).
[2] Michels *et al.*, Physica **4**, 981 (1937).
[3] Michels and de Groot, *ibid.* **16**, 183 (1950).
[4] Slater, J. Chem. Phys. **1**, 687 (1933).
[5] Linnett, Trans. Faraday Soc. **36**, 1123 (1940).

Configuration of the Tartaric Ion

CLÉMENT DUVAL
Laboratoire de Chimie
AND
JEAN LECOMTE
Laboratoire des Recherches Physiques, Sorbonne, Paris, France
June 14, 1950

IN a Letter to the Editor, E. E. Turner and K. Lonsdale[1] have recently called attention to the two possible configurations for *d*-tartaric acid in the crystalline state, H-atoms and OH-groups being arranged approximately in a plane and the carboxyl groups staying either both in front of behind the plane of the paper, or one in front and the other behind. We think the second configuration is the only correct one.

Some years ago, we recorded and studied[2] the infra-red absorption spectra, between the wave-lengths of approximately 6–15 μ, for a series of metallic tartrates (11 dextro, 7 laevo, 8 meso and 5 racemic) in the powder state. *d*- (and *l*-) *tartrates have a spectrum formed of numerous bands, whose number is greatly reduced in the case of mesotartrates and racemates; the individual positions of bands differ in the three cases of d (or l), meso, and racemic.*

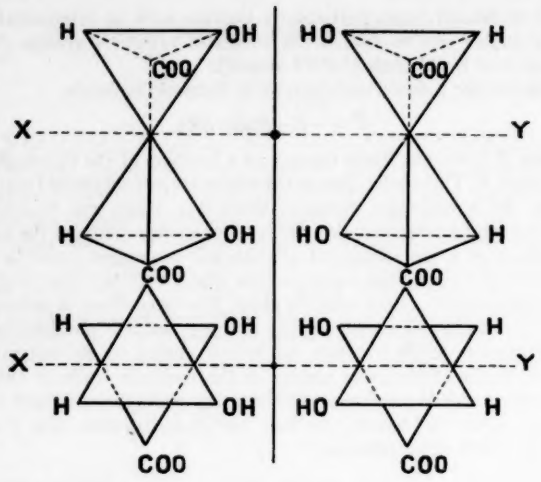

Fig. 1

Fig. 2

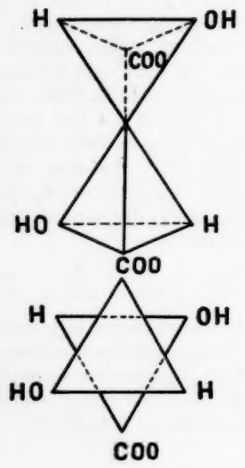

Fig. 3

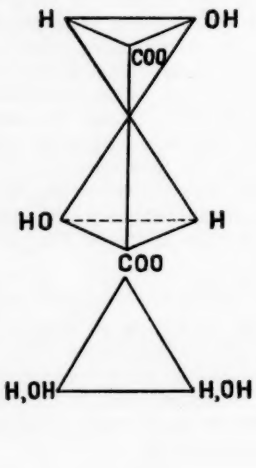

Fig. 4

With our hypothesis, the *d*-tartaric ion is shown in Fig. 1 and *l*-tartaric ion in Fig. 2 or inversely, but without any possible choice. We call again attention to the fact that this configuration is in accordance with the crystal structure as determined by x-rays.[3] On the other hand, the mesotartaric ion is represented by Fig. 3. In all cases, the horizontal projection is a hexagon.

We would like to point out that the *d*- (or *l*-) tartaric ion possesses but *one* binary axis XY located in the plane of the paper. Thence, a few molecular vibrations are forbidden in infra-red absorption; this fact explains the very complicated spectra we recorded. Moreover, a good agreement was found between infra-red bands and Raman lines. The mesotartaric ion possesses only *one* center of symmetry; thus, one-half of the fundamental vibrations is inactive in absorption; accordingly, the infra-red spectrum has been simplified and we may notice an alternance between absorption and diffusion spectra; the racemic ion is then formed as a *compound* (not a mixture) of a dextro and laevo-ion. The whole assembly possesses but *one* center of symmetry, and in accordance with the selection rules, the racemic differs from the mesotartaric ion only by the fact that an assembly of two ions is concerned. If racemates were formed by simple juxtaposition of a *d*- and *l*-ion, we would find exactly the same number of infra-red band in the active and racemic forms, but experiments show that it is not the case.

If Fischer's convention be kept (with the carboxylic groups either ahead or behind the plane determined by hydrogen and OH-groups), the meso-tartaric ion should be shown as in Fig. 4; but this picture is false since there is no element of symmetry to explain a decrease of the recorded infra-red bands with regard to those of the active tartrates.

[1] E. E. Turner and K. Lonsdale, J. Chem. Phys. **18**, 156 (1950).
[2] C. Duval and J. Lecomte, Comptes Rendus **219**, 483 (1944); Communication à la Société Chimique de France, January 26, 1945; Bull. Soc. Chim. **19**, 477 (1946); Communication à la Société de Minéralogie, April 12, 1945; Bull. Soc. franç. Min. **69**, 56 (1946).
[3] Bevers and Stern, Nature **162**, 864 (1948).

Microwave Spectra of Bromodiborane and Vinyl Bromide*

C. D. CORNWELL**
Mallinckrodt Chemical Laboratory, Harvard University, Cambridge, Massachusetts

June 1, 1950

SIXTY-EIGHT lines have been observed in the microwave spectrum of bromodiborane (B_2H_5Br). By assuming a configuration

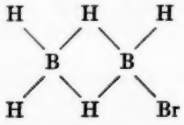

with the ring plane normal to the plane of symmetry, it is possible to assign forty-five lines as various bromine nuclear quadrupole multiplets of $J=2\rightarrow3$ and $J=3\rightarrow4$ transitions. Twenty-nine lines (belonging to the most abundant isotopic species, with both boron atoms having weight eleven) are fitted with six independent parameters. Lines were found for each of the four isotopic species with mixed boron weights expected for a structure in which the boron atoms are not symmetrically located (see Table I). The aplanarity, which is clearly observable ($I_A+I_B-I_C=4.1\pm0.8$ in atomic units) corresponds to a separation of the bridge hydrogen atoms of 2.0±0.2A. This and the parameters of Tables I and II reproduce the observed frequencies with an average error of 0.2 megacycle. A structural determination is now in progress. No fine structure attributable to boron quadrupolar effects was resolved.

In order to consider the possibility of a structure with the bromine atom in the bridge,

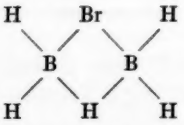

the frequencies to be expected for this configuration were calculated. They could not be made to conform to the observed spectrum for any reasonable ∠B-Br-B or B-Br distance. Now was the observed boron isotopic pattern compatible with a structure of

TABLE I. Rotational parameters of B_2H_5Br.*

Isotopic species	$b-c$	$b+c$	I_B	I_C
11–11–79	228.17±0.06	6511.13±0.10	149.989±0.004	160.883±0.004
11–11–81	225.80±0.06	6475.70±0.10	150.835±0.004	161.734±0.004
10–11–79	245.30±0.06	6802.13±0.10	143.431±0.004	154.163±0.004
10–11–81		6766.4 ±0.2		
11–10–79	222.57±0.06	6574.67±0.2	148.710±0.008	159.131±0.008
11–10–81	220.1 ±0.2	6539.8 ±0.2	149.53 ±0.01	159.95 ±0.01

* Isotopic weights are for the atoms B-B-Br reading from left to right in the structural formula given. b and c are the two smaller reciprocal moments of inertia in megacycles, I_B and I_C the corresponding moments in atomic units. Probable errors are given.

TABLE II. Nuclear quadrupole coupling constants in B_2H_5Br and C_2H_3Br.

Molecule	eQV_{aa}*
$B_2H_5Br^{79}$	293 mc
$B_2H_5Br^{81}$	244
$C_2H_3Br^{79}$	479
$C_2H_3Br^{81}$	399

* V_{aa} is the component along the principal axis of least moment of the molecular electric field gradient at the bromine nucleus, Q the electric quadrupole moment of the bromine nucleus. A ratio $Q^{79}/Q^{81}=1.20$ was assumed. Probable error is 5 mc.

TABLE III. Rotational parameters of C_2H_3Br.*

Isotopic species	$b-c$	$b+c$	I_B	I_C
$C_2H_3Br^{79}$	299.3 ±0.2	8025.2 ±0.2	121.43 ±0.01	130.83 ±0.01
$C_2H_3Br^{81}$	296.1	7979.9	122.14	131.55

* See Table I for definitions of parameters.

this symmetry, which has only two molecular species with mixed boron isotopes.

The bromodiborane was prepared by the reaction of bromine with diborane.[1] The melting point and vapor pressure of the product agreed with the reported values. Although it decomposes at room temperature, it was found to be quite stable at −78°C and hence all distillation paths and the absorption cell were packed in dry ice. The decomposition yields diborane and boron tribromide, which do not have microwave spectra. Di- and tribromodiborane are far less stable than bromodiborane and further more their lines could hardly be mistaken for those of the latter since the bromine isotopic pattern, which is striking because the two isotopes have equal abundances, would be different.

For the purpose of comparison with bromodiborane as well as on its own merits the structure of vinyl bromide

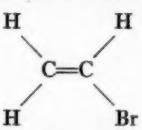

is of interest. Ten lines in its microwave spectrum have been assigned as $J=2\rightarrow3$ transitions. They are fitted with a maximum deviation of 0.5 megacycle by the parameters of Tables II and III. The few observable Stark effects of corresponding lines of this molecule and bromodiborane are qualitatively similar. A structural determination is planned for vinyl bromide also.

The author is grateful to Professor E. B. Wilson, Jr. for his encouragement and advice and to Dr. C. A. Brown for helpful suggestions concerning the preparation and handling of bromodiborane.

* This research was supported in part by the Navy Department through Contract N5Ori-76, Task Order V, ONR.
** Socony-Vacuum Oil Company Research Fellow.

[1] A. Stock, *Hydrides of Boron and Silicon* (Cornell University Press, Ithaca, New York, 1933), p. 117.

Low Frequency Raman Spectrum of a Benzene Single Crystal

A. FRUHLING
Laboratoire de Physique, Ecole Normale Supérieure, Paris, France
June 16, 1950

MAIR and Hornig[1] have reported recently that they have been able to detect by means of the infra-red combination lines the low frequency lines of solid benzene.

In this range, however, the Raman effect yields better results as these lines are not forbidden. Following the fragmentary results of several workers,[2–4] I have carried out a detailed experimental study of benzene, using all possible orientations of incident and scattered light vectors with respect to the axes of the single crystal, and given an interpretation of my results.[5]

There are four lines emitted, all very strong, with the respective frequencies 35, 63, 69 and 105 cm^{-1} at 0°C; the first and third are finer than the other.

These lines arise from rotatory oscillations of the whole molecules.[6,7]

Assuming that the ellipsoid of polarizabilities of the molecule does not get distorted during these oscillations, the theoretical form of the polarizability tensor of the unit cell can be determined. Comparison with the experimental result then shows that the 63 and 105 cm^{-1} lines arise from rotatory oscillations around the two axes of inertia situated in the plane of the molecule. Only two out of the four possible couplings (the unit cell of benzene contains four molecules[8] are shown to exist by the theory, but the corresponding frequencies are not separated experimentally.

The same perfectly symmetrical polarization characteristics are found for the 35 and 69 cm^{-1} lines. I would suggest that they take their origin in oscillations around the sixfold axis, together with strong distortions of the ellipsoid of polarizabilities due to the large mobility of the π-electrons. This would precisely give the observed type of polarization.

The corresponding coupling can be determined through examination of a model of the crystal: the intermolecular forces act essentially between the nearest hydrogen atoms, and the estimated value of the force constant between these atoms belonging to two neighboring molecules is 4.10^2 dyne/cm.

The study of the two couplings for the oscillations around the other axes, using this numerical value, shows that the corresponding lines cannot be resolved experimentally.

The low frequency lines depend strongly on temperature, especially the first and third ones. They become at −37°C: 45, 69, 78, 112 cm^{-1} and at −85°C: 53, 74, (?), 117 cm^{-1}.

The effect of pressure (700 atmos. applied) is to increase the frequencies by five percent, in agreement with London's dispersion formula.

The oscillation hypothesis is confirmed by the study of a crystal of diphenyl.

Finally, the results concerning diphenylmethane, diphenylether (structure unknown) and anthracene show that for aromatic compounds with one, two or three rings, the restoring torques C for low frequency lines is related to the melting point T_f according to the formula $C=A(T_f-T_0)$, where A and T_0 are constants.

[1] R. D. Mair and F. D. Hornig, J. Chem. Phys. **17**, 1236 (1949).
[2] E. Gross and M. Vuks, J. de phys. et rad. **7**, 113 (1936).
[3] S. C. Sirkar, Ind. J. Phys. **10**, 109 (1936); **10**, 189 (1936).
[4] A. Fruhling, Diplôme d'Etudes Superieures, Paris, 1944. A. Kastler and A. Fruhling, Comptes Rendus **218**, 998 (1944).
[5] A. Fruhling, J. de phys. et rad. **9**, 88 (1948). State Doctorate Thesis to be published in Ann. de Physique.
[6] A. Kastler and A. Rousset, J. de phys. et rad. **2**, 49 (1941).
[7] T. M. K. Nedungadi, Proc. Ind. Acad. Sci. **A13**, 161 (1941); **A15**, 376 (1942).
[8] E. G. Cox, Proc. Roy. Soc. **135A**, 491 (1932).

Carrier-Free Radioisotopes from Cyclotron Targets. X. Preparation and Isolation of Mg^{27} from Aluminum*

HERMAN R. HAYMOND, JOHN Z. BOWERS, WARREN M. GARRISON, AND JOSEPH G. HAMILTON
Crocker Laboratory, Radiation Laboratory, and Divisions of Medical Physics, Experimental Medicine, and Radiology; University of California, Berkeley and San Francisco, California
May 8, 1950

THE 10.2-min. Mg^{27} was produced from aluminum by the nuclear reaction $Al^{27}(d, 2p)Mg^{27}$ using the 20-Mev deuteron beam of the 60-in. cyclotron at the Crocker Laboratory. With deuterons of this energy, 14.8 hr. Na^{24} is also produced in comparable yield by the reaction, $Al^{27}(d, \alpha p)Na^{24}$. Other possible concurrent reactions produce radioisotopes having half-lives of

only a few seconds, with the exception of the 2.3-min. Al^{28}. The separation described here is based on our observation that carrier-free Mg^{27} in alkaline solution forms radio-colloidal aggregates[2,3] which may be removed by filtration.

A block of "magnesium-free" aluminum[4] was clamped to a water-cooled aluminum target plate and bombarded for 10 minutes at an average beam intensity of 10 μa. The bombarded surface (approx. 0.2 g) was removed by dissolution in 50 ml of hot ten percent sodium hydroxide. This solution containing sodium aluminate, sodium hydroxide and radio-colloidal Mg^{27} was diluted with an equal volume of water and drawn through two consecutive Whatman No. 50 filter papers. The first paper retained over 95 percent of the carrier-free Mg^{27} as adsorbed radio-colloid. This was washed with five percent sodium hydroxide until aluminum could not be detected in the filtrate followed by distilled water to remove the sodium hydroxide retained in the filter paper. Less than five percent of the magnesium activity was lost during the washing. The Mg^{27} was then removed from the filter paper with a minimum volume of 0.1N hydrochloric acid which on neutralization gave an isotonic solution of carrier-free radio-magnesium for biological investigations. Corrected for decay, a yield of 2.5 millicuries per microampere hour was obtained.

The decay curve was followed for 15 half-lives and showed a single period of 10.7 min. which agrees closely with previously reported values.[5,6] Absorption measurements in aluminum showed the 1.8-Mev beta-particle assigned[7] to Mg^{27}. The activity was further identified by chemical separation through the use of aluminum, sodium and magnesium carriers.

We wish to thank Mr. T. Putnam, Mr. B. Rossi and the crew of the 60-in. cyclotron for bombardments and Professor G. T. Seaborg for his continued interest in this work.

* This document is based on work performed under Contract No. W-7405-eng-48-A for the AEC.

[1] G. T. Seaborg and I. Perlman, Phys. Rev. **52**, 777 (1937).
[2] O. Hahn, *Applied Radiochemistry* (Cornell University Press, Ithaca, New York, 1936).
[3] M. H. Kurbatov and J. D. Kurbatov, J. Chem. Phys. **13**, 208 (1945).
[4] Spectrographic analysis showed less than 0.001 percent magnesium.
[5] M. C. Henderson, Phys. Rev. **48**, 306 (1935).
[6] S. Eklund and N. Hole, Arkiv. f. Mat. Astro. Fys. **29A**, 4, No. 26 (1943).
[7] E. Bleuler and W. Zünti, Helv. Phys. Acta **20**, 195 (1947).

Orbital and Spin Contributions to Paramagnetism of Hexavalent Chromium Compounds

D. S. DATAR
Central Laboratories for Scientific and Industrial Research, Hyderabad, India
June 6, 1950

IN previous communications[1,2] we have shown that feeble paramagnetism exhibited by certain ions in S state is due to partial freedom of the electronic spin owing to imperfect pairing. The free spin in chromium trioxide and potassium chromate was determined from structural diagrams constructed using x-ray data, the paramegnetism calculated from the free spin being in fair agreement with the experimental results.

Potassium polychromates also show feeble paramagnetism.[3] As their x-ray diagrams are not available, the unpaired spin may be computed on the basis of the structural formulas $K_2CrO_4\ CrO_3$, $K_2CrO_4\ 2CrO_3$, and $K_2CrO_4\ 3CrO_3$ for potassium dichromate, potassium trichromate and potassium tetrachromate respectively and 0.0571 and 0.0536 as factors[2] for the residual spin in CrO_3 and K_2CrO_4. The paramagnetism of the several compounds of hexavalent chromium was calculated from the free spin and the sp. susceptibility experimentally observed by Grey and Drakers[3] using values given by Augus[4] for diamagnetism of the different ions and 1249.8 for paramagnetism at 25°C for one unpaired electron. The paramagnetism per chromium atom obtained by dividing the total paramagnetism by the number of chromium atoms in the molecule has been given in Table I. The values of

TABLE I.

	Sp. susceptibility	Free spin per chromium atom	Paramagnetism per chromium atom calculated from: Sp. susceptibility	Free spin	Orbital contribution by difference
CrO_3	0.41	0.0571	81.7	71.3	10.4
Na_2CrO_4	0.12	0.0536	76.3	67.0	9.3
K_2CrO_4	0	0.0536	77.5	67.0	10.5
$K_2Cr_2O_7$	0.183	0.0553	84.5	70.9	13.6
$K_2Cr_3O_{10}$	0.241	0.0559	83.0	71.0	12.0
$K_2Cr_4O_{13}$	0.391	0.0562	96.3	71.1	25.2

paramagnetism obtained from the sp. susceptibility and the spin show a small difference. This gap may be explained as being the contribution of the high frequency elements of the orbital moment as represented by the second term in the formula for magnetic susceptibility given by Van Vleck[5]

$$\chi \text{ mole} = -\frac{Ne^2}{6mc^2}\sum \bar{r}^2 + \tfrac{2}{3}N \sum_{n' \neq n} \frac{[Mo(n';n)^2]}{h\nu(n';n)}.$$

The only attempt so far made to calculate the orbital paramagnetism is by Frank and Van Vleck[6] for the hydrogen molecule where the paramegnetism is about ten percent of the diamagnetism. The orbital paramagnetism in the compounds under study obtained by difference of the paramagnetic values calculated from the sp. susceptibility and the spin is between ten and 50 percent of the total diamagnetism of the constituent ions. It is not expected that the paramagnetism of the orbital origin ascertained in this manner is of any degree of accuracy but the results clearly show that the paramagnetism consists of two parts namely the spin and the orbital contributions. The orbital contribution is a small fraction and is of no consequence when normal paramagnetism is shown but becomes appreciable in molecules exhibiting low paramagnetism. It will be seen that in case of hexavalent chromium compounds the orbital contribution is generally one-sixth to one-eighth of the total paramagnetism, the balance being due to the free spin.

My thanks are due to Dr. S. K. K. Jatkar and Dr. S. S. Datar for helpful discussion.

[1] Datar and Datar, Nature **158**, 518 (1946).
[2] Datar and Datar, Ind. J. Phys. **23**, 16 (1949).
[3] Grey and Drakers, Phil. Mag. **7X**, 297 (1931).
[4] Augus, Proc. Roy. Soc. **136**, 569 (1932).
[5] Van Vleck, *Electric & Magnetic Susceptibilities*, 275 (1932).
[6] Frank and Van Vleck, Proc. Nat. Acad. **15**, 539 (1929).

The Role of Molecular Vibrations in Chemical Reactivity

JULES DUCHESNE
Department of Chemical Physics, University of Liége, Belgium
May 25, 1950

AN outstanding feature of the theories[1] of chemical reactivity lies in the fact that they deal with a static pattern of the molecules. This limiting assumption has nevertheless permitted a successful interpretation of reactivities in terms of the distribution of electronic densities of the molecules in a great number of cases.[2] However, in spite of significant predictions as to the reactivity of certain conjugated systems, one has been faced, especially in unconjugated systems, with fundamental difficulties which have not been overcome as yet. A striking example of this failure is concerned with the behavior of acetylene which is very much less reactive toward hydrogen bromide than ethylene is.

This is unexpected on various grounds which have been summarized recently by P. B. D. de la Mare.[3] We should especially point out the fact that the greater density of unsaturation electrons available for attack, which occurs for acetylene, would be in favor of a greater reactivity. This anomaly shows quite clearly

that reactivity is conditioned by another factor than electronic density of the molecule in its equilibrium position.

A detailed analysis of this problem has convinced us that the only simple way to solve the present contradiction between the accepted ideas and the facts was to abandon the static pattern and to adopt a dynamic one involving the molecular vibrations.

It is indeed well known that one of the out-of-plane fundamental vibrations of ethylene is a twisting vibration [$\delta \leqslant 1015$ cm^{-1}].[4] This gives rise to a torsion of the CH_2 groups with respect to one another through an angle amounting to several degrees in the first excited state ($v=1$). According to our knowledge of the electronic structure of a double bond it is to be expected, therefore, that the overlapping of the π-orbitals decreases in the course of such a motion, which means that the strength of the π-bond also decreases. In other words, one might say that several percent of the electrons forming the bond become effectively free and are responsible for the nucleophilic reaction of addition with the halogenated acids.

In the case of acetylene, on the other hand, such a dissociating twisting vibration does not appear among the fundamental movements on account of the linearity of the molecule. This has the important consequence of decreasing to a great extent its relative reactivity.

This specific vibrational effect not only provides a way out of an important particular difficulty of reactivity, but is furthermore able to furnish a unifying principle embracing any additional reaction. For instance, we should mention that it is easy to show that the reactions between benzene and the halogens, and the very peculiar 1.4 addition of the halogens to butadiene, can now be explained by making use of appropriate out-plane vibrations, which characterize the symmetry of these molecules. We therefore suggest identifying as addition-vibrations those twisting vibrations which are able to dissociate π-bonds.

Let us now turn our interest to another fundamental type of reaction, i.e., substitution reactions. It is well known[5] that, above 350°C, substitution of ethylene by halogens starts to predominate over addition, giving such products as C_2H_3Cl. This change of reactivity cannot be reconciled with the current ideas based on a static pattern. Indeed, in such a case the distribution of the electronic density in the molecule is not expected to be changed by a rise of temperature. Furthermore, the static dipole moment bound to the CH bond being practically zero for ethylene,[6] no electrophilic point of attack is available on the hydrogens to react with Cl^- of the supposed Cl^+Cl^- chlorine molecule. As for the addition reaction, it is possible, if we adopt a dynamic system, to recognize ethylene vibrations, especially valency and bending vibrations $\nu_{\sigma\sigma}$(1343 cm^{-1}) and $\delta_{\pi\sigma}$(3107 cm^{-1}), required by our accepted scheme of reaction. These vibrations indeed are able to bring a negative charge on the carbons and a positive charge on the hydrogens. This possibility arises from a discussion of changes of hybridization at the carbon atom when the molecule is distorted in a certain way from its equilibrium position.[7] That the magnitude of these charges appearing on the atoms as a consequence of their motion is not negligible is strongly supported by a recent work[8] which shows that the correct intensity of infra-red absorption in ethylene can only be interpreted on the assumption that a rather important dipole moment bound to the CH vibrating bonds does exist. Therefore, it is quite permissible to admit that positive charges at least as large as $e/50$ could be brought up to, and then taken away from a hydrogen atom in the course of the vibration. It is to be noticed that the σ-electrons and consequently only planar vibrations are involved in the substitution process, whereas the π-electrons alone, i.e., out-of-plane vibrations, are responsible of the addition reaction. This specific character of vibrations toward reactivity is also of great significance in explaining the influence of temperature on the orientation of the reaction. Indeed, out-of-plane vibrations are small with respect to planar ones, which means that by increasing temperature, we produce a relative increase in the proportion of molecules in states such as $\nu_{\sigma\sigma}$ and $\delta_{\pi\sigma}$ with respect to δ. This is not in disagreement with the experimental fact that the substitution reaction predominates at higher temperatures. On the other hand, arguments can be put forward in favor of the idea that the π-electrons tend to lose their normal properties when, at high temperature, the amplitude of the twisting frequency becomes large. This would tend to support the observed fact that addition reactivity even decreases in these conditions.

It is now to be strongly presumed that the specific properties of vibrations should be considered in the field of reactivity. This new factor, which seems of a very general importance, opens the road to a development of a theory through which we could envisage the possibility of determining *a priori* the best conditions to orient a chemical reaction in the direction desired. Of course, these considerations do not destroy the importance of the part played by effects connected with the static pattern, such as inductive and mesomeric effects. These last phenomena have, on the contrary, to be considered, as well as the vibrational effect, in order to reach a satisfactory representation of the facts. It follows from the present developments that infra-red photoactivation should be possible.

A full account of this preliminary note will appear elsewhere.

My best thanks are due Professors C. A. Coulson and C. K. Ingold for a helpful and stimulating correspondence.

[1] C. K. Ingold, Ann. Repts. Chem. Soc. **23**, 144 (1926).
[2] A. E. Remick, *Electronic Interpretations of Organic Chemistry* (John Wiley and Sons, Inc., New York, 1946).
[3] P. B. D. de la Mare, Quat. Rev. **3**, 126 (1949).
[4] R. L. Arnett and B. L. Crawford, J. Chem. Phys. **18**, 118 (1950).
[5] W. A. Waters, *The Chemistry of Free Radicals* (Oxford University Press, London, 1946), p. 100.
[6] W. L. G. Gent, Quat. Rev. **2**, 383 (1948).
[7] C. A. Coulson, *V. Henri Mem. Vol.* (Desoer, Liége, 1947), p. 15; J. Duchesne, Nature **159**, 62 (1947).
[8] Thorndike, Welles, and Wilson, J. Chem. Phys. **15**, 157 (1947).

The Coordinate Scheme in Crystalline Boron

T. N. Godfrey and B. E. Warren
Massachusetts Institute of Technology, Cambridge, Massachusetts
June 7, 1950

PRELIMINARY x-ray diffraction studies of crystalline boron have been reported,[1] but as yet it has not been possible to index the powder pattern, or to get satisfactory crystals for single

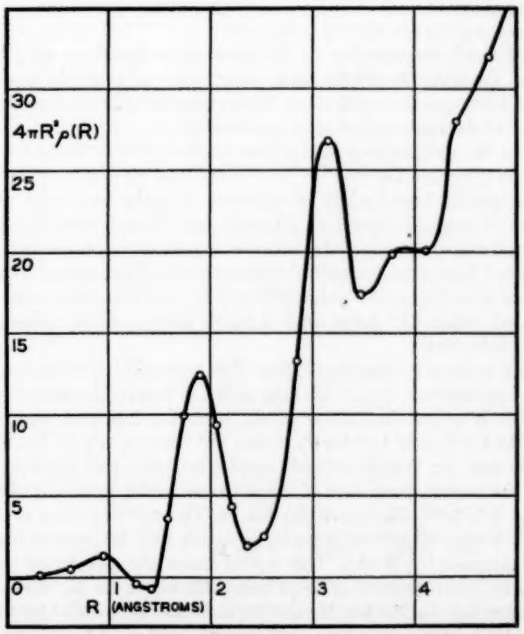

FIG. 1. Radial disribution curve for crystalline boron.

crystal patterns. The coordination scheme (number of nearest neighbors and interatomic distances) can be determined by a Fourier integral analysis[2] of the powder pattern, even when the pattern cannot be indexed and a complete structure determination is not possible.

The sample used in this investigation was boron of density 2.30 g/cm³ and of purity presumably greater than 99 percent. The crystalline form can be partially characterized by the prominent "*d*" values: 7.99, 5.52, 5.05, 4.69, 4.48, 3.57, 2.94, 2.86A. The Fourier analysis was made from the microphotometer record of a powder pattern made with crystal monochromated MoKα-radiation in a camera of diameter 8.93 cm. The area of the first peak of the radial distribution curve (Fig. 1) corresponds to 6.15 atoms. The area and position of this peak indicate six nearest neighbors at an average distance of 1.89A in crystalline boron.

[1] Laubengayer, Hurd, Newkirk, and Hoard, J. Am. Chem. Soc. **65**, 1924 (1943).
[2] Hultgren, Gingrich, and Warren, J. Chem. Phys. **3**, 351 (1935).

The Absorption Spectrum and the Dissociation Energy of Fluorine

M. W. NATHANS*
Department of Chemistry, University of California, Berkeley, California
May 29, 1950

RECENT spectroscopic and thermal data on the heats of formation and dissociation of ClF[1] have cast doubt upon the value of 60 kcal. of the heat of dissociation, D_0, of F_2. The indications are that D_0=30–40 kcal. Pitzer[2] more or less arbitrarily assumed a tentative value of 50 kcal.

Wicke[3] has questioned the interpretation of the absorption spectrum of ClF, suggesting that the low intensity of the bands are not in agreement with the Franck-Condon principle. He also measured the thermal conductivity of fluorine as a function of the temperature and found it to agree with the conductivity of nitrogen. Since his calculated curves for F_2 and N_2 almost coincide if no dissociation occurs, Wicke concluded that his experiments supported a high dissociation energy. Finally, a low D_0 of F_2 would correspond to an electron affinity of fluorine which would be below that of chlorine.

These arguments are not conclusive.

1. If the interpretation of the absorption spectrum of ClF is wrong, the true D_0 of ClF could only be lower than the one obtained from spectroscopic data. This would lower the dissociation energy of fluorine, rather than increase it.

2. In the calculations of the heat conductivity a value for the collision cross section and for the vibrational frequency occurring in the specific heat had to be assumed. For the latter the value 856 cm^{-1} was calculated by Murphy and Vance with Badger's rule and the values for the other halogens and the interatomic distance.[4] Recently Andrychuk[5] obtained the Raman spectrum of fluorine and found the value 892 cm^{-1}. The difference with the assumed value will have only a small effect on the calculated heat conductivity.

More serious is the assumption that the collision cross section of F_2 lies between that of O_2 and of N_2, although the interatomic distance is larger than either of the two, *viz.*, 1.48A as compared to 1.10A for N_2 and 1.21 for O_2. Using the values given by Pauling,[6] for the van der Waals radii of oxygen, nitrogen and fluorine, one finds the largest dimension of the diatomic molecules to be: 4.01A for O_2, 4.10A for N_2 and 4.18A for F_2. The collision cross section at $T=\infty$ may be several percent, probably five-ten percent higher than assumed by Wicke. This would cause the calculated curve for F_2 to be ten percent or more below the curve for N_2. Since the experimental results for N_2 and F_2 coincide to within $\pm$10 percent, the heat conductivity experiments conducted by Wicke are not at all conclusive.

The probability of a low D_0 for F_2 was reason to investigate the absorption spectrum of F_2 in the photographic infra-red. The visible region was investigated by Gale and Monk[7] who could not detect any absorption. The region covered by the present work extended from 7000A to 9600A.

The spectra were obtained in a Baird spectrograph with a 3m concave grating and photographed on Eastman I-N and (hypersensitized) I-M plates. The light source was a tungsten ribbon lamb. A Corning-3480 filter was placed in the light beam in order to cut out the blue, which would otherwise have shown up as a second-order spectrum. A 185-cm Pyrex tube was used as the absorption cell. The fluorine was introduced into the cell under a pressure of approximately one atmos.

The only absorption that could be detected was the forbidden oxygen band at 7600A and water absorption around 9000A, due to the long light path through air (7m). The detection of the oxygen band is evidence of the sensitivity of the method, and it may be concluded that there is no allowed transition for F_2 from the ground state to an attractive upper state in the region 7000–9600A. The sensitivity of the instrument toward detection of a possible weak continuous absorption resulting from a transition to a repulsive state is not as high, however, as that toward the detection of discrete absorption lines, because of the large dispersion (5.55A/mm). No definite conclusions can, therefore, be drawn about the dissociation energy of fluorine from this work.

The thermochemical work on ClF, however, as well as the large interatomic distance of fluorine presumably caused by outer shell repulsion, and the doubtfulness of the interpretation by Wicke of his thermal conductivity measurement, favor the low value of the dissociation energy of fluorine.

I would like to thank Professor L. Brewer for the many discussions on the subject and also for providing the fluorine; Professor F. A. Jenkins for the discussions, and Dr. C. Thurmond for his aid in building the transferring system for the fluorine.

* Present address: Institute of Engineering Research, University of California, Berkeley, California.
[1] See, e.g., R. L. Potter, J. Chem. Phys. **17**, 957 (1949).
[2] K. S. Pitzer, J. Am. Chem. Soc. **70**, 2140 (1948).
[3] E. Wicke, Zeits. f. Elektrochemie **53**, 212 (1949).
[4] Murphy and Vance, J. Chem. Phys. **7**, 208 (1939).
[5] D. Andrychuk, J. Chem. Phys. **18**, 233 (1950).
[6] L. Pauling, *Nature of Chemical Bond* (Cornell University Press, Ithaca, New York, 1945) p. 188.
[7] Gale and Monk, Phys. Rev. **29**, 211 (1927); Mulliken, Phys. Rev. **46**, 549 (1934), footnote 12a.

The Ionization Potential of Cyclopropane of Electron Impact

F. H. FIELD AND E. A. HINKLE
Department of Chemistry, University of Texas, Austin, Texas
May 29, 1950

We have determined the ionization potential of cyclopropane by electron impact and find its value to be 10.14$\pm$0.05 volts.

The measurements were made with a Westinghouse Type LV mass spectrometer using the vanishing current method.[1] The calibrating gas of known ionization potential and the cyclopropane were introduced simultaneously. The potential normally used to move the ions from the region in which they are formed through the slit in the first ion-accelerating electrode (the ion-drawout or pusher potential) was maintained at zero in order to obtain a satisfactory degree of reproducibility of results. The sensitivity of the instrument was thus diminished, but the energy spread of the ionizing electrons was also diminished. The voltage of the ionizing electrons was measured by means of a voltage divider placed across the electrodes of the electron gun and a Leeds and Northrup Type K-2 potentiometer. The accuracy of the voltage

TABLE I.

Substance	Ionization potentials (volts) Found	Literature
A	Pri. Std.	15.77[a]
N_2	15.60±0.06[b]	15.58[a]
CO_2	13.87±0.03	13.79,[c] 13.85[d]
CS_2	10.06±0.07	10.027,[e] 10.3[f]
C_3H_6[g]	10.14±0.05	
C_3H_6[h]	10.13±0.05	

[a] R. F. Bacher and S. Goudsmit, *Atomic Energy States* (McGraw-Hill Book Company, New York, 1932).
[b] All uncertainties calculated by multiplying the standard absolute errors by a factor which gives odds of 19 to 1 that the true mean lies within the resultant limits. See G. W. Snedecor, *Statistical Methods* (The Iowa State College Press, Ames, 1946), p. 65.
[c] Spectroscopic value. W. C. Price and D. M. Simpson, Proc. Roy. Soc. **A169**, 501 (1939).
[d] Electron impact value. R. E. Hornig, J. Chem. Phys. **16**, 105 (1948).
[e] Spectroscopic value. W. C. Price and D. M. Simpson, Proc. Roy. Soc. **A168**, 272 (1938).
[f] Electron impact value. T. M. Sugden and W. C. Price, Trans. Faraday Soc. **44**, 109 (1948).
[g] CO_2 used as secondary standard.
[h] CS_2 used as secondary standard.

measurements was greater than 0.1 percent. The temperature of the ionization chamber was maintained at 213±3°C.

Argon was used as the primary standard in calibrating the voltage scale. Unfortunately, the mass spectrum of cyclopropane[2] contains a contribution at mass 40, which prevented the direct use of argon as the calibrating gas in the determination of the cyclopropane ionization potential, but satisfactory results were obtained using carbon dioxide and carbon disulfide as secondary standards. The ionization potentials of these compounds were measured against argon.

The mass 42 peak of cyclopropane was symmetrical with no shoulders, and the peak height was a linear function of the pressure over the pressure range involved in the ionization potential determinations.

The cyclopropane, carbon dioxide, and argon were obtained from the Matheson Company and were used without further purification. The minimum purity given by the manufacturer for any of these substances was 99.5 percent. Commercial grade carbon disulfide was twice distilled through a packed column at a high reflux ratio, but the ionization potential was not altered by the purification.

Ten determinations of the ionization potentials of carbon disulfide and cyclopropane and thirteen determinations of the ionization potential of carbon dioxide were made. In general five separate samples were used, duplicate determinations being made on each. The results are summarized in Table I. The results of some measurements on nitrogen are also included in Table I. The good agreement of the ionization potentials of carbon dioxide, carbon disulfide, and nitrogen with previously reported values constitutes a check on the accuracy of the apparatus and method.

The ionization potential of cyclopropane can be compared with the values for propane (11.21 volts[3]), ethylene (10.62 volts by electron impace;[3] 10.50 volts by spectroscopic methods[4]), and propylene (9.84 volts by electron impact,[3] 9.6 volts by spectroscopic methods[4]). The ionization potentials of olefinic hydrocarbons are generally about a volt lower than those of the corresponding paraffinic compounds;[3] thus the ionization potential of cyclopropane indicates the presence of considerable unsaturation in this molecule. The value is compatible with Walsh's[5] concept of cyclopropane as a three-centered ethylene.

Using Walsh's model, Music and Matsen[6] calculated the wavelengths of the near ultraviolet spectrum of phenylcyclopropane, obtaining qualitative agreement with the observed values. It was assumed that the carbon π-bond Coulomb integrals are the same for all unsaturated hydrocarbons and that $|\beta\text{-cyclopropane}| \cong 0.9|\beta\text{-ethylene}|$ where β is the resonance integral. On the basis of these assumptions and the further assumption that the ionization potential of cyclopropane is given by $-(\alpha-\beta)$, the calculated ionization potential is lower than that of ethylene, which is in agreement with the experimental findings. Such agreement may be interpreted as evidence in favor of Walsh's model.

We should like to thank the Humble Oil and Refining Company of Baytown, Texas for the gift of the mass spectrometer.

[1] T. Mariner and W. Bleakney, Phys. Rev. **72**, 807 (1947).
[2] "Catalog of Mass Spectral Data," A.P.I. Project 44, Serial numbers 115, 172, and 181, National Bureau of Standards, Washington, D. C.
[3] R. E. Hornig, J. Chem. Phys. **16**, 105 (1948).
[4] W. C. Price and W. T. Tutte, Proc. Roy. Soc. **A174**, 207 (1940).
[5] A. D. Walsh, Trans. Faraday Soc. **45**, 179 (1949).
[6] J. F. Music and F. A. Matsen, J. Am. Chem. Soc. (to be published).

Remarks on a Paper by Riddell and Uhlenbeck

H. S. GREEN
Institute for Advanced Study, Princeton, New Jersey
May 1, 1950

PROFESSOR UHLENBECK has been kind enough to send me a copy of a manuscript by Mr. Riddell and himself,[1] already submitted for publication, in which reference is made to two other papers by de Boer[2] and myself.[3] As this contains a number of statements which appear to me inexact, I should welcome the opportunity to make the following comments.

As a preliminary remark, I do *not* consider that the thermodynamic and kinetic pressures are identical *only* in classical approximation, but also in a gas, where the surface energy is negligible, and in a liquid above a certain temperature. Further, neither de Boer nor myself introduces the complication of an external potential W into our considerations, for a reason which Riddell and Uhlenbeck appear to have overlooked. I affirm the following statements concerning their paper: (i) that, as a consequence of the inclusion of the potential term $W(q/L)$ in the Hamiltonian, the quantity p defined by Eqs. (4) and (5) is not the required thermodynamic pressure, *except* when the function $W(q/L)$ is infinite outside a region of volume $V=L^3$; (ii) that, when $W(q/L)$ has this character, Eq. (6) is incorrect; and (11) is also incorrect; and (iii) that, although (14) is correct, the considerations of Section 5 fail to justify the conclusion that the term containing μ_0 contributes to the pressure, but not the terms containing μ_1, μ_2, etc.

To prove the statement (i), it is sufficient to consider the classical limit. One sees immediately that the density of the fluid varies from place to place as $\exp-\beta W(q/L)$, and that in the classical limit the quantity p is given by

$$Vp=N/\beta+\tfrac{1}{3}\overline{\Phi}, \qquad \text{(a)}$$

where $V=L^3$, N is the number of molecules, and $\overline{\Phi}$ is the total virial of the molecular forces for *the volume* V_1 occupied by the fluid. The two volumes V_1 and V are only identical if $W(q/L)$ is infinite outside a region of volume L^3. Only then, therefore, will p represent the thermodynamical pressure. If the pressure is to be unique, it is necessary also for $W(q/L)$ to vanish inside the volume V.

To prove the statement (ii), suppose that the function $W(q/L)$ is of the type required; then one may no longer use "the hermitian property of $\mathcal{H}$" to derive (6). For

$$\int\left\{\Psi_n^*\left(\mathcal{H}\frac{\partial\Psi_n}{\partial L}\right)-(\mathcal{H}\Psi_n)^*\frac{\partial\Psi_n}{\partial L}\right\}d\tau = -\frac{\hbar^2}{m}\Sigma_i\int\frac{\partial}{\partial q_i}\left\{\Psi_n^*\frac{\partial^2\Psi_n}{\partial q_i\partial L}-\frac{\partial\Psi_n^*}{\partial q_i}\frac{\partial\Psi_n}{\partial L}\right\}d\tau, \qquad \text{(b)}$$

and, since $\partial\Psi_n/\partial q_i$ and $\partial\Psi_n/\partial L$ are both finite on the wall, however large the value of L, the surface integral arising from the second term cannot generally be discarded. One might attempt to remedy the argument in replacing $\mathcal{H}$ by $\exp-\beta\mathcal{H}$; this has been

done by T. Nishiyama,[4] who obtains, however, by this method a result equivalent to that which I have derived.

It is very difficult to reconstruct the argument of Riddell and Uhlenbeck between (10) and (11), but an independent calculation shows that their result (11) is incorrect. In fact, one obtains for the right-hand side an expression which may be written simply

$$\left(q\frac{\partial}{\partial q}+q'\frac{\partial}{\partial q'}\right)\langle q|\exp-\beta\mathcal{H}|q'\rangle, \qquad (c)$$

on the understanding that $\partial/\partial q$ and $\partial/\partial q'$ do not operate on $W(q/L)$. Since $W(q/L)$ must in any case be zero except outside the fluid, this last stipulation does not have any quantitative effect, the integration being limited to the region occupied by the fluid.

The statement (iii) above is almost self-evident. The condition necessary for the permutation of the operators is that the expectation values of certain physical quantities should be negligible at the wall; and Riddell and Uhlenbeck have not investigated the circumstances under which this condition is satisfied. I find that the condition is not satisfied in quantum liquids, and I believe that many of the properties of He II can be understood from this point of view.

[1] Riddell and Uhlenbeck, J. Chem. Phys. **18**, 1066 (1950).
[2] J. de Boer, Physica **15**, 843 (1949).
[3] H. S. Green, Physica **15**, 882 (1949).
[4] A short note on the virial theorem. I am much indebted to Dr. Nishiyama for sending me a copy of his manuscript.

Investigations on the Hydrated Molybdenum Blue

LUIGI SACCONI AND RENATO CINI
Institute of Physical Chemistry, University of Florence, Florence, Italy
May 28, 1950

IN connection with the different conclusions reported[1] on the constitution of hydrated molybdenum blue, the composition of this compound, prepared from hydrochloric solutions of Mo^{V} and Mo^{VI}, has been investigated.

Varying the ratios of Mo^{VI}:Mo^{V} in the solutions from 9.0 to 0.56, the empirical unitary formula of the produced molybdenum blue lies between $Mo_{2.89}\cdot x\,H_2O$ and $MO_{2.93}\cdot x\,H_2O$ and the ratios of Mo^{VI}:Mo^{V} in the blues varies from 3.4 to 6. The amount of water present in the compounds ranges from 17.96 to 19.38 percent. The slight paramagnetism exhibited by the compounds (about one-tenth to one-twentieth that for one unpaired electron) suggests that pentavalent molybdenum, in the blue, is mainly bound with covalents Mo^{V}-Mo^{V} linkages.

The hydrated blue, treated at 195°C in an atmosphere of nitrogen, loses nearly all the water of hydration. At 350°C decomposition takes place with separation of MoO_3 and formation of a more reduced blue oxide. X-ray analysis showed that both hydrated and dehydrated (at 195°C) molybdenum blues are essentially amorphous. The few diffuse halos on continuous background in the powder photographs are coincident with the x-rays lines produced by MoO_3. Electric resistance determinations on molybdenum blue showed that the blue treated at 195°C behaves as a typical semiconductor. The values of conductivity range from 10^{-5} ohm^{-1}-cm^{-1} at 20°C to 10^{-3} ohm^{-1}-cm^{-1} at 180°C. The temperature coefficient is strongly positive and the classical relation $\sigma=Ae^{-E/T}$ is satisfied. The results indicate that amorphous molybdenum blue, behaving as a reduction semiconductor, is a non-stoichiometric compound with a stoichiometric defect of oxygen.

Treatment of the blue at 350°C causes the conductivity to reach values of the order of 1 ohm^{-1}-cm^{-1} and the temperature coefficient, between 350°C and 20°C, becomes almost nil, which confirms that thermal treatment at 350°C causes decomposition and yields a different blue oxide. This oxide, indeed, separated with aqueous ammonia, exhibits a similar conductivity, while the conductivity of MoO_3, the variation of which with temperature has not yet been reported, varies from 10^{-8} ohm^{-1}-cm^{-1} at 20°C to 10^{-3} ohm^{-1}-cm^{-1} at 350°C.

The investigation continues chiefly in regard to the study of the compounds which arise from thermal treatment of hydrated molybdenum blue.

[1] J. W. Mellor, *A Comprehensive Treatise on Inorganic and Theoretical Chemistry* (Longman and Company, London), Volume XI; R. Abegg and Fr. Auerbach, *Handbuch der Anorganischen Chemie* (Verlag S. Hirzel, Leipzig), Volume IV; O. Glemser and E. Lutz, Naturwiss. **34**, 215 (1947).

Erratum: Parabolic Oxidation Rates of Metals

[J. Chem. Phys. **18**, 231 (1950)]
WALTER J. MOORE
Catholic University of America, Washington, D. C.

IN footnote 2 of this letter it is stated that the theoretical equation of Mott and Gurney for the parabolic rate constant K contains an incorrect factor of 2. Actually their equation is given correctly in *Electronic Processes in Ionic Crystals* (Oxford University Press, London, 1940), p. 257. The author regrets this mistake.

The Quadrupole Coupling of Three Nuclei in a Rotating Molecule

RICHARD BERSOHN*
Harvard University, Cambridge, Massachusetts
May 25, 1950

RECENTLY the microwave spectra of a number of molecules ($AsCl_3$,[1] PCl_3,[1] $CHBr_3$,[2] PBr_3,[2] $CHCl_3$ [3]) with three quadrupolar nuclei have been measured. The calculation of the energy levels of such a molecule is most simply done by the tensor methods of G. Racah.[4] His procedure in fact yields directly the matrix elements for any quadrupole coupling problem.

Let the spins be I_1, I_2, I_3, the quadrupole moments Q_1, Q_2, Q_3 and $(\partial^2V/\partial z^2)$ (i) be the derivative of the potential taken at the position of the ith nucleus with respect to a z-axis fixed in space. Let $\mathbf{I}=\boldsymbol{I}_1+\boldsymbol{I}_2$, $\mathbf{I}=\boldsymbol{I}+\boldsymbol{I}_3$, $\boldsymbol{F}=\boldsymbol{I}+\boldsymbol{J}$. The matrix elements of the molecular quadrupole Hamiltonian are

$$(IIJF|H_Q|I'I'J'F)=\frac{5}{4}(-1)^{I_1+I_2+I_3-\mathbf{I}-\mathbf{I}'+J'-F}$$
$$\times\frac{eQ_1(J|(\partial^2V/\partial z^2)(1)|J')[(2\mathbf{I}+1)(2\mathbf{I}'+1)(2I+1)(2I'+1)]^{\frac{1}{2}}}{(I_1I_1-I_1I_1|I_1I_120)(JJ'-JJ|JJ'20)}$$
$$\times W(I_1II_1\mathbf{I}';I_22)W(I\mathbf{I}'I';I_32)W(IJI'J';F2)$$
$$+\frac{5}{4}\frac{(-1)^{I_1+I_2+I_3-2\mathbf{I}'+J'-F}eQ_2(J|(\partial^2V/\partial z^2)(2)|J')}{(I_2I_2-I_2I_2|I_2I_220)(JJ'-JJ|JJ'20)}$$
$$\times W(I_2II_2\mathbf{I}';I_12)W(I\mathbf{I}'I';I_32)W(IJI'J';F2)$$
$$\times[(2\mathbf{I}+1)(2\mathbf{I}'+1)(2I+1)(2I'+1)]^{\frac{1}{2}}$$
$$+\frac{5}{4}(-1)^{\mathbf{I}+I_3+I-I'+J'-F}eQ_3\left(J\left|\frac{\partial^2V}{\partial z^2}(3)\right|J'\right)$$
$$\times\frac{[(2I+1)(2I'+1)]^{\frac{1}{2}}\delta_{\mathbf{I},\mathbf{I}'}W(I_3II_3I';\mathbf{I}2)}{(I_3I_3-I_3I_3|I_3I_320)(JJ'-JJ|JJ'20)}$$
$$\times W(IJI'J';F2).$$

$W(j_1j_2j_1'j_2';jk)$, introduced by Racah, is essentially the matrix element of the scalar product of two irreducible tensors of rank k

between the states $(j_1j_2jm|$ and $(j_1'j_2'jm|$. In the special cases that the three nuclei are identical, have identical coupling constants, and have spins of 1 or $\frac{1}{2}$, the matrix elements have been calculated as a function of J.[5] For each energy level $J(J \geqslant 2)$, six cubic and two quartic equations must be solved.

* Now at Columbia University, New York, New York.
[1] P. Kisliuk and C. H. Townes, Phys. Rev. **78**, 347 (1950); J. Chem. Phys. **18**, 1109 (1950).
[2] Q. Williams and W. Gordy, Phys. Rev. **79**, 195 (1950).
[3] Unterberger, Trambarulo, and Smith, J. Chem. Phys. **18**, 565 (1950).
[4] G. Racah, Phys. Rev. **62**, 438 (1942).
[5] R. Bersohn, thesis, Harvard University, 1949.

Electron Deficient Compounds. V. The Structure of Dimethylberyllium*

R. E. Rundle and A. I. Snow
Department of Chemistry, Iowa State College, Ames, Iowa
May 29, 1950

EMPIRICAL[1] and theoretical[2] justification has been given for the rule that metals tend to use all low energy orbitals for bond formation, even when orbitals exceed valence electrons numerically. This accounts for known electron deficient compounds, and allows prediction of their occurrence.

On the basis of the above rule dimethylberyllium, a compound subliming at 200°C, should involve four tetrahedral, electron-deficient bonds to beryllium. The structure fulfills these predictions.

Dimethylberyllium is body-centered, orthorhombic, $a_0=6.14$, $b_0=11.53$, $c_0=4.18$A, $\rho=0.9$, $z=4$. Reflections $(h0l)$ and $(0kl)$ occur with even indices only, so the space group is Ibam or Iba. In either case the eight carbon positions are $(000, \frac{1}{2}\frac{1}{2}\frac{1}{2})\pm xy0$, $\pm x\bar{y}\frac{1}{2}$, with $x=0.182\pm0.003$, $y=0.101\pm003$. The beryllium positions are $(000, \frac{1}{2}\frac{1}{2}\frac{1}{2})+00z$, $00z+\frac{1}{2}$, with $z\equiv\frac{1}{4}$ for Ibam. Reflections $(00l)$ limit z to 0.25 ± 0.026 for Iba. The structure determination, when refined, will be published elsewhere.

The structure, isomorphous with SiS_2, consists of chains,

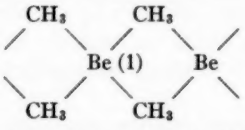

The configuration about Be is approximately tetrahedral with Be−C=1.92±0.03A, *versus* 1.84 calculated by Pauling's radii and rule,[3] assuming half an electron pair per bond. The C−Be−C angle, (1), is 114°. The Be−Be distance is 2.09±0.01A, which, by Pauling's rule, indicates a bond number of 0.3. The larger than tetrahedral C−Be−C bond angle, (1), lends support to the idea that Be−Be bonding is important. The angle may also be explained by the need for a sharp Be−C−Be angle. The distance is long enough to suggest that the Be−Be bond does not share electrons equally with the Be−C bonds.

Symmetry of even the lower space group rules out methyl bridges like those suggested by Pitzer and Gutowsky for the trimethylaluminum dimer,[4] and the distances rule out analogous bridges,

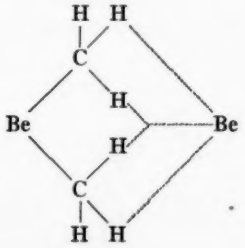

By analogy this structure suggests symmetrical bridges in trimethylaluminum, as has been proposed.*,[5] There is nothing in the distances to suggest material contribution of C−H bonds to the electrons of the bridge. The bonding probably consists essentially of one tetrahedral orbital from carbon symmetrically overlapping tetrahedral orbitals from each of two beryllium atoms to form one molecular orbital for the Be−C−Be half-bond pair. The Be−C−Be angle, only 66°, permits good utilization of the carbon tetrahedral orbital in this arrangement, first suggested by Mulliken.[6] An analogous type of geometry of the migrating group in molecular rearrangements would account for the observed retention of configuration.

The structure does not appear to be predominantely ionic. Moreover, negative methyl ions should require larger C−C distances between chains than the 4.1A observed.

Electron deficient compounds, historically limited to third group elements, now include platinum and beryllium compounds. Extension to other groups of the periodic table is to be expected from the rule above.

* Paper No. 96 from the Institute for Atomic Research, Iowa State College, Ames, Iowa. This work was performed in the Ames Laboratory, AEC.
[1] R. E. Rundle, J. Am. Chem. Soc. **69**, 1327 (1947).
[2] R. E. Rundle, J. Chem. Phys. **17**, 671 (1949).
[3] L. Pauling, J. Am. Chem. Soc. **69**, 542 (1947).
[4] K. Pitzer and Gutowsky, J. Am. Chem. Soc. **68**, 2204 (1946).
[5] R. S. Mulliken, Chem. Rev. **41**, 207 (1947).

A Theoretical Calculation of Valence-Bond Parameters

J. van Dranen and J. A. A. Ketelaar
Laboratory for General and Inorganic Chemistry, University of Amsterdam, Amsterdam, Netherlands
May 29, 1950

THE valanece bond method enables us to express the energy of the π-electrons in terms of two parameters: the Coulomb integral Q and the (single) exchange integral α. E.g., for benzene, we have

$$Q=\int a(1)b(2)c(3)d(4)e(5)f(6)Ha(1)b(2)c(3)d(4)e(5)f(6)d\tau$$

and

$$\alpha=\int a(1)b(2)c(3)d(4)e(5)f(6)Ha(2)b(1)c(3)d(4)e(5)f(6)d\tau.$$

Here a, b, c, etc., are the p_z-wave functions of the carbon atoms and the π-electrons are labeled by 1, 2, 3, etc.[1]

In this treatment the non-orthogonality integrals $s_{12}=\int a(1)b(1)d\tau$, etc., the single-exchange integrals between non-neighboring atoms and all double-, triple-, etc., exchange integrals are neglected. So it is possible to express the energy of a certain structure of a molecule as $Q+m\alpha$. For instance the Kékule-structure of benzene has the energy $Q+1.5\alpha$; the stationary ground state $Q+2.61\alpha$.

If we take now the energy difference between two states, e.g., to calculate a resonance energy (R.E.) or an ultraviolet transition, Q cancels out and we are left with an expression in α. By putting this equal to the experimental R.E., α can be calculated. It is possible however to evaluate theoretically $\alpha(\alpha')$ and also other exchange integrals neglected hitherto. Hence it is no longer justifiable to neglect the non-orthogonality integrals and so we have to transform α into $\alpha'\equiv\alpha-S_{12}^2Q$, for only after this transformation Q cancels out in the expression for the R.E.'s and the excitation energies. Of course the other exchange integrals have to be transformed in an analogous way. In general, an exchange integral becomes $\lambda'=\lambda-lQ$, where l is equal to the integral for λ with the Hamiltonian H replaced by unity; thus l is the product of a number of non-orthogonality integrals.

According to the absolute valence-bond method the R.E. of the hypothetical compound cyclobutadiene is equal to: $0.8747\alpha' - 0.8747\beta' - 0.08028\delta' - 0.8747\zeta'$. Distance between two C-atoms 1.39A; effective nuclear charge $Z=3.18$.

$\alpha'=\alpha-s_{12}^2Q=-1.04$ ev (exchange between 1 and 2)
$\beta'=\beta-s_{13}^2Q=-0.16$ ev (exchange between 1 and 3)
$\delta'=\delta-s_{12}^4Q=-0.13$ ev (exchange between 1 and 2; 3 and 4)
$\zeta'=\zeta-s_{12}^2s_{13}Q=-0.11$ ev (cycle exchange $1\to2\to3\to1$)
($s_{12}=0.2600$; $s_{13}=0.0943$).

Substituting these values yield a value of 15 kcal. for the R.E. (Inclusion of the other exchange integrals does not alter this value appreciably.)

For benzene we computed the values:

$\alpha'=\alpha-s_{12}^2Q=-1.03$ ev
$\beta'=\beta-s_{13}^2Q=-0.03$ ev (exchange between 1 and 3)
$\gamma'=\gamma-s_{14}^2Q=-0.002$ ev (exchange between 1 and 4)
$\delta'=\delta-s_{12}^4Q=-0.23$ ev(!) (exchange between 1 and 2; 3 and 4)

We are engaged in calculating the R.E. of benzene with the aid of this absolute valence-bond method.

For the valence-bond method with empirical parameters there occurs in the literature a discrepancy between the values taken for the single exchange integral of the C−N bond. A. Maccoll[2] takes a lower and W. T. Simpson[3] a higher value as compared with that of the C−C bond. By expanding the absolute method discussed in the present paper to heterocyclic molecules we evaluate for the α_{en}' of pyridine the value -0.93 ev ($\alpha_{en}'\equiv\alpha_{en}-s_{en}^2Q$) for a C−N distance of 1.37A, thus slightly lower than that for the C−C bond.

Mathematical Appendix.—The Hamiltonian for the π-electrons in benzene is

$$H=-\frac{\hbar^2}{8\pi^2m}\sum_{i=1}^{i=6}\nabla_i^2+\sum_{\substack{j=1\\ j>i}}^{j=6}\sum_{i=1}^{i=6}\frac{e^2}{r_{ij}}+\sum_{k=a}^{k=f}\sum_{i=1}^{i=6}H_k(i)$$

+interaction integrals which cancels out in the expression for λ'.

Using the symbols already given,[4] we get for α' in benzene:

$$\alpha'=\alpha-s_{12}^2Q=2s_{12}Ae(r_{12})+4s_{12}^2Ad(rm3,rm4)$$
$$-2s_{12}^2Ad(r_{12},r_{12},r_{13},r_{13},r_{14})-2s_{12}Be(r_{12})+s_{12}^2Bd(r_{12})+Bf(r_{12}).$$

Bf is a new symbol to denote the exchange integral

$$Bf(r_{ij})=\int\varphi_i(\gamma)\varphi_j(\gamma)\frac{e^2}{r_{\gamma\mu}}\varphi_i(\mu)\varphi_j(\mu)d\tau.$$

A numerical value for α' can now be calculated with the values for the integrals as given by Parr and Crawford.[5] $\delta'=\delta-s_{12}^4Q$ for cyclobutadiene (m is a point midway between C_1 and C_2 with a virtual charge equal to $s_{12}e$). On the left side we write the symbols for δ; on the right side the symbols for $-s_{12}^4Q$ after canceling the equal terms.

$$\delta'=4s_{12}^3Ae(r_{12})+8s_{12}^4Ad(rm3)-4s_{12}^4Ad(r_{12},r_{12},r_{13})$$
$$+2s_{12}^2Bf(r_{12})+4s_{12}^4Bd(r_{12})-2s_{12}^4Bd(r_{12},r_{12},r_{13})$$
$$-4s_{12}^3Be(r_{12})-8s_{12}^4Bd(rm3)+4s_{12}^4Bd(r_{12},r_{12},r_{13}).$$

It is not possible to evaluate Q or α in this way, since certain integrals involved, referring to the interaction between neutral C-atoms at short distances, cannot be solved. On the other hand, if we transform λ into $\lambda'-lQ$ these integrals cancel out.

[1] Eyring, Walter, and Kimball, *Quantum Chemistry* (John Wiley and Sons, Inc., New York, 1948).
[2] A. Maccoll, J. Chem. Soc. **132**, 670 (1946).
[3] W. T. Simpson, J. Chem. Phys. **16**, 1124 (1948).
[4] J. van Dranen and J. A. A. Ketelaar, J. Chem. Phys. **18**, 15 (1950).
[5] R. G. Parr and B. L. Crawford, J. Chem. Phys. **16**, 1049 (1948).